NASA CR-
160582

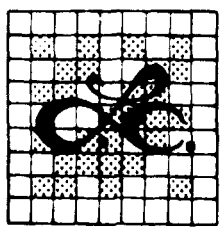

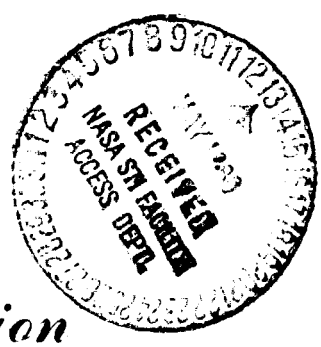

LinCom Corporation
P.O. Box 2793D, Pasadena, Calif. 91105

LinCom

SPS PHASE CONTROL SYSTEM PERFORMANCE VIA ANALYTICAL SIMULATION

PREPARED FOR

NASA JOHNSON SPACE CENTER
HOUSTON, TX 77058

TECHNICAL MONITOR: JACK SEYL

CONTRACT NAS9-15725

PREPARED BY

W. C. LINDSEY
A. V. KANTAK
C. M. CHIE
R. W. D. BOOTH

LINCOM CORPORATION
P.O. BOX 2793D
PASADENA, CA 91105

MARCH, 1979

TR-7903-0977

LinCom

ACKNOWLEDGEMENT

The authors wish to acknowledge the discussions held with Mr. Jack Seyl and Dr. G. D. Arndt of the Johnson Space Center and for providing us with various articles of interest. In addition, the support and encouragement of Mr. R. H. Dietz and Mr. R. O. Piland of the Johnson Space Center is greatly appreciated.

TABLE OF CONTENTS

TABLE OF CONTENTS

TABLE OF CONTENTS

TABLE OF CONTENTS

1.0 INTRODUCTION

In Ref. 1 a Solar Power Satellite Transmission System incorporating automatic beam forming, steering and phase control was presented. The phase control concept, which was discussed in great detail in Ref. 1, centered around the notation of an active retrodirective phased-array, ([Refs. 2,3]. Figure 1.1 illustrates the major elements required in the operation of an SPS system which employs retrodirectivity as a means of automatically pointing the beam to the appropriate spot on the Earth. From Figure 1.1 we see that these include: (1) the transmitting antenna, hereafter called the spacetenna, (2) the receiving antenna, hereafter called the rectenna, and (3) the pilot signal transmitter. The rectenna and pilot signal transmitter are located on the Earth. The purpose of the spacetenna is to direct the high-power beam so that it comes into focus at the rectenna. Since the rectenna is to be approximately 10 km in "diameter," the beamwidth of the high power beam must be extremely narrow, in fact, on the order of one-half minute of arc. The pilot signal, transmitted from the center of the rectenna to the spacetenna, provides the signal needed at the SPS to focus and steer the power beam. As a by-product of this requirement a command link to the SPS is provided.

As seen from Fig. 1.1 the SPS phase control system is faced with several key problems. They include: (1) path delay variations due to imperfect SPS circular orbits, (2) ionospheric effects, (3) initial beam forming, see Figs.1.2 and 1.3, (4) beam pointing, see Fig. 1.4, (5) beam safing, Figs. 1.2 to 1.4, (6) high power amplifier phase noise effects, (7) interference (unintentional and intentional), etc.

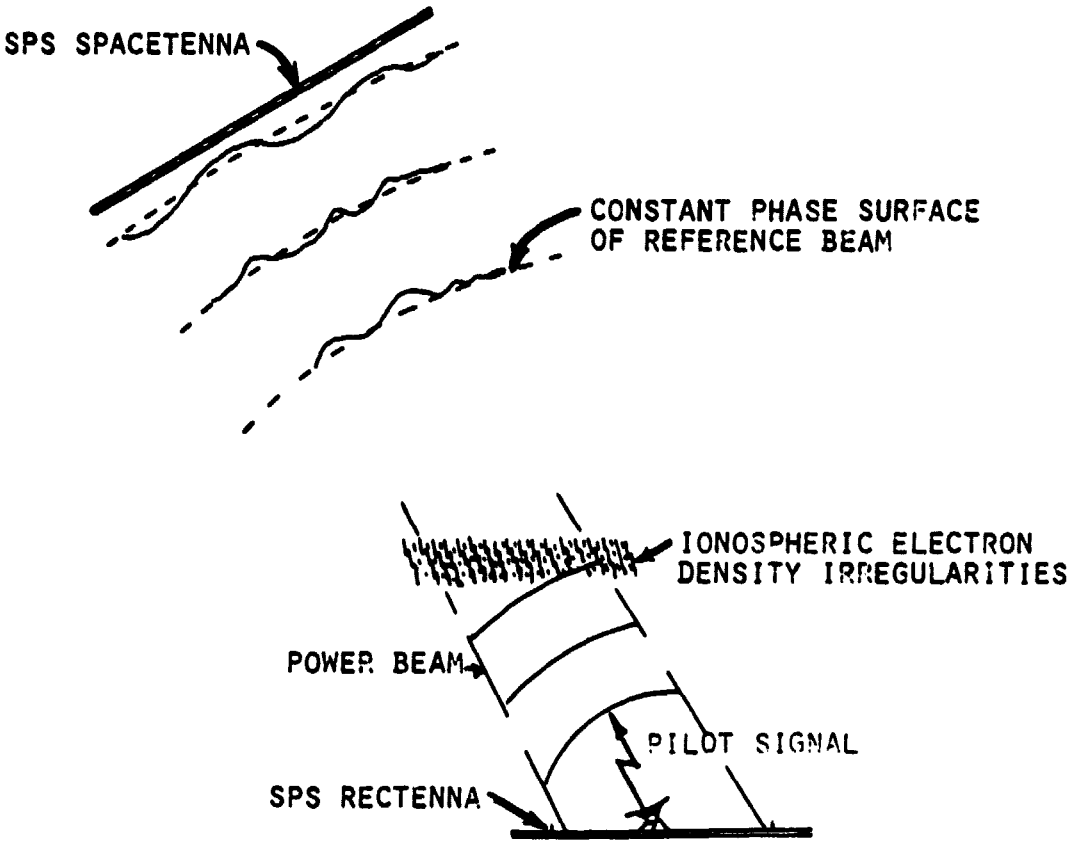

- PATH DELAY VARIATIONS
- IONOSPHERE EFFECTS
- INITIAL BEAM FORMING
- BEAM POINTING
- BEAM SAFING
- PHASE NOISE (HPA)
- INTERFERENCE
- SELF-JAMMING

Figure 1.1. Space Based Solar Power Satellite and Earth Based Energy Collection System Concept.

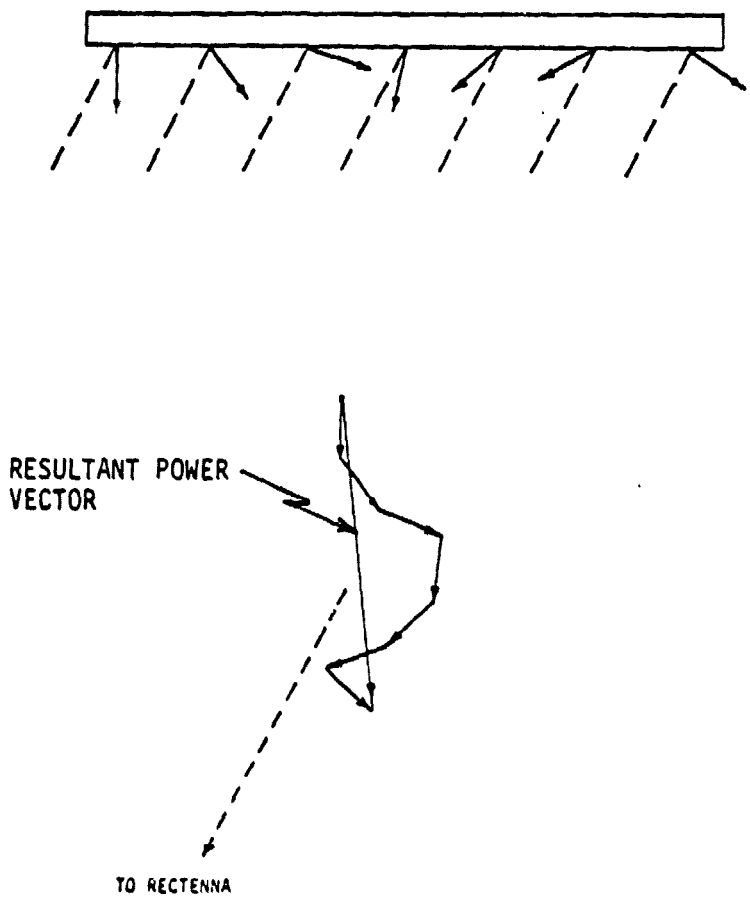

Figure 1.2. Initial Phasing of the SPS Power Amplifiers.

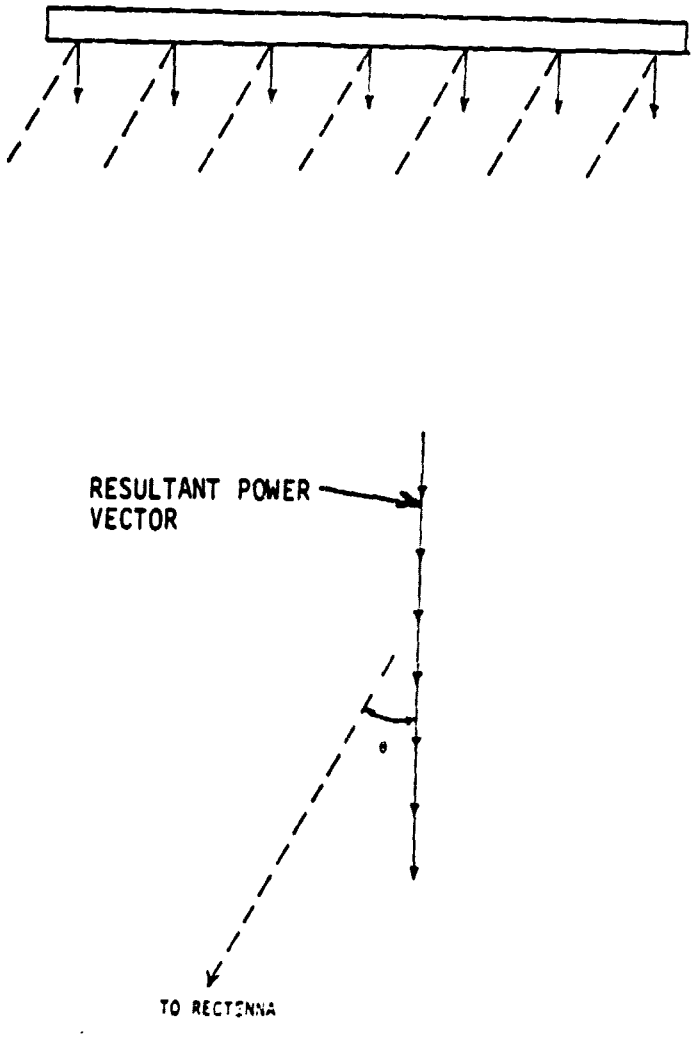

Figure 1.3. SPS Power Amplifier Phased at Angle θ Relative to Rectenna Sight.

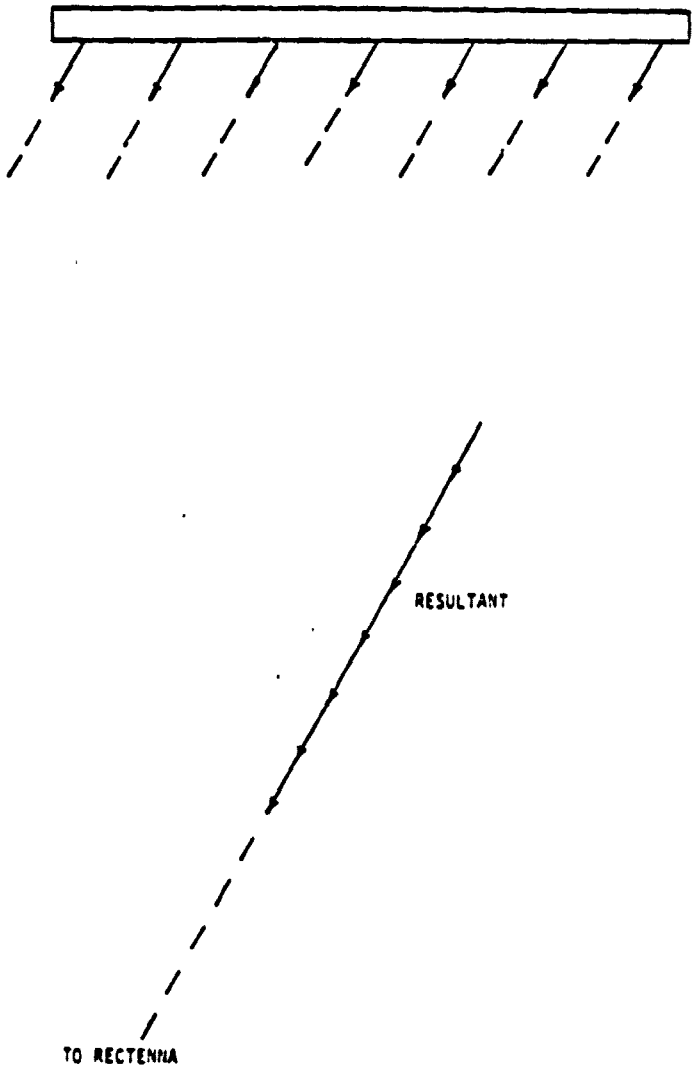

Figure 1.4. SPS High Power Amplifiers Phased and Pointed so as to Form a High Power Beam.

1.1 SPS Transmitting System Concept

From the system engineering viewpoint, the SPS transmitting system which incorporates retrodirectivity is depicted in Figure 1.5. A central feature of the SPS Transmitting System is 101,552 element retrodirective active phased-array (spacetenna) [2],[3] of 1-km diameter designed to focus and point the phase-coherent microwave beam to a ground-based rectifying antenna (rectenna) which is approximately 10 km in diameter. As seen from Figure 1.5 the SPS Transmission System consists of three major systems: (1) The Reference Phase Distribution System, (2) The Beamforming and Microwave Power Generating System, and (3) The Solar Power to Electrical Power Conversion System. In what follows we shall be concerned with establishing the far-field performance associated with the Reference Phase Distribution System and the Beamforming and Microwave Power Generating System. The major technique used in the performance evaluation is that of analytical simulation, i.e., a combination of analysis and computer simulation.

1.2 The Phase Control System Concept

To achieve retrodirectivity, the microwave power transmission system requires an on-board Phase Control System (Figure 1.5) phase-locked or synchronized to the pilot signal transmitted from the center of the ground based rectenna. One major purpose of the Phase Control System is to coherently reconstruct the instantaneous frequency and phase of the received pilot signal and use this to generate and distribute a set of constant phase conjugation reference signals. This set of signals is used to advance the phase of the pilot signal received at each spacetenna element by an amount equal

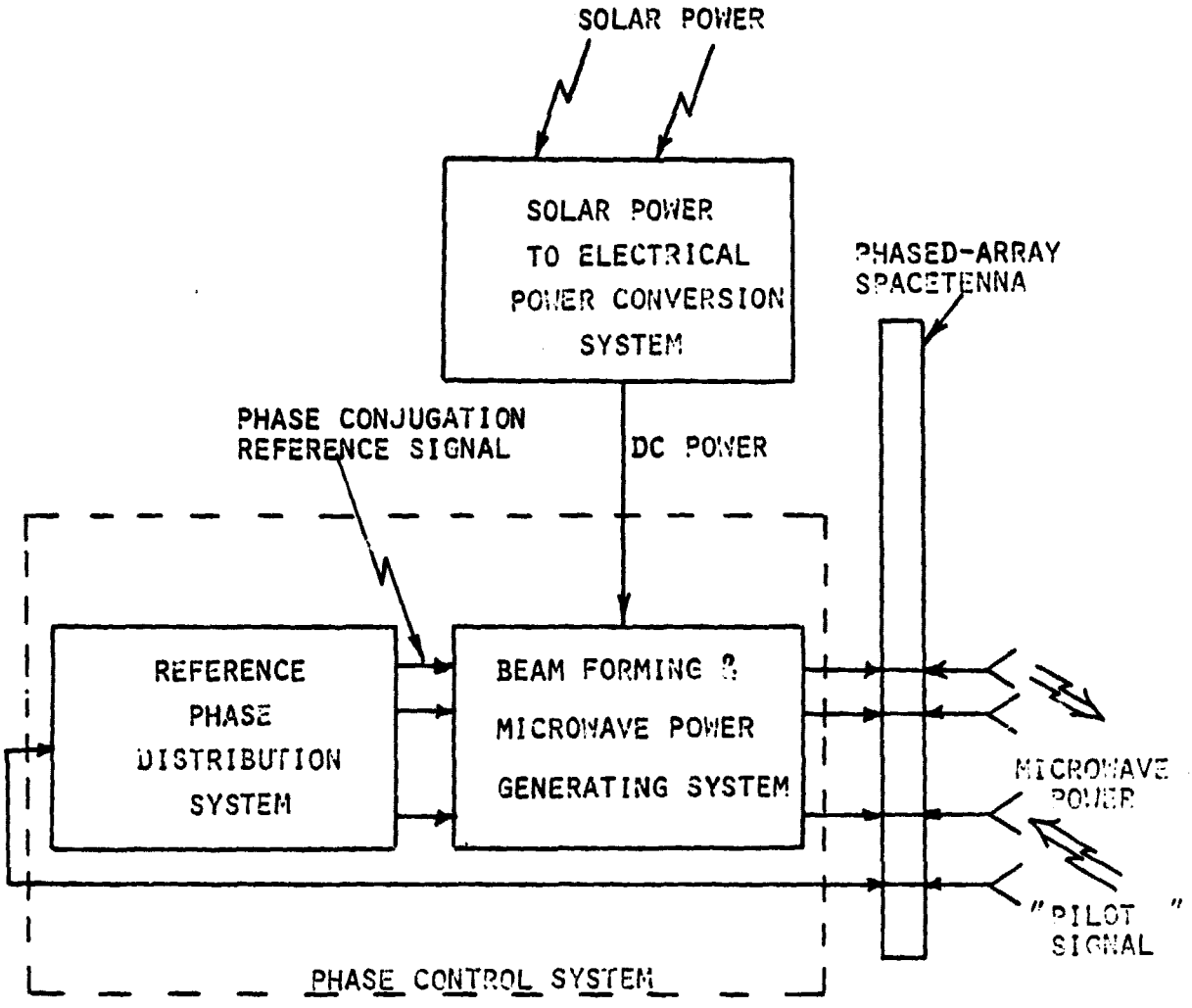

Figure 1.5. Solar Power Satellite (SPS) Transmission System (Phase Conjugation).

to the phase delay accumulated on the uplink. By a constant phase conjugation reference signal is meant a signal whose instantaneous phase characteristic, at any spatial point (x_1,y_1,z_1) on the spacetenna, is perfectly correlated with the phase characteristic distributed from the spacetenna center to any other point (x_2,y_2,z_2) on the spacetenna. Such instantaneous "phase-matching" in time and space implies synchronization [4], i.e., bringing about and maintaining a synchronous state at all points on the spacetenna where phase conjugation is to take place. In essence, the generation of a set of constant phase conjugation reference signals from the received pilot signal is equivalent to transfering precise time and time interval to a set of remote points (subarray centers) located on the spacetenna. At these subarray centers we locate Phase Control Centers (PCCs). In Reference 1 we illustrated and discussed their location on the SPS.

1.3 Beamforming and Microwave Power Generating System Concept

To form a coherent, high power microwave beam a cooperating Microwave Power Generating System is required, see Figure 1.5. One of its main functions is that of delivering large amounts of microwave power to the radiating subarrays, Refs. 4, 5. By taking advantage of the retrodirective feature of the active phased-array the power generated by the high power amplifiers is automatically returned (transponded) to the direction from which the pilot signal came. Thus the SPS system directs the power generated by the Space-Based Energy Station to the Earth based rectenna. The retrodirective phase conjugate concept, currently selected as the reference system.

will be further elaborated upon in what follows. Needless to say, there are other approaches to beam forming and power transmission: viz., ground control techniques which are currently being investigated at LinCom.

1.4 The Reference Phase Distribution System and the Microwave Power Generating System Interface

As previously mentioned the phase conjugate reference signals generated by the Reference Phase Distribution System are coherently distributed to Phase Control Centers (PCCs) located on the SPS. From these PCCs, the signals are then distributed and used to drive the set of phase conjugate circuits associated with the Beam Forming and Power Generating System, Figure 1.5. These processors, which contain the phase controlled high-power amplifiers operating in unison, automatically form the high power beam by causing advancement in the phase of the power amplifier output signals. This advancement is such that the accumulated phase on the downlink signal equals the phase accumulated on the uplink signal. Accomplishing this "zero phase accumulation process" on the up and downlink signals requires that the uplink frequency of the pilot signal "appear" to equal the downlink carrier frequency; this creates the SPS Pilot Signal Design problem.

2.0 THE SPS PILOT SIGNAL MODULATION FORMAT FOR A RETROFIRE ARRAY

The major factors of concern in the design of the SPS pilot (see Fig 2.0) waveform include: (1) ionospheric effects, (2) beam squint, (3) isolation of the up and downlink waveforms, (4) phase noise associated with the high power amplifiers, (5) diplexer characteristics, (6) security, (7) multiple access capability and anti-jamming margin, (8) privacy of a command link to the SPS, (9) radio frequency interference

- MAIN CONSIDERATIONS
  - IONOSPHERIC EFFECTS
  - BEAM SQUINT
  - ISOLATION OF UP/DOWN LINK
  - PHASE NOISE OF PA's
  - DIPLEXER CHARACTERISTICS
  - SECURITY (AJ MARGIN)
  - COMMANDS
  - AMBIGUITY
  - POWER ROBBING
- MAIN APPROACHES
  - SINGLE-FREQUENCY TONE
  - DOUBLE-FREQUENCY TONE
  - BI-ϕ CODED TONE

Figure 2.0. SPS Pilot Signal Design Considerations.

/

including that from other signals which may be generated in the SPS network (multiple access), (10) bandwidth requirements, (11) oscillator instability, and (12) phase ambiguities generated in the Phase Control System. Appendix I provides analytical support to the selection of SPS pilot signal.

Figure 2.1 summarizes the single-frequency pilot tone/retrofire concept investigated in Ref. 8. The major disadvantages of this approach are also summarized in Fig. 2.1. To overcome some of the disadvantages a two-frequency pilot-tone/retrofire concept has been considered. This approach is summarized in Fig. 2.2 along with its major disadvantages. Appendix I provides an analysis of the ambiguity resolution problem associated with the two-frequency pilot tone concept.

To overcome the uplink pilot signal interactions with the high energy downlink power beam a pilot waveform has been designed (Ref. 1) which isolates the uplink from the downlink while simultaneously providing for anti-jam protection (security and privacy) and multiple access operation of any reasonable number of SPSs. In addition, the pilot waveform design has the added attributes that it tends to minimize the deleterious effects (beam squint and jitter) produced by the ionosphere's index of refraction. The modulation characteristics of the reference system pilot waveform is Binary Phase-Shift Keying (BPSK) of the pilot carrier for command transmission to the SPS and split-phase (Manchester coded), direct sequence (DS) pseudo-noise modulation for uplink/downlink isolation and anti-jam protection [4,7]. Code-division multiple access (CDMA) modulation is used to provide the needed multiple access capability required in the operation of a network of SPS's, see Figure 2.3. The SPS Pilot waveform design is

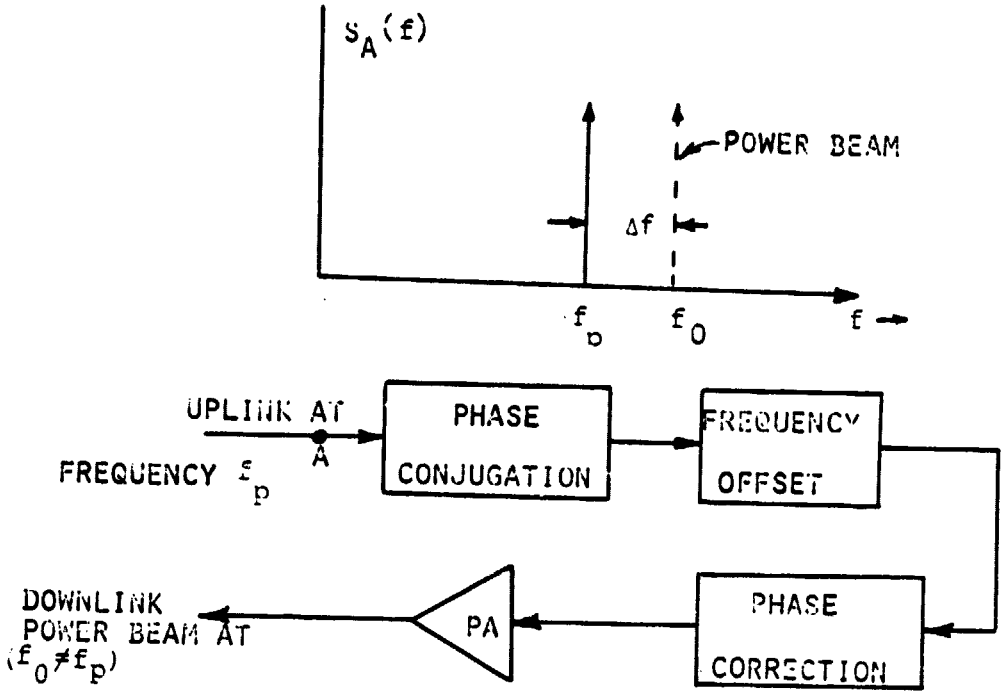

- BEAM SQUINTING PROBLEM
- IONOSPHERIC EFFECT
- SUSCEPTABLE TO INTERFERENCE
- POWER ROBBING
- PHASE CORRECTION SYSTEM REQUIRED

Figure 2.1. SPS Single-Frequency Pilot Signal Design and Retrofire Concept.

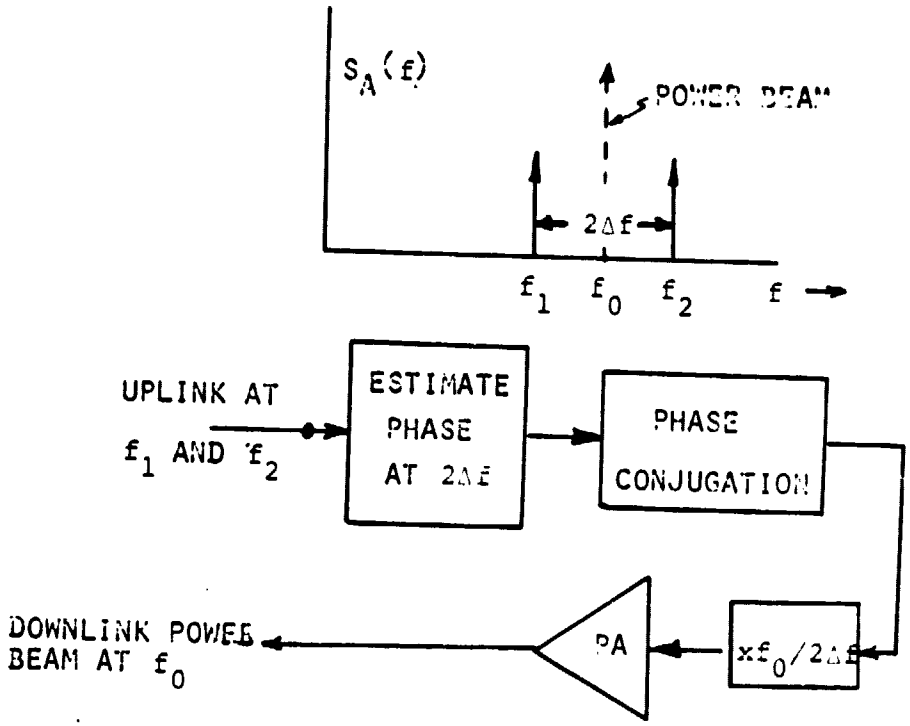

- SUSCEPTIBLE TO INTERFERENCE
- POWER ROBBING
- PHASE ERROR MULTIPLIED BY $f_0/2\Delta f$
- $f_0/2\Delta f$ MUST BE INTEGER

Figure 2.2. SPS Two-Frequency Pilot Signal Design and Retrofire Concept.

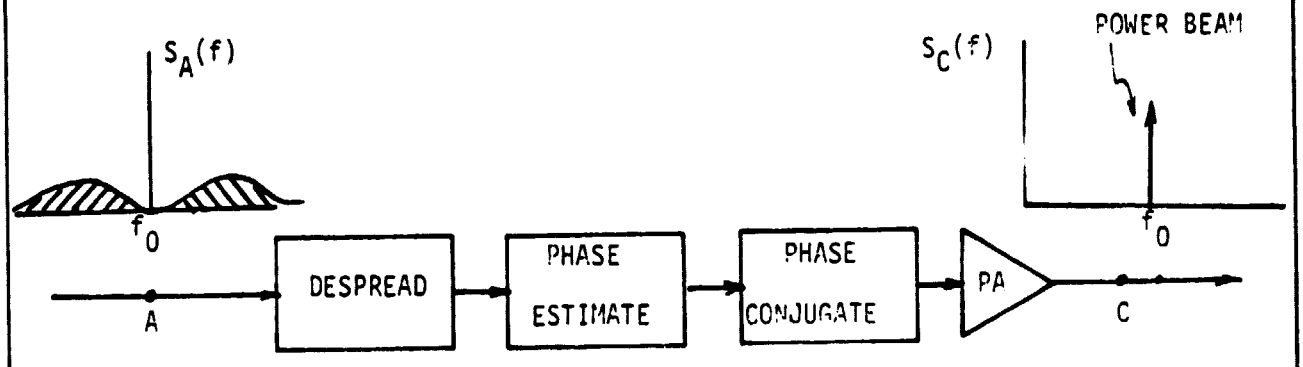

- COMMAND LINK PROVIDED
- SECURITY (AJ) PROVIDED
- BEAM SQUINT ELIMINATED
- PRIVACY (IF NEEDED)
- INTERFERENCE IMMUNITY
- AVOIDS POWER ROBBING
- SPS NETWORKING
- AMBIGUITIES RESOLVABLE
- ISOLATION UP/DOWN LINK

Figure 2.3. SPS Bi-ϕ Coded Pilot Signal and Retrofire Concept.

summarized as NRZ/BPSK/BI-ϕ-DS/CDMA, Ref. 1, i.e., for simplicity the signal is a Bi-ϕ coded tone, see Fig. 2.3.

The math model for the SPS pilot signal $s(t,\varsigma)$ is characterized as the product of three complex random modulations, i.e.,

$$s_u(t,\varsigma) = \mathrm{Re}\{\sqrt{2P_u}\, \underbrace{d(t,\varsigma)}_{①} \underbrace{c(t,\varsigma)}_{②} \underbrace{\exp[j\omega_0 t+\theta(\varsigma)]}_{③}\} \qquad (2.1)$$

① Command Modulation ② Code Modulation ③ Carrier Modulation

Here P_u represents the average transmitted power. In the notation used here, (e.g. $d(t,\varsigma)$), ς simply indicates that the quantity involved should be viewed as being random in some way. A functional diagram indicating the mechanization of the pilot signal transmitter is shown in Fig. 2.4. As illustrated the data clock and code clock are coherent so that the uplink operates in a data privacy format. If the switch at the output of the RF oscillator is moved to the alternate position shown, then the data clock, code clock and carrier are all coherent. This configuration would simplify the implementation of pilot signal receivers located at the SPS; the concern could be transmitter, media and oscillator phase instabilities. The purpose of the spread spectrum (SS) code generator is several fold. First it provides link security, second it provides a multiple access capability for the operation of a network of SPSs, See Fig. 2.5, and third, the anti-jamming protection can be provided if needed. Proper choice of this code modulation will also provide the needed isolation between the uplink and the downlink. The expression for the SPS transmitted signal $s(t,\varsigma)$, indicated in (1.1),

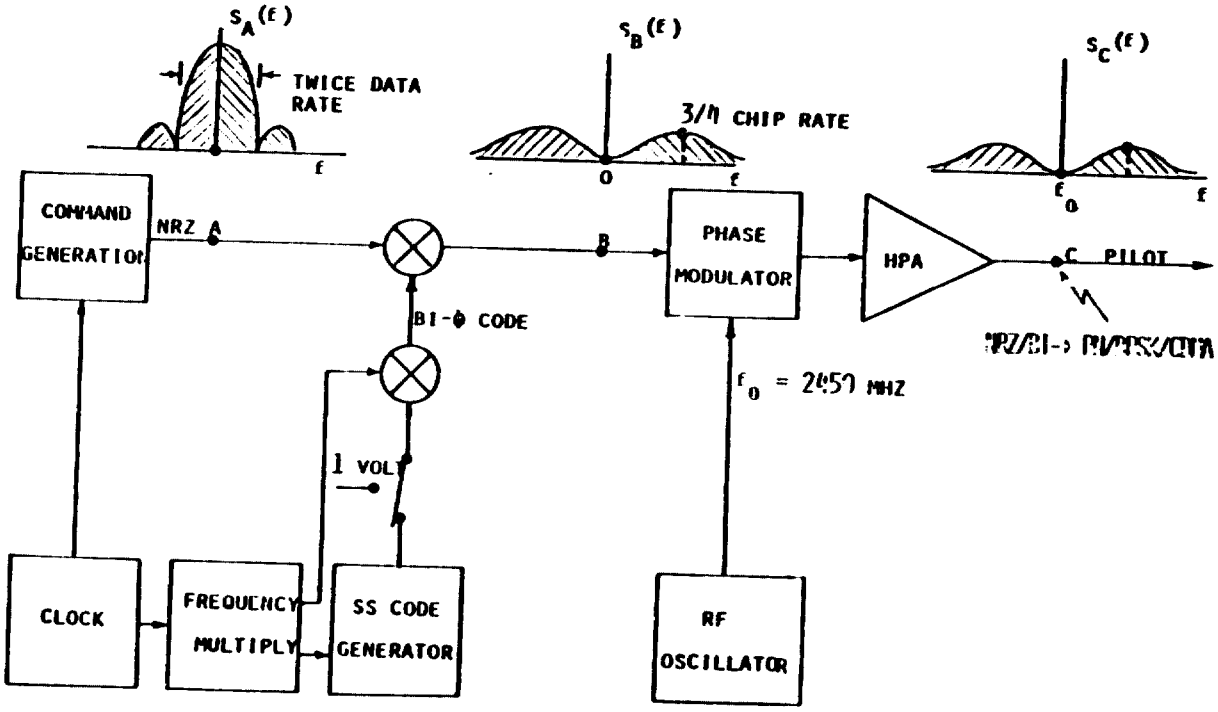

Figure 2.4. Reference System Pilot Signal Transmitter Functional Diagram.

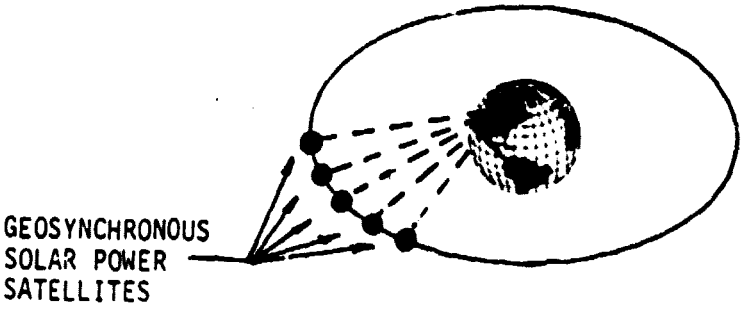

Figure 2.5. SPS Network Scenario.

would be the same even if the uplink signal does not employ the spread spectrum modulation $c(t,\zeta)$, i.e., $c(t,\zeta) = 1$ for all time. We shall refer to the signal $c(t,\zeta)$ as the SPS spread spectrum (SS) code signal. To simplify the demodulation process required in the spacetenna receiver, the SPS spread spectrum codes (multiple access) will product phase modulation of the complex carrier $\exp[j(\omega_0 t+\theta(\zeta))]$, i.e.,

$$|c(t,\zeta)| \equiv 1 \tag{2.2}$$

A mathematical characterization of the code is given by

$$c(t,\zeta) = \sum_n a_n p_c(t-nT_c) \tag{2.3}$$

where $\{a_n\} = 1$ for all n and T_c represents the chip time. Such an expression models Direct Sequence Pseudo-Noise Code modulation [1] and contains no random parameters. The notation $p_c(t)$ is used there to denote a square T_c second pulse of unit amplitude centered at the time origin and hence it is easily seen that the direct sequence (DS) signals satisfies the constant power and constant envelope condition.

The complex sequence $\{a_n\}$ must be agreed upon in advance by the pilot signal transmitter and the SPS pilot signal receiver. In fact, it has a status similar to that of a key used in a cryptographic system. Thus with knowledge of the appropriate sequence, demodulation is possible and without knowledge of that sequence, demodulation is extremely difficult. It is of interest to make the DS code purely random with no mathematical structure; however, all systems have a finite memory constraint and thus all practical DS codes have some periodic structure, i.e., $a_n = a_{n+L}$ for all n where L denotes the period of the SPS code sequence.

2.1 Power Spectrum of the SPS Pilot Signal

The term spread spectrum comes from the fact that the spectral density of the key signal $c(t,\zeta)$ is very much wider than the spectral density of the data modulation $d(t,\zeta)$. This means that the spectral density of the pilot signal $s(t,\zeta)$ is much wider than it would be in the absence of the key $c(t,\zeta)$.

If we now let $z(t,\zeta) = d(t,\zeta)c(t,\zeta)$ then

$$(\sqrt{2P_u})^{-1}s(t,\zeta) = \mathrm{Re}\{z(t,\zeta)\exp[J(\omega_0 t+\theta(\zeta))]\} \qquad (2.4)$$

and under reasonable assumptions about the process $d(t,\zeta)$ and $c(t,\zeta)$ it is easy to show that the power spectral density of the amplitude process $z(t,\zeta)$ is given by

$$S_z(f) = S_d(f) * S_c(f) \qquad (2.5)$$

where $S_d(f)$ and $S_c(f)$ are the power spectral densities of the data modulation and DS code modulation respectively. Here "*" denotes the convolution operation. We now discuss the power spectral densities of the data modulation and DS code modulation respectively. Here "*" denotes the operation convolution. We now discuss the power spectral densities for $S_d(f)$ and $S_c(f)$.

2.2 Power Spectral Density of the Data Source

A convenient representation for the SPS uplink command modulation is

$$d(t,\zeta) = \sum_{n=-\infty}^{\infty} a_n(\zeta)p_d(t-nT_b-\varepsilon) \qquad (2.6)$$

where ε is a random pulse epoch uniformly distributed over the bit duration T_b seconds. Additionally, $\{a_n(\zeta)\}$ is assumed to be a

sequence of independent, equally probable command data bits taking on values plus one or minus one. The uplink command data rate is therefore

$$R_b = \frac{1}{T_b} \text{ bits/sec} \tag{2.7}$$

Using the Wiener-Khintchin theorem, it is easy to show that [7]

$$S_d(f) = T_b \frac{(\sin \pi f T_b)^2}{(\pi f T_b)^2} \tag{2.8}$$

This power spectral density is indicated in Figure 2.6. Notice that the main lobe occupies a bandwidth of approximately $B = 2/T_b$ Hz.

2.3 Power Spectral Density of the DS Code Modulation

If the SPS code modulation $c(t,\varsigma)$ is to be used it should possess the following features:

(1) Wide power spectral density in order to achieve anti-jam (AJ) margins if required.

(2) No line spectrum components to prevent jamming by narrowband interference.

(3) Spike-like autocorrelation function for accurate code synchronization.

(4) Non-predictability for use against intelligent jammers and to maintain complete security and privacy on the uplink modulation.

(5) Low cross-correlations with other possible DS codes to render the multiple access capability required in the SPS network.

(6) Possess spectral characteristics such that the SPS uplink and downlink signals do not lie in the same frequency.

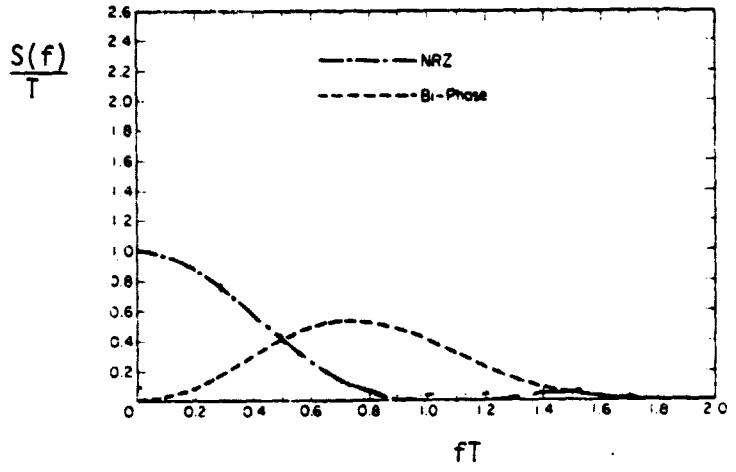

Fig. 2.6. Power Spectral Density of Command and Code Baseband Modulation

(7) Possess spectral characteristics so as to isolate the SPS uplink signal from the downlink SPS high power amplifier output phase noise characteristics.

(8) Possess spectral characteristics such that the effects produced by the ionosphere delay on the upper sideband frequency components averaged with those of the lower sideband frequency components equals the average ionospheric effects produced on the carrier component at frequency f_0 Hz. This minimizes the effect of the varying index of refraction produced in the ionosphere on the downlink power beam.

Particular types of random key sequences most frequency used for constructing DS code keys are the so-called pseudo-noise (PN) sequences possessing a period of 2^L-1 code chips. The discrete periodic correlation function, say $R_c(\tau)$, of a PN sequence $\{a_n\}$ is defined as

$$R_c(\tau) = \sum_{n=1}^{2^L-1} (-1)^{a_n \oplus a_{n-\tau}}$$

where $\oplus$ denotes mod 2 arithmetic in the exponent. Using the properties of PN sequences [7,8] the correlation function becomes

$$R_c(\tau) = \begin{cases} 2^L-1 & \tau = 0 \\ -1 & \tau \neq 0 \end{cases}$$

Since the sum is over one period of a periodic sequence, the result is independent of the starting state of the PN sequence. The code period is actually $(2^N-1)T_c$ seconds in duration.

In order to satisfy requirements (6), (7), and (8) in the above list an additional modulation must be applied to the generated code, viz., that of bi-phase (Bi-ϕ) modulation of the code chip pulses, Ref. 14. This is sometimes referred to as Manchester coding and is most frequently applied to the data source pulses for the purposes of guaranteeing a certain data transition density in the data modulation $d(t,\zeta)$ for purposes of clock recovery. Applying this modulation to each code chip pulse results in the modified code generated output waveform of

$$c(t,\zeta) = \sum_n a_n(\zeta)p_c(t-nT_c)p_m(t-nT_c) \qquad (2.9)$$

where $p_m(t)$ constitutes the Bi-ϕ pulse waveform

$$p_m(t) = u(t) - 2u(t-T_c/2) + u(t-T_c) \qquad (2.10)$$

and $u(t)$ is the unit step waveform. Using the Wiener-Khintchin theorem it is easy to show, under suitable assumptions, that the power spectral density of the Bi-phase code key is [7]

$$S_c(f) = T_c\left[\frac{\sin^4(\pi fT_c/2)}{(\pi fT_c/2)^2}\right] \qquad (2.11)$$

where T_c is the code chip duration. This power density is illustrated in Figure 2.2 for the case where the code processing gain

$$PG = T_b/T_c \qquad (2.12)$$

is much greater than one. Now approximately 90% of the area under the $(\sin x/x)^2$ curve lies in the central peak between the first zeros of the data modulation spectrum and the first side lobes on

both sides contain another 5% of the area. If PG >> 1, then the spectrum of $d(t,\zeta)$ is much narrower than that of $c(t,\zeta)$; hence, $S_d(f)$ behaves approximately like a delta function when convolved with $S_c(f)$. Thus from (2.8), (2.11), and (2.5) we have

$$S_z(f) = T_c \left[\frac{\sin^4(\pi f T_c/2)}{(\pi f T_c/2)^2} \right] \tag{2.13}$$

while the power spectral density of the transmitted SPS pilot signal, as found from (2.4) and (2.13), is

$$S_s(f) = \frac{P_u T_c}{2} \left[\frac{\sin^4[\pi(f-f_0)T_c/2]}{[\pi(f-f_0)T_c/2]^2} + \frac{\sin^4[\pi(f+f_0)T_c/2]}{[\pi(f+f_0)T_c/2]^2} \right] \tag{2.14}$$

This spectral shape is illustrated in Figure 2.7. Notice from (2.14) that as the chip time T_c becomes smaller the spectral null around f_0 broadens and the overall power spectral broadens (features (1) and (2) in Section 2.2) and decreases in amplitude. Thus the code chip duration T_c serves as the parameter which can be used to control the degree of uplink/downlink isolation, see feature (6) in Section 2.2. Variation of T_c can also be used to tradeoff uplink bandwidth requirements with diplexer and other receiver filter requirements.

If the switch appearing at the output of the code generator were switched to the alternate position then the uplink is no longer secure nor would it possess the multiple access capability; however, the pilot signal still retains the required spectral and sideband averaging properties needed to isolate the up and downlink signal. The transmitter output power spectrum for this configuration is sketched in Fig. 2.8 for the case where the transmitted carrier is not modulated with the spread spectrum code. The split-

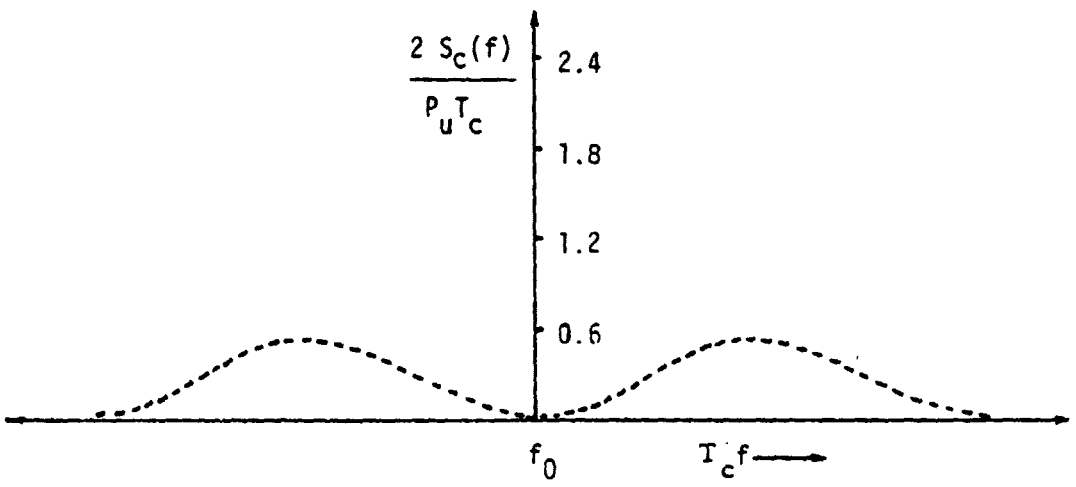

Fig. 2.7. One-Sided Power Spectral Density of the Pilot Signal

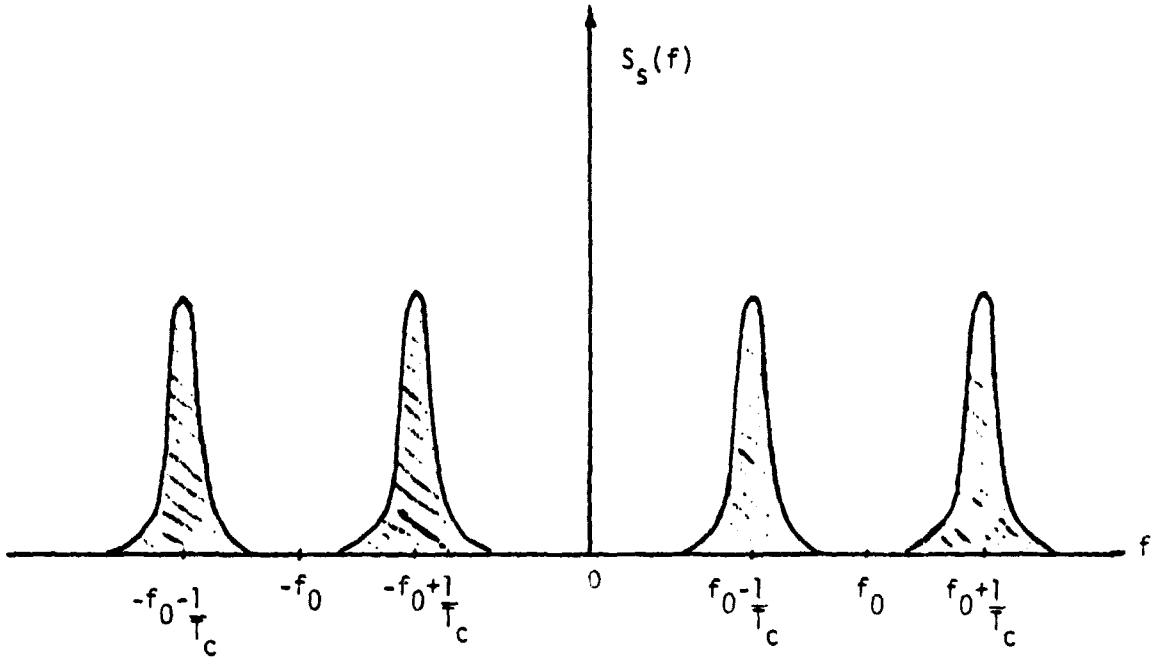

Fig. 2.8. Power Spectrum of the SPS Pilot Signal When the SS Code is Removed. (Manchester Clock Present)

phase format of the PN (pseudo-noise sequence results in a spectral distribution of energy which peaks either side of the carrier at approximately $3/4T_c$, where R is the PN code chip rate. Proper selection of T_c will thus allow RF diplexing at the power transponder receiver to provide isolation between the desired pilot signal and the unwanted power signal which is present at the pilot carrier frequency of 2,450 MHz.

2.4 Code Division Multiple Access (CDMA) Modulation

The spread spectrum code $c(t,\zeta)$ possess an inherent multiple access capability which will be needed in the operation of a network of SPSs. For example, each SPS can be assigned a pseudo-random (PN) code (or one from the so-called Gold family) each of which is orthogonal (or near orthogonal) with respect to each of the other assigned SPS codes. In fact, a single PN code generator design can be used for all SPSs with differing logic combinations used to derive the desired set of orthogonal codes.

CDMA techniques therefore offer an attractive multiple access approach and some anti-jam protection if desired. They require little or no additional equipment complexity in their generation and the bandwidth occupancy requirement is equal to that required for a single SPS. The geometric dispersions of the SPSs should not be overly severe to impose restrictive constraints on CDMA performance.

3.0 REFERENCE SYSTEM SPS PILOT WAVEFORM SUMMARY

The reference system SPS pilot waveform utilizes: (1) NRZ command modulation, (2) split phase, direct sequence pseudo-noise or spread

spectrum modulation, BI-ϕ-DS. This combined data-code modulation is used to bi-phase modulate (BPSK) the RF carrier. Multiple access in the SPS network is to be achieved via code division multiple access techniques (CDMA). Thus the baseline SPS pilot waveform is characterized via four modulation products summarized by the symbols:

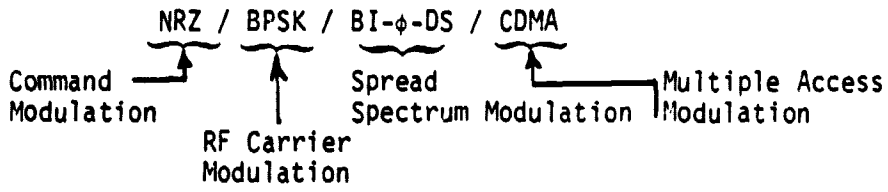

The command data rate, $R_b = 1/T_b$ bits/sec, nor the code chip rate, $R_c = 1/T_c$ chips per second, is not specified in this report; however, LinCom has just developed preliminary chipping rates. The baseline SPS up and downlink signals are designed to occupy a band of frequencies centered at f_0 = 2450 MHz; thus the bandwidth requirement is currently under study at LinCom.

4.0 REFERENCE PHASE CONTROL SYSTEM

As previously noted, the phase control system (see Fig. 1.2) must accomplish three major functions. These include: (1) power beam forming, (2) power beam pointing, and (3) power beam safing. The first involves the generation of a highly directional narrow beam microwave signal. This is accomplished at the spacetenna by coherently phasing each radiating power module (subarray) in the one kilometer diameter spacetenna to produce the desired broadside spacetenna far-field pattern. In addition, in order to improve power transfer efficiency, the power transmitted over the spacetenna "spelling" aperture is tapered by approximately 10 dB from the spacetenna center to its outer edge. This power taper effects the

beam shape by concentrating more of the microwave energy into the center portion of the main beam by widening the main lobe of the antenna pattern. Later on we present some average power patterns resulting from the computer simulation of the phase control system.

Once a coherent beam is achieved, the center of the beam must be precisely pointed at the Earth-based rectenna. Since the mechanical pointing accuracy of the spacetenna and the individual subarrays within the spacetenna is expected to be on the order of one to three minutes of arc, the potential miss distance on the Earth's surface from the geosynchronous orbit would be on the order of 10 to 30 kilometers which would completely miss the 10-kilometer diameter rectenna site. To compensate for this pointing inaccuracy, the phase control system of the SPS must be capable of adjusting the phase of each radiating element power module (subarray) to shift the power beam center without degrading the beam shape.

The final function to be provided by the phase control system is power beam safing. This aspect is characteristic of the phase control process selected since the power beam intensity becomes diffused if phasing of the high power amplifiers is uniformly random. As we shall see complete loss of phasing results in increased sidelobe levels, the resultant increase remains well below the USA and USSR standards. The other aspect of dephasing has to do with power robbing by intentional or unintentional jamming. By utilizing the concept of a retrodirective phased-array incorporating the pilot signal design discussed in the previous section, and perhaps ground sensors for additional safing considerations, the phase control

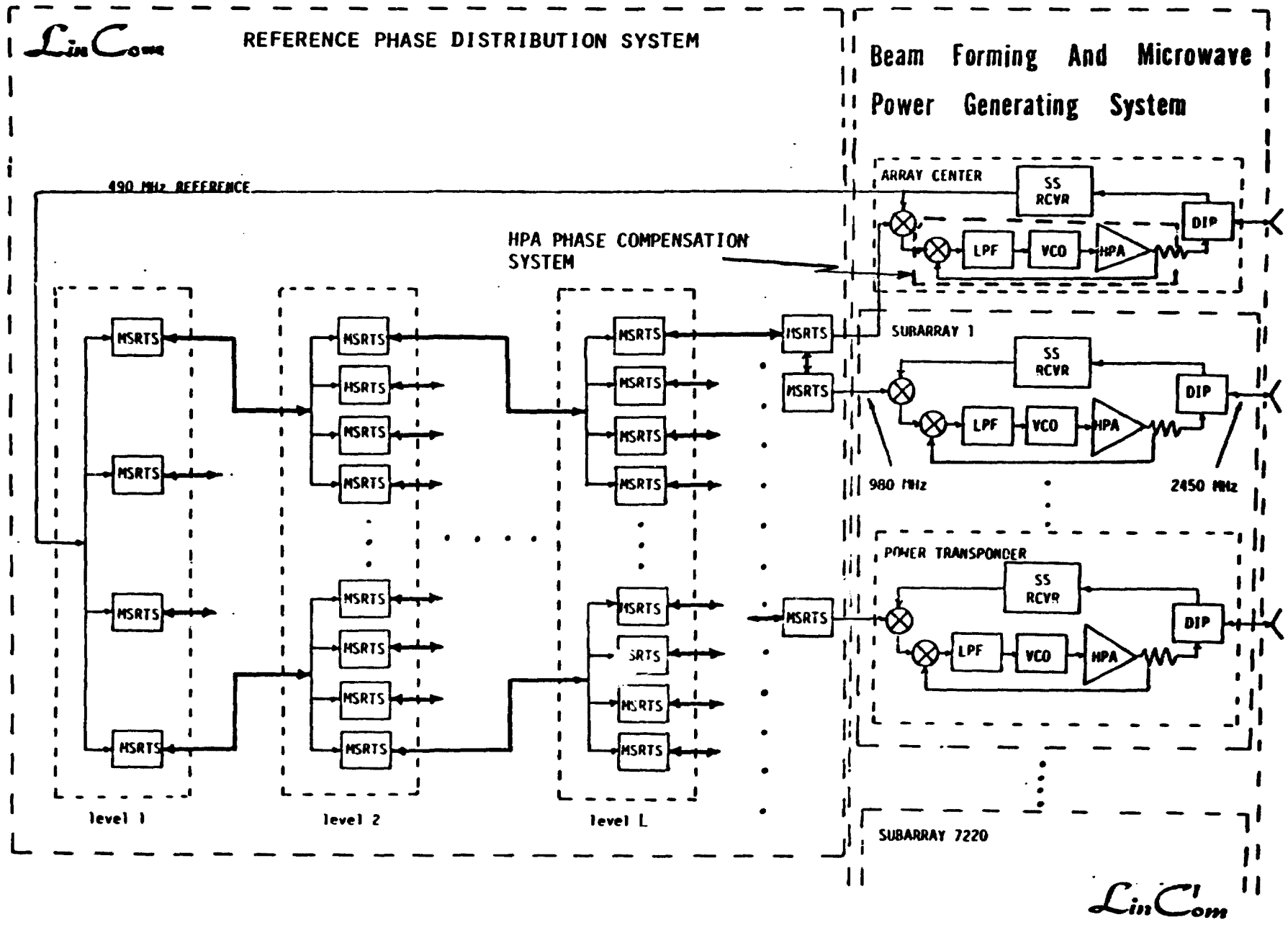

Figure 4.1. Reference Solar Power Satellite Transmission System.

system summarized in the next section meets the general functional requirements.

4.1 Phase Control Via Retrodirectivity

The phase control system concept to be simulated was presented in detail in Ref. 1; its major features will be summarized in this section. Based upon earlier study efforts (Refs. 1,8), a phase control system concept has been proposed which partitions the system into three major levels. Figure 4.1 demonstrates the partitioning and represents an expanded version of Fig. 1.2. The first level in Fig. 4.1 consists of a reference phase distribution system implemented in the form of phase distribution tree structure. The major purpose of the tree structure is to electronically compensate for the phase shift due to the transmission path lengths from the center of the spacetenna to each phase control center (PCC) located in each subarray. The second level is the Beam Steering and Microwave Power Generation System which houses the SPS Power Transponders. This transponder consists of a set of phase conjugation multipliers driven by the reference phase distribution system output and the output of a pilot spread spectrum receiver (SS RCVR) which accepts the received pilot via a diplexer connected to a separate receive horn or the subarray itself. The output of the phase conjugation circuits serve as inputs to the third level of the phase control system. The third level of phase control is associated with maintaining an equal and constant phase shift through the microwave power amplifier devices while minimizing the associated phase noise effects (SPS RFI potential) on the generated power beam. This is accomplished by providing a phase-locked loop around each high power amplifier. The amplifier phase is therefore stabilized by

phase locking to the conjugated phase reference provided at the output of the phase conjugation multipliers.

4.2 Optimal Topological Design of a Reference Phase Distribution Feed Structure

Based upon an earlier LinCom study (Ref. 8) various techniques to the problem of generating, maintaining and distributing a coherent reference signal over a large area were considered. These techniques were modeled and mathematically analyzed with respect to their ability to minimize: phase-error build up, beam diffusion, beam pointing jitter, cable length and maximize power transfer efficiency. To accomplish this distribution a tree structure has been selected: in fact, Appendix II, presents preliminary results related to the optimal design of a survivable feed structure for the reference phase distribution system. As seen from Fig. 4.1, the reference distribution tree consists of three major parameters and one functional building block. The parameters of the tree to be optimized include: (1) the number of levels in the tree, (2) the number of branches per level and (3) the interconnecting cable length. The functional building block consists of the Master Slave Returnable Timing System (MSRTS) units which is briefly discussed in what follows.

4.2.1 The Master Slave Returnable Timing System (MSRTS)

To maintain the precise phase distribution accuracy required over the one kilometer aperture of the SPS, some method of active phase control is necessary. In the present baseline this is accomplished using the MSRTS technique. Figure 4.2 illustrates the functional diagram associated with the MSRTS technique. Appendix III provides a mathematical modeling and analysis which provides insight into the principle of operation of the MSRTS concept. In Fig. 4.2 we see that

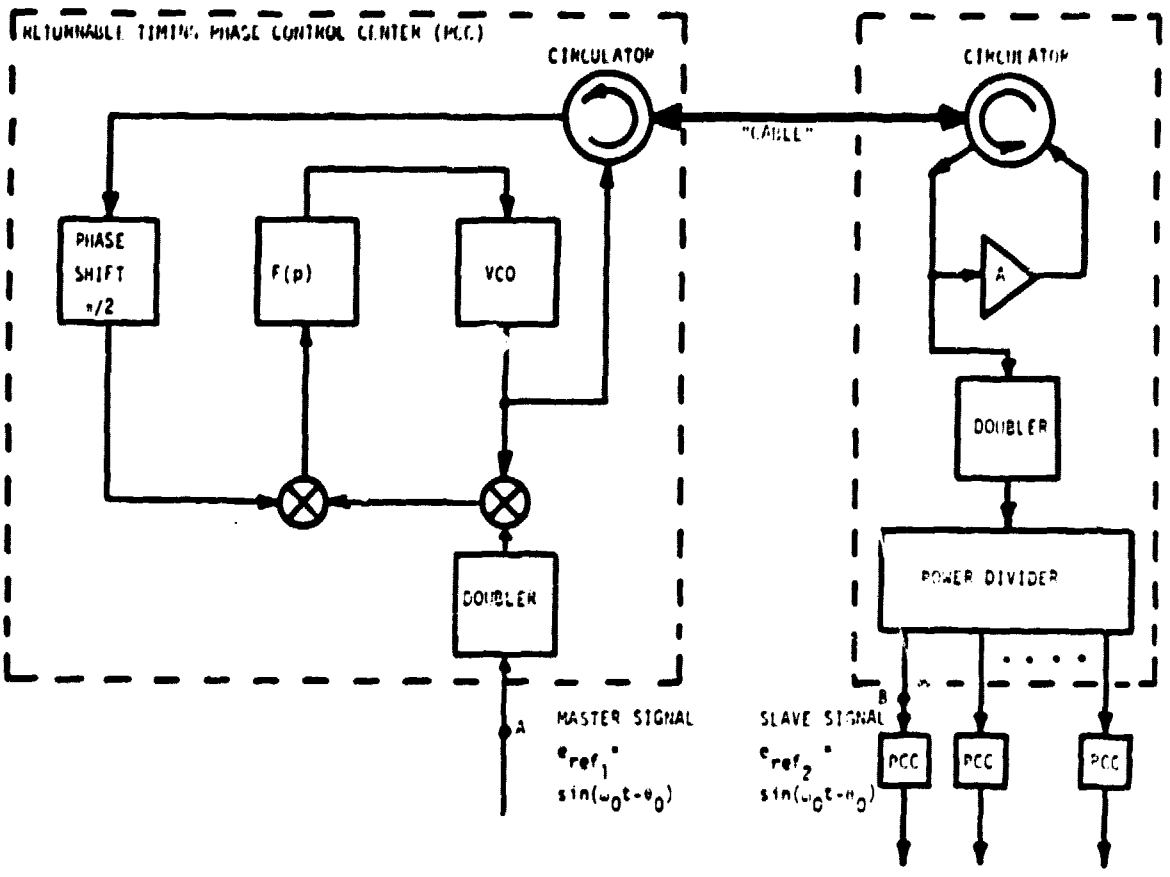

Figure 4.2. Master Slave Returnable Timing System.

a portion of the reference signal at the received location is amplified and coupled back into the phase distribution cable via a circulator. This return signal component is then used for phase locking to the original reference input of the Phase Control Center (PCC). Thus the phase of the VCO in the PCC is advanced by an appropriate amount so that the phae of slave signal $e_2(t)$ equals the phase of the reference signal $e_1(t)$ transmitted via the "cable*," see Appendix II. Since the same frequency is transmitted both directions over the cable, phase error build up due to frequency dispersion on the cable is eliminated. When phase lock is achieved in the PCC, the resultant phase at point B in Fig. 4.2 equals the phase at point A even if the effective cable delay varies. If the connection cable is cut to within plus or minus one-fourth of an integer number of wavelengths at the distribution signal frequency, the phase can be distributed accurately over various lengths of cable without phase ambiguity. For example, for a frequency of 490 MHz, the cable lengths must be cut to within plus or minus fifteen centimeters to avoid ambiguities.

4.2.2 Phase Transfer Between the Phase Control Centers

The MSRTS discussed in the previous section is used as building blocks to transfer the phase of the SS pilot reference receiver output to various points on the spacetenna where phase conjugation can take place. Since each building block in the MSRTS contains a PCC, see Figures 4.1 and 4.2, one must specify the PCC locations and ultimately how the phase conjugator reference signals are to be supplied as inputs to the Power Amplifier Conjugation Electronics which feeds the radiating elements. There are three basic configura-

*By "cable" is meant any suitable propagation medium connecting the two desired points.

tions which use the MSRTS concept to transfer the phase between PCCs. This includes: (1) Series Fed PCCs, (2) Parallel of Tree Fed Pccs, (3) Hybrids of the first two, and (4) Attachment of PA's at each tree level. In what follows we discuss the parallel or tree fed structure which has been chosen for use in the baseline.

4.2.2.1 Tree Structure Used to Transfer Phase Between PCCs

Figure 4.3 illustrates a typical tree structure connecting the PCCs which transfer and maintain the reference signal phase characteristic over the spacetenna aperture. As can be seen from Figure 4.3, the pilot reference signal (R) is transferred to four PCCs appearing at level 1 in the tree. Each PCC in level 1 is connected to n PCCs located at the next level in the hierarchy. Each PCC at this level feeds n PCCs located at the next level in the hierarchy. This process is repeated until the required number of PCCs is fed.

In general, a symmetrical tree is defined by two parameters, viz., the number of levels, say L, and the number, n, of branches per level. For this case there would be generated n^L tree nodes (PCCs). In such a case, the tree structure could be used to provide n^L phase conjugator reference signals. Here the parameter "n" defines the number of output terminals associated with power dividers required in the implementation.

4.2.2.2 Tree Structure Generated Using the MSRTS Configuration

Figure 4.4 illustrates how the phase characteristic (derived in the reference SS receiver) can be transferred using the MSRTS. Here we have selected the MSRTS which uses a single frequency and circulator shown in Figure 4.2. The 490 MHz signal provided by the

TOTAL NUMBER OF PCCs = n^L

n = NUMBER OF BRANCHES PER LEVEL

L = NUMBER OF LEVELS

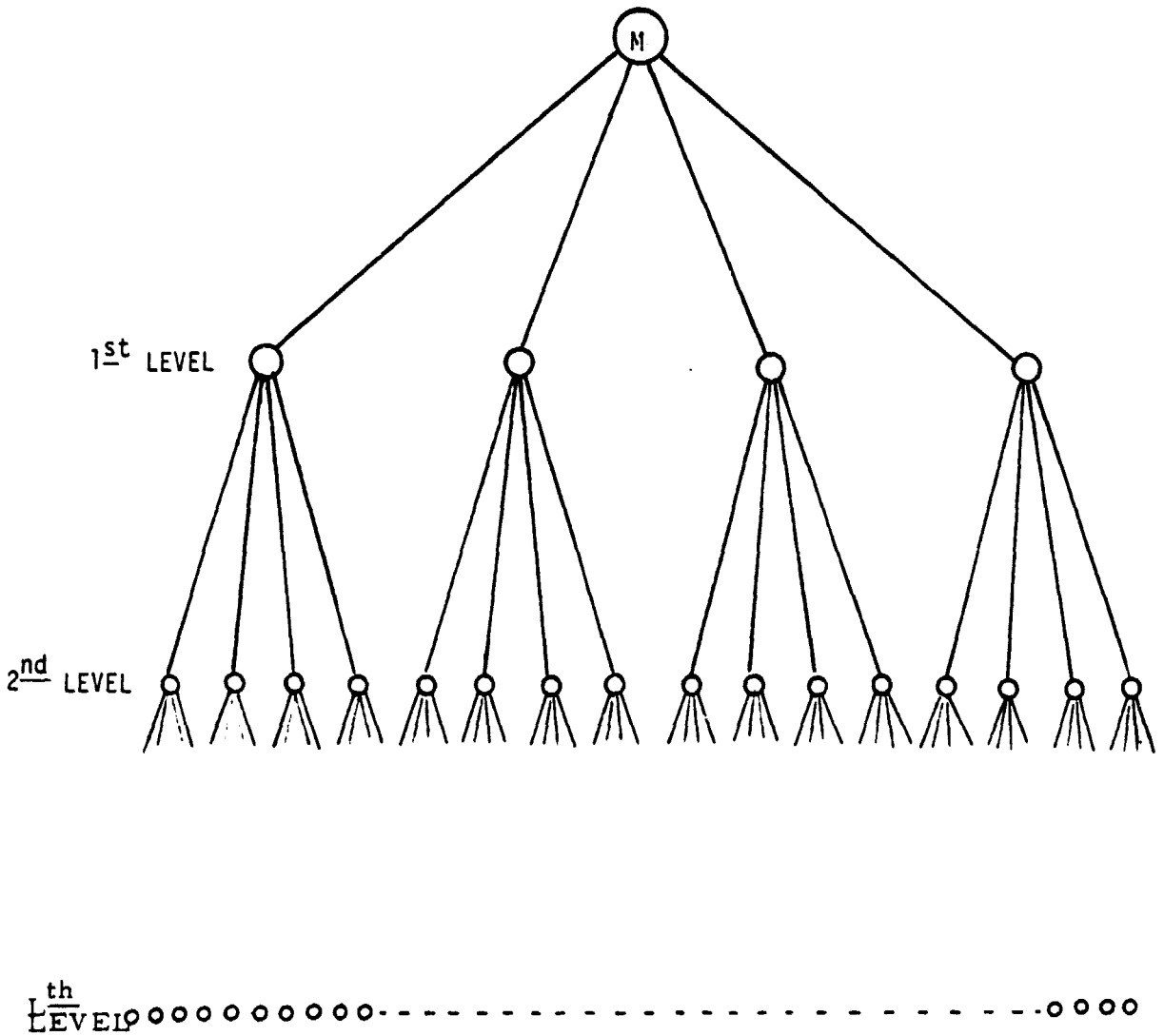

Figure 4.3. Hierarchial Tree Structure.

Costas loop in the reference receiver of Figure 4.1 is frequency multiplied by two and used to drive the PCCs located at the first level in the tree, see Figure 4.4. As seen each MSRTS feeds a power splitter and a times two multiplier at the next tree level. This partitioning continues until the tree structure is completed. At the final stages of the tree the set of phase conjugator signals required for driving the conjugation circuits in Fig. 4.1 can be generated. Since there are 101,552 power amplifiers and 101,552 radiating/receiving elements are specified then the parameters n and L must be selected so as to best "match" these characteristics to the tree. Once this "match" has been determined one must specify the layout on the SPS. Performance tradeoffs between the parameters are presented later on in this report.

4.2.3 The Reference Phase Distribution System Functional Diagram

Figure 4.3 demonstrates the first three levels in the layout of the reference phase distribution system. Here we illustrate reception of the pilot signal at the center of the spacetenna. This signal passes through the diplexer (D) to the reference spread spectrum receiver (R). The SS receiver reproduces the carrier component in the received pilot signal. The frequency of this signal is doubled to produce the 980 MHz reference. The reference is subsequently power divided and supplied to four PCCs via the MSRTS, see Fig. 4.5. The MSRTS process is replicated until the appropriate number of levels in the tree are developed. The outputs of the tree then serve as phase conjugator reference signal needed for beam steering and for stabilization of the high power amplifier phase characteristics by means of a phase-locked loop.

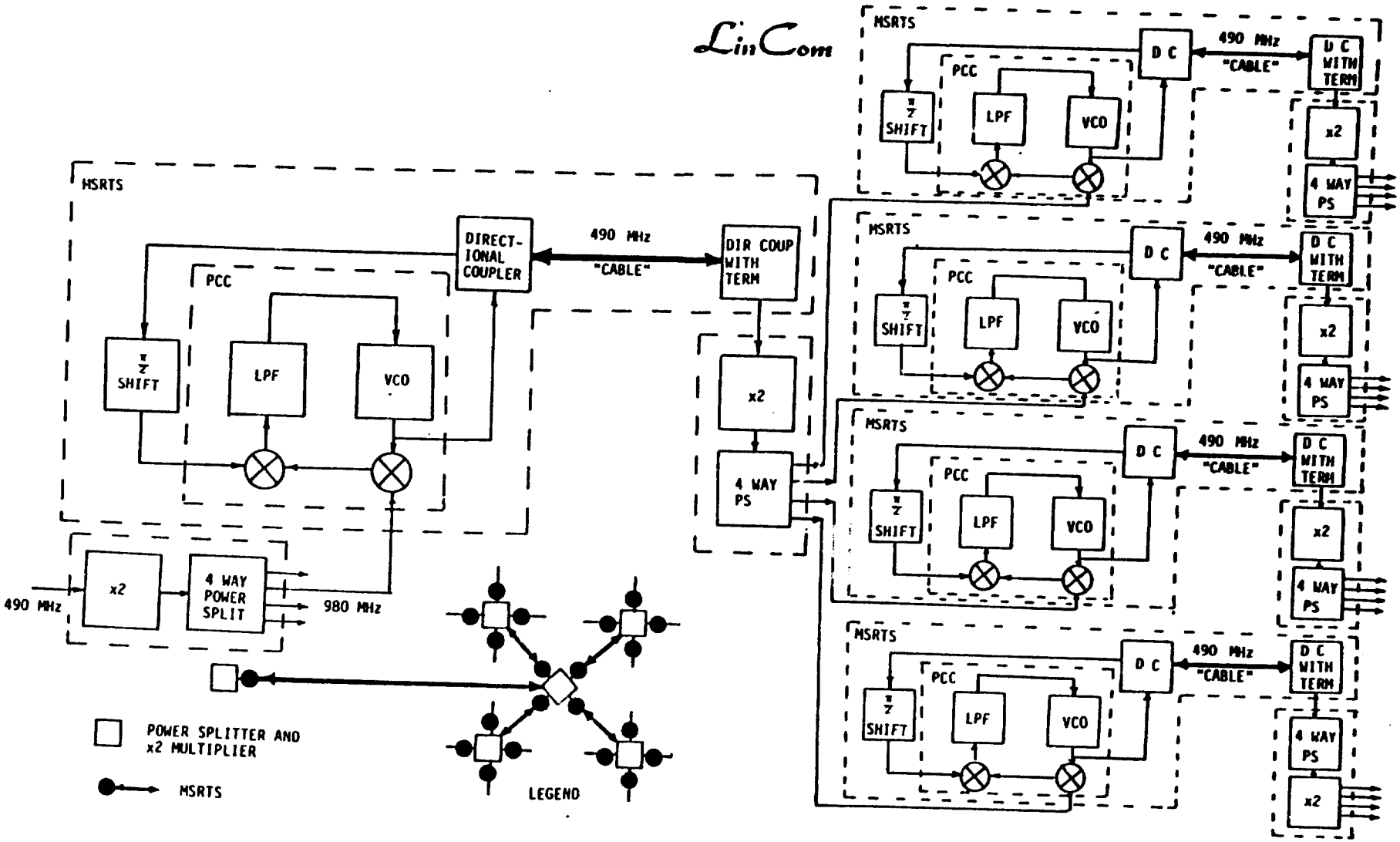

Figure 4.4. Phase Control System Configuration Near Spacetenna Center.

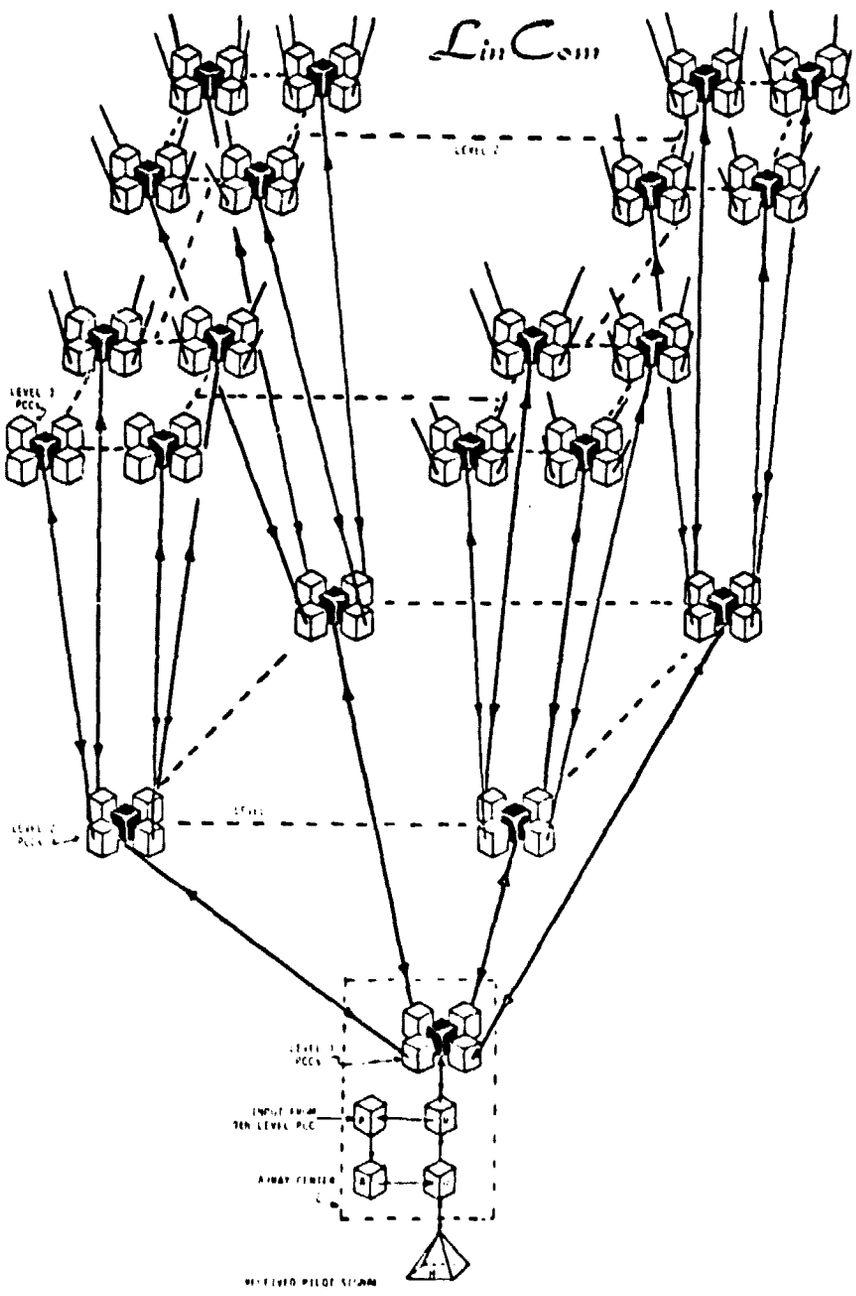

Figure 4.6. Three Levels of the Reference Phase Distribution System Illustrated in all Components.

The number of levels in the tree, L, as well as the number of branches per level, k, represents parameters to be optimized from a far-field performance point of view. As we shall see, the rms pointing error and the main beam gain reduction are affected by these design and layout of the tree structure. Thus the far-field performance for various tree structure designs. The redundancy requirements and possible other mechanical layouts are under investigation to insure that the reference phase distribution network will exhibit high survivability and reliability characteristics, see Appendix I.

5.0 REFERENCE SYSTEM SPS POWER TRANSPONDER

In addition to distributing the constant phase reference signal over the spacetenna as discussed in the last section, a method for recovering the phase of the received pilot signal is required. Figure 5.1 represents the functional diagram of the SPS power transponder. This includes the pilot signal receiver, phase conjugation electronics and the high power amplifier phase control subsystem.

In the mechanization of the SPS power transponders, two receiver "types" will be required; however, most of the hardware will be common between two receivers. One receiver, the Pilot Spread Spectrum Receiver, is located at the center of the spacetenna or the reference subarray. It serves two major functions: (1) Acquires the SS code, the carrier and demodulates the command signal, (2) provides the main input signal to the Reference Phase Distribution System, see Figure 5.1.

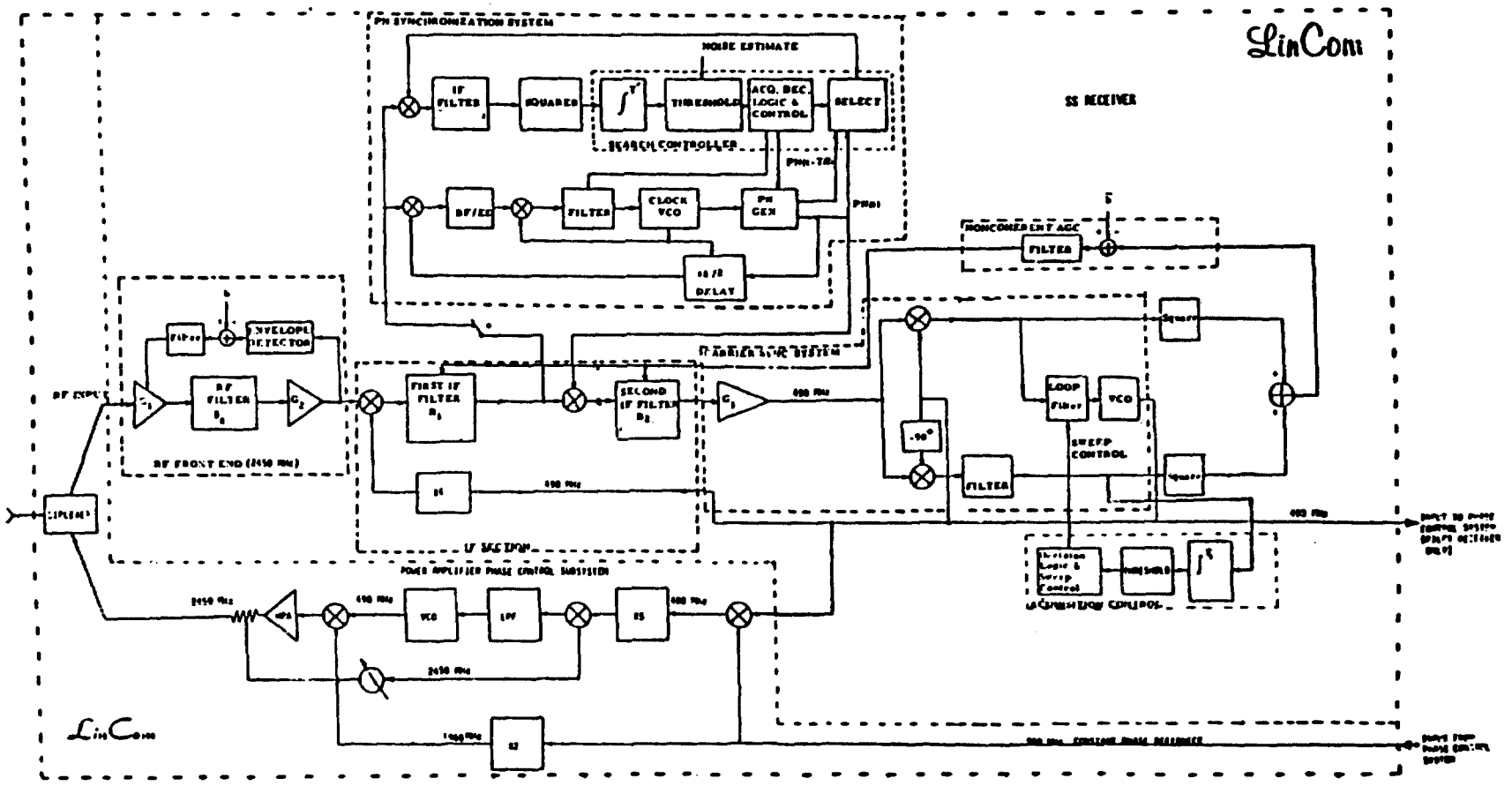

Figure 5.1. Central SPS Power Transponder Located at Spacetenna Center.

The second receiver "type" will be located in the Beam Forming and Microwave Power Generating System, see Figure 5.2. Its main purpose is to phase conjugate the received pilot signal and transpond power via the j-th spacetenna element, j = 1,2,...,101,552. We now discuss the functional diagram indicating the mechanization of the SS power transponder and discuss its operation.

From Fig. 5.1 we note that each SS receiver element must be capable of despreading and demodulating the received pilot signal based upon the gain provided by a single element of the SPS spacetenna. The receiver consists of several major subsystems. These include,(see Fig 5.1 and 5.2): (1) the RF Front End centered at 2450 MHz, (2) The SS Code (PN) Sync Subsystem (PNSS), (3) The AGC Subsystems, (4) The Carrier Sync Subsystem (CSS), (5) The Carrier Lock Detection Subsystem, (6) Carrier Sync Acquisition Subsystem, (7) Symbol Synchronization Subsystem, (8) The Viterbi Decoder (if the uplink employs convolutional coding), and (9) The Ambiguity Resolving Subsystem.

The philosophy used in partitioning the receiver is summarized below:

- Rapid acquisition in the Carrier Sync System
- Despreading Process Independent of Carrier Acquisition, Tracking and the Demodulation Process

The carrier, with nominal frequency of 2450 MHz, is first processed via an RF filter. The bandwidth of this filter must be sufficiently wide to pass the PN chips and the roll-off must be sufficient to meet the desired rejection requirements.

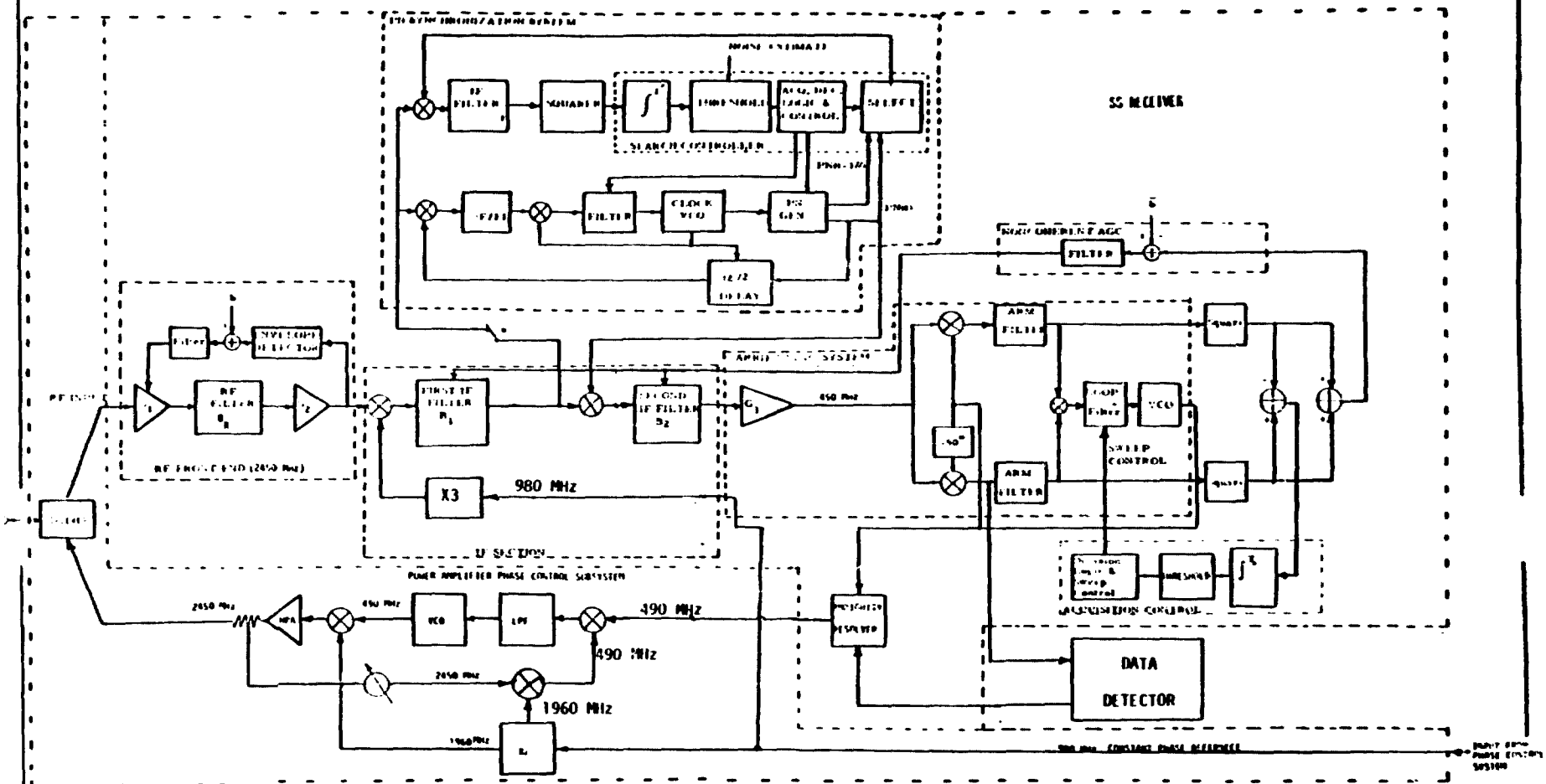

Figure 5.2. SPS Power Transponder

The signal level into the first IF mixer is held constant by the noncoherent AGC . The first LO is selected to run at 1960 MHz; therefore, the first IF frequency, at zero Doppler, is 490 MHz. The output of the first IF mixer is further filtered by the first IF filter whose bandwidth is sufficiently wide to pass the PN chips. The cascaded frequency response of the RF filter and the first IF filter are collectively designed to meet the desired front end rejection requirements. The IF filter output serves as the input to the PN synchronization system. The PN synchronization system (PNSS) of Figure 5.1 incorporates a noncoherent τ-dither PN acquisition and tracking design. The details associated with the particular algorithms selected for the code acquisition will not be discussed here.

The PNSS is configured to give rapid acquisition of the chosen PN code in noise and in the presence of worst-case Doppler frequency shifts. The PNSS also provides highly reliable code loop tracking performance under a chosen minimum input signal-to-noise level without severely degrading the symbol synchronizer, carrier tracking loop and data detection processes.

As shown in Figure 5.1, the output of the second IF mixer (despreader) is processed via two paths. One path is selected for signal demodulation and carrier recovery while the other for PN code acquisition and tracking. Based upon hardware considerations a τ-dither early/late gate code tracking loop has been chosen. This loop generates a code error signal proportional to the phase difference between the locally generated PN code and the received signal code. The code error signal generated at IF is filtered in the bandpass filter/ envelope detector arrangement shown. A loop filter integrates the

code phase error signal and drives a VCO to null the error signal. This assures precise code alignment at the on-time correlator or PN despreading mixer. The PN despreading mixer output contains the data signal without the code and is then processed as a normal BPSK suppressed carrier signal by means of the CSS, see Figure 5.1.

The PNSS noncoherent code acquisition design point signal-to-noise ratio has not been determined; however, a code phase synchronization search would be performed over the entire doppler-expanded code length by stepping the local PN code generator at half-chip intervals, integrating the envelope detector's output for a dwell time of T_d seconds, and then making a sync decision based upon a threshold comparison of this integrated output. The threshold is established by means of a noise estimate produced via an appropriately chosen algorithm. If the decision is not in favor of the particular code phase being searched, the code-tracking loop filter is quenched and the search proceeds to the next code phase position. The PN code acquisition stage of synchronization ends with the two codes (transmitted and local) most probably aligned to within an average of one-quarter of a chip. The second-order early-late, τ-dither, code tracking loop will then pull the system into final alignment.

The code error signal is recovered at the output of the bandpass filter/envelope detector shown in Figure 5.1. The error signal polarity is toggled in synchronism with the early-late switching of the local PN code thereby creating a voltage proportional to the phase difference between the locally generated and received PN waveforms. This voltage is filtered by the loop filter and used to drive the VCO so as to null the error signal. Once the code loop

locks, the loop filter positions the code loop VCO frequency so that the phase error between the local and received codes approach zero.

The arriving NRZ/BPSK/BI-ϕ-DS/CDMA signal is despread prior to filtering by the second IF filter. This gives rise to an ordinary BPSK signal when the τ-dither loop is locked. The output from the second IF filter goes to the output of the carrier recovery circuit. The bandwidth of the second IF filter is chosen to be wide with respect to the data rate. This avoids creating intersymbol interference in the data stream thereby minimizing command data detection errors, avoiding false lock problems in the suppressed carrier tracking loop as well as minimizing phase jitter on the reference signal which drives the Phase Control System.

A Costas (I/Q) loop configuration is chosen for carrier acquisition, tracking and data demodulation. This configuration was chosen because it was determined to be optimum when all considerations, including the ability to square perfectly over temeprature and signal level, are traded against lock detection and synchronization monitoring. We note that the bandwidth of the Costas loop serves to control the time dependent phase jitter fed into the Phase Control System. In order to minimize this effect the bandwidth of the Costas must be as small as oscillator and media instabilities will allow.

Noncoherent AGC is derived from the sum "I" and plus "Q" Channels appearing in the arms of the Costas Loop. In addition, lock detection for the carrier circuit is accomplished by using the difference between the "I" and "Q" channels of the Costas arms.

The noncoherent AGC_2 controls the receiver gain (prior to phase detection) with the signal plus noise level appearing in the outputs of the Costas loop arm. This feature is used to control the loop bandwidth and damping factor during acquisition and tracking. The bandwidth of the arm filters are chosen to minimize the so-called squaring loss and their roll-off characteristics selected to avoid the false lock problem.

The loop filter receives the signals from the phase detector (third multiplier) and supplies an error signal to the VCO which control the local frequency. The loop filter sets the tracking loop bandwidth and damping factor. An AGC voltage, proportional to the incoming signal plus noise power, is low pass filtered and amplified to drive variable gain elements in the IF amplifiers. (These amplifiers are included here in the first and second IF filters for simplicity.) Additional integrate and dump circuits and threshold detector circuits control the sweep and the lock indicator needed for loop supervisory control. It is to be noted that the carrier sweep is not activated until PNSS is synchronized.

The carrier lock detector circuit monitors the integrate and dump voltage formed at the discrete points in time by differencing the squares of the inphase and quadrature arm outputs. The output of the integrate and dump circuit is compared to a fixed threshold level. If the I and D output exceeds the fixed threshold level a preliminary indication of lock is given and the search sweep is disabled. When lock is verified the loop bandwidth could be reduced, if necessary, to further reduce loop jitter. In such a case the loop bandwidth would be optimized for both acquisition and tracking.

Data extraction can be derived in two different ways. The most convenient way is to extract the data from the output of the Q channel and apply the symbol stream to the symbol sync system as shown in Figure 5.1. The symbol synchronizer extracts the NRZ baseband waveform and applies the symbol (soft decision) voltages to the Viterbi decoder (if coding is used) for further processing. The 180 degree phase ambiguity in the Costas loop is of no consequence if a convolutional code (assuming the link is coded for error control) is selected that is not sensitive to code polarity. On the other hand, if a code is selected that is sensitive to code polarity (transparent vs nontransparent code) then the decoder can be used to resolve the 180° ambiguity in the Costas loop. Whether coding is used or not, proper operation of the phase conjugation circuitry cannot be achieved unless this ambiguity is resolved. A method for achieving this is provided in Appendix I.

An alternate approach to extraction of the command data is to use a wideband phase detector and reflect the data to baseband by using the despread signal which appears at the input to the second IF filter. However, the differential phase shift accumulated between the second IF filter input and the input to the wideband phase detector created by the loop must be controlled if this approach is used. It is not recommended here.

The 490 MHz reference appearing at the pilot receiver VCO output, see Figure 5.1, serves as the only input to the Phase Control System. This phase characteristic is then distributed over the aperture of the spacetenna. The output of the Phase Control System consists of 101,552 980 MHz constant phase reference signals which are used to conjugate

the incoming signal and to stabilize the high power amplifier (HPA) outputs. This is acheived by placement of an automatic phase control around each HPA, see Figure 5.1. This will be discussed further later.

Overall transponder performance is affected by various system interactions. These include the AGCs, PNSS, CSS, SSS, and the power power amplifier phase control system. Their performance will not be further discussed here. A time domain simulation of the SPS receiver elements is currently available at LinCom for operation in both the acquisition and tracking mode. This simulation is currently being extended to include other elements of the Power Trandponder, viz., the Phase Control System and the Power Amplifier Phase Control System and associated phase conjugation circuitry. Figure 5.3 provides a summary of the "high level" electronic subsystems required in the implementation of the SPS Reference Phase Distribution System shown in Fig. 4.1.

5.1 Conjugation in Groups of Power Modules

The reference system described above needs a conjugator at each power amplifier and hence needs 101552 conjugators. An alternate way of doing the same thing is to put a single conjugator at the center of constant size subarray (10 mx10 m), conjugate the received pilot phase at that point and then sending this conjugated phase to all the power amplifiers in the subarray via MSRTS. This arrangement simplifies the hardware implementation. If there are no mechanical errors, i.e., jitters due to random errors are negligible then this system works just as well as the baseline but this system is very sensitive to the random errors and tilts of one subarray. This is described in greater detail in Section 10 of this report. Figure 5.4 depicts the system concept and functional diagram which serves to perform the

(1) NUMBER OF SS RECEIVERS	
•COSTAS LOOPS	101,553
•DESPREADERS	101,553
(2) NUMBER OF DIPLEXERS	101,552
(3) NUMBER OF POWER MODULES	101,552
(4) NUMBER OF PHASE CONJUGATOR MULTIPLIERS	101,552
(5) NUMBER OF 4-WAY POWER SPLITTERS	40,960
(6) NUMBER OF MSRTSs	22,000
(7) APPROXIMATE "CABLE LENGTH" REQUIRED*	120 MILES

*SEE FOOTNOTE ON PAGE 34.

Figure 5.3. Summary of the High-Level Electronic Subsystems Required in the Implementation of Phase Distribution System, the Beamforming and Microwave Power Generation System.

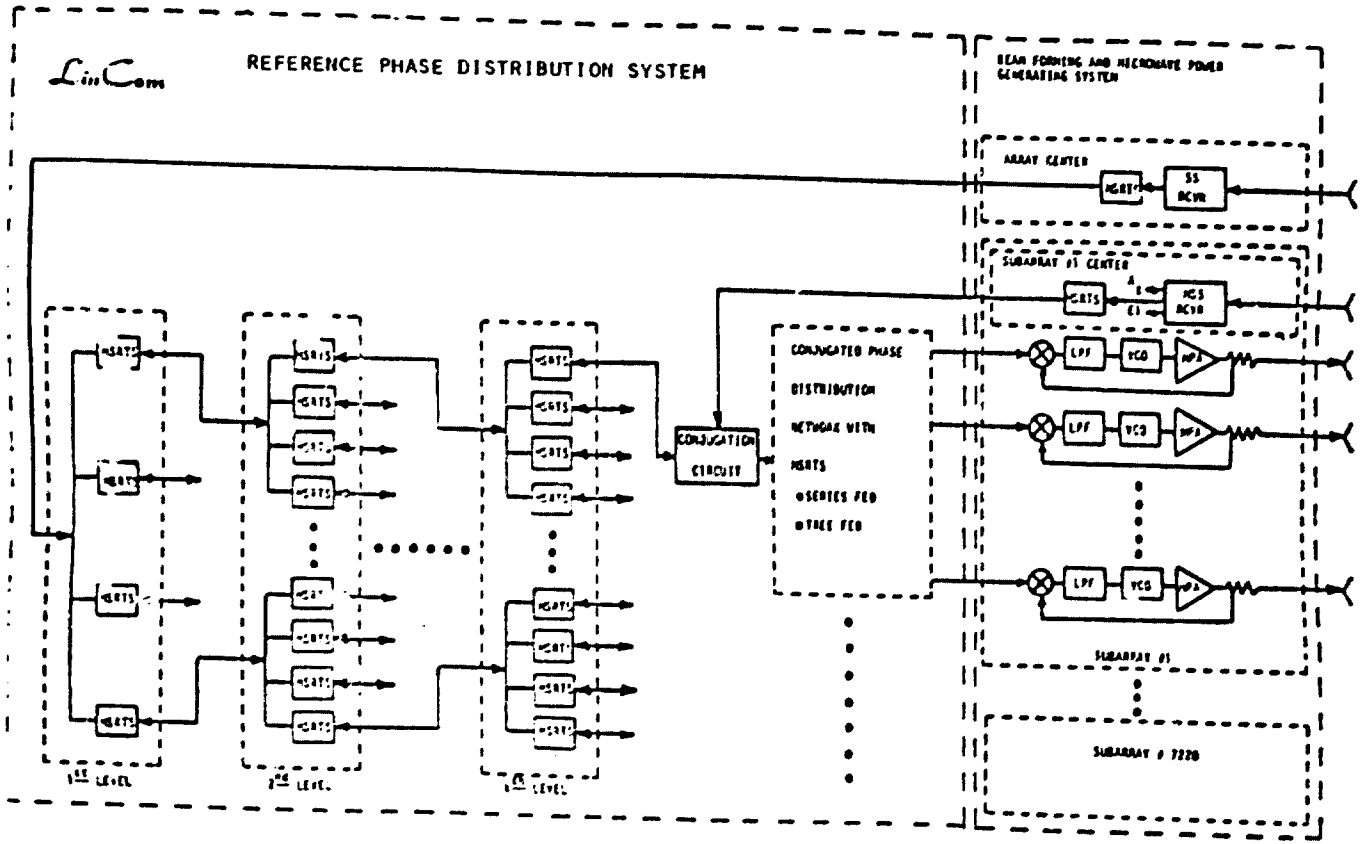

Figure 5.4. Conjugation in Groups of Power Modules.

conjugation at the center of each constant sized subarray. This simplification should be compared with the reference system concept in Fig. 4.1.

6.0 SPS PHASE CONTROL SYSTEM PERFORMANCE EVALUATION VIA THE METHOD OF STATISTICAL ANTENNA THEORY

Because of the complicated nature of the problem of evaluating performance of the SPS phase control system and because of the multiplicity and interaction of the problems as they relate to subsystem interfaces, the methods of analytic and computer simulation (analytical simulation) have been combined to yield performance of the SPS system. Figure 6.1 illustrates the approach which has been taken in order to develop the performance of the phase control system described in the previous sections of this report. As seen from this figure various inputs in the form of requirements, technology status, constraints, and other NASA/DOE contracts have been used in the problem formulation. From this formulation it has been convenient to break the analysis of the phase control system into three major problem areas. Outputs from these analytical efforts have been used to provide direction for development of a computer simulation (called SolarSim) whose major output is the performance of the SPS retrofire phase control system. The SolarSim outputs (to be discussed later) are then used to make System Engineering tradeoffs and perhaps support modifications in the baseline system.

6.1 SPS Phase Control System Performance Measures

In this section of the report we shall discuss the pertinent performance measures associated with evaluating the far-field characteristics and performance of the SPS antenna when its current excitation is driven by random fluctuations arising in the Phase

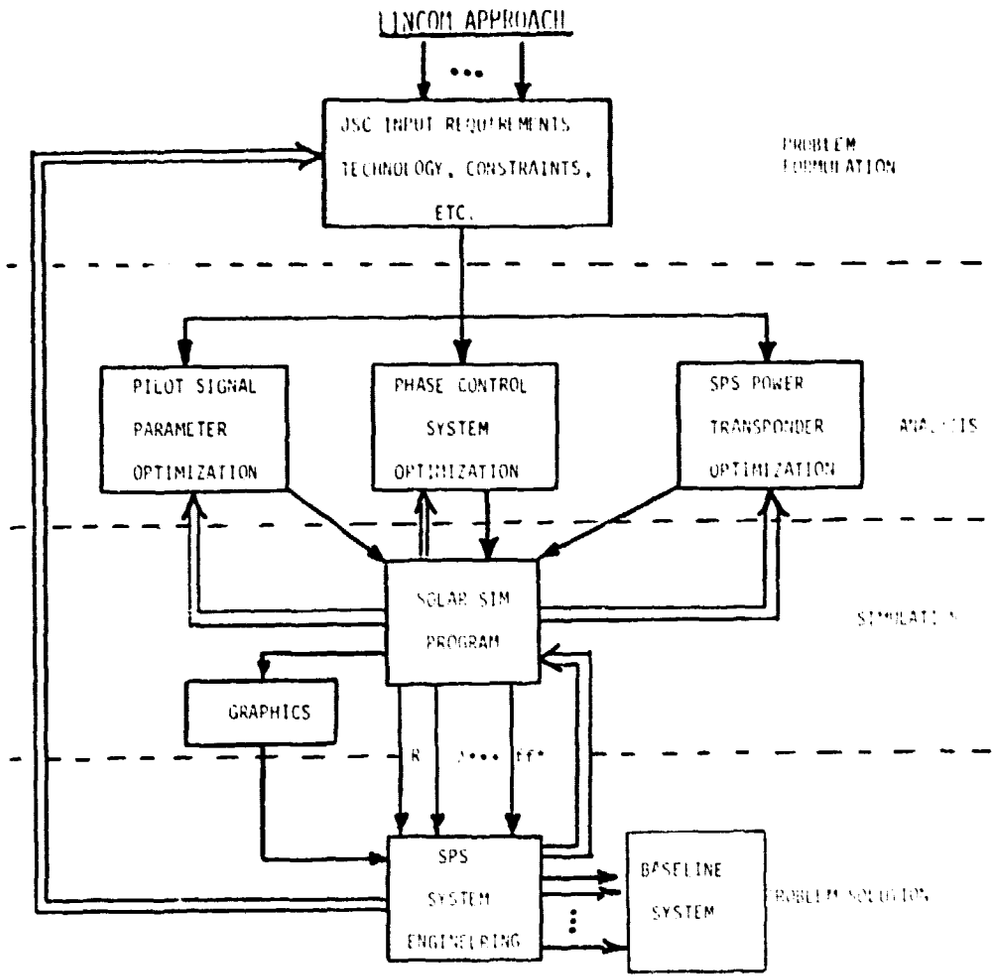

Figure 6.1. Block Diagram of LinCom Approach to SPS Problem.

Control System. The randomness produces errors in the amplitude and phase components of its element feed currents.

The major sources of errors are due to: (1) ionosphere (propagation medium), thermal , PA phase noise, etc., (2) subarray defects and fabrication error, (3) phase error buildup in the phase control system and (4) motion induced irregularities and thermal stresses. In conjugation with the possible error sources responsible for the random fluctuations, one must distinguish between the statistics taken over the ensemble of similar antennas and the statistics in time from an individual SPS antenna.

In the first case, one investigates the scatter of the parameters of antennas of the same type with respect to the ensemble of antennas. Such a scatter may be caused by inaccuracies in the production of the feed structure, by the inhomogeneity of the material of which the SPS antenna is made, etc.

In the second case, one investigates the scatter of parameters of one and the same spacetenna in time. This scatter may be caused by instabilities of the feeder elements of the spacetenna, random changes of the spacetenna surface due to solar pressure or temperature changes, changes in the parameters of the ionosphere through which the pilot signal has propagated, etc.

The problem of analyzing the SPS spacetenna performance as effected by the Phase Control System is divided into two partial problems, viz., the internal and the external problem. The former problem deals with modeling of the statistics of the amplitude and phase excitation currents in accordance with the implementation of the phase control system. This problem is approximation methods, viz., modeling of the actual mechanisms responsible for error

sources. On the other hand, the external problem consists of characterizing the statistics of the far-field using the solution to the internal problem.

Using the statistical characterization of the far-field a number of important characteristics of the transmitted power beam can be studied. They include the spacetenna pattern and such associated parameters as gain, beamwidth, sidelobe level, the phase and polarization patterns. In this study we have concentrated on the evaluation of the mean (average) spacetenna far-field characteristics as a function of the phase amplitude error build-up in the phase control system. The approach has been to develop an analytical simulation capable of predicting the performance of the phase control system. By analytical simulation is meant the combination of using analysis and computer simulation to develop a computer program, called SolarSim, to develop the far-field performance characteristics.

6.1.1 Phase Control System Performance via SolarSim

In order to assess the phase control system performance, it has been necessary to put the multidimensional phase control problem under computer control via the development of the analytical simulation called SolarSim. SolarSim, see Fig. 5.2, is an SPS system engineering computer simulation designed to reduce the entropy of the SPS phase control system problem. A description of the SolarSim software is given in Appendix 1. Because of the inability to implement a full scale model of the SPS phase control system to demonstrate performance, it appears that the only way to obtain performance of a full size system is to simulate a full-scale model. Thus the implementation of a reduced size model can be used to verify its performance concurrently with the program. Once the program is fully developed

- SPS FAR-FIELD PERFORMANCE FOUND VIA SOLARSIM
  - MAGNITUDE OF PROBLEM PROHIBITS HARDWARE DEMONSTRATION
  - SYSTEM ENGINEERING DESIGN AND SPEC TOOL ONLY PROVIDED BY COMPUTER SIMULATION

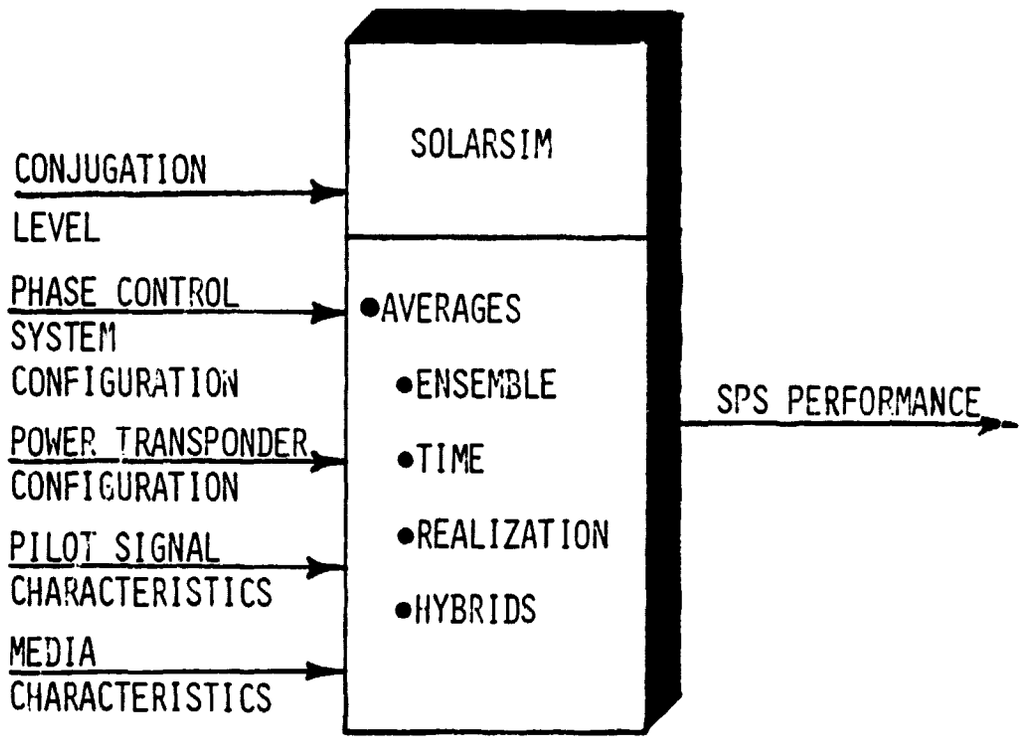

Figure 6.2. SPS System Engineering Computer Simulation.

- INDIVIDUAL REALIZATION
- MEAN FAR-FIELD OR RADIATION PATTERN
- MEAN POWER PATTERN
- MEAN DIRECTIVE GAIN
- MEAN OF MAXIMUM DIRECTIVE GAIN*
- MEAN BEAMWIDTH*
- BEAMWIDTH OF MEAN POWER PATTERN
- MEAN SIDELOBE LEVEL
- SIDELOBES OF MEAN POWER PATTERN
  - SHIFTING OF NULLS
  - VARIATION OF MAXIMUM SIDELOBES

*CURRENTLY NOT AVAILABLE.

Figure 6.3. Far Field Performance Measures.

it can be used to write system specifications, perform design tradeoffs, optimize performance and provide system engineering direction. Figure 6.3 summarizes the far-field performance measures affected by the phase control system performance.

7.0 MATHEMATICAL DEFINITIONS OF THE FAR-FIELD PERFORMANCE MEASURES

In this section we shall define the various performance characterization of the SPS spacetenna in terms of the far-field pattern. The geometric center of the spacetenna coordinates of interest are illustrated in Fig. 7.1. The particular realization of the antenna pattern for a retrodirective antenna can be written as

$$f(\theta,\phi) = \sum_k \sum_\ell I_{k\ell} e^{j\psi_{k\ell}} e^{jK_T[(\sin\theta\cos\phi - \sin\theta_r\cos\phi_r)x_{k\ell} + (\sin\theta\sin\phi - \sin\theta_r\sin\phi_r)y_{k\ell}]} \quad (7.1)$$

With

$$\sin\theta\cos\phi = u \qquad \sin\theta_r\cos\phi_r = u_r$$

$$\sin\theta\sin\phi = v \qquad \sin\theta_r\cos\phi_r = v_r$$

This can be rewritten as

$$f(u,v) = \sum_k \sum_\ell I_{k\ell} e^{j\psi_{k\ell}} e^{jK_T[(u-u_r)x_k + (v-v_r)y_k]} \quad (7.2)$$

where $\psi_{k\ell}$ represents the total phase error build up at the $(k,\ell)\underline{\text{th}}$ radiating element having coordinates (x_k,y_ℓ) and $I_{k\ell}$ is the magnitude of current associated with $(k,\ell)\underline{\text{th}}$ radiating element. This amplitude factor may indeed be random. Notice that in this formula the effect of phasing the tree structure is not explicit hence we have

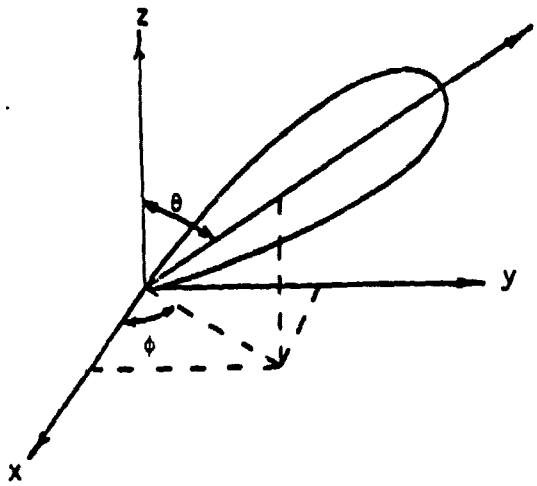

ANALYTICAL SI ULATIC' OF RANDOM
FOWER PATTERN

$$u = \sin\theta \cos\phi$$

$$v = \sin\theta \sin\phi$$

Figure 7.1. Spacetenna Coordinate Geometry.

$$f(u,v) = \sum_{m_1}\sum_{m_2}\cdots\sum_{m_L} I_{m_1\ldots m_L} e^{j\psi_{m_1\ldots m_L}} e^{jK_T[(u-u_r)x_{m_1\ldots m_L}+(v-v_r)y_{m_1\ldots m_L}]} \tag{7.3}$$

where $\psi_{m_1\ldots m_L}$ signifies the random phase generated by the distribution tree by going through the $m_1^{\underline{th}}$ branch at the $i^{\underline{th}}$ level $i = 1,\ldots,L$.

The <u>power pattern</u> is then defined as $f(u,v)f^*(u,v) = |f(u,v)|^2$, i.e.,

$$|f(u,v)|^2 = \sum_{m_1}\cdots\sum_{m_L}\sum_{n_1}\cdots\sum_{n_L} I_{m_1\ldots m_L} I_{n_1\ldots n_L} e^{j(\psi_{m_1\ldots m_L}-\psi_{n_1\ldots n_L})} \cdot e^{jK_T[(u-u_r)(x_{m_1\ldots m_L}-x_{n_1\ldots n_L})+(v-v_r)(y_{m_1}\ldots y_{m_L}-y_{n_1\ldots n_L})]} \tag{7.4}$$

while the <u>average power pattern</u> becomes

$$E|f(u,v)|^2 = \sum_{m_1}\cdots\sum_{n_L}\sum_{n_1}\cdots\sum_{n_L} E[I_{m_1\ldots m_L} I_{n_1\ldots n_L}] \cdot E[e^{j(\psi_{m_1\ldots m_L}-\psi_{n_1\ldots n_L})}] e^{jk_T[(u-u_i)(x_{m_i\ldots m_L}x_{n_1\ldots n_L})} +(v-v_r)(y_{m_1\ldots m_L}y_{n_1\ldots n_L})] \tag{7.5}$$

Here we have assumed that the current amplitudes and phases are independent random processes. The effect of the randomness introduced by the phasing tree is clearly seen in this equation. Note that the difference of phases between elements is more important than the absolute phase of the element. Also note that the currents are only the amplitudes. From this average power pattern one can observe the beamwidth, sidelobe levels, shifting of the nulls, variation of sidelobe levels.

7.1 The Mean Normalized Directive Gain

Let $f(\theta,\phi|\underline{x})$ characterize the far-field at the point (θ,ϕ) given the parameter set $\underline{x}$. With $G_0 \triangleq |f_0|^2$ denoting the boresight gain of the spacetenna in the absence of errors, then the mean normalized directive gain in the direction of the principal maximum is defined by

$$\frac{G}{G_0} \triangleq \frac{E[|f|^2]}{|f_0|^2_{\theta=\phi=0}}$$

7.2 SPS Beamwidth of the Far-Field Pattern

The beamwidth of the mean power pattern is the angle θ at which the value of the power pattern is 3 dB below the maximum value. Figure 7.2 shows the beamwidth of the mean radiation pattern.

7.3 RMS Pointing Error

Equation 7.4 says that in the noise free environment ($\psi_{m_1 \ldots m_L}=0$) the direction of the main beam would be exactly towards the pilot source. But as soon as the phase control system noise is added to the equation, this direction changes. The next direction of the main beam as given by

$$\frac{\partial|f(u,v)|^2}{\partial u} = 0 = \frac{\partial|f(u,v)|^2}{\partial v}$$

This shifting of the main beam is depicted in Fig. 7.3. Using small angle approximation, after differentiating the power pattern with respect to the variables u and v and then setting these to zero gives

$$u-u_r = \frac{B_u C_v - A_v C_u}{A_u A_v - B_u B_v}$$

and

$$v-v_r = \frac{B_v C_u - A_u C_v}{A_u A_v - B_u B_v}$$

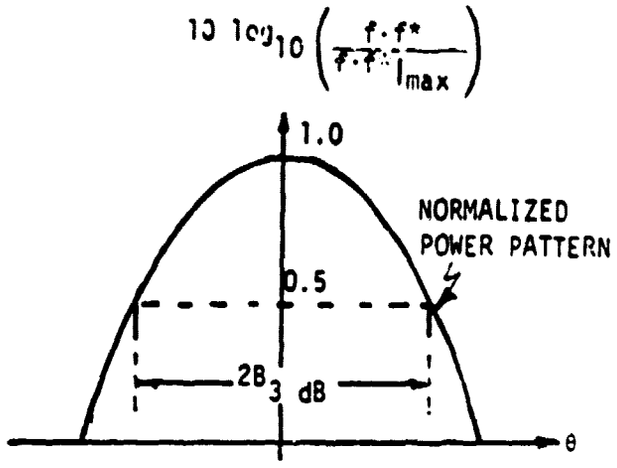

Figure 7.2. Beamwidth of Mean Power Pattern.

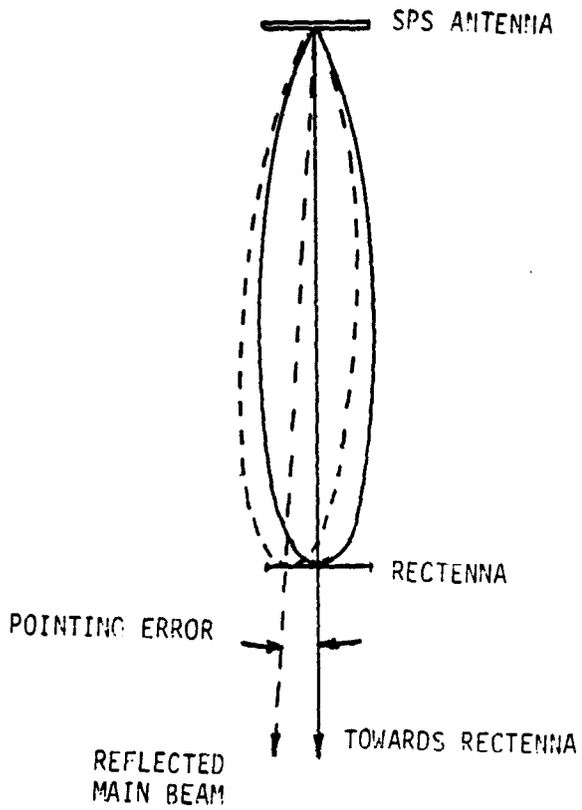

Figure 7.3. Pointing Error Due to Phase Control System Noises.

where

$$A_u = \sum_{m_1}\cdots\sum_{m_L}\sum_{m_1'}\cdots\sum_{m_L'} k_T I_{m_1\ldots m_L} I_{m_1'\ldots m_L'} (x_{m_1\ldots m_L} - x_{m_1'\ldots m_L'})^2$$

$$B_u = \sum_{m_1}\cdots\sum_{m_L}\sum_{m_1'}\cdots\sum_{m_L'} k_T I_{m_1\ldots m_L} I_{m_1'\ldots m_L'} (x_{m_1\ldots m_L} - x_{m_1'\ldots m_L'}) \cdot (y_{m_1\ldots m_L} - y_{m_1'\ldots m_L'})$$

$$C_u = \sum_{m_1}\cdots\sum_{m_L}\sum_{m_1'}\cdots\sum_{m_L'} I_{m_1\ldots m_L} I_{m_1'\ldots m_L'} (x_{m_1\ldots m_L} - x_{m_1'\ldots m_L'}) \cdot (\psi_{m_1\ldots m_L} - \psi_{m_1'\ldots m_L'})$$

A_v, B_v, C_v are the same as A_u, B_u and C_u respectively, but with x and y interchanged. Note that $(u-u_v)$ and $(v-v_r)$ define the pointing error The variance of the pointing error is then given by $E(u-u_r)^2$ and $E(v-v_r)^2$. It should be noted that the mean pointing error becomes zero assuming that the phase errors added by the phasing tree have zero mean values.

8.0 POWER TRANSFER EFFICIENCY

Since the power efficiency is directly related to the beam forming and the beam pointing ability of the antenna, there are two different effects that degrade the power transmission efficiency. They can be generally classified under Random and Nonrandom effects. Figure 8.1 lists various sources of random and nonrandom effects while Figure 8.2 presents typical random effects added by the phase distribution system.

The combination of random effects has a mean value and a variance. The mean value of the random effects combined with the nonrandom effects produces the beam pointing error. In what follows,

- MEAN (NONRANDOM) COMPONENTS
  - PHASE INTRODUCED BY THE UNCOMPENSATED PATH DELAYS IN THE REFERENCE PHASE DISTRIBUTION SYSTEM
  - UNCOMPENSATED BIASES
  - FREQUENCY OFFSETS
- RANDOM COMPONENTS
  - TEMPERATURE INDUCED FLUCTUATIONS IN THE PATH DELAYS
  - FLUCTUATION IN PATH DELAYS INTRODUCED BY THE ANTENNA FLEXING
  - PHASE INSTABILITY ASSOCIATED WITH THE PHASE CONTROL CENTERS IN THE REFERENCE PHASE DISTRIBUTION SYSTEM
  - POWER AMPLIFIER INSTABILITIES
    - AM-AM
    - AM-PM
    - PHASE NOSIE
  - MEDIA INSTABILITIES
  - OSCILLATOR PHASE NOISE

Figure 8.1. Random and Nonrandom Effects Affecting the Power Transfer Efficiency.

- POWER SPLITTERS
- PHASE LOCKED LOOP NETWORK
  - MIXERS
  - PHASE SHIFTER
  - DIRECTIONAL COUPLER
- CABLE
  - DISPERSIVE EFFECTS IN TWO FREQUENCY SYSTEM
- TERMINATION
  - DIRECTIONAL COUPLER
  - TERMINATION
  - X2 MULTIPLIER
  - POWER SPLITTER

Figure 8.2. Power Transfer Efficiency Degrading Effects Added by the Reference Phase Distribution System.

we will investigate the effect of the random and nonrandom parameters described above on the power transfer efficiency.

8.1 SPS Power Transfer Efficiency Formulation

8.1.1 Definition

$$\text{POWER TRANSFER EFFICIENCY} = \frac{\text{Power Received by the 10 km Diameter Rectenna}}{\text{Total Power Radiated by the Spacetenna}} \qquad (8.1)$$

Figure 8.3 makes the idea clear. The power transfer efficiency can be redefined as

$$\text{POWER TRANSFER EFFICIENCY} = \frac{\text{Power Output at Terminals A \& B}}{\text{Power Output at Terminals C \& D}} \qquad (8.2)$$

This definition is convenient because the multiplying constants due to the propagation through the medium cancel out from the numerator and denominator. The computer program uses this efficiency definition. It may be noticed that the power received by the rectenna as well as the total power radiated by the spacetenna are functions of several parameters such as the spacetenna mechanical pointing error, jitters on the pointing error, jitters on locations of the radiating elements, feed current and phase jitters, to name a few.

8.1.2 Computation of Efficiency

Computation of total radiated power and the power received by the rectenna is done by integrating the averaged power pattern of the spacetenna over the appropriate regions.

$$\text{TOTAL RADIATED POWER} = \iint_H (\text{averaged power pattern}) \sin\theta d\theta d\phi$$

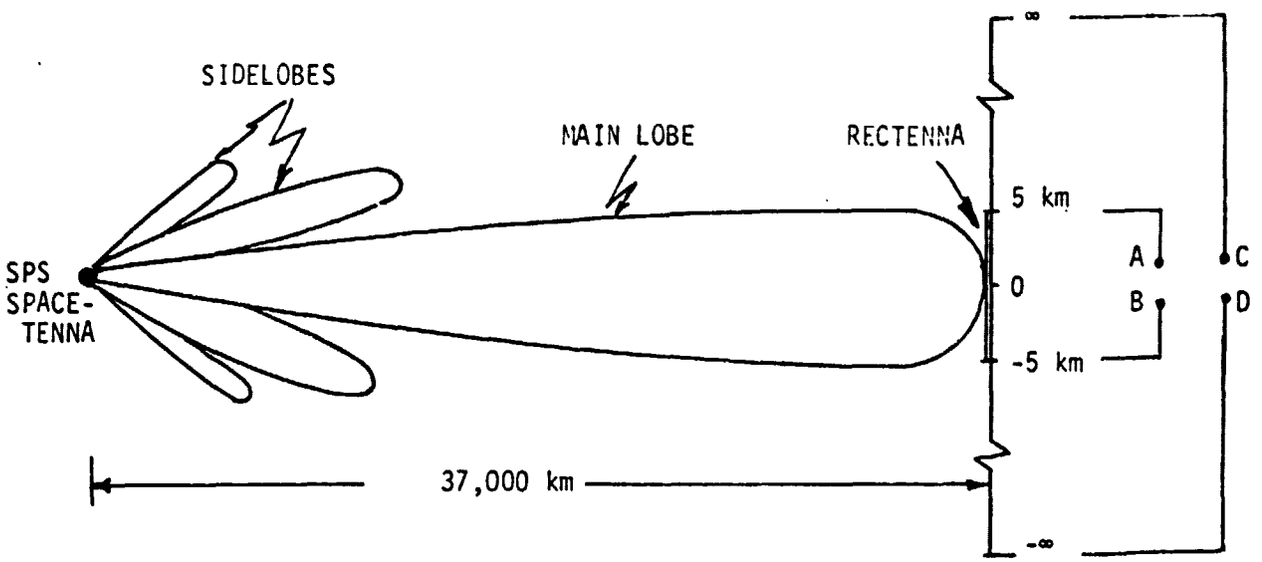

Figure 8.3. Geometry of the Power Pattern.

where the averaged power pattern is obtained from the spacetenna configuration and the feed currents, and H is the hemisphere [$\theta = (0,\pi/2)$ and $\phi = (0,2\pi)$].

The actual radiating elements are the slots cut in the waveguides (slots are separated from each other by a distance of $\lambda/2$, where λ is the wavelength of the waves in the waveguide). The pattern multiplication principle tells us that the radiation pattern of spacetenna is the multiplication of the element pattern of the radiating elements and the array factor (based on the location of the radiating slots) of the antenna. Array factor of the antenna remains the same regardless of the nature of the radiating elements. The array factor of the spacetenna has a very highly peaked mainlobe having a 3 dB beamwidth of a few tenths of a minute of arc which is comparable to the angle subtended by the rectenna at the spacetenna center. The element factor of the slot is so flat around the boresight for several minutes of arc that the region of interest (the 3 dB beamwidth region) this factor could be approximated by a constant. Hence the radiation pattern of the spacetenna in the region of interest, could be approximated by considering isotropically radiating elements instead of the slots. The spacetenna power pattern using the above approximation has two main parts comprising it. One part depends on the direction (θ,ϕ) which will be called the anisotropic term and the other part independent of (θ,ϕ) will be termed the isotropic part, i.e.,

$$\text{Averaged Power Pattern} \triangleq E(f \cdot f^*) = \text{Anisotropic Term} + \text{Isotropic Term}$$

The spacetenna averaged power pattern takes into account all the

system imperfections in the form of jitters. The isotropic term is a function of independent phase disturbances at the slot level. It should be noted that the isotropic term carries into existance only if the phase disturbances at the slot level are statistically independent, e.g. the location jitter on the radiating slots this does not include, for example, the phase disturbance added by the phase distribution system because all the slots in the subarray are affected by the same phase disturbance. One more fact may be pointed out that if the slot element pattern is used in the computation, the only change is that the isotropic term becomes directional due to the element pattern and the total power due to this term reduces by the gain factor (of the slot) from the total power radiated by the isotropic term. Here we point out that

$$\text{THE TOTAL RADIATED POWER} = \iint_H (\text{anisotropic term}) \sin\theta d\theta d\phi + \iint_H (\text{iostropic term}) \sin\theta d\theta d\phi \qquad (8.4)$$

Figure 8.4 shows that the isotropic term is independent of (θ,ϕ), the direction (that is the reason it is called isotropic). Hence

$$\text{TOTAL RADIATED POWER} = \iint_H (\text{anisotropic term}) \sin\theta d\theta d\phi + (\text{isotropic term}) \underbrace{\iint_H \sin\theta d\theta d\phi}_{\text{Constant}} \qquad (8.5)$$

Similarly,

$$\text{RECEIVED POWER} = \iint_{\theta,\phi\epsilon R} (\text{anisotropic term}) \sin\theta d\theta d\phi + (\text{iostropic term}) \iint_{\theta,\phi\epsilon R} \sin\theta d\theta d\phi \qquad (8.6)$$

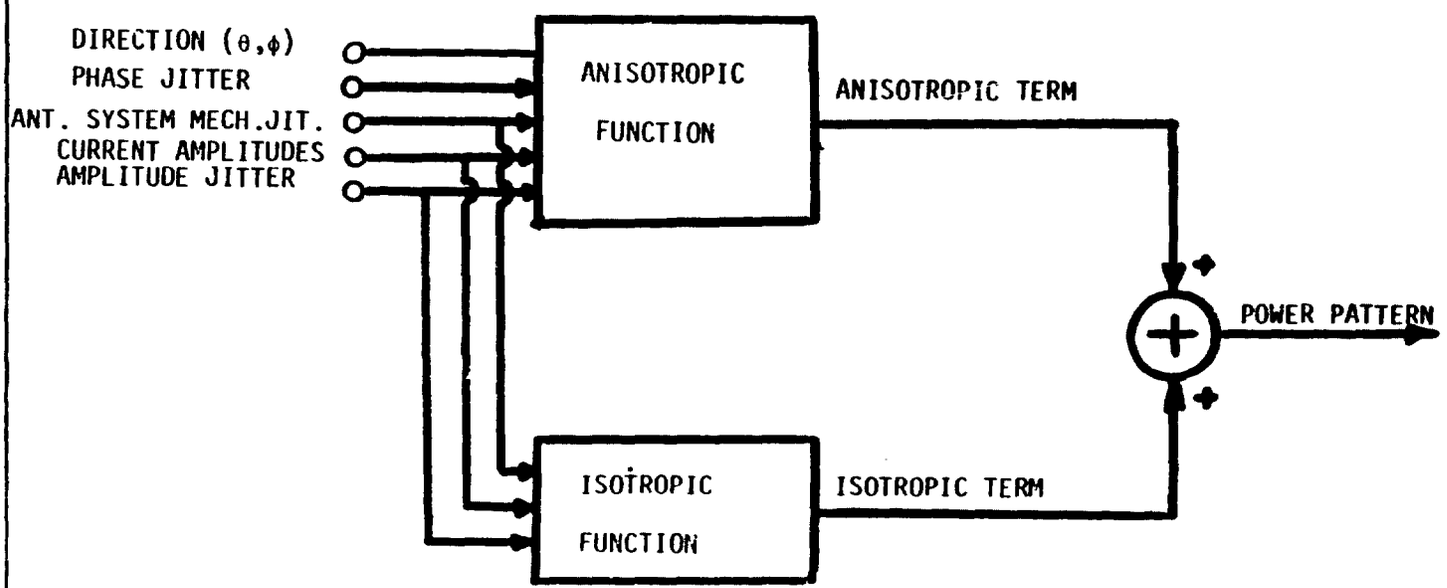

Figure 8.4. Components of the Power Pattern Due to Dipoles.

where R is the region of the rectenna.

Numerical results pertaining to efficiency computation are given in Section 10.3.

9.0 MODELING OF THE PHASE ERROR BUILD UP IN THE DISTRIBUTION OF PHASE BY THE TREE STRUCTURE

The practical implementation of a retrofire array based on the phase conjugation principle requires the existence of a reference carrier at twice the frequency and constant phase at every phase conjugation circuit. The phase of this reference carrier must be exactly the same at every phase conjugation circuit; thus, the differential phase between the reference available at any two phase conjugation circuits is ideally zero. The distribution of this phase is a problem of considerable practical interest. The topic of this section is the modeling of errors in the distribution of this reference by the tree structure.

9.1 Tree Structure for the Distribution of the Reference Phase

As previously noted, the tree structure is a method of providing a constant reference phase to several physically remote points in space. This distribution is done in parallel; that is, several oscillators are "locked" simultaneously to one central reference oscillator. These remotely located oscillators serve as local reference oscillators to the oscillators located in their neighborhood. These new local references may now distribute the phase to another layer of "local" references. This process continues until it is possible to accurately distribute the phase to several phase conjugation circuits. This tree structure is illustrated in Fig. 9.1. (The single frequency method was drawn since it's simpler and the principle is the same.) A multiplied version of the reference drives four (in this case) PLL assemblies that are ultimately connected to

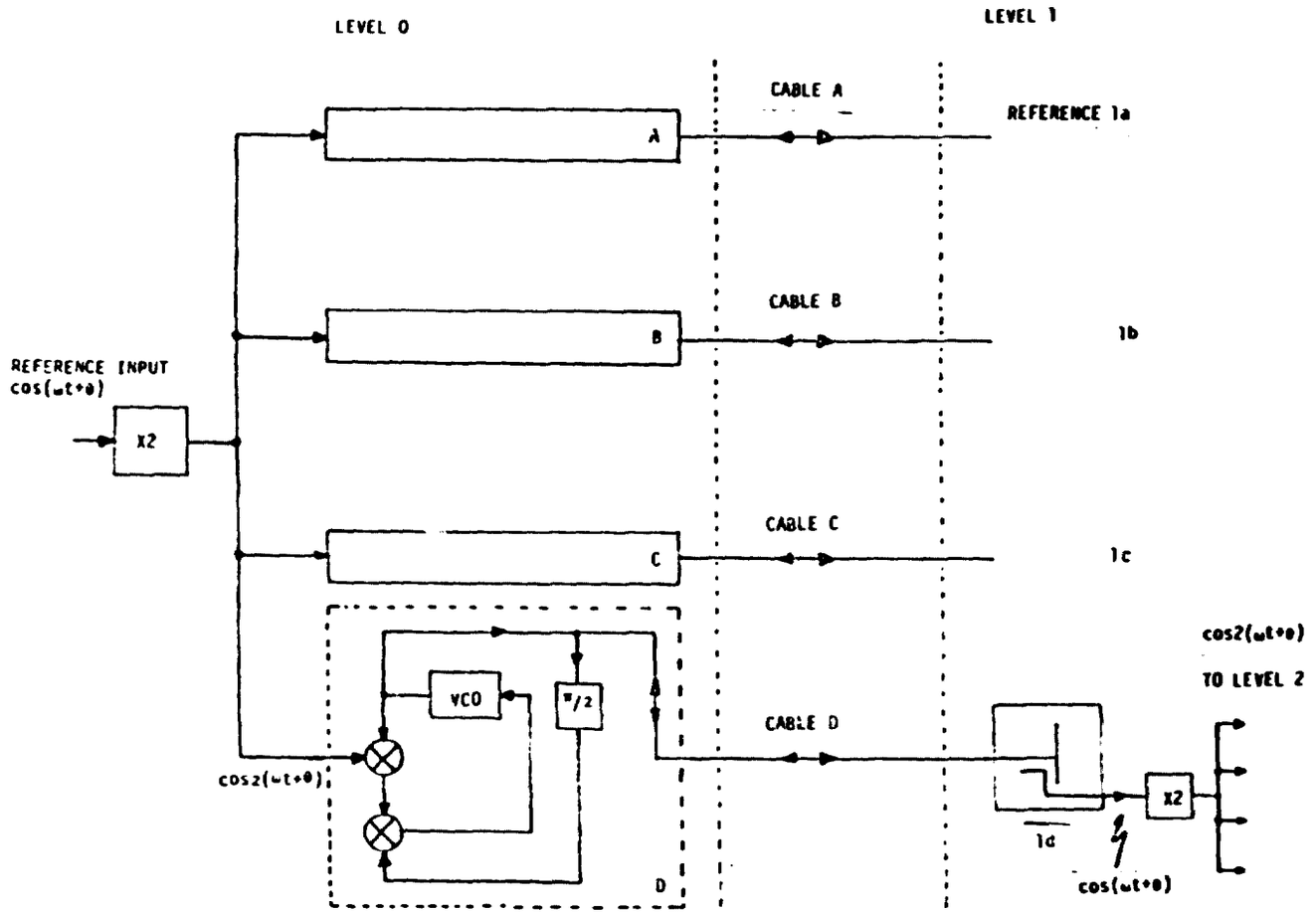

Figure 9.1. Tree Phase Distribution Network.

the cables. The other end of each cable is terminated in a short circuit or similar connection so that the signal transmitted down the cable is reflected back to the driven end of the cable. A portion of the incident signal is removed by the directional coupler and used as the reference for the next level in the tree. This circuit is a remarkably straightforward solution to a complicated problem. It may be readily verified that the reference available at each side 1a-1d is exactly equal to $\cos(\omega t+\theta)$, the input reference phase at level 0 for an ideal implementation. Departures of this model from ideal are the topic of the remainder of this section.

Keeping in mind that the purpose of the phase distribution network is to provide the same reference at all phase conjugation circuits then it is clear that the phase at references 1a through 1d must all be the same. Any variations at this level cannot be removed by hardware at lower levels. First consider the transmission of the reference signal at the input of the X2 multiplier at level 0 through to the reference regenerated at location 1d. The signal is injected into the multiplier and then distributed by a power splitter (4-way for this example) and injected into the PLL network. The PLL network generates a signal with the same frequency as the reference. The phase of this signal is equal to the reference phase minus the amount of phase shift that is cortributed by the cable. Finally, the signal passes down the cable and is removed by the directional coupler. Since the hardware is designed to subtract out the phase effects in the cable only the hardware will contribute some phase shifts. These phase shifts are such that the references generated at level 1 outputs 1a-1d will differ from the reference phase injected at level 0.

The points where phase shifts occur are at the multiplier, the four way power splitter, the PLL network (including the directional couplers, etc. that allow the two signals propagating in different directions to coexist on the cable), the reflective termination, and the directional coupler at the end of the cable that removes the desired signal reference at ld. For example, mismatches in the terminating impedances in the power splitter will cause undesired phase shifts, and nonideal termination of the cable will result in an additional (undesired) phase shift of the signal returned to the PLL network. Each of these phase errors is a static error (neglecting thermal effects) and is set for all time.

These static phase errors result in level 1 references with phases that differ from the reference injected at level 0. Since these phases are statistical in nature it is desirable to characterize them. Consider as an example the four way power splitter. Suppose there exists an ensemble of these four way power splitters. Each power splitter will have a specific phase shift between the input port and each output port. Given a specific output port then there is a certain mean value (averaged over the ensemble) of the phase shift between the input port and the chosen output port. In addition there is a variance associated with this mean. Now there is the possibility that the mean value (and associated variance) between the input and one of the other remaining output ports is some other value. This can be carried out for all the ports. The net result is summarized in Fig. 9.2. This is an extremely complicated model for a power splitter. The following basic symmetry assumption will now be used. If the power splitter is a symmetric design that there is no a priori reason to suspect that

$m_i \neq m_j$. Furthermore, the variances should all be equal. This is probably a valid assumption since the ideal power splitter has zero relative phase shifts between the output ports; thus any design that tends to favor a static relative phase shift between the output ports is a poor design. Thus the final model for a power splitter is to assume that the static phase shift between the input and any particular output port is a random variable drawn from some distribution with a certain mean and variance. This final model is illustrated in Fig. 9.3.

This modeling philosophy can be carried through to the rest of the circuitry. For example now consider the PLL networks, cable and termination. The mixers, phase shifters, power splitters and directional couplers will all contribute some phase errors. The net result is the phase of the recovered reference at a particular level 1 node, say 1d, will be different than the input phase at level 0. Now it may be assumed that the relative phase shift between the input to the PLL network and the recovered reference at a particular node is drawn from a particular distribution with a specific nonzero mean and specific variance. This means that the mean value does not change from network to network!

There are several final notes. First, it has been assumed that the hardware is an ensemble with an associated ensemble mean and variance. This, of course, implies zero average static phase shift between the references recovered at level 1. There may exist an average phase shift between the reference at level 0 and all the recovered references at level 1. Second, since any overall phase shift between the reference at level 0 and all the phase conjugation circuits will not squint the beam or produce any other deleterious effects, it may

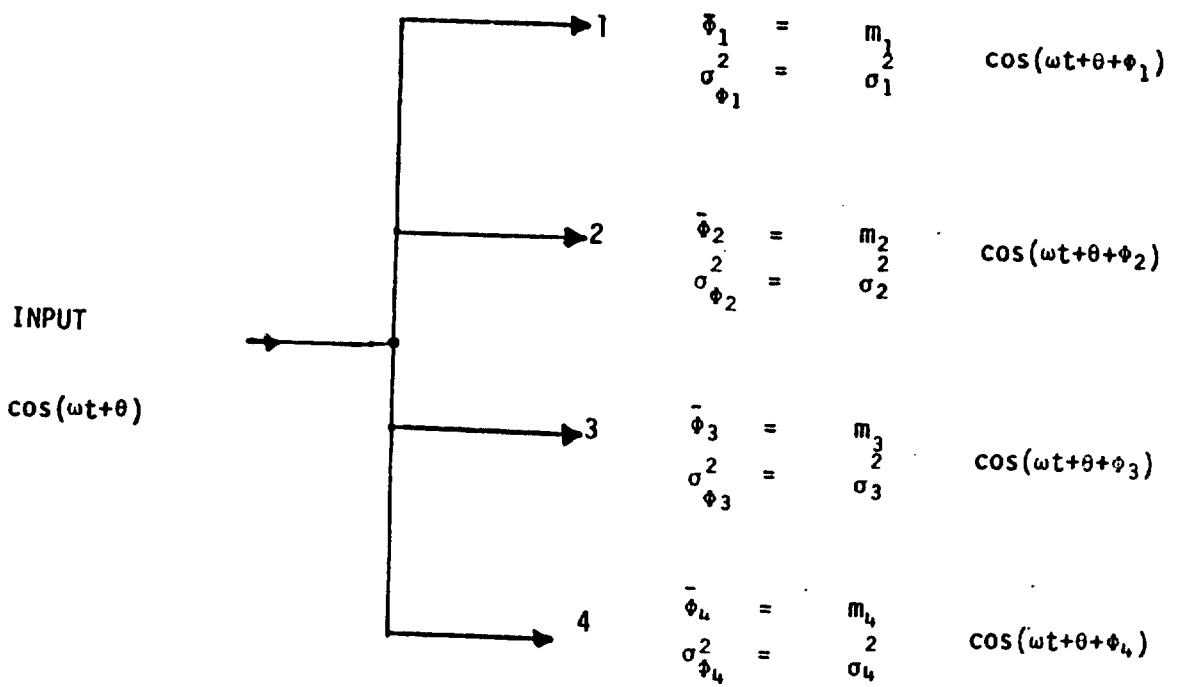

FIGURE 9.2. GENERAL STATISTICAL CHARACTERIZATION OF FOUR WAY POWER SPLITTER

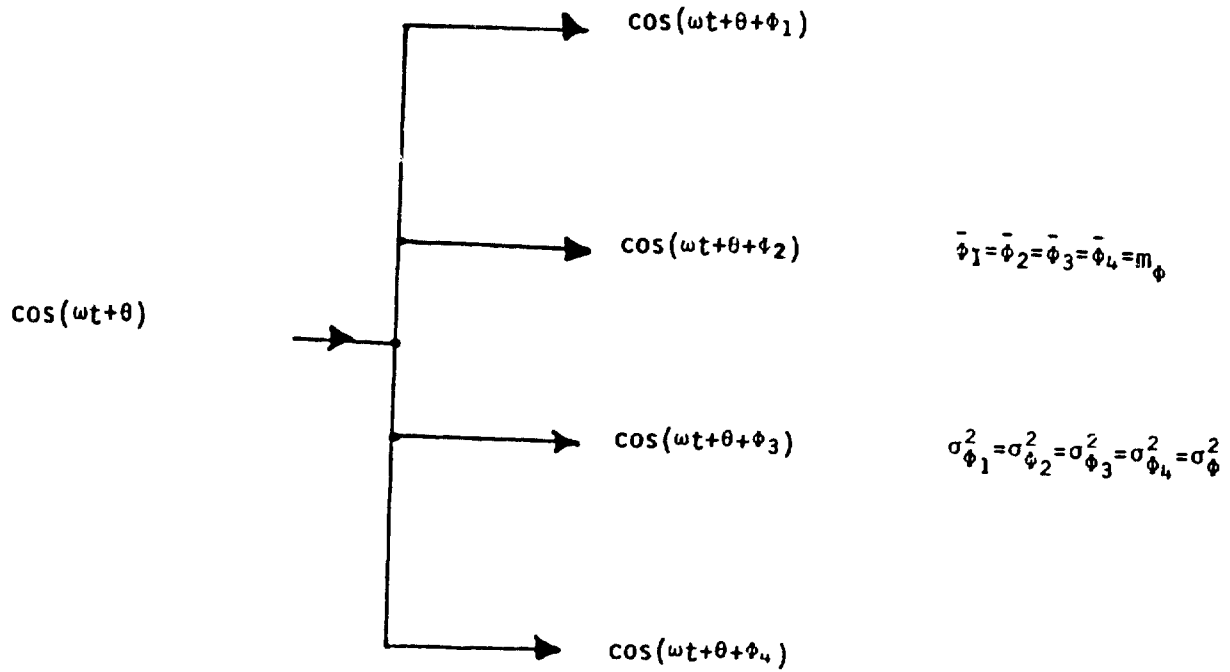

FIGURE 9.3 .FINAL CHARACTERIZATION OF FOUR WAY POWER SPLITTER

as well be assumed to be zero. Thus, it may be assumed for the example considered here that the phase shift between the reference at level 0 and any particular recovered reference at level 1 is a zero mean random variable with a variance of σ^2. Finally, note that the processes considered here are not ergodic. These phase shifts are static errors that will exist for all time. In spite of the fact that the ensemble average of the phase shift between level 0 and level 1 is assumed to be zero, the actual phase shift will be some value that will exist forever, thus causing some static beam shift anomaly peculiar to that particular array.

9.2 Phase Error Build Up and Tree Correlation Matrix

As we saw above, the phase distribution structure takes the form of a tree. Ideally the phase at any tip of the tree should be exactly the same as the master phase but as indicated above, there are sources of phase shift (random or otherwise) in which phase distribution structure which alter the value of the master phase delivered to the tip. Figure 9.4 depicts the sources of phase shift per level of the phase distribution tree structure using MSRTS and the power splitters. The phase disturbance added at any point in the phase distribution tree travels through the tree towards the tip giving rise to nonzero cross correlation of the phase at a tip with the phases at the other tips. The value of the cross-correlation depends upon the value of the variances of the phase errors added by the system to the signal as well as where in the distribution tree it was introduced. Figure 9.5 depicts a phase distribution tree having L levels of slave nodes, each node having

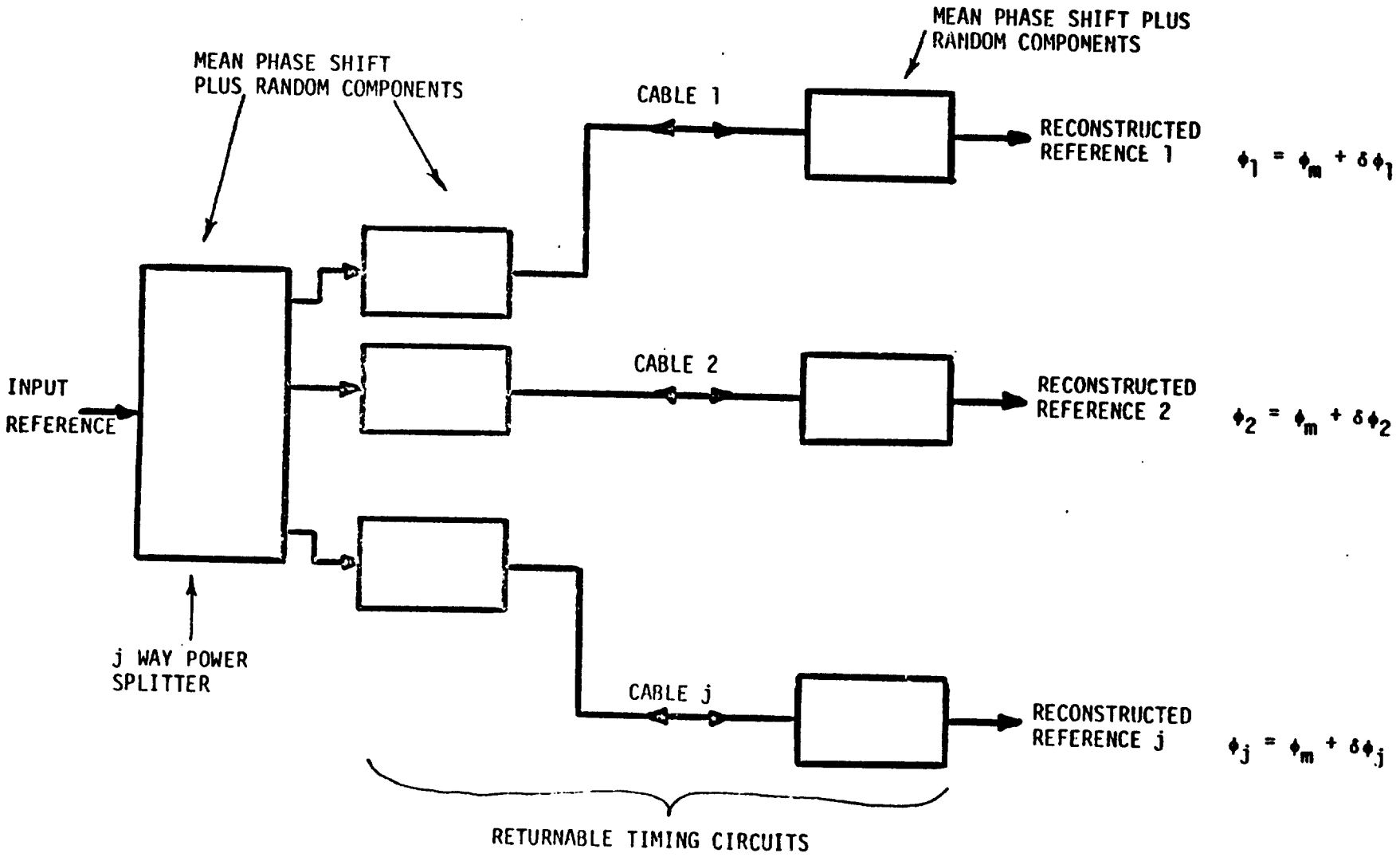

Figure 9.4. Sources of Phase Shifts Fer Level of the Phase Distribution Tree.

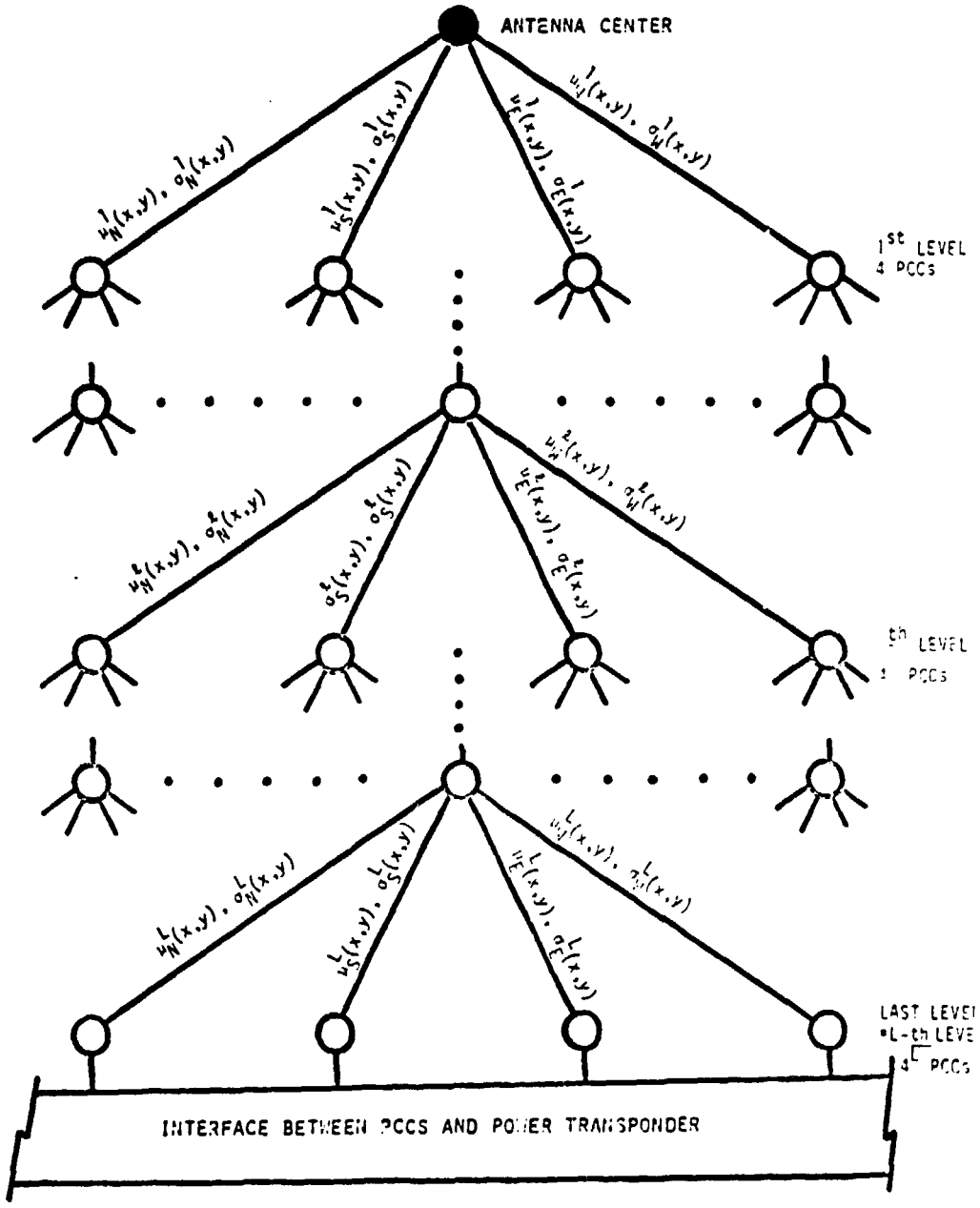

Figure 9.5. A Phase Distribution Tree Network.

four branches. The phase error added by the phase distribution system at the 1^{st} level slave node comes from a distribution having a mean value μ^1 and standard deviation σ^1. The subscripts on μ and σ indicate the north, south, east and west direction in which the slave node is, with respect to the center of the spacetenna. At the second level of slave nodes depending on which node is under consideration (north, south, east or west with respect to the immediate level 1 node) phase error from the distribution having a mean value μ^2 and standard deviation σ^2 is added to the phase error handed down by the immediate level 1 node. This combined phase error is then handed down to the third level slave nodes. The process of handing down the phase error from level to level continues until the tip of the tree is reached, at that point the phase with the accumulated phase error is used in the conjugation circuit to conjugate the pilot wave phase received at that point. An example of the phase error build up in a two level phase distribution tree having four branches per node is shown in Fig. 9.6. A general computer program was written for this particular application and it was executed with the value of phase errors and level 1 and level 2 nodes from a Gaussian random number generator with zero mean and standard deviation of 5°. The resultant phase error at each tip is shown in the same figure.

Thus we see that the correlation of phase at one tip of the phase distribution tree with the phases at the other tips depend on the routes taken by the signal from the center to arrive at those tips. An example of the correlation matrix for a two level phase distribution tree having four branches per node with the phase error

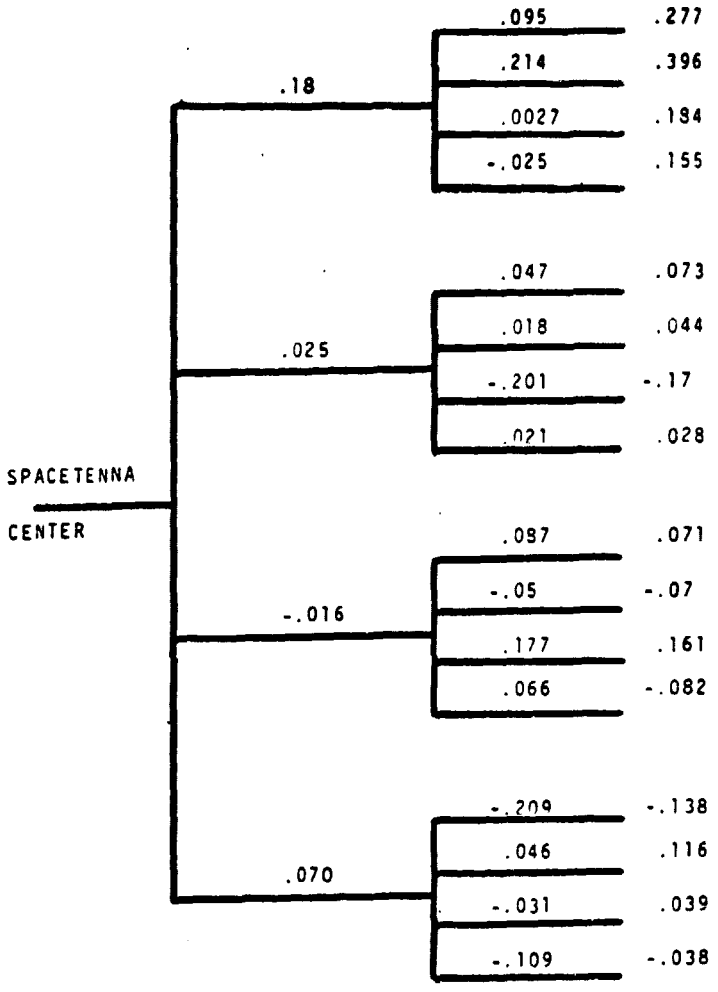

σ_1 = 5°, SEED(1) = 11.

σ_2 = 5°, SEED(2) = 21.

Figure 9.6. A Sample Phase Error Build Up in a Two Level Phase Distribution Network

added at level 1 and at level 2 having a standard deviation of 5° (both the phase errors have zero means) is shown in Figure 9.7. The matrix elements are normalized by $\sigma^2_{\text{Level},1} + \sigma^2_{\text{Level},2}$. Note that the matrix has more zero entries than nonzero entries. An ideal matrix would be an identity matrix which results in maximum power transfer.

9.3 Modeling of the Phase Error Build Up in the Distribution of Phase When PAs are Present at Each Level of the Phase Distribution Tree

Ideally the phase distribution tree transfers the master phase from level to level with no errors, hence it seems possible to put the PAs and the related conjugation circuits at each level reducing the cable weight necessary for the phase distribution system. When the circuit components are not ideal, randomness with nonzero mean (biases) are added to the phase being transmitted from level to level of the distribution system. Assuming that the master signal is a pure tone, the spectra of signals supplied to the PAs and the conjugation circuits is shown in Fig. 9.8. The spectrum seen by the conjugation circuit gets progressively broader and shifted as we proceed towards the tip of the phase distribution circuit. The variance of the phase after ℓ^{th} level is given by $\sum_{i=1}^{\ell} \sigma^2_{\text{Level } i}$ which is smaller than the variance of the phase at the tip of the phase distribution tree for ℓ total number of levels in the phase distribution tree. Thus the variance of the phase used in the conjugation circuits and PAs on the average becomes smaller than when the PAs and conjugation circuits are at the tip of the phase distribution tree structure. This results in

L = 2

$\sigma_1 = 5°, \sigma_2 = 5°$

.01523	.00762	.00762	.00762	.00000	.00000	.00000	.00000	.00000	.00000	.00000	.00000	.00000	.00000	.00000	.00000
.00762	.01523	.00762	.00762	.00000	.00000	.00000	.00000	.00000	.00000	.00000	.00000	.00000	.00000	.00000	.00000
.00762	.00762	.01523	.00762	.00000	.00000	.00000	.00000	.00000	.00000	.00000	.00000	.00000	.00000	.00000	.00000
.00762	.00762	.00762	.01523	.00000	.00000	.00000	.00000	.00000	.00000	.00000	.00000	.00000	.00000	.00000	.00000
.00000	.00000	.00000	.00000	.01523	.00762	.00762	.00762	.00000	.00000	.00000	.00000	.00000	.00000	.00000	.00000
.00000	.00000	.00000	.00000	.00762	.01523	.00762	.00762	.00000	.00000	.00000	.00000	.00000	.00000	.00000	.00000
.00000	.00000	.00000	.00000	.00762	.00762	.01523	.00762	.00000	.00000	.00000	.00000	.00000	.00000	.00000	.00000
.00000	.00000	.00000	.00000	.00762	.00762	.00762	.01523	.00000	.00000	.00000	.00000	.00000	.00000	.00000	.00000
.00000	.00000	.00000	.00000	.00000	.00000	.00000	.00000	.01523	.00762	.00762	.00762	.00000	.00000	.00000	.00000
.00000	.00000	.00000	.00000	.00000	.00000	.00000	.00000	.00762	.01523	.00762	.00762	.00000	.00000	.00000	.00000
.00000	.00000	.00000	.00000	.00000	.00000	.00000	.00000	.00762	.00762	.01523	.00762	.00000	.00000	.00000	.00000
.00000	.00000	.00000	.00000	.00000	.00000	.00000	.00000	.00762	.00762	.00762	.01523	.00000	.00000	.00000	.00000
.00000	.00000	.00000	.00000	.00000	.00000	.00000	.00000	.00000	.00000	.00000	.00000	.01523	.00762	.00762	.00762
.00000	.00000	.00000	.00000	.00000	.00000	.00000	.00000	.00000	.00000	.00000	.00000	.00762	.01523	.00762	.00762
.00000	.00000	.00000	.00000	.00000	.00000	.00000	.00000	.00000	.00000	.00000	.00000	.00762	.00762	.01523	.00762
.00000	.00000	.00000	.00000	.00000	.00000	.00000	.00000	.00000	.00000	.00000	.00000	.00762	.00762	.00762	.01523

Figure 9.7. The Correlation Matrix for a Two Level Phase Distribution Network.

higher gain of the spacetenna. The biases added by the phase distribution circuit components portray a different picture altogether. It is well known that the conjugation scheme is very sensitive to differential phase shifts of the currents feeding the radiagint elements of the antenna. Fig. 9.8 shows that the differential phase shifts (biases) are considerable for the system with PAs and conjugation circuits at each level as compared to the phase distribution system with PAs and conjugation circuits at the tips of the distribution tree having negligible differential phase shift.

One serious source of biases is the power splitters. With some additional hardware at each power splitter the problem of biases can be eliminated. One such scheme is shown in Fig. 9.9. A VCO is added to the power splitter assembly which has a feedback from the power splitter output, when the VCO locks. The biases are eliminated.

10.0 REFERENCE FAR-FIELD SYSTEM PERFORMANCE AND TRADEOFFS FOUND VIA SOLARSIM

In this section of this report we shall demonstrate the far-field performance characteristics of the reference system phase control system as found using SOLARSIM discussed in Appendix IV. Since the problem is too massive and expensive to implement in the form of early experiments which could provide meaningful performance results, a computer simulation supported by analysis has been developed (Appendix IV). Effective use of simulation techniques as a system engineering tool allows one to establish performance tradeoffs as hardware technology develops without the extreme costs of full scale testing of various concepts. In the following sections, certain

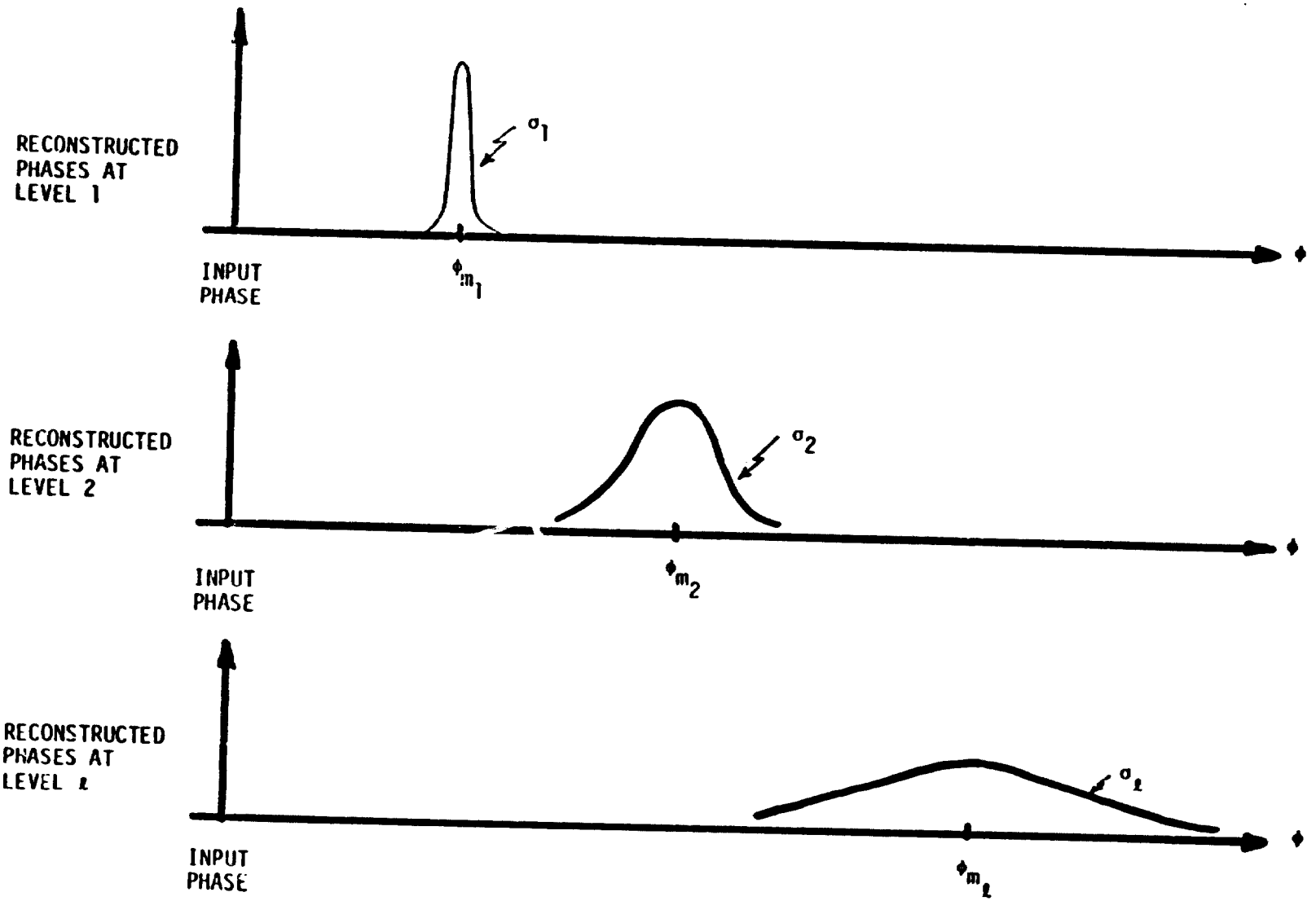

Figure 9.8. Diffusion of Phase Through Tree Reference Phase Distribution System.

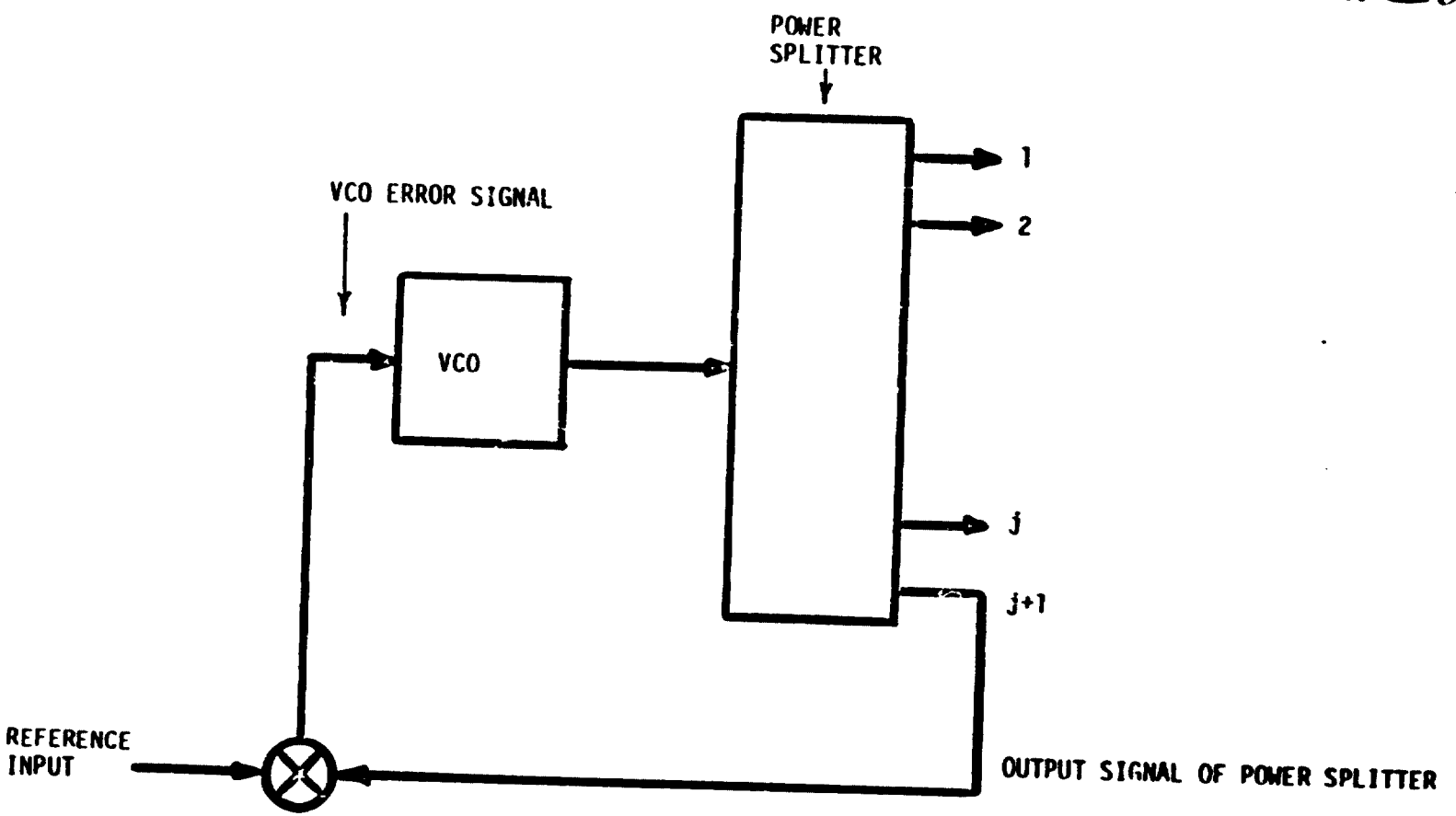

Figure 9.9. Circuit for Compensation of Power Splitter Bias.

performance characteristics of the SPS reference system are presented as found using SolarSim--an analytical simulation of the SPS phase control system.

10.1 Phase-Error Build Up and Tree Structure Optimization

In order to evaluate different phasing tree structure, one has to study the effects of the tree structure on the spacetenna performance. In particular, the boresight gain reduction and the spacetenna pointing error are two important performance measures for merit comparisons. The boresight gain reduction is proportional to the transmission efficiency of the microwave transmission system. The pointing error measures the ability of the spacetenna to focus on the center of the rectenna. SOLARSIM has been developed to investigate these effects. The current reference phase distribution tree consists of four levels and is shown in Fig. 10.1. Note that a total of 102400 nodes (PAs) at the last level are fed by the structure. Phase noises are introduced to the nodes at each level by the MSRTS discussed in Section 4.2.1. In addition, in the last level (PA level), additional phase noises are introduced by the power transponders.

10.1.1 Effect of Tree Structure on Main Beam Gain Reduction

The main beam gain reduction is a function of the magnitude of and the level where the phase errors are introduced by the phasing tree. It is interesting to see the extent to which the phase errors introduced at each level individually contributes to reduce this gain. In Fig. 10.2, we show the effect of the phase errors introduced at a particular level in the phase distribution tree, while the phase error at the other levels are neglected. A phase jitter of 5° is shown for a four level tree. The normal main beam gain loss of gain in dB is

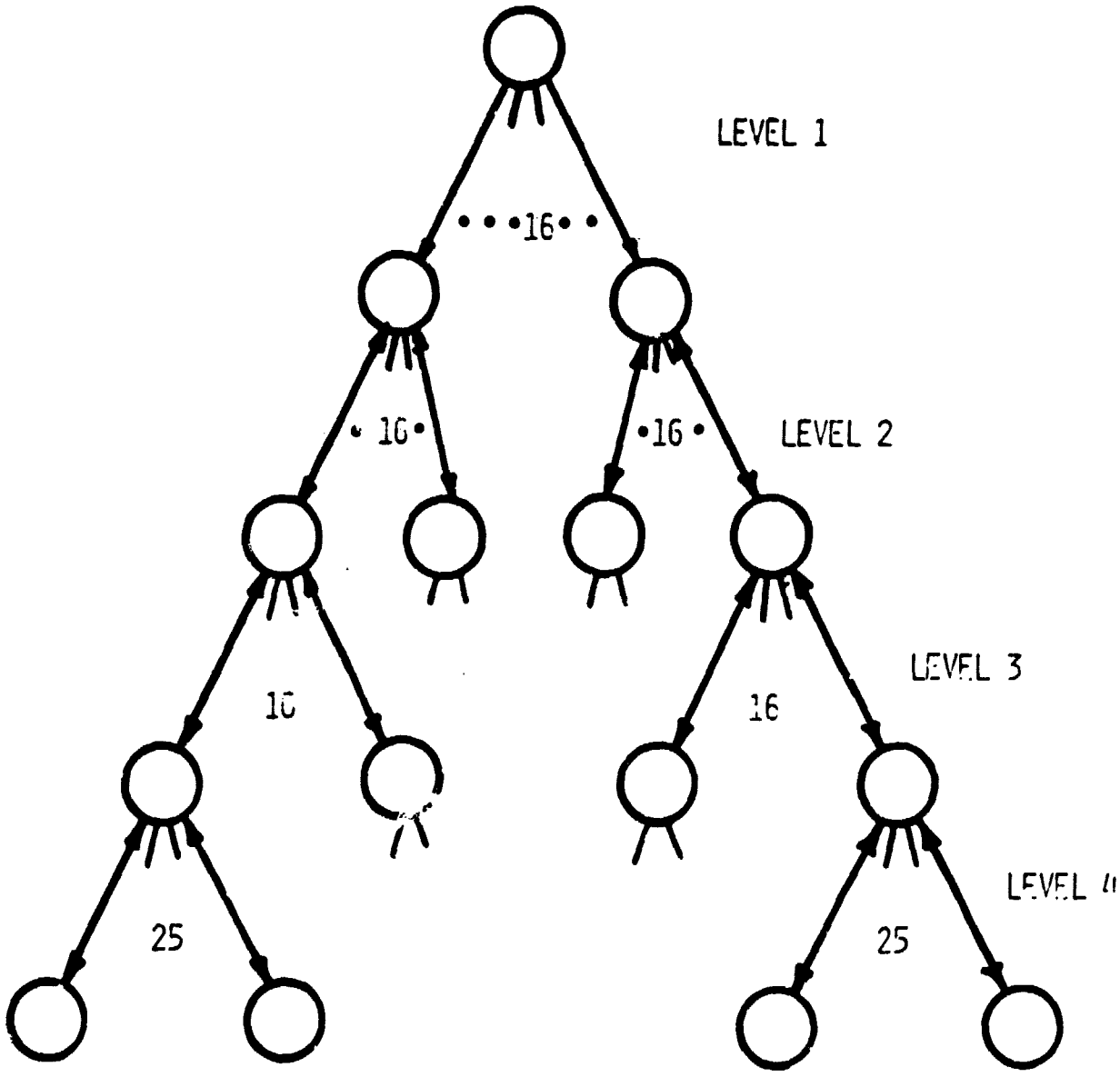

- PHASE NOISES ARE CORRELATED
- POWER SPLITTERS, POWER TRANSPONDERS, PHASE TRACKING PLLS, MULTIPLIERS, MICROWAVE HARDWARE COMPONENTS

Figure 10.1. Four Level Phase Distribution Tree.

is plotted in Fig. 10.2.

The quantity G_0 is obtained when all the phase errors introduced in the phasing tree are set to zero. From Fig. 10.2, we see that as far as the gain reduction is concerned, phase errors introduced in the last level (4^{th} level) results in the worst performance. Intuitively, phase errors introduced at the beginning levels of the tree cause the total phase error build up at the radiating elements to be correlated. As a result, individual patterns all add up in the same general direction. On the contrary, when phase errors are introduced in the last level, radiating elements have uncorrelated phase errors which results in reduced main beam gain. In any case, the differences are small.

10.1.2 Effect of Tree Structure on RMS Pointing Error

The ideal spacetenna attains its peak power density in the direction of the rectenna center. Under the assumption that the power beam is focused properly, the purpose of the phase control system is to phase its individual radiating elements so that the boresight gain is maximized. When random errors are introduced by the phasing system, the antenna power pattern peaks at some other direction other than the boresight. The variance of this direction is spacetenna pointing error.

Depending on the level where phase errors are introduced, the resulting pointing error is different. From Fig. 10.3, we can see that the phase error introduced at the first level causes the largest rms pointing error while the phase error from the last level (level four) has the least impact. The same trend is observed from the 8- and 9-level phase distribution tree which is depicted in Fig. 10.4. In essence, if

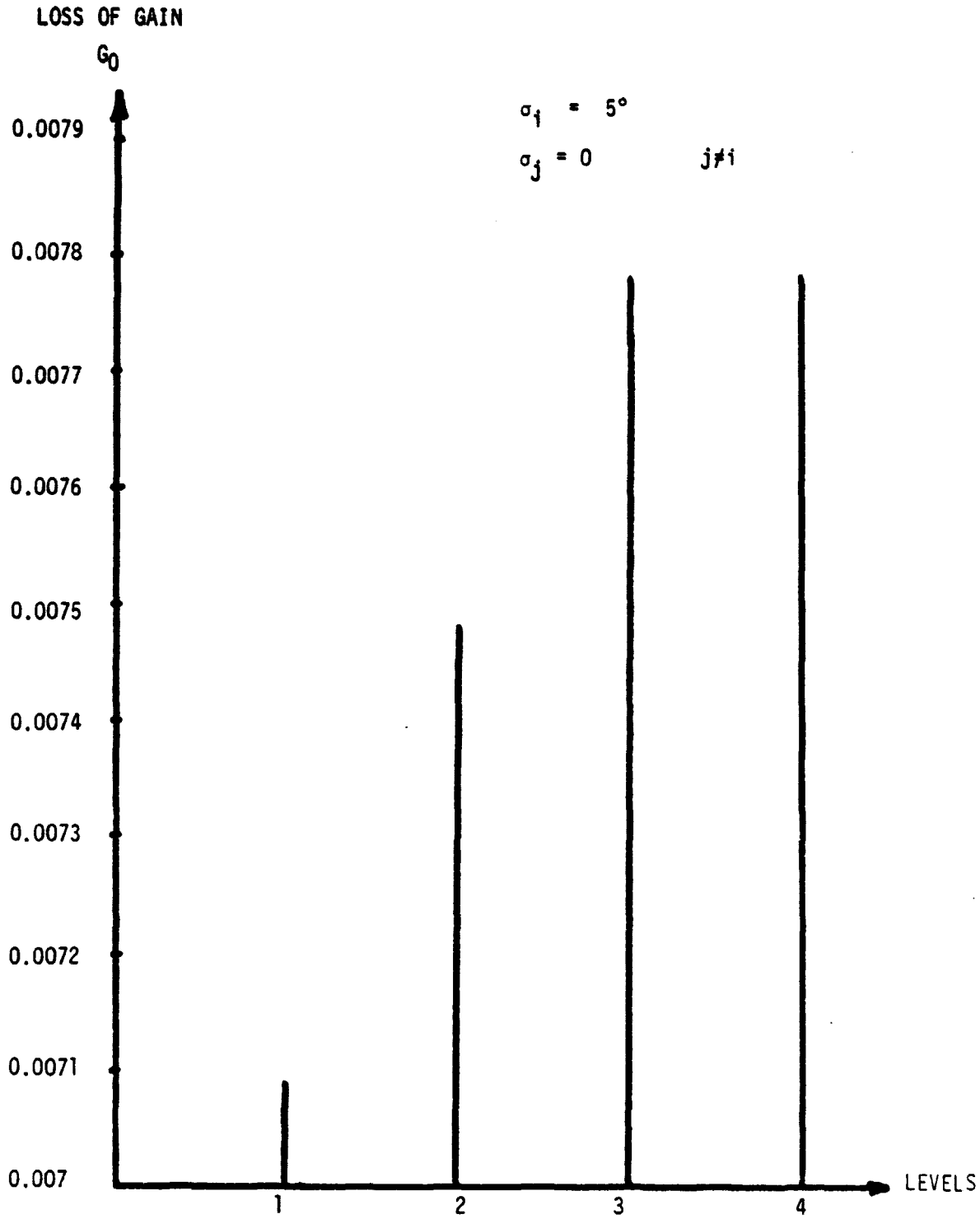

Figure 10.2. Effect of Phase Jitter Introduced in Different Levels of the 4-Level Phase Reference Tree.

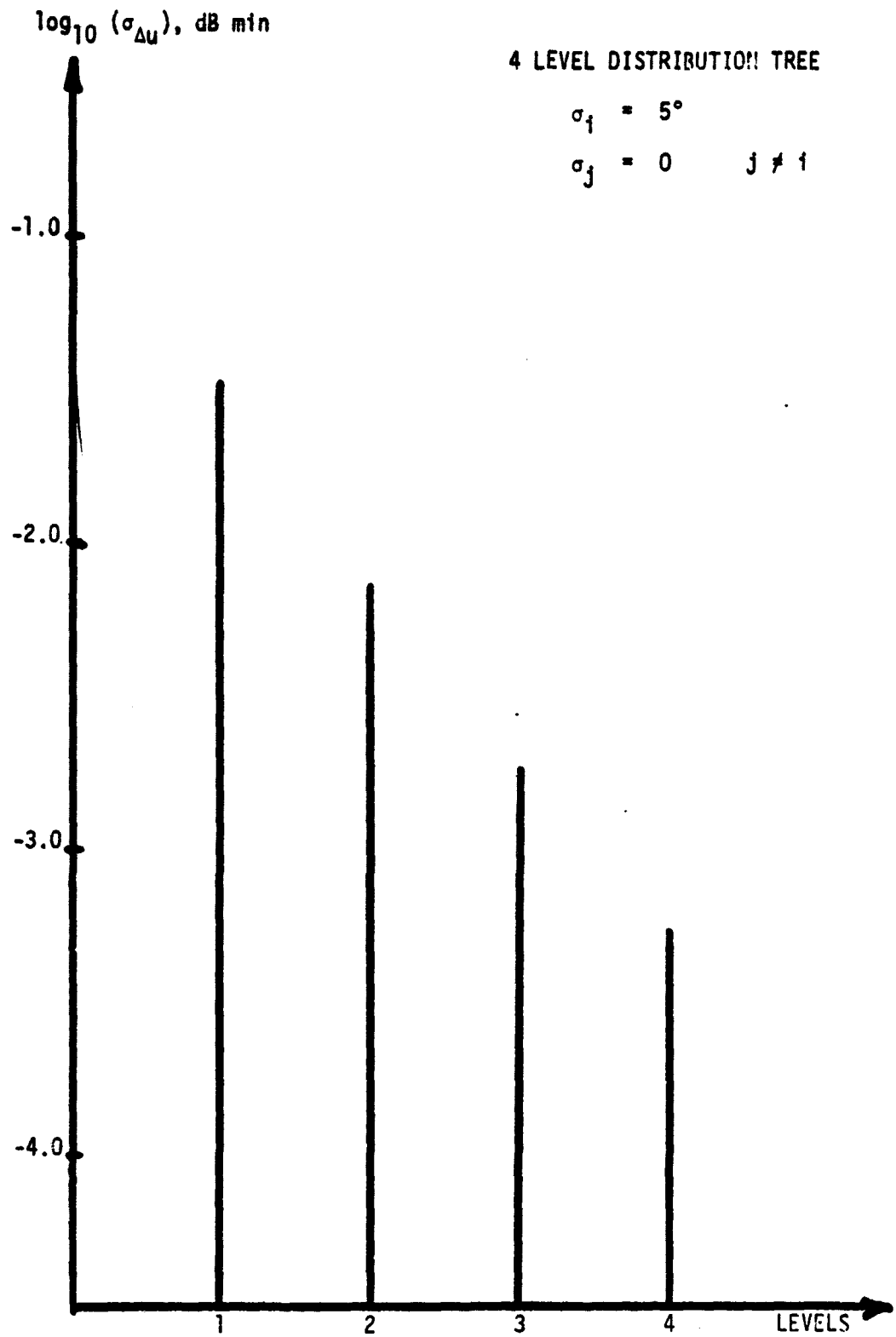

Figure 10.3. RMS Pointing Error as a Function of the Level When Phase Errors are Introduced for a Four-Level Tree.

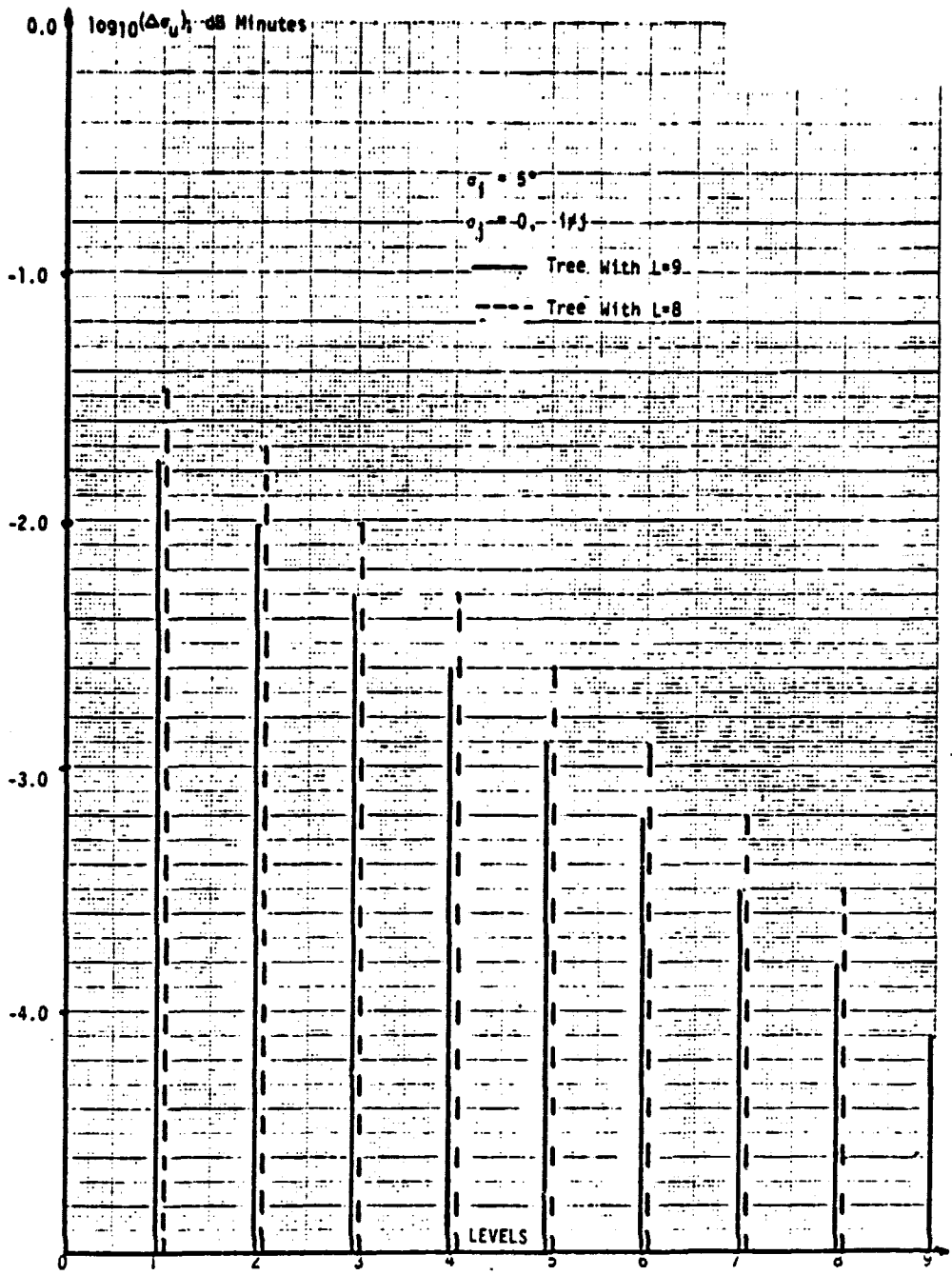

Figure 10.4. RMS Pointing Error as a Function of the Level where Phase Errors are Introduced.

independent phase errors are introduced at the last level, the resultant phase error variance on the beam is reduced roughly by the number of radiating elements (101552). This follows from the law of large numbers. However, if the phase errors are introduced at the first level, the resultant phase error variance on the beam is reduced by the number of nodes in the first level. For the baseline (4-level tree), that number is 25. The square root of the ratio 101552/25 is roughly 18 dB, which can be observed in Fig. 10.3.

10.2 Performance Evaluation Using SOLARSIM

10.2.1 Phase Error Build Up Effects on Far-Field Power Pattern

One of the current capabilities of SOLARSIM is to compute and display the received power pattern. The set of patterns shown in Figs. 10.5 to 10.9 represents its use to investigate the effect of phase error on the received power pattern for the 4-level distribution tree baseline. Fig. 10.5 is a typical power pattern with the phase jitter per level set to be 5°. The power pattern is normalized so that it is unity if all phase errors are negligible. This corresponds to a maximum microwave power density of 23 nW/cm^2 at the center of the rectenna. The power pattern is shown as a function of θ which is the angle from the boresight of the spacetenna. At any point on the rectenna, its distance d from the center is approximately given by $d = R\theta$ where R is the distance of the spacetenna from the rectenna (3.7×10^5 Km). The edge of the rectenna is approximately equivalent to half a minute of arc, which is depicted in the figure. Both the power patterns for the 0 dB taper (dashed line) and 10 dB taper (solid line) are shown in Fig. 10.5. We can observe that the power taper serves to bring down the sidelobes while broadening the main beam. For the reference system

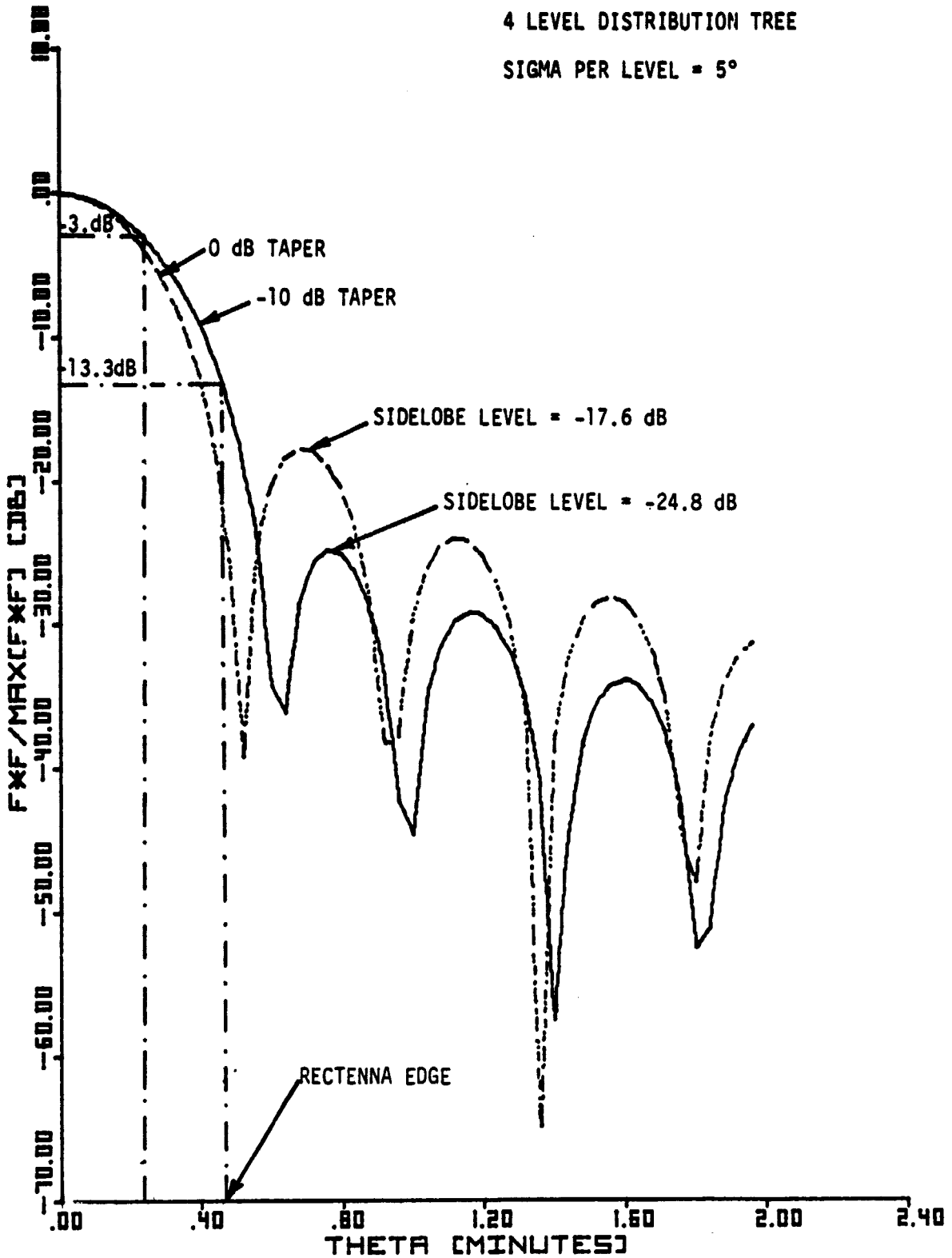

Figure 10.5. Power Pattern for 5° rms Phase Error.

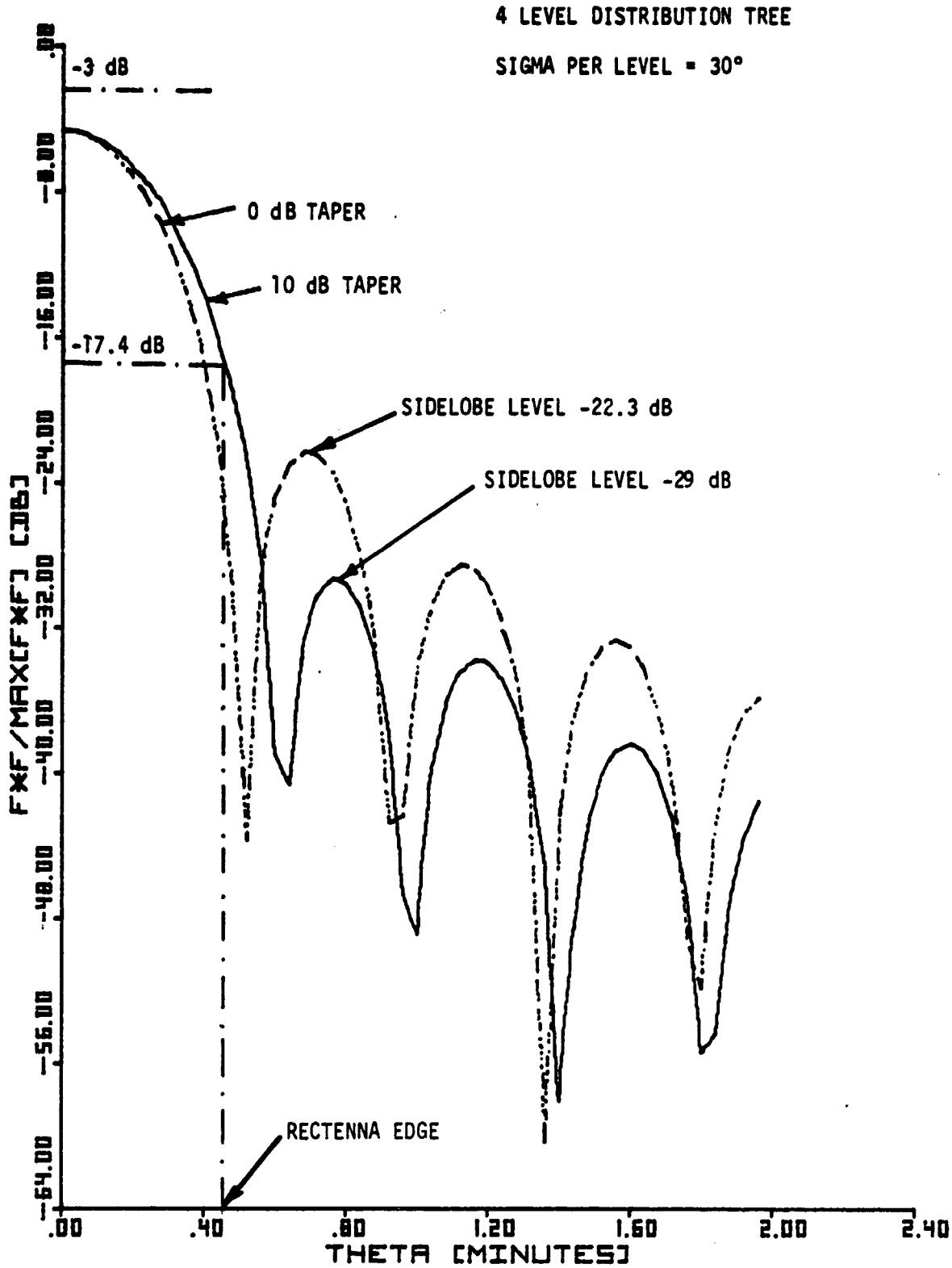

Figure 10.6. Power Pattern for 30° rms Phase Error.

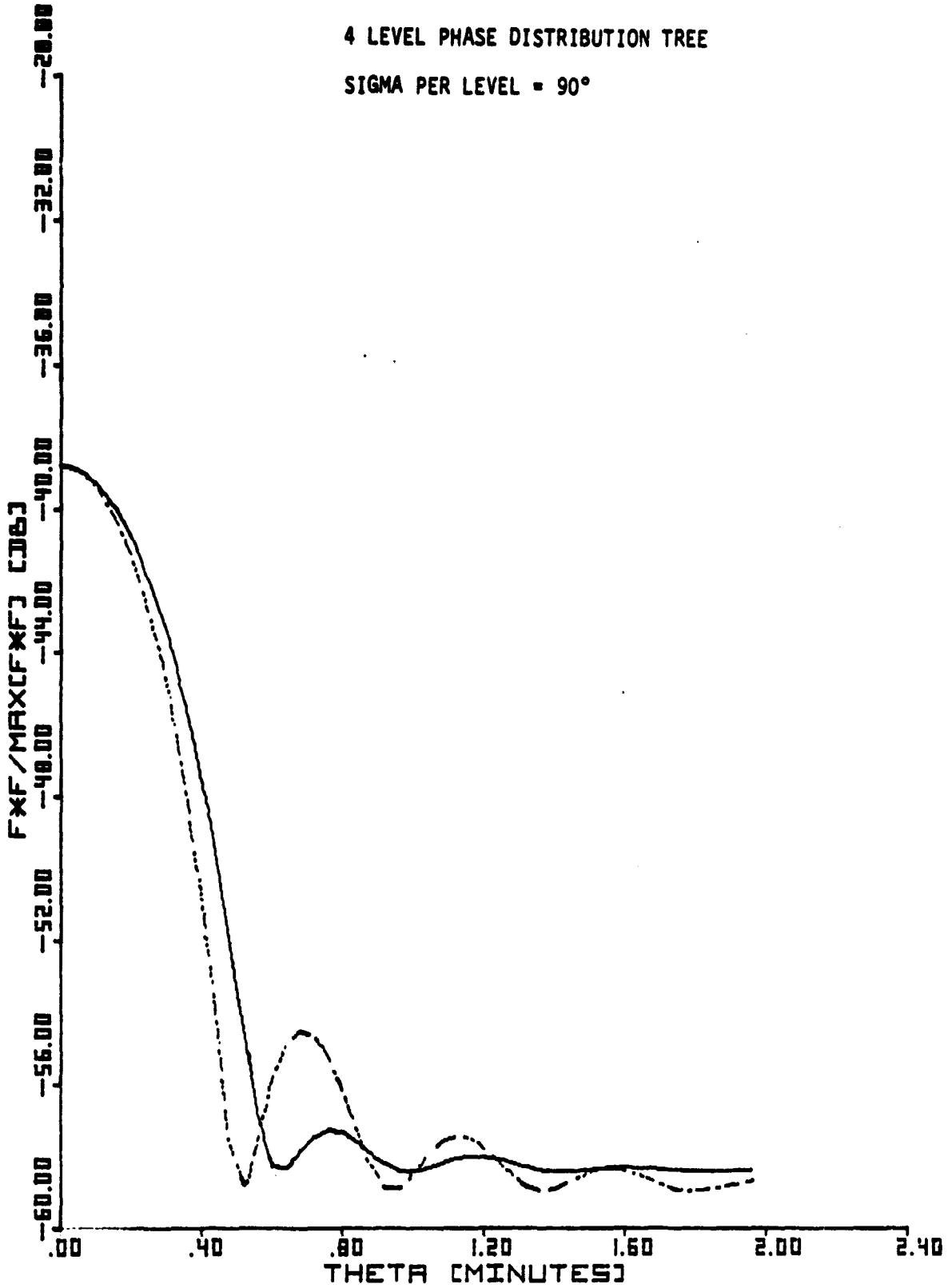

Figure 10.7. Power Pattern for 90° rms Phase Error.

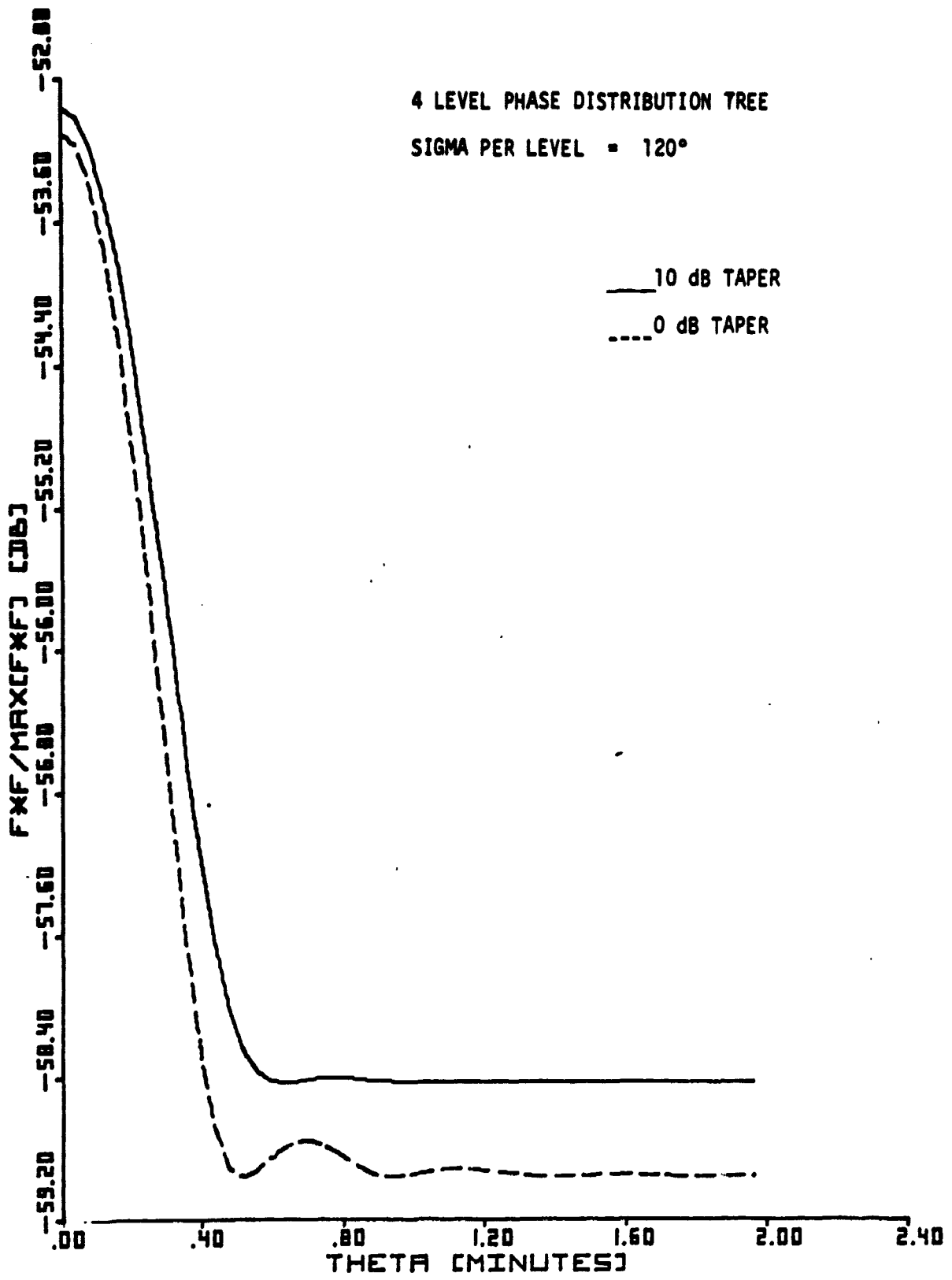

Figure 10.8. Power Pattern for 120° rms Phase Error.

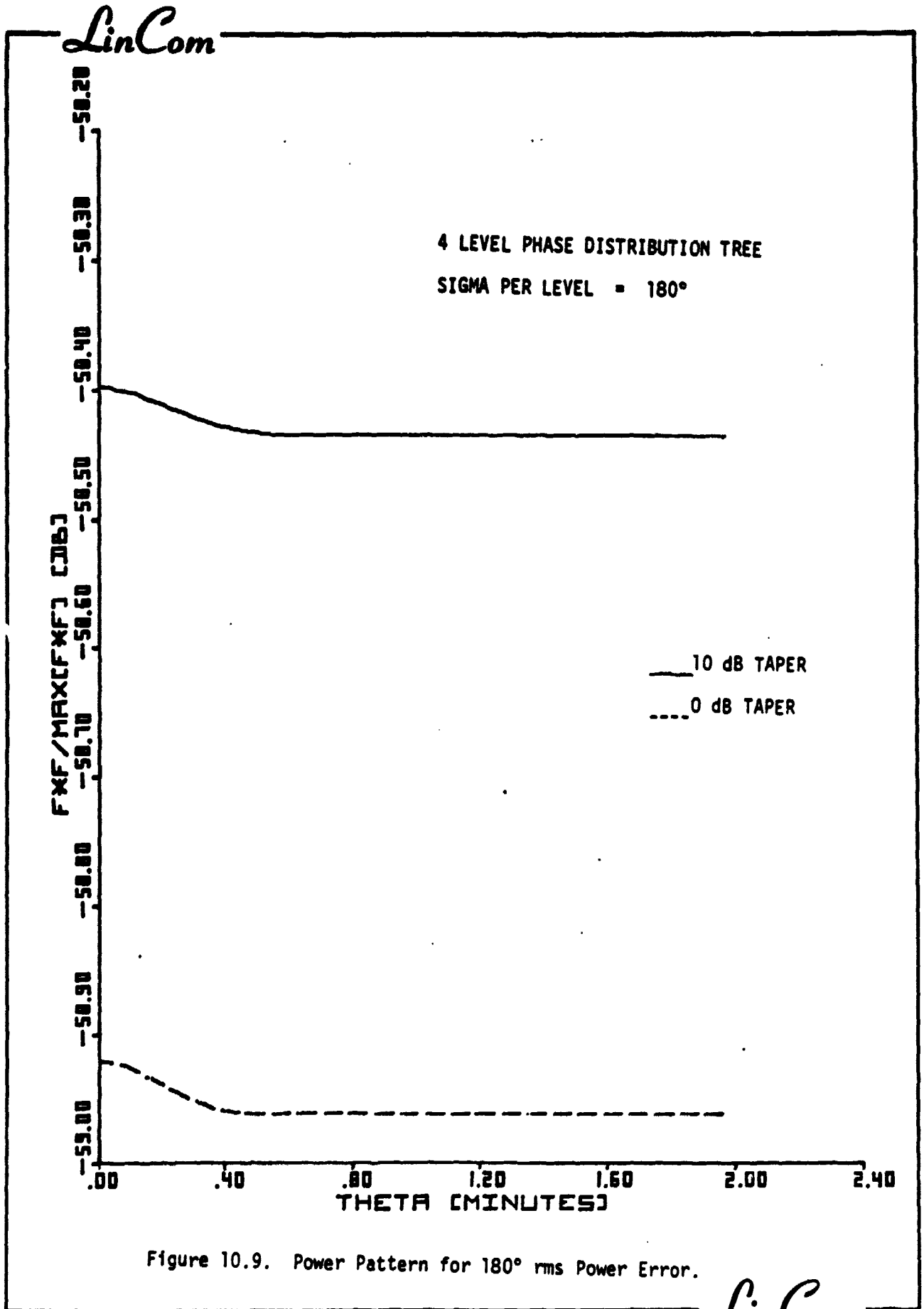

Figure 10.9. Power Pattern for 180° rms Power Error.

(10 dB taper), the power density is down to -13.3 dB at the rectenna edge. This corresponds to a power density of 1.08 mW/cm^2. The series of figures show that as the phase jitter per level increases, the boresight power density decreases and the sidelobe levels become closer together. Finally, for an rms phase error of 180° per level, i.e., initially no phase control, the spacetenna appears to be an isotropic radiating element (see Fig. 10.9). Under this condition, the power density is approximately 3 x 10^{-5} mW/cm^2. This level is far below either the U.S. radiation limit (10 mW/cm^2) or the USSR guideline (10^{-2} mW/cm^2) and hence does not appear to pose any biological hazard.

10.2.2 Main Beam Gain Reduction Due to Phase Error Build Up in Tree of Phase Control System

We have seen qualitatively how the efficiency of the microwave transmission system is reduced if the phase error build up is not kept under control. Fig. 10.10 investigates this effect by plotting the boresight gain reduction vs the total rms phase error build up through the phasing tree. As we have seen earlier, the shape of the power pattern is relatively insensitive to the phase error, at least to the first few lobes shown provided the rms phase error is not excessive (e.g. < 30°). In that case, the main beam reduction is proportional to the power received by the rectenna. In Fig. 10.11 and in what follows, total rms phase error is defined to be the total phase error build up through the phase distribution tree, assuming each level in the tree adds in the same amount of phase error. The phase error processes introduced at different nodes on the same level are assumed to be independent of one another. For an efficiency of 96%, Fig. 10.11 indicates that one can only tolerate about 11.8° of total rms

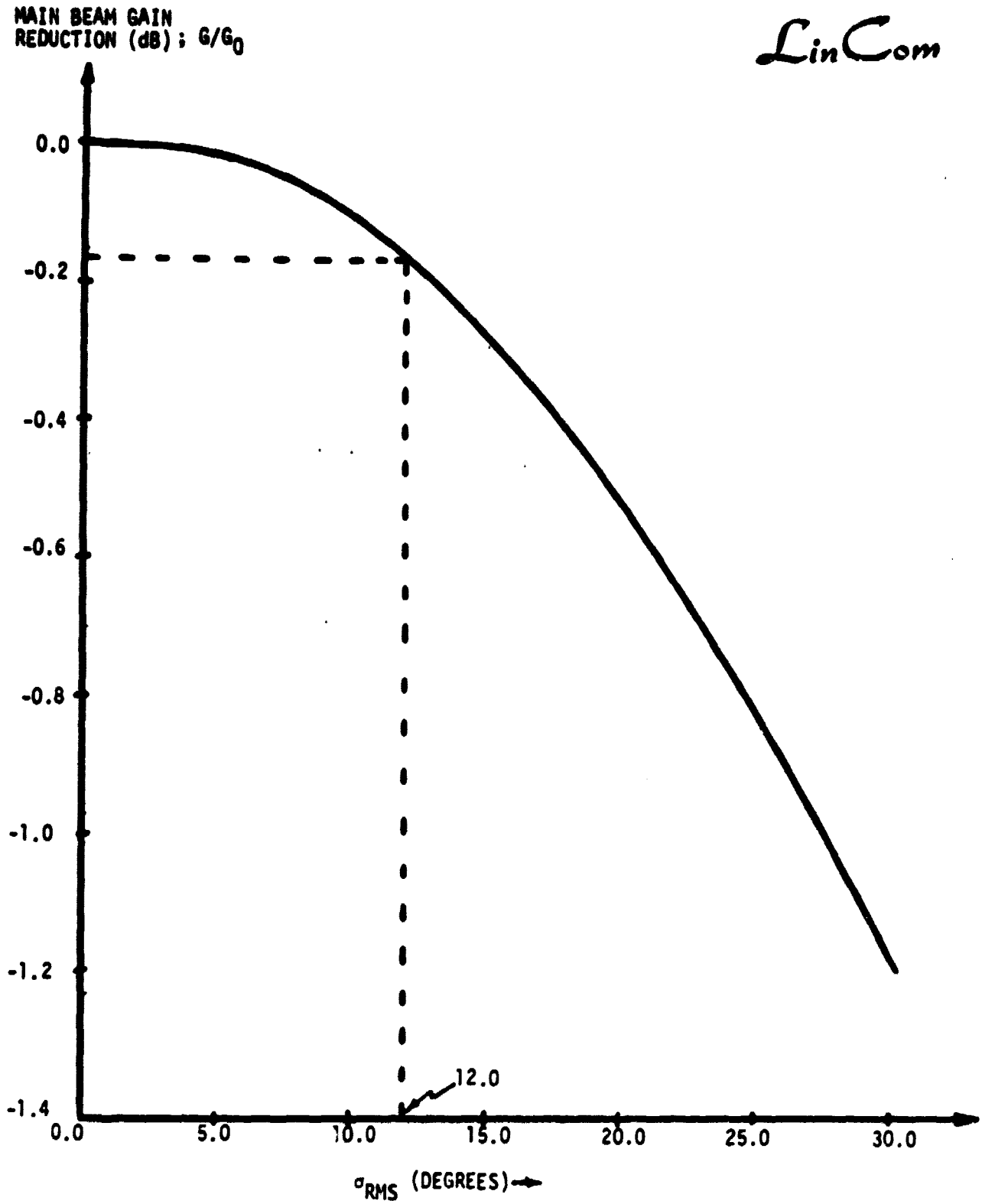

Figure 10.10. Main Beam Gain Reudction Due to Phase Erorr Build Up in Tree of Phase Control System.

G/G_0 EFFICIENCY (PERCENT)	PHASE ERROR BUILD UP (DEGREES)			
	TOTAL RF P.E. BUILD UP°	TOTAL IF P.E. BUILD UP°	RF P.E. BUILD UP PER LEVEL	
			L=9	L=4
96.0	11.8	2.4	3.93	5.9
90.0	18.8	3.8	6.5	9.7
85.0	23.0	4.6	7.7	11.5
80.0	27.0	5.4	9.0	13.5
75.0	30.5	6.1	10.17	15.25

Figure 10.11. Efficiency Performance of Baseline Phase Distribution System vs Phase Error Build Up.

phase error. The allowable phase error build up in the tree structure for a fixed efficiency is tabulated in Fig. 10.11. For the 96% efficiency, the total (RF) phase error build-up of 11.8° reflects into an IF phase error build-up of 2.4° for the 490 MHz IF baseline. For a four level tree (baseline system) the maximum error tolerable is 5.9° per level. If a nine level tree is used, we have to tighten the phase error specification to 3.9° per level. In this respect, the 4 level tree system seems to be superior. However, since different amounts of hardware and layout is required for different structures, the above remark is not conclusive.

As we have eeen earlier, the phase errors introduced at the last level result in the most severe reduction in the main beam gain. This effect is further investigated in Fig. 10.12 in which the total phase error build up through the phasing tree up to, but excluding the last level, is held fixed at 15° rms, and we vary the phase error introduced at the last level. The resultant gain reduction is identical for the four and the nine level tree. In general, one expects the magnitude of the phase error introduced in the last level to be higher than the earlier levels, since we must now take into account the phase errors introduced by the power transponder, in addition to the phase reference distribution system.

10.2.3 RMS Pointing Error Due to Phase Error Build Up in Tree of Phase Control System

The sensitivity of the rms pointing error to the total phase error build up is investigated in Fig. 10.13. As to be expected, the pointing error is directly proportional to the phase error. It is of interest to relate the rms pointing error to the probability that the beam misses the rectenna center by a given amount. This is rather straightforward

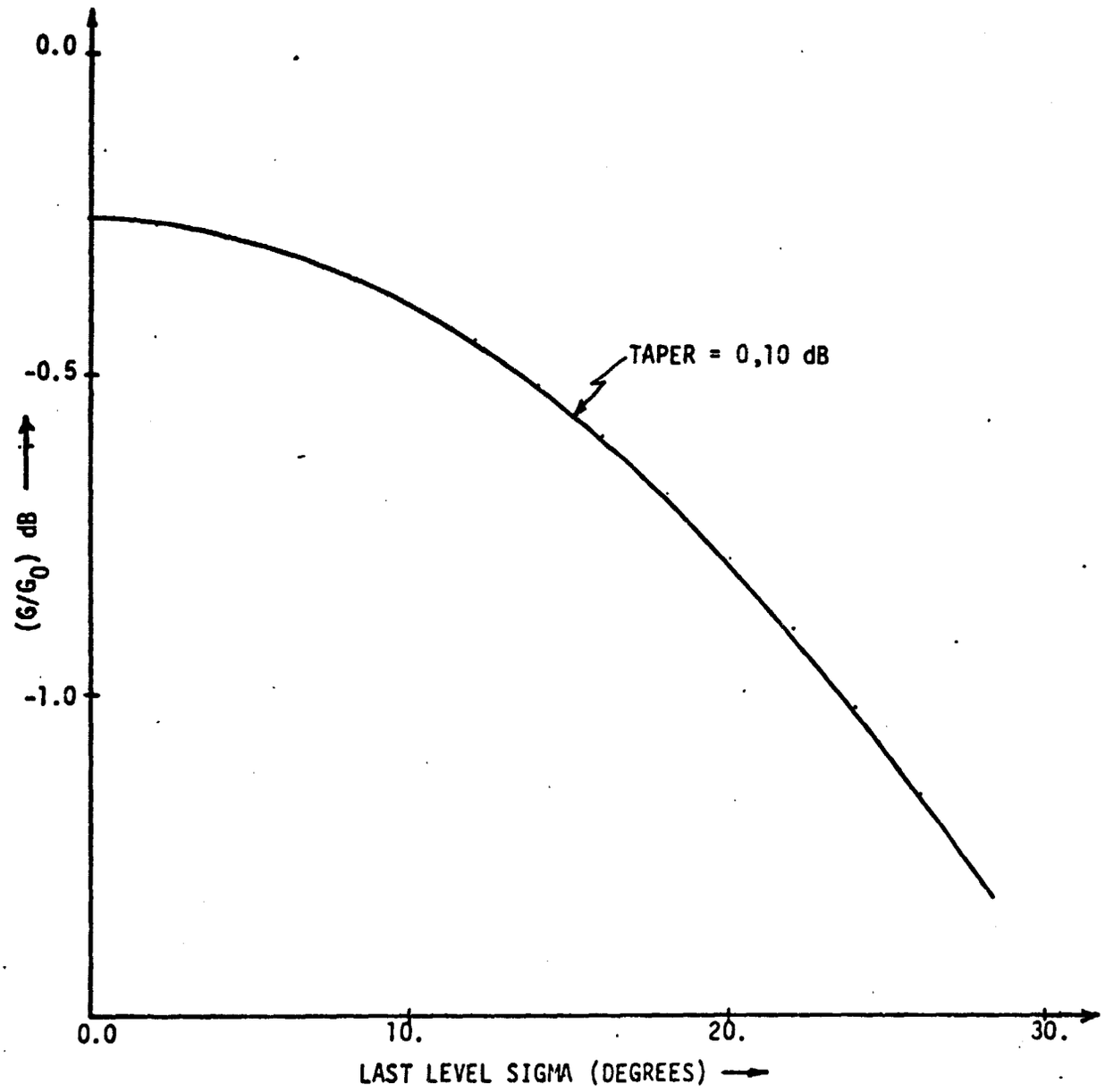

Figure 10.12. Gain Reduction for 4 and 9 Level Trees with the Last Level Sigma Changing.

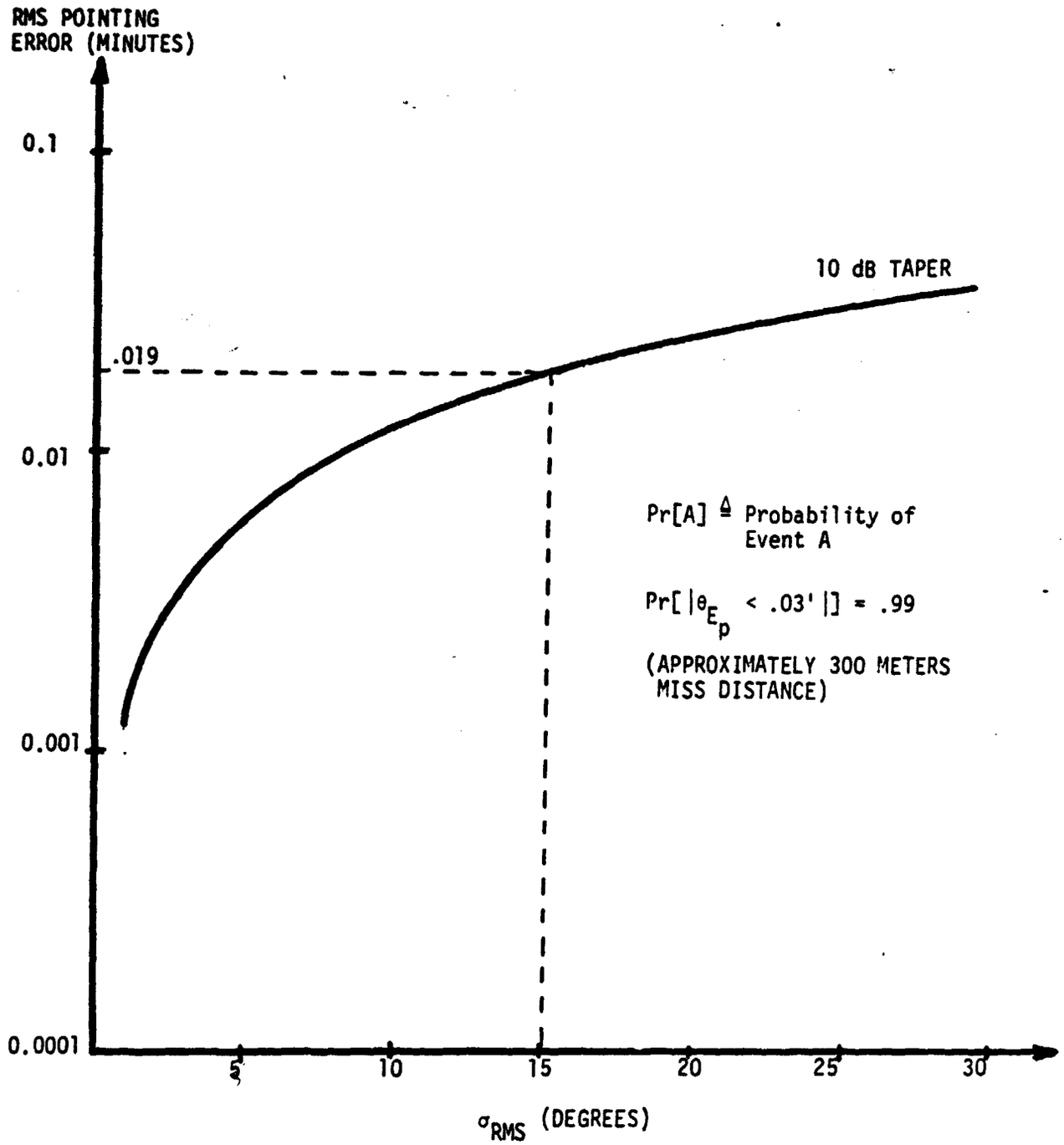

Figure 10.13. RMS Pointing Error Due to the Phase Error Build Up in Tree of the Phase Control System.

if we assume that the pointing error is approximately Gaussianly distributed. For a typical total rms phase error of 15°, we can see from Fig. 10.13 that the rms pointing error is 0.019 min. This translates into a probability of 0.99 that the main beam will be restricted to 0.03 min off boresight. In terms of distances, this means that the probability that the main beam misses the rectenna center by 300 meters is less than 10^{-2}.

10.2.4 Summary of Performance of the Baseline Phase Control System in Terms of Main Beam Gain and Pointing Error

The table in Fig. 10.14 summarizes the performance of the baseline phase control system. The projected efficiency is compiled as a function of the RF phase error build up (both total and per level). The associated rms pointing error and the 99 percentile range of the main beam are also given under the corresponding phase error conditions. For a target efficiency of 96%, the RF rms phase error allowed is 12° total or 4° per level. The corresponding rms pointing error is 10^{-2} min while the 99 percentile distance is 437 meters. Hence if we can keep the phase error to be less than 4° per level, the performance of the phase control system is satisfactory.

From [11], the gain reduction is approximately $\exp(-\sigma_\phi^2)$ where σ_ϕ^2 is the total phase error variance and the rms pointing error is proportional to the rms phase error. These relationships were developed for a linear array. Nonetheless, they also seem to apply for the present system. As a matter of fact we can verify that $G/G_0 \cong \exp(-\sigma_\phi^2)$ and $\sigma_u \cong \sigma_\phi/4.5\times10^4$ from Fig. 10.14.

10.2.5 Effects of Antenna Imperfections on SPS Performance

In an ideal retrodirective array where phase conjugation is performed

(G/G_0) (PERCENT)	PHASE ERROR BUILD UP (DEGREES)		RMS POINTING ERROR (MINUTES)	Pr[|Miss Distance < x|] = .99
	TOTAL R.F. P.E.BUILD UP	R.F. P.E. BUILD UP PER LEVEL		
96.0	12.0	4.0	0.016	x = 437m
90.0	19.0	6.33	0.026	710m
85.0	24.0	8.0	0.032	874m
80.0	27.0	9.0	0.036	983m
75.0	31.0	10.33	0.041	1120m

Figure 10.14. Performance of Baseline Phase Control System.

on each and every radiating element, the performance of the array is insensitive to imperfections on the array structure. In reality, the phase conjugation required for retrodirectivity is feasible only at the subarray level. As a result, the performance of the spacetenna as a retrodirective array is severely affected by the layout, size, surface roughness and tilt of the subarray. The latter phenomena are caused by structural imperfections due to engineering tolerances, bending and shearing forces, aging, and thermal effects, to name a few. SOLARSIM provides the capabilities to investigate these effects on the spacetenna performance.

10.2.5.1 Spacetenna Layout, Tilts and Location Filters

The 10 dB power taper in the present reference system is achieved by dividing the spacetenna into 10 distinct power density rings. A quadrant of the spacetenna is shown in Fig. 10.15. The radii of these rings run from about 94 meters to a maximum of 500 meters as shown. The power density per ring is varied by changing the number of PAs feeding per unit radiating surface. For example, the number of PAs feeding a 10.4 m x 10.4 m square of slotted waveguide changes from 36 to 4 from the inner most to the outer most ring. The power taper from the spacetenna center to its edge is thus 9.5 dB to be exact.

The current reference system assumes that phase conjugation is performed on each PA that feeds a subarray. By a subarray we mean a group of slotted waveguides grouped into a square in the center of which phase conjugation is performed. Hence only the central radiating element is truly retrodirective. The other elements on the same subarray will experience differential phase shifts defined by the projections of the location of the elements along the boresight. The size of subarray in

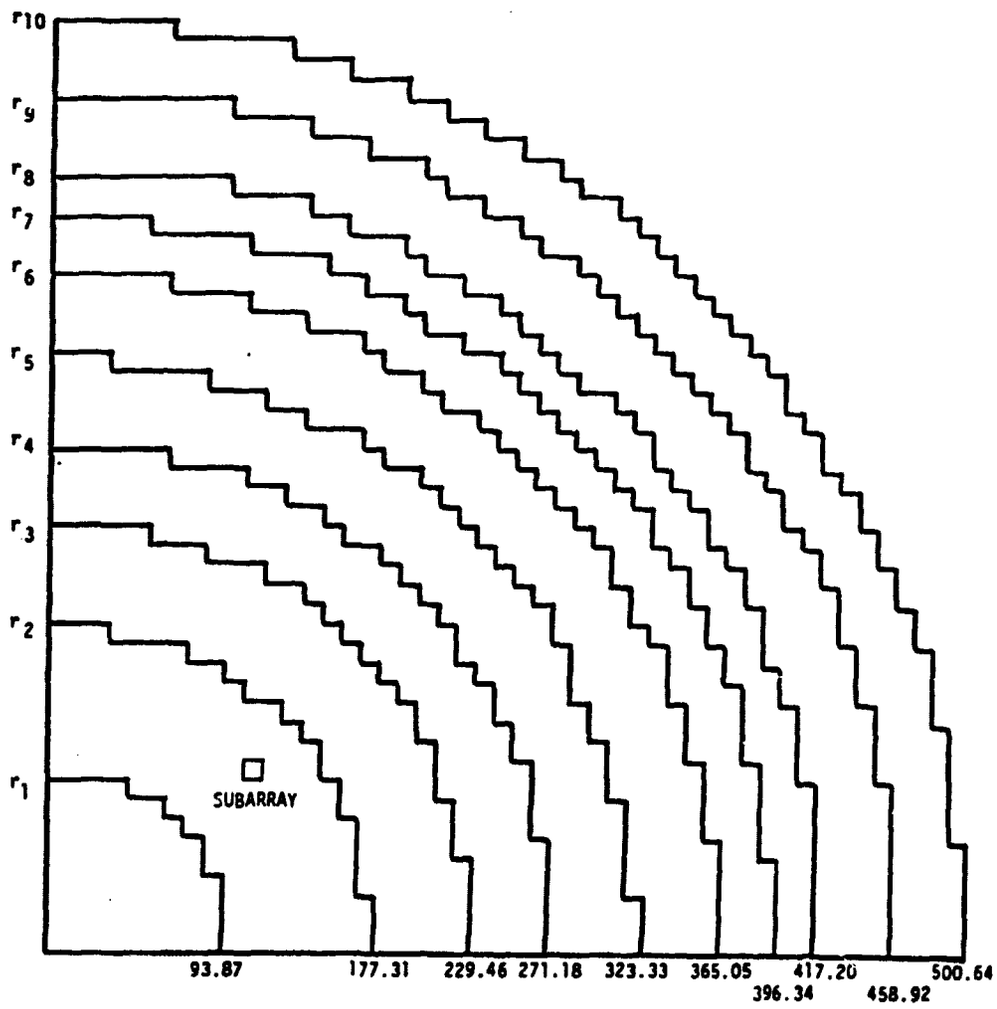

Figure 10.15. Spacetenna Power Density Rings.

the reference system varies from 1.73x1.73 m^2 to 5.2x5.2m^2 from the center to the edge of the spacetenna. The details are given in Fig. 10.16. Also shown in the same figure is the fixed size subarray geometry conceived by Boeing. In that configuration all subarrays have a fixed size of 10.4 x 10.4 m^2. Only one conjugation center is provided on each subarray.

For a perfectly flat spacetenna, the normal directions of each subarray are all identical, i.e., they all coincide with the normal direction of the spacetenna as a whole. Since the spacetenna is never perfectly flat in reality, each subarray will point in a different direction. For SOLARSIM, we adopt the subarray tilt model depicted in Fig. 10.17. The dashed line shows the ideal position of the subarray. With tilts, the subarray is depicted by the solid line. Note that the tilted subarray makes an angle θ_x with the x axis and an angle θ_y with the y axis. The angle between the present normal direction and the ideal direction is given by $\theta^2 = \theta_y^2 + \theta_x^2$. The tilted angles θ_x and θ_y have mean components denoted by $E(\theta_x)$ and $E(\theta_y)$. They represent the errors in the SPS steering mechanism made in pointing the spacetenna towards the rectenna center. The mean values $E(\theta_x)$ and $E(\theta_y)$ are the same for all the subarrays and they are referred to as the mechanical pointing error in the x- and y-direction. The perturbation about these means, i.e., $\theta_x - E(\theta_x)$ and $\theta_y - E(\theta_y)$ represent the variations of the tilt angles from one subarray to another. They are assumed to be Gaussian with variances $\sigma^2_{\theta_x}$ and $\sigma^2_{\theta_y}$.

In the above model, we have modeled the subarrays to be flat surfaces. This assumption is justifiable since we are only interested in the global behavior of the subarray. However, when we are concerned with the

FIXED SIZE SUBARRAYS

POWER DENSITY STEP	NUMBER OF SUBARRAYS	NUMBER OF POWER MODULES PER CONJUGATION PT.	TOTAL # OF POWER MODULES PER DENSITY STEP
1	276	36	9936
2	632	30	18960
3	644	24	15456
4	628	20	12560
5	784	16	12544
6	900	12	10800
7	664	9	5976
8	612	8	4896
9	1052	6	6312
10	1028	4	4112
TOTAL FOR FULL ARRAY	7220		101552

SIZE OF THE SUBARRAY = 10.4m x 10.4m

VARIABLE SIZE SUBARRAYS

POWER DENSITY STEP	SIZE OF SUBARRAY	NUMBER OF SUBARRAYS	TOTAL # OF POWER MODULES PER CONJUGATION POINT	# OF POWER MODULES
1	1.73m x 1.73m	9936	1	9936
2	1.89m x 1.89m	18960	1	18960
3	2.12m x 2.12m	15456	1	15456
4	2.32m x 2.32m	12560	1	12560
5	2.6 m x 2.6 m	12544	1	12544
6	3. m x 3. m	10800	1	10800
7	3.46m x 3.46m	5976	1	5976
8	3.67m x 3.67m	4896	1	4896
9	4.24m x 4.24m	6312	1	6312
10	6.2 m x 6.2 m	4112	1	4112
		101552		101552

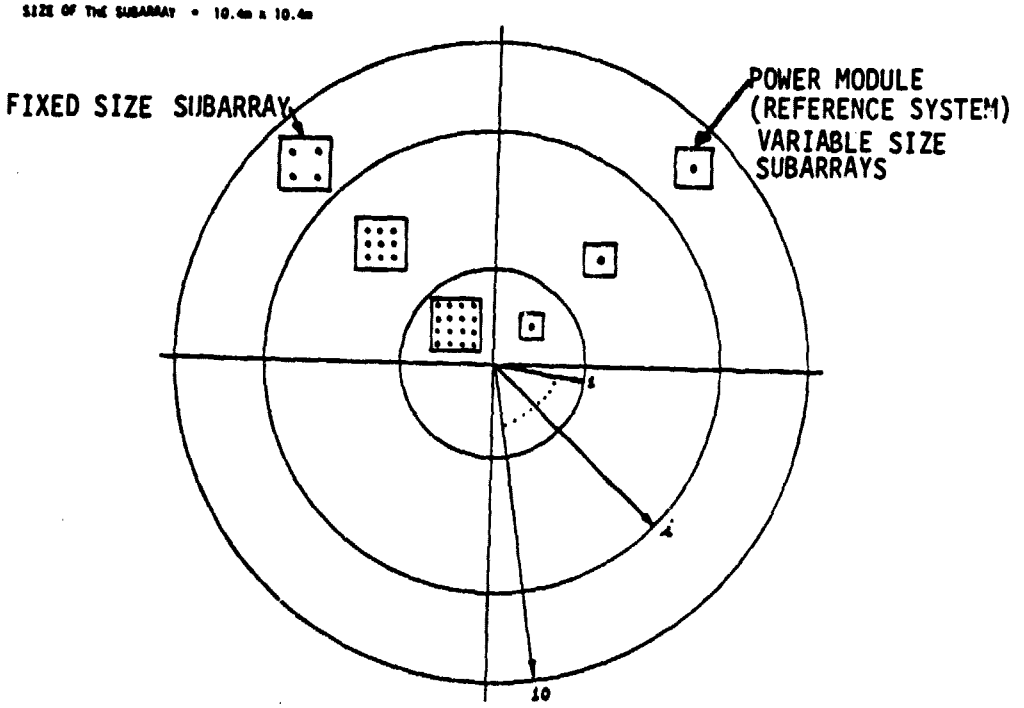

Figure 10.16. Variable and Fixed Size Subarray Geometry.

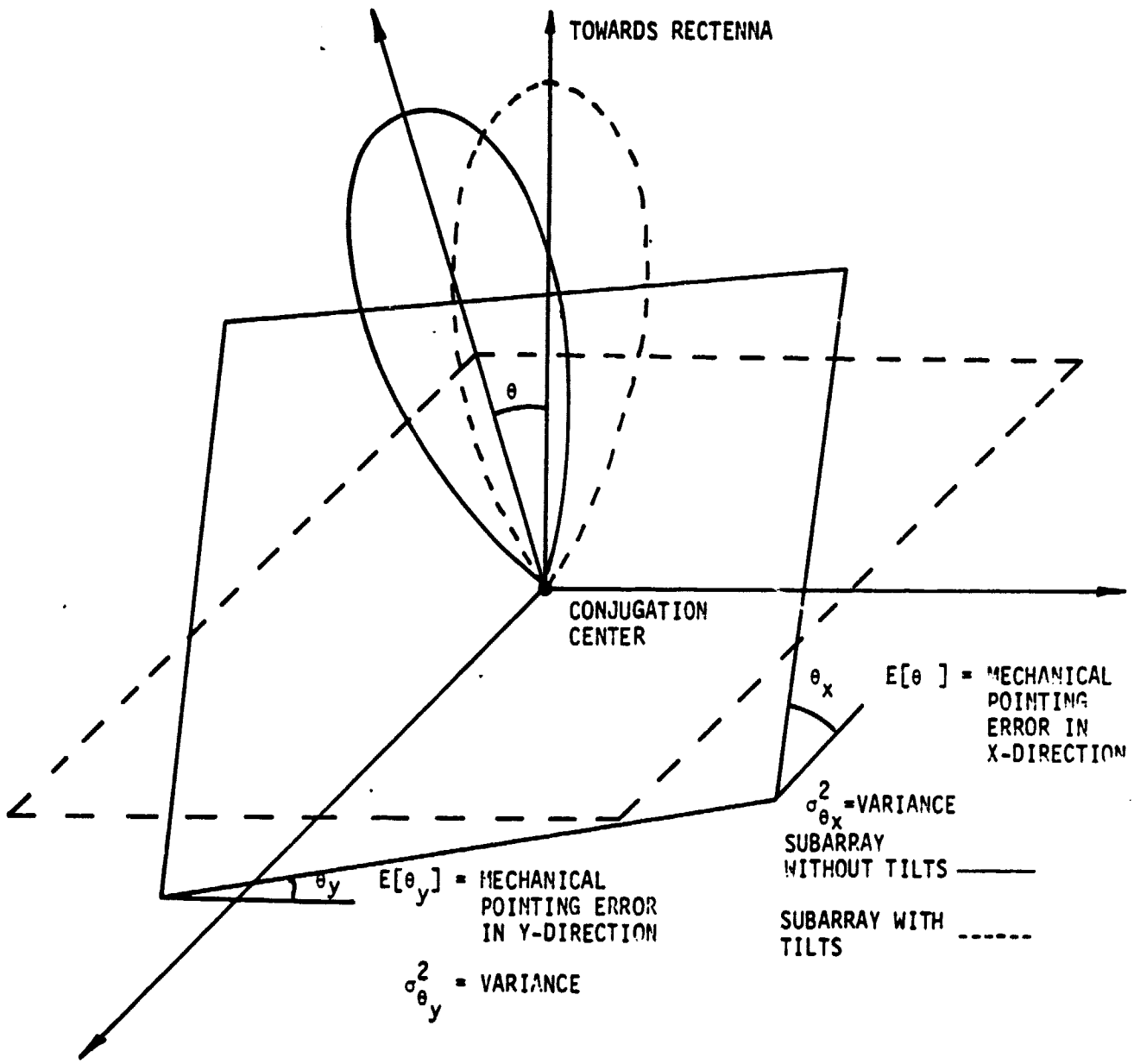

Figure 10.17. Effect of Subarray Mean Tilt and Jitter.

radiating elements, we need a more refined model for SOLARSIM. Figure 10.18 defines the location uncertainty of the radiating elements and the conjugation point primarily resulting from the unevenness of the subarray surface. The average plane through the subarray defined the ideal subarray used to model the tilt effects. However, the actual locations of the radiating elements and the conjugation point will be perturbed from the average plane. A cross section of a typical subarray surface running through the conjugation point parallel to the y-axis is shown in Fig. 10.18. The location jitter is defined to be the projection of the location of a point along the line joining the ideal center of the subarray and the center of the rectenna.

10.2.6 Sensitivity to Tilt Effects as a Function of Conjugation Level

In the absence of tilt effects, the performance of the spacetenna is not sensitive to the conjugation levels. In practice, the presence of tilt effects determines the level required. Fig. 10.19 compared the sensitivity of the gain reduction G/G_0 vs the mechanical pointing error with the location jitters (assumed equal for conjugation points and radiating elements) as a parameter. A typical rms tilt $\sigma_\theta = \sqrt{\sigma_{\theta_x}^2 + \sigma_{\theta_y}^2}$ of 2 min is assumed. We can observe that the baseline system degrades more gracefully than the fixed subarray (Boeing) scheme.

10.3 SPS Power Transfer Efficiency

In Section 8 the power transfer efficiency was defined. That definition is used to generate the results below.

The computer program evaluates the received power as given in the equation (8.6), i.e., $\phi\epsilon(0,2\pi)$ and $\theta\epsilon(0,0.464')$. The total radiated power is computed in two parts. The first part integrates the anisotropic term of the power pattern over the main lobe and 5 sidelobes, i.e., 'H'

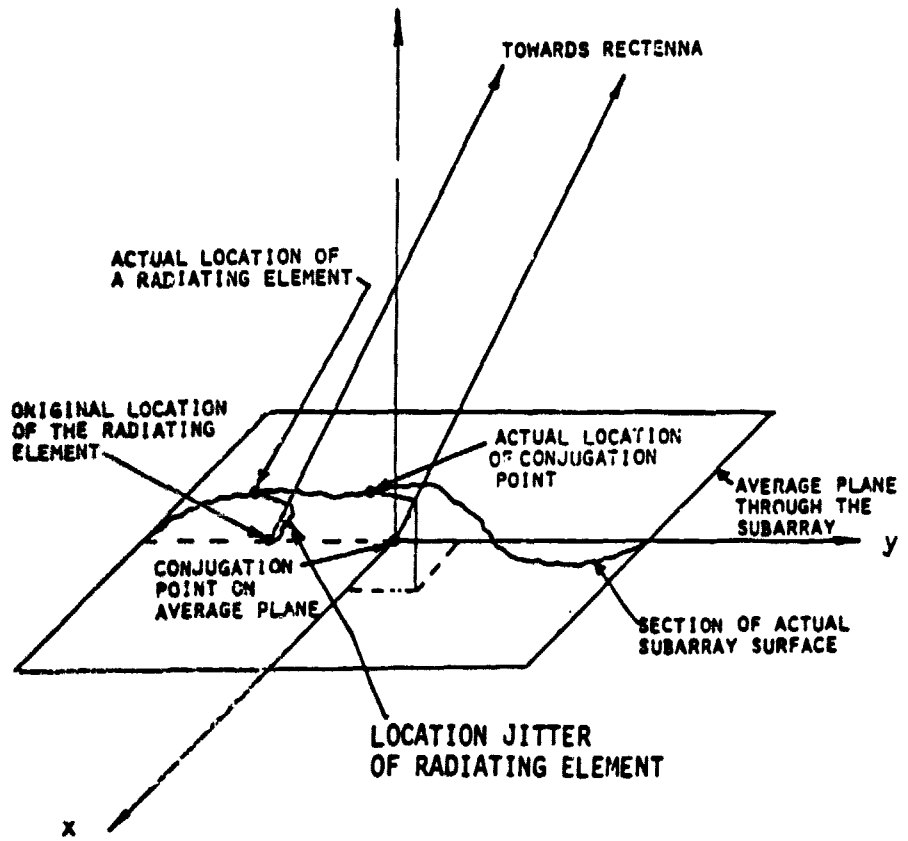

Figure 10.18. Jitters Added Due to Location Uncertainty of Radiating and Conjugation Points.

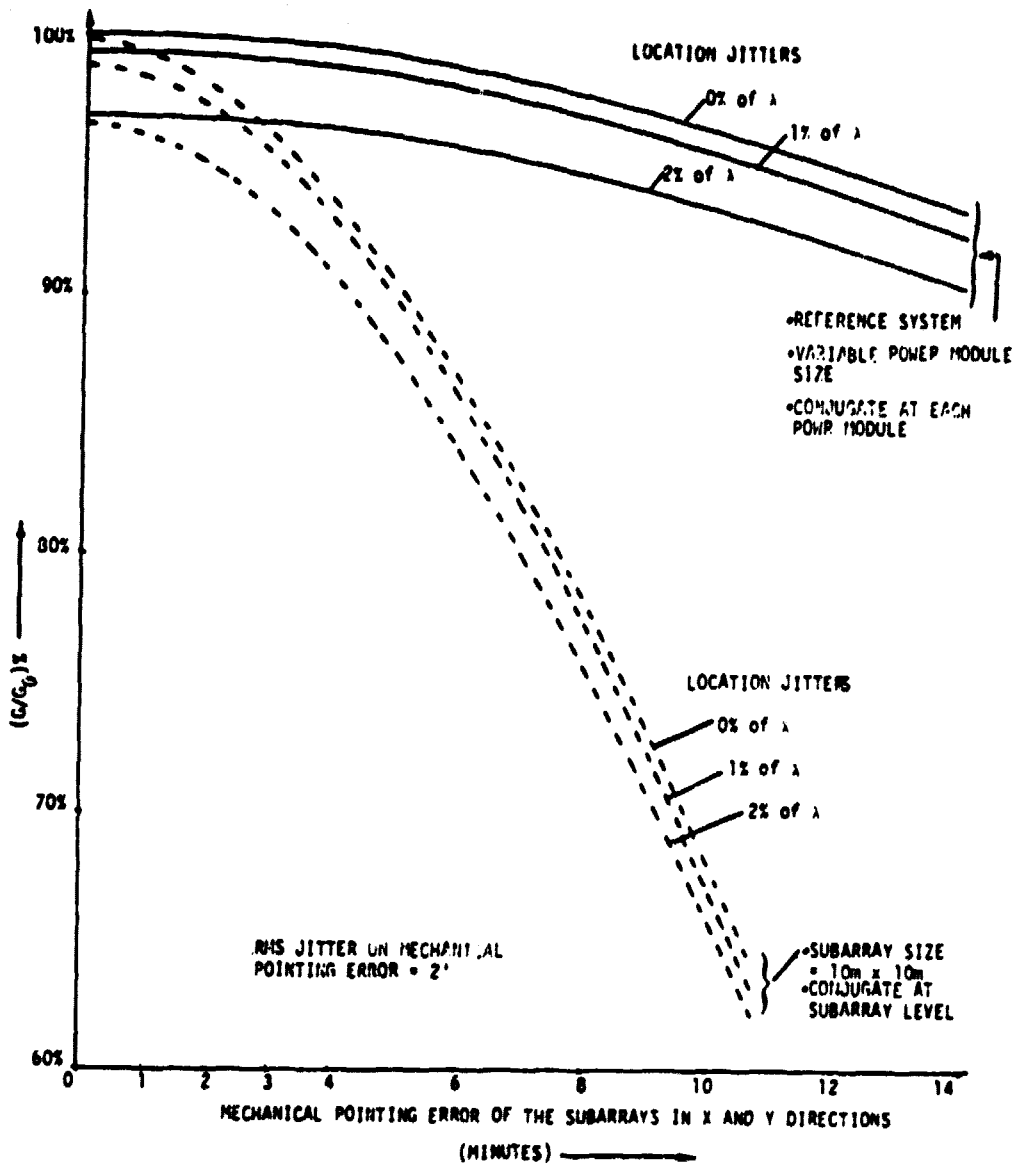

Figure 10.19. Sensitivity to Tilt Effects as a Function of Phase Conjugation Level.

in equation (8.5) is approximated by $\phi_c(0,2\pi)$ and θ_c(0,main lobe + 5 sidelobes). The second part computes the isotropic part of the power pattern and multiplies it with the 'constant' shown in equation (8.5). Notice that the constant is hand computed with H to be $\phi_c(0,2\pi)$ and $\theta_c(0,\pi/2)$. Addition of these two parts gives the total radiated power. The important thing to notice is

$$\text{(isotropic term)} \int_{\phi=0}^{2\pi} \int_{\theta=0}^{\pi/2} \sin\theta d\theta d\phi \;>>\; \text{(isotropic term)} \int_{\phi=0}^{2\pi} \int_{\theta_c(5B.L.)} \sin\theta d\theta d\phi \tag{10.3.1}$$

or

$$\int_{\phi=0}^{2\pi} \int_{\theta=0}^{\pi/2} \sin\theta d\theta d\phi \;>>\; \int_{\phi=0}^{2\pi} \int_{\theta_c(5B.L.)} \sin\theta d\theta d\phi \tag{10.3.2}$$

The computer program computes the received power and the total radiated power as described above and their ratio gives the efficiency. This efficiency is plotted against the total rms phase error in Figure 10.20.

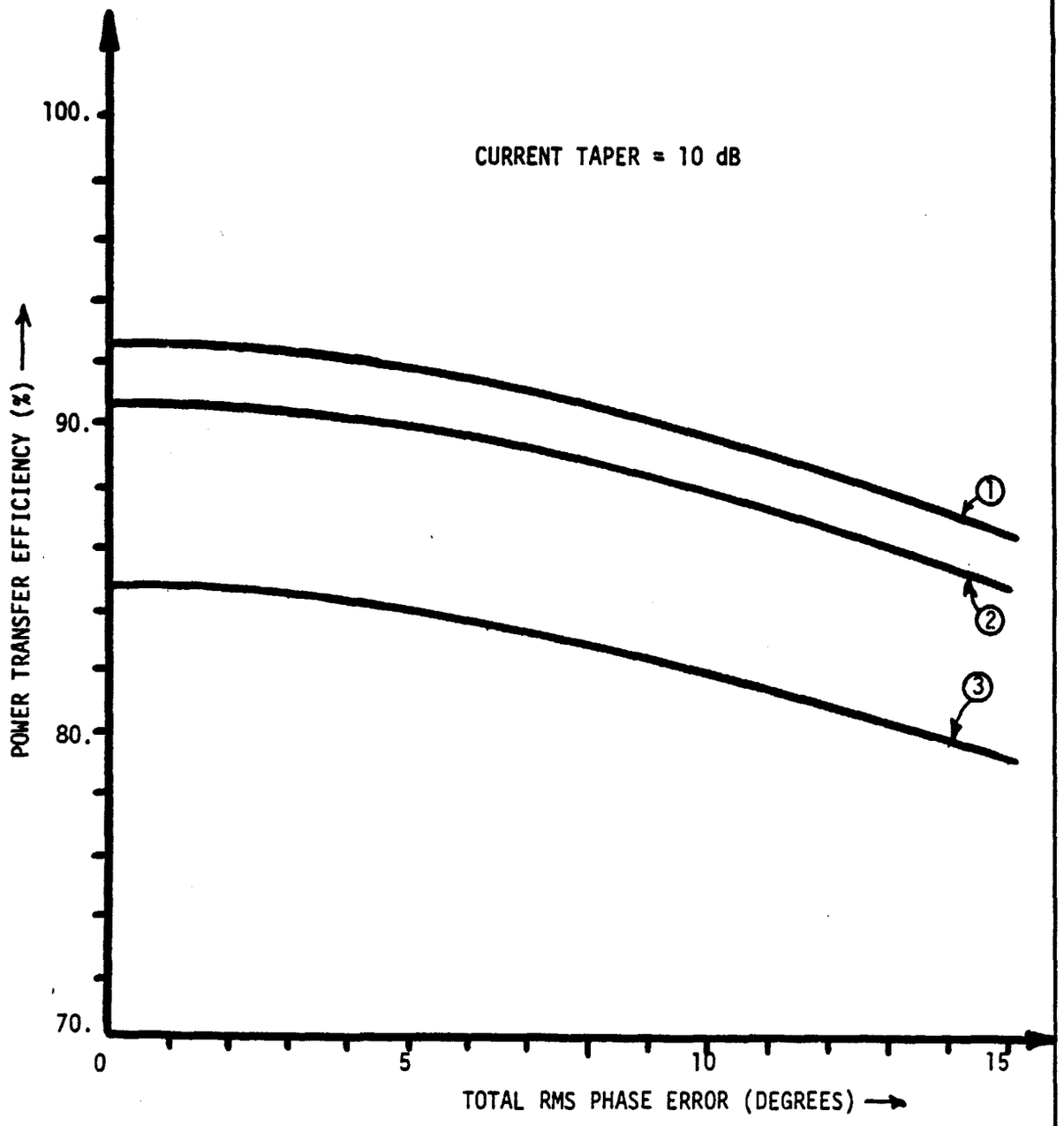

LEGEND

① MECHANICAL POINTING ERROR (MPE) = 0, LOCATION JITTER (LJ) = 0, JITTER ON MECHANICAL POINTING = 0

② MPE = 10', LJ = 0, JITTER ON MPE = 2'

③ MPE = 10', LJ = 2% of λ, JITTER ON MPE = 2'

Figure 10.20. Curves of Power Transfer Efficiency vs Total RMS Phase Error.

10.4 Observations and Improvements

The first observation one makes from Fig. 10.20 is that the efficiency of the system is below 95% even with no phase errors present as indicated by curve (1) . At a phase error of 10° rms, the efficiency drops to about 90% with no other error present. The following suggestions are made to increase the efficiency:

a. Put more conjugators in each subarray (increase in efficiency would be minimal).

b. Use radiators with more directivity instead of dipoles (slots).

c. Increase the size of the rectenna.

REFERENCES

1. Lindsey, W. C., "A Solar Power Satellite Transmission System Incorporating Automatic Beam Forming, Steering and Phase Control," prepared for NASA/JSC, June, 1978, LinCom Corporation, Pasadena, CA.

2. Hansen, R. C., Microwave Scanning Antennas, Part II and Part III, Academic Press, New York, 1966.

3. Chernoff, Ralph C., "Large Active Retrodirective Arrays for Space Applications," Jet Propulsion Laboratory Report, October 31, 1977.

4. Lindsey, W. C., Synchronization Systems in Communication and Control, Prentice-Hall, Inc., Englewood Cliffs, NJ, 1972.

5. "Microwave Power Transmission System Studies, Vols 1-4," prepared for NASA/Lewis Research Center by Raytheon Company, NAS 3-17835, December 1975.

6. "Solar Power Satellite System Definition Study, Vols. 1-6," prepared for NASA by Boeing Company, NAS 7-15636, December 1977.

7. Lindsey, W. C., and Simon, M. K., Telecommunication Systems Engineering, Prentice-Hall, Inc., Englewood Cliffs, NJ, 1973.

8. Lindsey, W. C., and Kantak, A. V., "Automatic Phase Control in Solar Power Satellite Systems," Prepared for NASA/JSC, TR-7809-0977, September 1977, LinCom Corporation, Pasadena, CA.

9. Lindsey, W. C., and Kantak, A. V., "SPS Phase Control System Performance via Analytical Simulation," Prepared for NASA/JSC, February, 1979, LinCom Corporation, Pasadena, CA.

10. Booth, R. W. D., "Two Frequency Technique for Retrofire Arrays," LinCom Memo SPS-77-RWB-1, December 9, 1977. Also see Appendix 1.

11. Steinberg, B. D., Principles of Aperture and Array System Design, John Wiley and Sons, NY, November 1975.

APPENDIX I

ANALYSIS OF THE TWO-FREQUENCY PILOT SIGNAL CONCEPT AND AMBIGUITY RESOLUTION

As we saw above, the necessary evil of frequency separation in the single frequency separation in the single frequency conjugation scheme introduces the phase correction necessary and that necessitates the computer. Besides there is a question of feasibility and accuracy of such a system. There exists, however, an easier way to circumvent the frequency separation problems. Consider an array of transponders located at positions $\vec{R}_0, \vec{R}_1, \ldots, \vec{R}_N$ relative to the location of the pilot transmitter. A carrier $u_T(t) = e^{j\omega t}$ emitted by the pilot is received at the $i^{\underline{th}}$ transponder. This received signal is $e^{j(\omega t + 2\pi \cdot |\vec{R}_i|/\lambda)}$. The amplitude factor has been neglected for the sake of this illustration. The net phase shift accumulated by the signal in traversing the distance $|R_i|$ is $2\pi|R_i|/\lambda$. The complex conjugate circuit conjugates the amplitude factor $e^{j2\pi \cdot |\vec{R}_i|/\lambda}$ and the reradiated signal is $e^{j(\omega t - 2\pi|\vec{R}_i|/\lambda)}$. This reradiated signal is received at the pilot location. This signal is $e^{j(\omega t - 2\pi|\vec{R}_i|/\lambda + 2\pi|\vec{R}_i|/\lambda)} = e^{j\omega t}$! This is independent of the location R_i. Thus the signal received at the pilot tone location is the same for <u>any</u> transponder location. Since the reradiated signals from each transponder are all in phase at the pilot transmitter location then the power is maximized

and the peak of the array beam is in exactly the same direction as the pilot tone transmitter location.

Consider now the case where the down link frequency is $\omega_0 \neq \omega$. Then the reradiated signal is $e^{j(\omega_0 t - 2\pi|\vec{R}_i|/\lambda)}$ and the received signal is $e^{j(\omega_0 t - 2\pi|\vec{R}_i|/\lambda + 2\pi|\vec{R}_i|/\lambda_0)}$. The phase is $-2\pi|\vec{R}_i|(1/\lambda - 1/\lambda_0)$. Since $\omega \neq \omega_0$, $\lambda \neq \lambda_0$ and now the phase does depend on $|R_i|$. Now the beam does not peak in the direction of the pilot signal. Note that $-2\pi|\vec{R}_i|(1/\lambda - 1/\lambda_0) = -2\pi|\vec{R}_i| \cdot (\omega - \omega_0)/c$ The amount of the phase shift is proportional to the difference in frequency between the uplink and the downlink. This suggests that if two frequencies were used for the uplink, $\omega_0 = \omega_0 + \Delta\omega$ and $\omega_2 = \omega_0 - \Delta\omega$, then the phase shift for each frequency could be measured and the two phase shifts could be summed and divided by two. This average phase shift is just the phase shift that will be undergone on the downlink carrier with frequency ω_0.

Phase shift at $\omega = \omega_1 \triangleq \omega_0 + \Delta\omega = \frac{2\pi}{c} |R_i| (\omega_0 + \Delta\omega)$

Phase shift at $\omega = \omega_2 \triangleq \omega_0 - \Delta\omega = \frac{2\pi}{c} |R_i| (\omega_0 + \Delta\omega)$

Average is $\frac{2\pi|R_i|}{c} [(\omega_0 + \Delta\omega) + (\omega_0 - \Delta\omega)]/2$

$= \frac{2\pi|R_i|}{c} \omega_0$

= phase shift on downlink

The phase shift on the two frequencies is measured and averaged. This phase shift is added to a carrier at the center frequency $\omega_0=(\omega_1+\omega_2)/2$. At this point the remaining operation is the same as an ideal Van Atta array, i.e., the complex conjugate of the signal formed and this signal is reradiated. This operation is illustrated in Figure I.1 The uplink signal is

$$r(t) = d(t)[\cos(\omega_1 t+\theta_1)+\cos(\omega_2 t+\theta_2)] \qquad (I.1)$$

where $\omega_1=\omega_0+\Delta\omega$, $\omega_2=\omega_0-\Delta\omega$, $\theta_1 = \frac{2\pi}{c}|R_i|(\omega_0+\Delta\omega)$, $\theta_2 = \frac{2\pi}{c}|R_i|(\omega_0-\Delta\omega)$ and d(t) is some data.

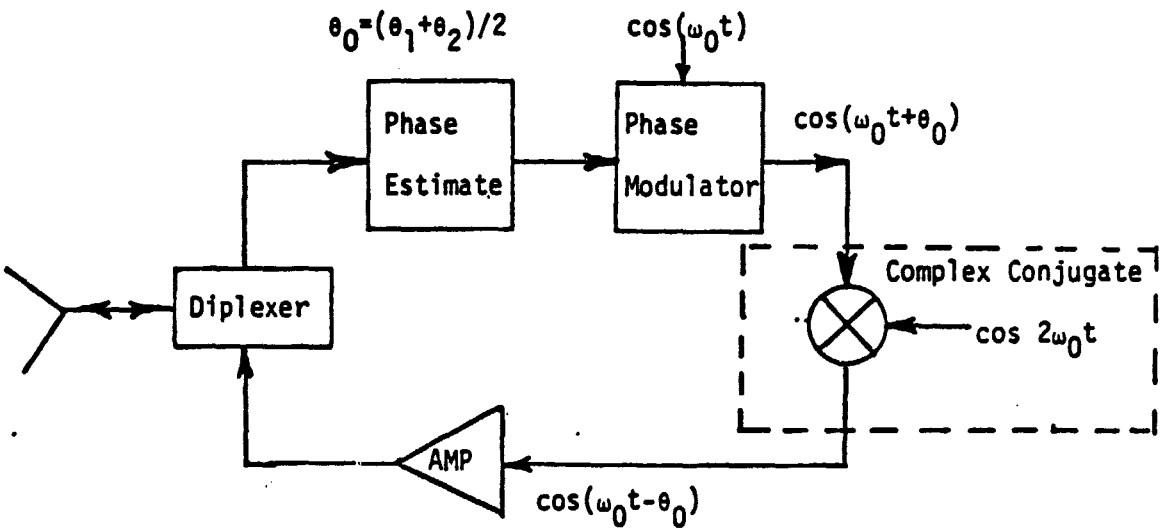

Figure I.1. Block Diagram of Two Frequency Phase Estimation and Conjugation Transponder.

The problem of performing the phase estimation and phase modulation may be solved fairly easily. A circuit that performs this is illustrated in Figure I.2.

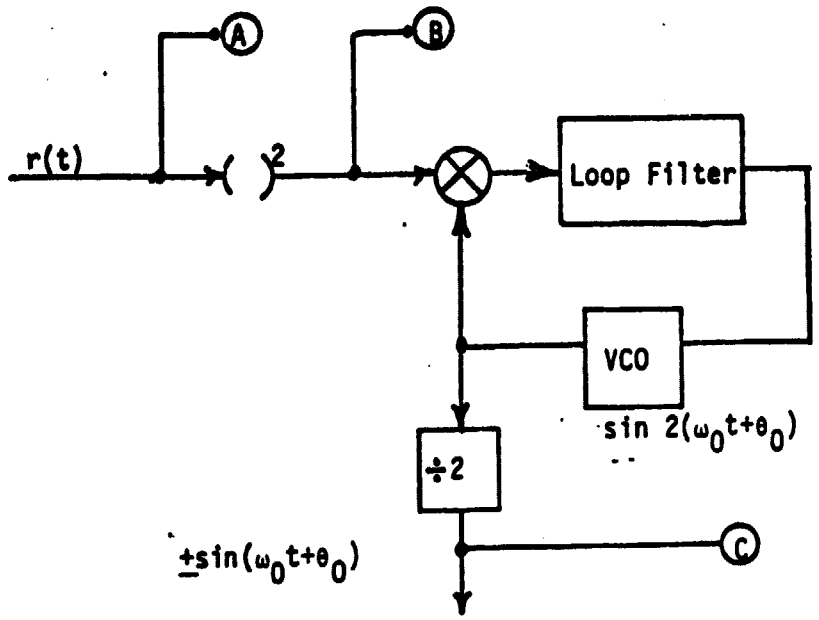

Figure I.2. Phase Estimator and Modulator Circuit.

This circuit operates as follows:

$$x(t) = r^2(\ ) = [\cos(\omega_1 t+\theta_1)+\cos(\omega_2 t+\theta_2)]^2$$

$$= \cos^2(\omega_1 t+\theta_1)+\cos^2(\omega_2 t+\theta_2)+2\cos(\omega_1 t+\theta_1)\cos(\omega_2 t+\theta_2) \quad (I.2)$$

The desired signal is contained in the product terms

$$2\cos(\omega_1 t+\theta_1)\cos(\omega_2 t+\theta_2) = \cos 2(\Delta\omega t+\Delta\theta)+\cos 2(\omega_0 t+\theta_0) \quad (I.3)$$

where $\Delta\theta = \frac{2\pi}{c}|\vec{R}_1|\Delta\omega$ and $\theta_0 = \frac{2\pi}{c}|\vec{R}_1|\ \omega_0$. The second term is tracked by the phase locked loop. The PLL output is $\sin 2(\omega_0 t+\theta_0)$. This is frequency divided by two in a frequency divider. The output is $\pm\sin(\omega_0 t+\theta_0)$. Except for the $\pm(0°\text{-}180°)$ phase ambiguity due to the divide by two circuit this signal is exactly the desired signal. It has the correct center frequency $\omega_0 = (\omega_1+\omega_2)/2$ and

the same phase shift $\theta_0 = 2\pi|R_1|\omega_0/c$ that would have occurred if the uplink signal was a single sinusoid at frequency ω_0. One serious problem remains to be solved. The divide by two results in a 0°-180° phase ambiguity. This is a potentially disastrous situation since phase reversals represent cancellation of signal power and thus result in a serious deterioration in array performance. This phase ambiguity may be resolved by the following circuit which is connected to points A, B and C in Figure I.2.

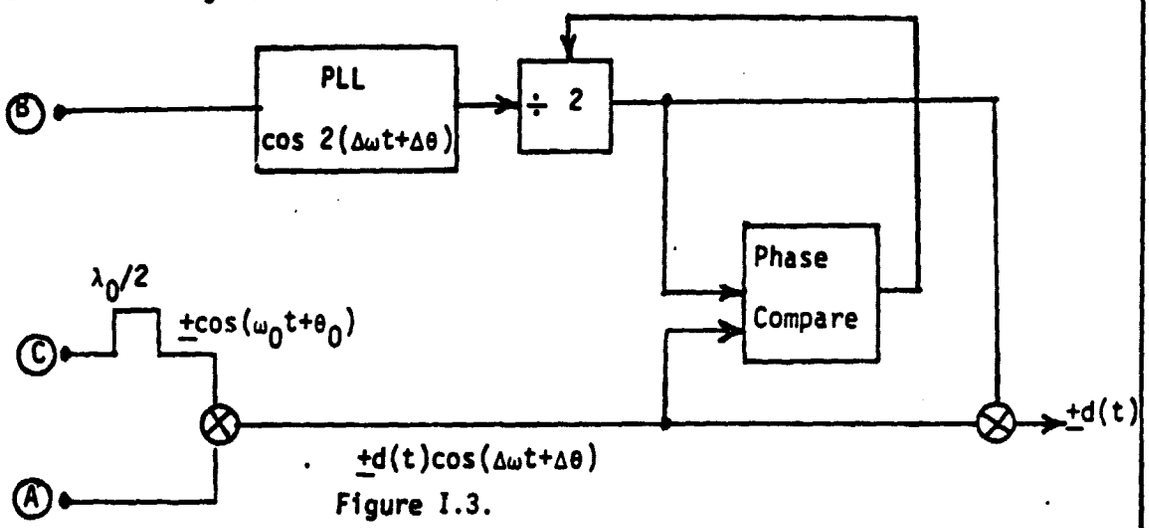

Figure I.3.

The circuit works in the following fashion. At point C is available the reference $\pm\sin(\omega_0 t+\theta_0)$ will contain the 180° phase ambiguity. This is delayed by $\lambda_0/2 \rightarrow 90°$ to get $\pm\cos(\omega_0 t+\theta_0)$. This is multiplied by the input from point (A). The result of this multiplication is $\pm d(t)\cos(\Delta\omega t+\Delta\theta)$. This contains the data on a carrier at the difference frequency. This signal contains the 180° phase ambiguity. At point (B) is the second harmonic of this carrier which is the first term in equation (I.3). This

component is removed using the PLL. The output of this PLL is frequency divided by two to give $\pm\cos(\Delta\omega t+\Delta\theta)$ where the $\pm$ indicates another 180° phase ambiguity due to this second divider. These ambiguities may now be resolved using the data d(t). This is a two step acquisition procedure. First d(t) = +1, for a fixed period of time. During this time the output $\pm d(t)\cos(\Delta\omega t+\Delta\theta)$ is compared with $\pm\cos(\Delta\omega t+\Delta\theta)$ at the output of the divide by two. These two signals are compared to determine whether or not they are in phase or out of phase. This is used to resolve the ambiguity in the circuit of Figure I.3. The phase compare circuit is relatively straightforward and is illustrated in Fig.I.4 below. Thus the output of the

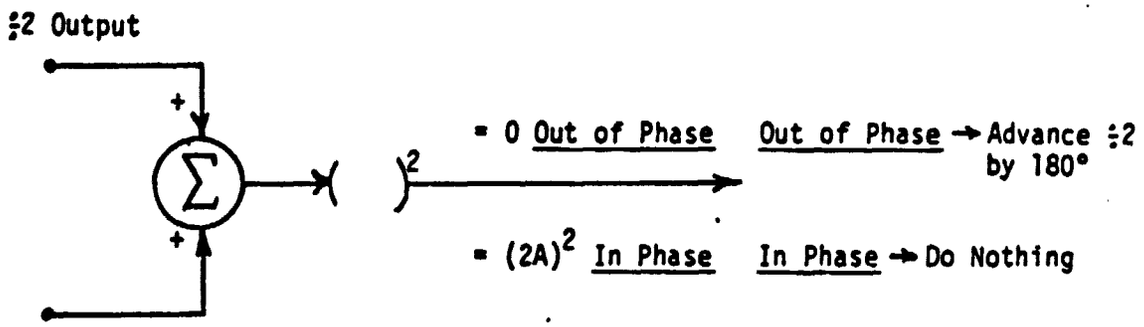

Figure I.4.

PLL/÷2 combination can be phase correctly with the data bearing signal. This signal is now used to demodulate d(t) as illustrated in Fig. I.3. The data is now modulated with a sequence of 1's and -1's. If the number of 1's is different than the number of -1's over a given interval of time then the number of 1's may be counted and used to resolve the final phase ambiguity in the divider in Figure I.2.

The squaring type of circuit in Fig. I.2 contains a divider that is probably impossible to implement at microwave frequencies. A Costas loop may be used instead which eliminates both the squarer and the divider. This removes one problem but introduces the problem of differential phase shift in the two arms of the Costas loop. Either one of these circuits must operate on the entire range of frequencies of interest, i.e., (ω_1, ω_2). This includes the center frequency and thus the possibility exists for leakage of ω_0 terms from the antenna back through the diplexer to the receiver. This isolation question is crucial to the operation of these circuits. A notch may need to be inserted at the center frequency.

APPENDIX II

SURVIVABLE TOPOLOGICAL CONFIGURATIONS FOR THE SPS PHASE CONTROL SYSTEM

Introduction

The object of this appendix is to apply the mathematical theory of graphs and topology to the problem of evaluating the reliability and survivability of the SPS Phase Control System due to failures. Graceful degradation in the power transmitted is required as failures occur in the Phase Control System. In doing so the cable lengths, number of connectors, etc. will be minimized for an a priori specified connectivity resulting from failures of parts in the Phase Control Centers and/or the Power Amplifiers and interconnecting cables. It is one purpose of this report to develop optimum survivable topological configurations which conform to a set of prescribed performance and structural measures. It is desirable to derive PCC and PA configurations which require the least overall cable length while attaining a properly low value of m = minimum number of cable pieces and connectors.

The synthesized PCC and PA configurations are required to be survivable to a specified degree when failures occur. These configurations should perform effectively under failures of certain PCCs and/or PAs or interconnecting cables. We will measure the survivability of the Phase Control System in terms of its invulnerability to PCC and/or PA failures, i.e., we required graceful degradation of power transmitted as a function of failures in the Phase Control System. We note that the resulting survivable PCCs and/or PAs are always invulnerable to cable failures. A variety of PCC/PA configuration invulnerability measures will be used including deterministic and probabilistic invulner-

ability measures. The results produced include the ability to predict PCC and PA interconnectivity so as to optimize power output as a function of failures in the SPS Phase Control System.

In what follows a more detailed discussion of the above concepts is given. This is followed by a few examples with recommendations for further investigation.

II.1 Topological Structures and Performance Configurations

The SPS reference phase distribution systems can be modeled from a topological configuration point of view, as follows.

Each amplifier node (containing the associated radiation antenna and other processing elements) is taken to be a node (vertex) in an underlying graph. We thus identify (n-1) nodes,

$$V_R = \{v_1, v_2, \ldots, v_n\} .$$

We also include in the graph a central node, denoted v_c or v_1.

The central node v_c distributes phase information to the "regular" nodes called Phase Control Centers (Refs.1,2). Each regular node must be able to obtain this "reference" phase information for it to effectively survive. A similar situation will exist for the power amplifiers.

To distribute phase information from the central (master) node to all others, one must connect by "cables" the regular and central nodes. A cable connection between node v_i and node v_j is designated by a line, denoted (v_i, v_j) or (i,j), or e_{ij}. The collection of nodes $V = \{v_i, i=1,\ldots,n\}$ and of lines E connecting them,

$$E = \{e_{ij}, i, j-1, \ldots, n\},$$

form the underlying graph $G = (V,E)$. This graph describes the pure topological structure of the network constituting the PCCs and the cables interconnecting them.

To incorporate geographical distances into the topological description of the antenna network, we generate the weighted graph G_W,

$$G_W = (V,W) \quad .$$

Here we have described the line connections by a distance matrix W, where

$$W = \{\omega_{ij},\ i,j=1,2,\ldots,n\}$$

and

ω_{ij} = distance from v_i to v_j, if they are connected

= ∞, otherwise.

Thus, W describes the network line connections as well as the associated distances of the connections.

It is the purpose of our study to develop optimal survivable topological configurations G_W, which conform to a set of prescribed performance and structural measures. The latter constitute a proper set of constraints to be incorporated in the tree synthesis procedure. We outline in the following, the major such topological constraints.

II.1.1. Number of Lines and Overall Distance Measures

The overall number of lines in the underlying graph is denoted by m. Thus, m represents the number of cable pieces used. Furthermore, since each cable piece is connected at its ends to two nodes, then 2m is equal to the number of connections (and connectors) used in the system.

It is therefore of interest to develop a survivable topological configuration which will have the minimal number of lines (minimum m) and thus the minimal number of cable pieces and connectors (as well as local connections).

If the cable pieces to be used in the network are generally of equal (or nearly equal) length, the number of lines m also represent the overall length of cables used in the system. Minimizing m, would thus also entail the utilization of the minimum overall cable length.

If cable pieces are of varying actual lengths, the overall cable length is given by

$$|W| = \sum_i \sum_j w_{ij}$$

It is then desirable to derive a network configuration which requires the least overall cable length $|W|$, while attaining a properly low value of m = minimum number of cable pieces and connectors.

II.1.2. Survivability, Invulnerability and Connectivity Measures

The synthesized tree network is required to be survivable. The tree network should perform effectively under the failures of certain regular nodes or lines. Node failure impose more serious effects on the network performance. They are also more liable to occur (than line-cable-failures) in our situation. We will thus measure the survivability of the network configuration in terms of its invulnerability to node failures. We will note that the resulting survivable networks are always also invulnerable to line failures.

A variety of tree network invulnerability measures can be utilized They can be classified into two general classes: deterministic and probabilistic invulnerability measures. We will mention here a set of deterministic and probabilistic connectivity measures which are proper for the tree network.

Network Connectivity Measure.

A network of PCCs or PAs is said to be k-connected if and only if the network remains connected under the failure of (k-1) or less nodes; k=1,2,... .

A network is said to be connected if and only if there exists an least one path between any two nodes; thus, any two nodes can "communicate" to one another phase information.

It can be shown that if a network is k-connected then there exists at least k (vertex disjoint) paths between any pair of nodes v_i and v_j. Thus, there exist at least k paths between v_i and v_j which have in common only nodes v_i, v_j. Then, upon the failure of any node and its associated path, the remaining paths could be used for intercommunication between the corresponding terminal nodes.

For our phase distribution network, a k-connected topological configuration ensures at least k (vertex disjoint) paths between the central node and any regular node. Subsequently, the central node can communicate its phase information to any regular node even if (k-1) or less other regular nodes have failed.

Note that a 1-connected network can assume a tree structure (having no cycles). Upon the failure of any single regular nodes, certain nodes become disconnected from the center of the tree.

A 2-connected network can be realized by a cycle structure.

We will show how k-connected networks with minimum number of lines, any $k \geq 1$, satisfying certain prescribed topological constraints can be developed.

A Probabilistic Connectivity Measure.

We can regard node failures as a random phenomena. The latter is then statistically characterized by the joint distribution of failure events associated with the network nodes.

For example, one can assume node i failure to be statistically independent of node j failure, $i \neq j$, with a given probability ϕ_i that node i will fail within a certain period of time.

A proper probabilistic invulnerability measure would then be given by ρ, where:

$$\rho = \min_{i:\ i \geq 2} \Pr\{\text{node } v_i \text{ is connected to the center}\} .$$

Thus, if a network G has $\rho(G) = \rho$, then the probability that a regular node will be connected to the center is not smaller than ρ; it will be disconnected from the central node with a probability not higher than $1-\rho$.

We will show how measure ρ can be computed and incorporated into the topological design.

II.1.3. Nodal Degree Constraints

The degree of a node is defined as the number of lines (cables) connected to this node.

Practical considerations impose actual constraints on the degree of a regular node, as well as on the (usually higher) degree of the central node. In our development of optimal topological configurations, we will incorporate these important degree constraints.

We note that if a network is k-connected, the degree of each node must be at least equal to k; i.e.,

$$\deg(v_i) \geq k, \quad \text{each } i.$$

It is generally desirable to synthesize the antenna topology such that every regular node will have a degree not much higher than k,

$$k \leq \deg(v_i) \leq k + N_k, \text{ each } i \geq 2, \text{ some } N_k \quad .$$

The central node should have a degree not higher than some constraint b, b > k,

$$k \leq \deg(v_c) \leq b \quad .$$

Note that if all network nodes have a degree equal to ℓ, $\ell \geq k$, then the network has a number of lines m equal to

$$m = \frac{1}{2} \ell n,$$

where n is the number of nodes in the network. Thus, increasing nodal degrees, clearly induced an increase in the network number of lines m. Also, increasing the network connectivity k, implies higher values for nodal degree, and a higher number of network lines m, as

$$m = \frac{1}{2} \sum_{i=1}^{n} \deg(v_i) \quad .$$

Such considerations will be an integral part in our topological studies.

II.1.4. Network, Radius and Radius-Stability Constraints

The length of a network path is defined as the number of lines included in this path.

The distance $d(v_i,v_j)$ between node v_i and node v_j, $i \neq j$, is defined as the length of the shortest path between v_i and v_j.

The diameter d = d(G) of network G is defined as the length of the longest distance between any two nodes; i.e.,

$$d = d(G) = \max_{i,J} d(v_i,v_j) \quad .$$

For our antenna network, we are interested in defining the following radius $r = r(G)$ measure:

$$r = r(G) = \max_{i:\, i \geq 2} d(v_i, v_1) .$$

Thus, for our centralized network G, the radius r(G) is equal to the maximal distance of any regular node from the central node.

The phase information distributed from the central node to the regular nodes across the network cables, experiences phase delays along each cable. To limit the overall phase delay experienced by the phase stream, we need to limit the lengths of the paths used for its distribution. Thus, we impose a constraint on the maximal radius of the topological structure:

$$r(G) \leq r_0,$$

for same proper r_0 value. Subsequently, any phase message between the central node and any regular node, is routed through a path not longer than r_0 cables (lines).

One can also incorporate actual geographical distances to define the above mentioned radius, diameter and distance measures.

Furthermore, from the viewpoint of graceful degradations of efficiency under failures, it is important to derive a topological structure which is radius-stable. For such a configuration, upon the failure of (k-1) nodes, or less, the radius of the antenna remains unchanged, or just changes by not more than a prescribed value. Thus, upon failures of certain nodes in the antenna network, we not only provide that it remains connected, but also prevent the new distances between any regular node and the center from increasing arbitrarily. Subsequently, as nodes fail, the remaining nodes are still able to

receive phase information which does not contain much extra phase delays.

We note that in making the PCC/PAs k-connected we have designed a topological structure which sets (at least) k (vertex disjoint) paths between v_c and any regular node. To make the network k-connected and radius-stable, we will also constrain the latter k paths to be not (much) longer than the prescribed network radius r_0. In this way, we will be able to provide acceptable phase distortions even under nodal failures.

We have recently developed new procedures and graph theoretical techniques, for the synthesis of optimal survivable topological structures applicable to PCC and PA layouts. We will extend these results and techniques to apply to the present problem and thus obtain the desirable optimal survivable topological configurations for the SPS phase control system.

In the following we illustrate the underlying topological design problem by presenting various optimal topologies of interest. As noted these structures will be extended and applied to satisfy other more general constraints that might be incorporated into the antenna network design problem.

II.2 The Reference Phase Distribution Network and the Graph Adjacency

In the performance analysis of the reference phase distribution network, the following connectivity matrix has been defined:

$$F = \{F_{ij}, i,j = 1,2,\ldots, n\}$$

where F_{ij} is a submatrix (row vector) of order 1xn, defined as

$$F_{ij} = \{0,0,\ldots,0\} \quad \text{if } i \neq j, \text{ each } i,j ,$$

$$F_{ii} = \{a_{i1}, a_{i2}, \ldots, a_{in}\} , \text{ each } i ;$$

where, for $i \neq j$:

$$a_{ij} \triangleq \begin{cases} 1, & \text{if vertex } v_i \text{ is connected by a line to vertex } v_j \\ 0, & \text{otherwise} \end{cases}$$

and

$$a_{ii} \triangleq 0 \ .$$

Thus, row vector F_{ii} represents the connections made between node v_i and all other nodes. Matrix F subsequently describes the topological structure of the cable network interconnecting the power amplifiers (nodes).

Clearly, for the sole sake of the network topological description, matrix F can be reduced to the adjacency matrix of the underlying graph.

For a graph $G = (V,E)$, with set of nodes $V = \{v_1,\ldots,v_n\}$ and set of lines $E = \{e_1,\ldots,e_m\}$, the <u>adjacency matrix</u> A is defined by

$$A = \{a_{ij}, i,j = 1,\ldots,n\} \ ,$$

where a_{ij} is defined as mentioned above.

Clearly, there exists a one-to-one correspondence between the matrices A and F. Given $A = \{a_{ij}\}$, we set $F_{ii} = \{a_{i1},\ldots,a_{in}\}$, $F_{ij} = \{0,\ldots,0\}$, $i \neq j$, and obtain $F = \{F_{ij}\}$. And conversely, given $F = \{F_{ij}\}$, we have F_{ii} as the $i^{\underline{th}}$ row of A:

$$A = \begin{bmatrix} F_{11} \\ F_{22} \\ \vdots \\ F_{nn} \end{bmatrix}$$

We note that the following normalized F_N matrix has been incorporated in the performance analysis:

$$F_N = \frac{F_{ij}}{F_{ij}} \quad ,$$

where

$$\frac{F_{ij}}{F_{ij}} = 0, \quad \text{if} \quad i \neq j$$

and

$$F_{ii} = \sum_{j=1}^{n} a_{ij}, \quad \text{each } i \ .$$

This induces the associated normalized adjacency matrix A_N:

$$A_N = \frac{a_{ij}}{\sum_{j=1}^{n} a_{ij}}$$

But one observes that

$$\sum_{j=1}^{n} a_{ij} = \text{number of lines connected from node } v_i = \deg(v_i) \ .$$

We can thus write:

$$A_N = \frac{a_{ij}}{\deg(v_i)} \quad , \quad \frac{F_{ii}}{F_{ii}} = \frac{F_{ii}}{\deg(v_i)}$$

We can distinguish between two main related performance analysis and design tasks.

Task A. Performance analysis and design of the antenna network, with respect to antenna radiation pattern characteristics (beam dispersion, etc.), when a proper topological configuration for the interconnection of the power amplifiers is assumed.

Task B. The design of proper survivable families of topological structures for connecting the power amplifiers.

The study described here is concerned with Task B. Incorporating the various important topological measures presented in Section II.1 we will develop survivable topologies satisfying a proper set of topological constraints.

The network designer would then be able to choose the proper survivable cable connection configuration that satisfies the desired beam characteristics, incorporating our Task B results, by incorporating the latter into his Task A performance analysis procedure.

To illustrate the significance of the synthesized topological structure, in yielding the proper measures of survivability, connectivity, number of lines, node degrees and network radius and diameter, we will present next certain optimal topological substructures.

II.3 Survivable Network Structures with Minimum Number of Lines

We have a set V of n nodes:

$$V = \{v_1, v_2, \ldots, v_n\} .$$

We wish to connect them by a graph G that is k-connected. There are many such graphs. As noted in Sec.II.1 , each k-connected graph must yield a node degree now lower than k:

$$\deg(v_i) \geq k \quad , \quad \text{each } i \quad .$$

Subsequently, the number of lines m(k,n) of a k-connected graph with n nodes must satisfy the relation:

$$m(k,n) \geq \frac{1}{2} nk \quad .$$

This lower bound is attained when all the nodes in the network have the same degree k.

In fact, it can be proved that there exists a family of graphs, to be denoted as {H(n,k)}, that attain this lower bound when nk is even. These graphs, attain the minimal possible number of lines of any n-node k-connected graph. This minimum number is given by

$$m^*(k,n) = \left\lfloor \frac{nk+1}{2} \right\rfloor ,$$

where $\lfloor x \rfloor$ denotes the integer part of x.

It can thus be seen that in a H(n,k) graph, either all nodes have degree k, or (n-1) nodes have degree k and one node has degree k+1.

The H(n,k) graphs are constructed as follows. Let the vertices of the graph now be indexed as 0,1,...,n-1. Assume $k \geq 2$.

For even k:

$$a_{ij} = \begin{cases} 1, & \text{if } |i-j| = m \pmod n,\ 1 \leq m \leq k/2 \\ 0, & \text{otherwise} \end{cases}$$

For odd k, even n:

$$a_{ij} = \begin{cases} 1, & \text{if } |i-j| = m \pmod n,\ 1 \leq m \leq k-1/2 \\ & \text{or if } |i-j| = n/2 \\ 0, & \text{otherwise} \end{cases}$$

For odd k, odd n:

$$a_{ij} = \begin{cases} 1, & \text{if } |i-j| = m \pmod n,\ 1 \leq m \leq k-1/2 \\ & \text{or if } |i-j| = n-1/2 \\ 0, & \text{otherwise} \end{cases}$$

We note that the adjacency matrix of an H(n,k) graph is constructed by following a very simple procedure. We have that A is symmetric,

$$a_{ij} = a_{ji}$$

and that

$$a_{i+1,j+1} = a_{ij} , \quad j > i ,$$

so that a-l the diagonals of A are either all 1's or all 0's. Therefore, we need to specify only the first row of A in order that all of A (and the topological structure) be specified. However, the first row of A for H(n,k) is specified simply by setting, symmetrically from both ends of the row, a total of k elements equal to 1. The elements inbetween are set equal to 0.

Example. n=7,k=4

$$A = \begin{array}{c} \\ 0 \\ 1 \\ 2 \\ 3 \\ 4 \\ 5 \\ 6 \end{array} \begin{array}{c} \begin{array}{ccccccc} 0 & 1 & 2 & 3 & 4 & 5 & 6 \end{array} \\ \begin{bmatrix} 0 & 1 & 1 & 0 & 0 & 1 & 1 \\ & 0 & 1 & 1 & 0 & 0 & 1 \\ & & 0 & 1 & 1 & 0 & 0 \\ & & & 0 & 1 & 1 & 0 \\ & & & & 0 & 1 & 1 \\ & & & & & 0 & 1 \\ & & & & & & 0 \end{bmatrix} \end{array}$$

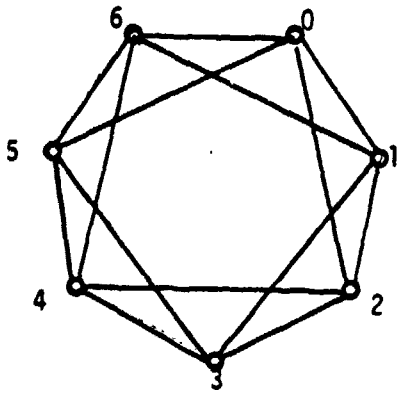

Note. Each vertex has degree k=4

Graph has number of lines $m = \frac{1}{2} nk = \frac{1}{2} \cdot 7 \cdot 4 = 14$

Graph has diameter d = 2

Graph is k=4-connected. There are 4 disjoint paths between any pair of nodes.

Examples. n=6.

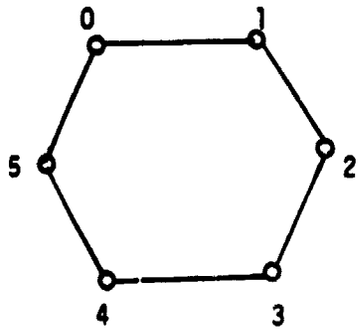

k=2

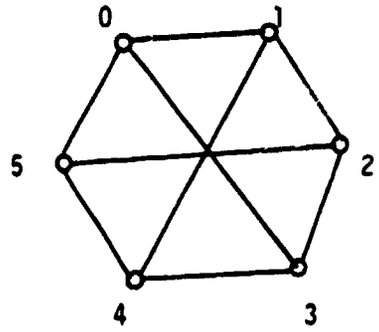

k=3

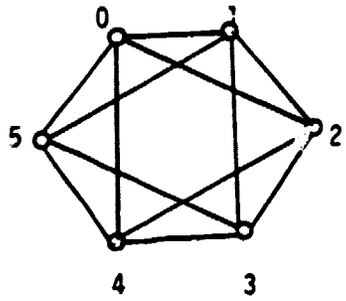

k=4

n=7

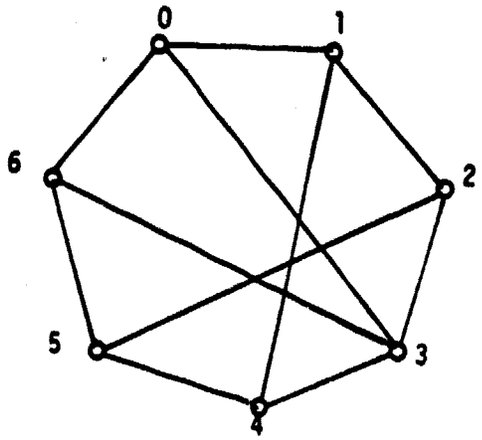

k=3

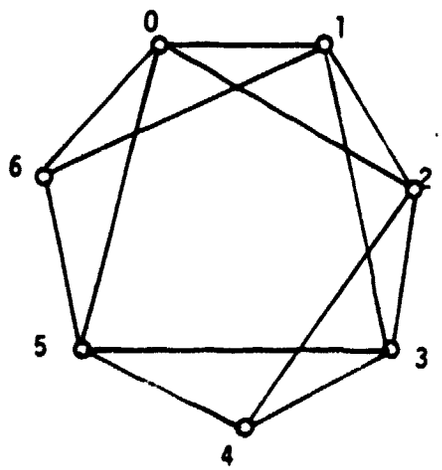

k=4

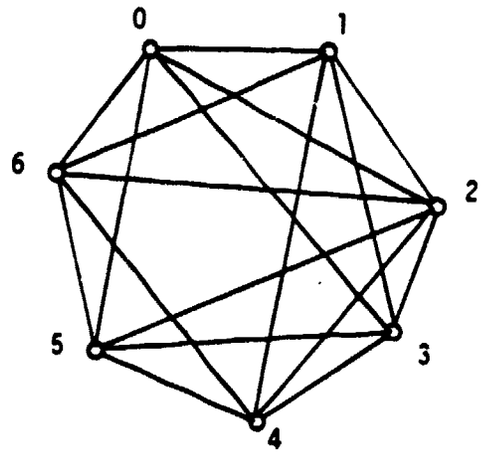

k=5

In summary, network structures H(n,k) have n nodes, are k-connected, and as such have the minimal number of lines. If nk is even, all the vertices in H(n,k) have the same degree k. If nk is odd, one vertex has degree k+1, the rest have degree k.

Example. n=7,k=3

	0	1	2	3	4	5	6
0	0	1	0	1	0	0	1
1		0	1	0	1	0	0
2			0	1	0	1	0
3				0	1	0	1
4					0	1	0
5						0	1
6							0

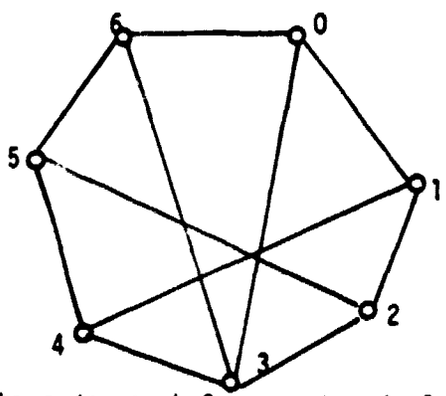

Note. All nodes have degree k=3, except node 3 which has degree k+1=4.

The graph diameter is d=2.

Example. n=8,k=4

	0	1	2	3	4	5	6	7
0	0	1	1	0	0	0	1	1
1		0	1	1	0	0	0	1
2			0	1	1	0	0	0
3				0	1	1	0	0
4					0	1	1	0
5						0	1	1
6							0	1
7								0

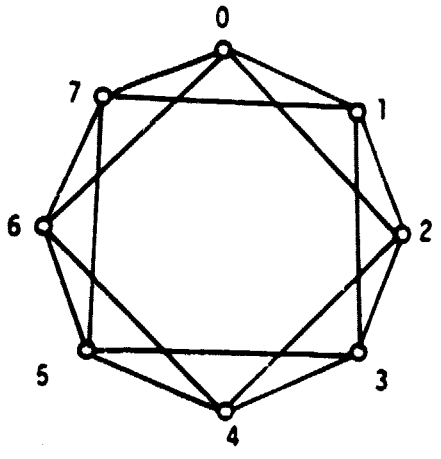

deg (v_1) = k = 4

Example. n=8, k=5

$$A = \begin{array}{c} \\ 0 \\ 1 \\ 2 \\ 3 \\ 4 \\ 5 \\ 6 \\ 7 \end{array} \begin{array}{c} \begin{array}{cccccccc} 0 & 1 & 2 & 3 & 4 & 5 & 6 & 7 \end{array} \\ \begin{bmatrix} 0 & 1 & 1 & 0 & 1 & 0 & 1 & 1 \\ & 0 & 1 & 1 & 0 & 1 & 0 & 1 \\ & & 0 & 1 & 1 & 0 & 1 & 0 \\ & & & 0 & 1 & 1 & 0 & 1 \\ & & & & 0 & 1 & 1 & 0 \\ & & & & & 0 & 1 & 1 \\ & & & & & & 0 & 1 \\ & & & & & & & 0 \end{bmatrix} \end{array}$$

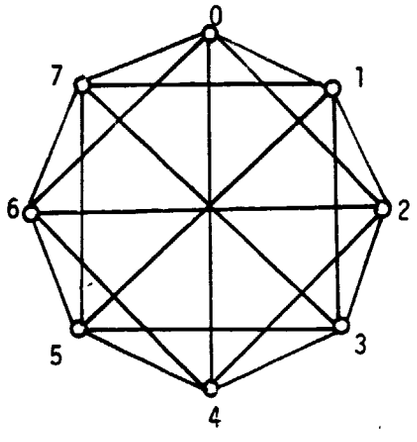

$\deg(v_i) = 5$

Graphs H(n,k) have a diameter which is proportional to n/k. This can be large for large n. Thus, such structures will require long cables for our network, and will thus be inappropriate. However, we will find that graphs H(n,k) are optimal for certain hierarchies within the global topological structure.

To obtain a k-connected topology with minimal number of lines that also incorporates radius constraints, as well as a set of central nodes, we next present the following optimal structures, recently developed and studied by us.

II.4 Reliable Centralized Topologies Under a Radius Constraint

Assume now the nodes in the network to be decomposed into two groups. The first group is that of regular nodes, V_R, the number of which is n. We require each regular node to have a degree not much higher than k, preferably not higher than k+2.

The second group is that of central nodes, V_c. Each central node is assumed to have a degree not higher than a prescribed number b, $b > k$. The number of central nodes is set to be equal to s.

We define the radius $r = r(G)$ of the network G connecting these nodes, as the longest distance of any regular node from any central node. Thus, if the SPS antenna has radius r, then

$$d_c(v) \leq r, \quad \text{for each regular node } v,$$

where $d_c(v)$ denotes the distance from regular node v to any central node.

We wish now to construct a graph which will be k-connected (reliable), have radius not larger than r, satisfy the node degree constraints, and have the minimal number of lines.

We have recently solved such problems, obtaining the following solution. For $k \geq 2$, to obtain radius r and central nodes with maximal degree b, the number s of central nodes must be at least s_0:

$$s \geq s_0 = \left\lceil \frac{n}{bs(k,r)} \right\rceil$$

where

$$s(2,r) = r$$

$$s(k,r) = \frac{(k-1)^r - 1}{k-2} \quad , \quad k \geq 3$$

It can then be shown that the topology with the minimum number of lines will then contain s_0 central nodes, and have the following topological structure.

We start from the s_0 central nodes. Each of them is then joined to the b distinct regular nodes, to form hierarchy 1 of nodes. Each of the latter is then joined to (k-1) other distinct regular nodes to form hierarchy 2. We continue in this manner until hierarchy r is reached. The resulting tree has a number of regular vertices not less than n. To obtain n regular vertices, we delete a sufficient number of groups of (k-1) end-nodes and add few more lines to obtain a graph where all regular nodes, except the end-nodes are of degree k. We have thus obtained a hierarchial tree T(n,r,k). The n_e end nodes of the tree are now joined as an $H(n_e,k-1)$ graph, which is (k-1)-connected and has minimal number of lines. The central nodes are connected together as desired. The overall graph is denoted as H(n,r,k) graph. We have shown it to virtually attain the minimal number of lines. Note that it is k-connected, has radius r and satisfies the nodal degree constraints.

The construction of an H(n,r,k) network is illustrated by the following example.

Example. H(n,r,k) graph, with s=1, single central node, r=5,k=3,b=4

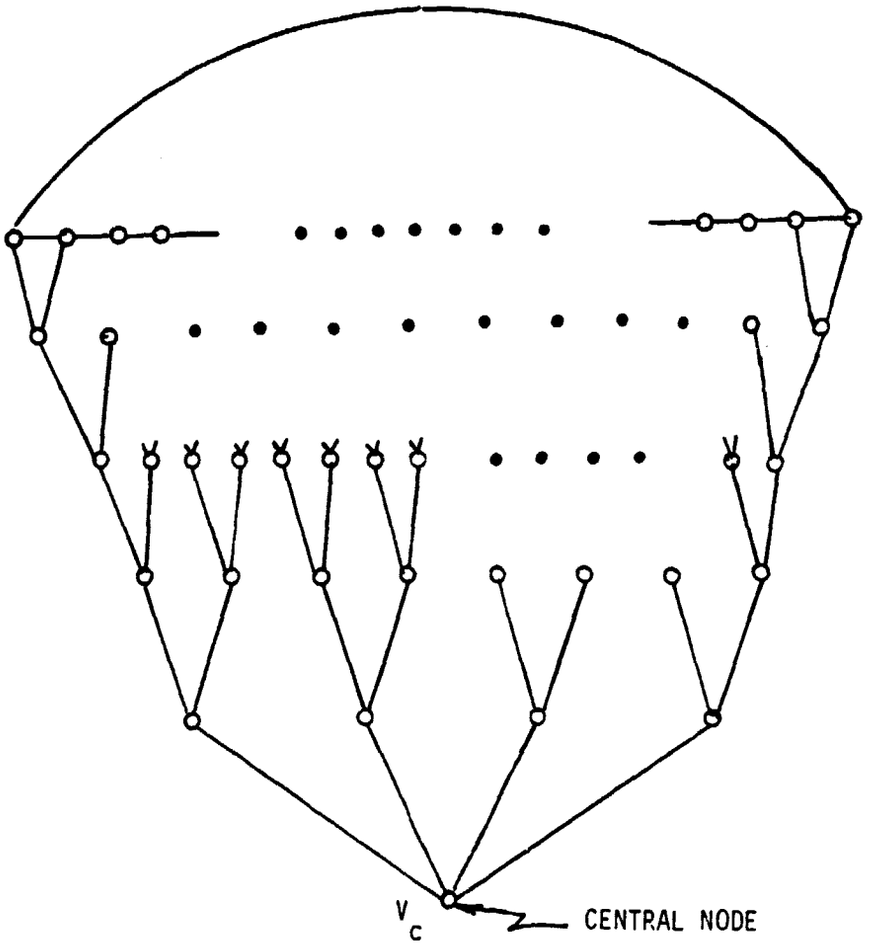

Note. •This network is k=3-connected. Between any pair of nodes there are at least 3 disjoint paths.

•In this network, every regular node can be connected to the central node through a path which contains no more than 5 lines. Network radius is r=5.

- Each regular node in this network has a degree equal to k=3, which is the minimal nodal degree for the network to be k=3-connected.
- The central node has a degree b=4, which is its specified maximal degree.

The number of lines in a H(n,r,k) network with s central nodes is noted to be given as

$$m \cong \frac{1}{2}(k(n+1)) + \frac{1}{2}s(b-k) + m_s \quad ,$$

where m_s represents the number of lines used to connect the s centers.

These H(n,r,k) topological structures and various proper extensions of them to be developed in our topological design studies, will serve as fundamental hierarchial topologies in the construccion of the desired families of survivable topologies.

II.5 Survivable Topological Structures for the Antenna Phase-Array Network

In arriving at the optimal topology for connecting the antenna center to the distributed power amplifiers, we are constrained by the existing locations ofthe amplifiers (regular nodes) and the center. Thus, we are bound by the geographical locations of the network nodes.

Subsequently, we are able to classify the network nodes into r levels, so that every node at the i-th level is at a distance of i distance units (or approximately so) from the center. Connections will generally be made in such a manner that usually a single cable piece (line in the underlying graph) will cover a single distance unit. On certain occasions, a cable piece will extend over a few distance units. Subsequently, a graph structure with minimum number of lines, satisfying the above distance structure constraints, will generally attain also the

minimal overall cable length.

To illustrate the geographical constraints, we draw again the H(n,r,k) network in the example in Section IV, incorporating now the actual geographical location of nodes, obtaining the following structure:

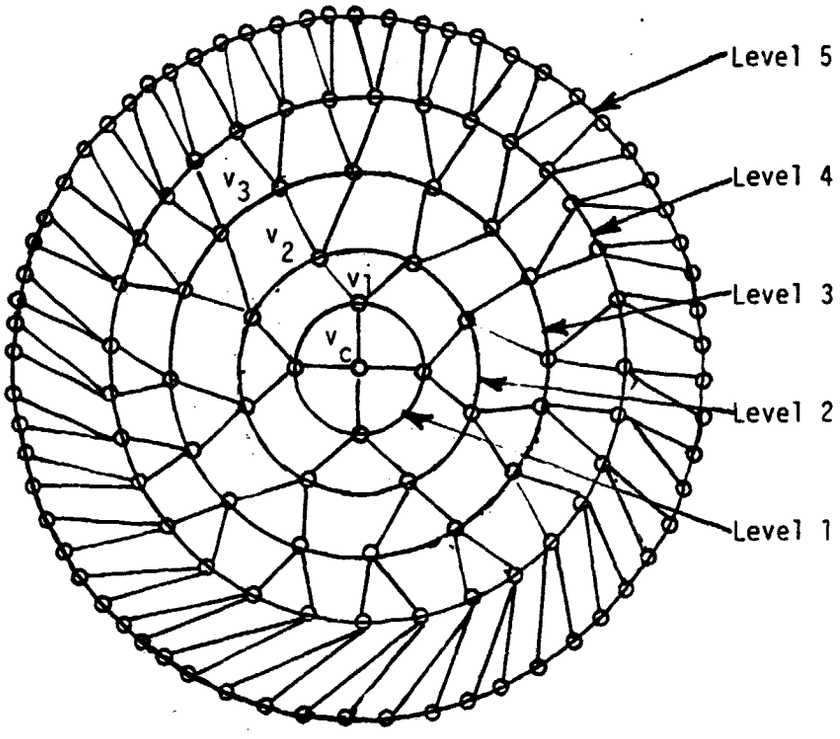

Recall that the illustrated structure is 3-connected; each node has degree 3 except the center, the degree of which is 4; it has radius 5; and it contains the minimum number of lines among all such graphs.

Of course, in the actual tree network structure the number of nodes in each level is already prescribed. This will be taken into consideration in developing the optimal structure.

The H(n,r,k) structure is k-connected, so that upon the failure of (k-1) or less nodes every remaining pair of nodes is able to communicate; and in particular, every remaining node stays connected to the center. This network has radius r, so that every node has a path not longer than r lines which connects it to the center, under no failures. However, under any failure, even though a remaining node stays connected to the center, its distance from the center will usually increase. This may induce an undesirable extra phase offset at such a node.

For example, node v_2 is at distance 2 from the center (through vertex v_1). If, however, vertex v_1 fails, node v_2 will be at a distance 9 from the center! Thus, it will have to experience a considerable possible phase offset due to the additional 7 lines in its shortest path from the center. Similarly, the distance of v_3 from the center increases from 3 to 8, upon the failure of v_2.

To prevent excessive additional phase offsets due to node failures, we need to develop topologies which are radius stable. Such structures will guarantee the distance for many node to the center to remain the same, or increase only in a restricted manner, upon certain node failures.

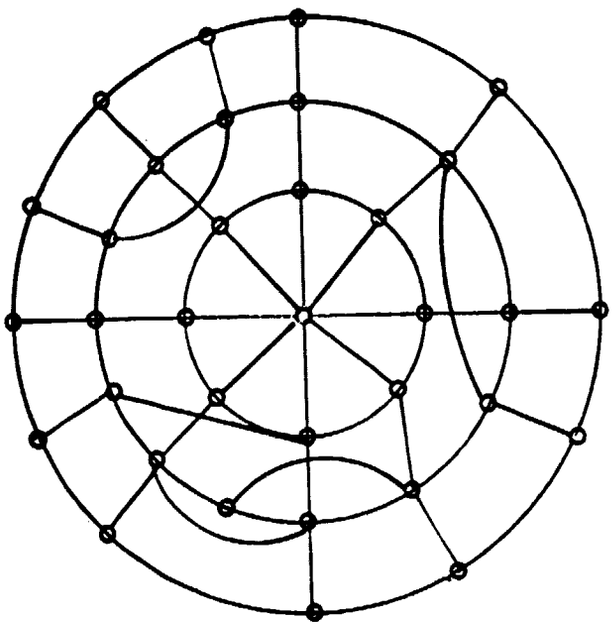

We have recently studied the topological design of radius stable reliable topologies. Results of these studies will be coupled with the considerations and results mentioned above to develop optimal tree network structures.

For example, it is possible to design topologies where certain node level assume proper H(n,k) structure, while the levels are connected approximately according to an H(n,r,k) topology. Such structures can be shown to have certain radius-stability properties.

For example, the following figure illustrates a 3-connected network structure which has certain radius stability properties. The network does not necessarily contain the minimum possible number of lines. Note that upon the failure of a node or two, the distance of a node from the center does not usually increase considerably.

II.6 Recommendations

It is our objective to incorporate the powerful methods, techniques and results mentioned here to derive optimal survivable topological tree structures for connecting the SPS phase control centers to the central (master) node and for connecting the power amplifiers.

In deriving these topologies we will impose the following topological constraints, which we have shown to be closely related to the desired phase control system performance objectives.

- Tree (deterministic and probabilistic) connectivity and invulnerability measures.
- Nodal degrees.
- Number of network lines and overall cable length measures.
- Network radius constraints and radius-stability measures.

We recommend subsequently developing families of optimal topologies satisfying the above prescribed measures. One would then be able to

incorporate these proper survivable structures in the performance analysis of the reference phase distribution tree, to conclude the associated beam dispersion characteristics. The topology yielding the desired dispersion properties could then be chosen. As such, our study will guarantee the latter to be highly reliable, highly insensitive to node failures and requiring the least amount of overall cable length and the least number of nodal connections.

REFERENCES

[1] W. C. Lindsey, "A Solar Power Satellite Transmission System Incorporating Automatic Beamforming, Steering and Phase Control," LinCom Technical Report, TR-7806-0476, June 1978.

[2] W. C. Lindsey and A. V. Kantak, "Automatic Phase Control in Solar Power Satellites," LinCom Final Report, TR-7802-0476, February, 1978.

APPENDIX III

MSTRS: A NEW METHOD OF TIME (PHASE) TRANSFER FOR THE SPS PHASE CONTROL SYSTEM

III.1 Introduction

Most time transfer systems in use today utilize MS (master to slave) mode of operation mainly because the alternate ways of achieving the time transfer such as Mutual Synchronization methods are not fully understood. Recently, there have been some attempts made to understand the mechanization of time transfer in a mutually synchronized system Refs. [1 - 3]. The steady state frequency and phase errors of the mutually synchronized systems are, as pointed out in Ref. [3], very sensitive to the path delays in the system, hence the necessity of delay compensation arises. Recently, the delay compensation is attempted in Refs. [4 - 5].

The Returnable Timing System (RTS) described in Ref. [5] is of particular interest because the delay compensation feature of this system can be combined with the MS system to create Master Slave Returnable Timing System (MSRTS), described in this paper to combine the advantages of MS as well as RTS configurations. MSRTS uses the basic MS hierarchial structure (tree structure) to transfer time from one station to any other station perfectly (delay independent) in a noise free environment. This method is particularly interesting because by addition of some equipment, the already existing MS systems can be made delay compensating and the theory developed here can be

used to predict performance of the system.

The basic idea in MSRTS is to send the signal received at a station via a delay back to the sending station via the same delay (path). The delay accumulated by this returned signal is used to advance the phase of the master (sending) station thereby canceling the effect of the delay introduced by the path. To understand this idea clearly, we shall start with only two stations one of them is the master station and the other one is a slave station.

III.2 Mathematical Model

Fig.III.1 depicts the system of two stations in a chain of stations completely. Each station has a signal processing equipment with a phase locked loop in it. Since our paper is primarily concerned with the synchronization of the stations, we will represent the stations by their respective phase locked loops only.

As described in the figure, we desire to transmit the phase of the master signal to the slave station. The master signal and the returned signal from the slave station are used to drive the PLL and the output of the VCO is sent to the slave station via a directional coupler. This directional coupler has the ability to sense the direction of energy flow and hence it can route the signals coming to it at the same frequency in the proper directions. At the far end of the cable there is a directional coupler with termination. The termination in the coupler simply reflects some of the incident energy back to the master station for the purpose of delay compensation. It should be noted that the mechanization can be brought about by using two diplexers (or four bandpass filters) instead of the two directional couplers.

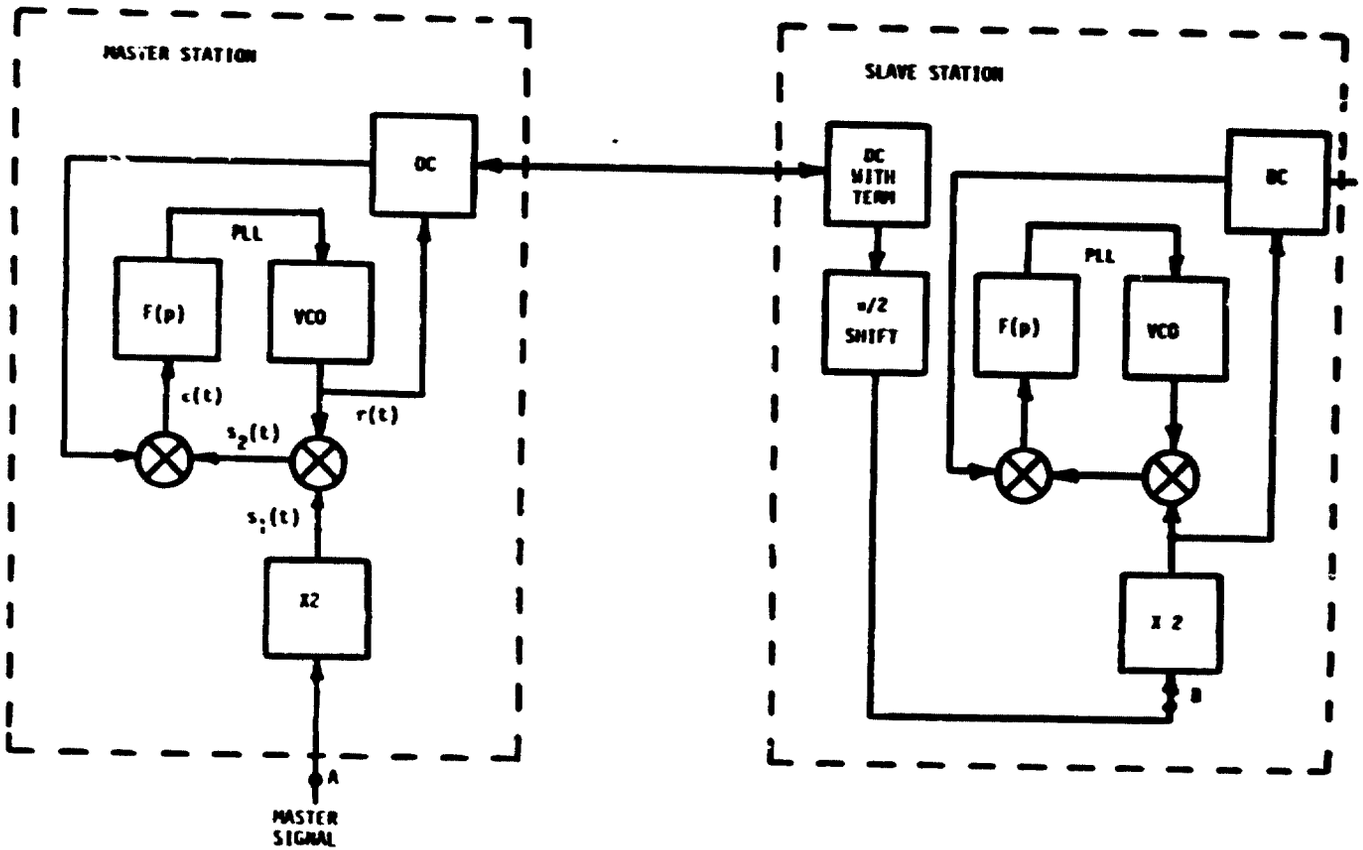

Figure III.1. A System of Two Stations in a Chain of Stations.

$$\text{Master Signal} = s(t) = A \sin(\omega t + \theta_M) \qquad \text{(III.1)}$$

where θ_M is the phase to be transferred to the slave state

$$r(t) = \hat{K} \cos(\omega t + \hat{\theta}(t))$$

where $\hat{\theta}(t)$ is the estimate of the master PLL of the phase θ_M

$$s_1(t) = A \sin 2(\omega t + \theta_M)$$

$$s_2(t) = A\hat{K} \sin(\omega t + 2\theta_M - \hat{\theta}(t))$$

$$s_3(t) = K \cos(\omega(t - \tau_{12} - \tau_{21}) + \hat{\theta}(t - \tau_{12} - \tau_{21}))$$

where τ_{ij} is the delay suffered by the signal from the $j^{\underline{th}}$ station to the $i^{\underline{th}}$ station

$$\varepsilon(t) = AK \sin(2\theta_M - \hat{\theta}(t - \tau_{12} - \tau_{21}) - \hat{\theta}(t) + \omega(\tau_{12} + \tau_{21}))$$

and with no frequency offsets and no biases, in the steady state we will have

$$\theta(t - \tau_{12} - \tau_{21}) \rightarrow \hat{\theta}_{ss}$$

$$0 = 2\theta_M - (2\hat{\theta}_{ss} - \omega_s \tau_{12} - \omega_s \tau_{21})$$

$$= 2\theta_M - 2\hat{\theta}_{ss} + (\omega_s \tau_{12} + \omega_s \tau_{21}) \; ; \; \text{mod } 2\pi \qquad \text{(III.2)}$$

where $\hat{\theta}_{ss}$ is the steady state value of $\theta(t)$ and ω_s is the steady state frequency.

$$\therefore \quad \hat{\theta}_{ss} = \theta_M + \omega_s \frac{(\tau_{12} + \tau_{21})}{2} \; ; \quad \text{mod } \pi \qquad \text{(III. 3)}$$

Thus the phase ambiguity goes away when multiplication is an even integer.

$$r(t)\Big|_{\substack{\text{steady}\\\text{state}}} = r_{ss} = K\cos(\omega_s t+\hat{\theta}_{ss})$$

$$= K\cos(\omega_s t+\theta_M+\omega_s\frac{\tau_{12}+\tau_{21}}{2})$$

Phase of r_{ss} at point B (at the slave station)

$$= \theta_M + \omega_s\left(\frac{\tau_{12}+\tau_{21}}{2}\right) - \omega_s\tau_{21}$$

$$= \theta_M + \omega_s\left(\frac{\tau_{12}+\tau_{21}}{2} - \tau_{21}\right)$$

$$= \theta_M + \omega_s\left(\frac{\tau_{12}-\tau_{21}}{2}\right)$$

$$= \theta_M + \omega_s\left(\frac{\Delta\tau}{2}\right) \qquad \text{(III.4)}$$

where

$$\Delta\tau \triangleq \tau_{12} - \tau_{21} \qquad \text{(III.5)}$$

Now $\Delta\tau=0$ because the same signal travels back and forth through the same line, therefore $\tau_{12}=\tau_{21}$. (This assumes a nondispersive cable). When $\Delta\tau=0$, in the steady state, the phase of the master signal at point A equals the phase of the received signal at the slave station at point B.

III.3 Chain of Stations

As shown above, the phase of the master signal is regenerated at the slave station (point B in FigIII1. This signal will be fed to the slave PLL and this PLL will act as the master for the next station in line. FigIII.2 shows the situation in a block diagram form. Phase of the signal at the input of any slave (in the steady state) is

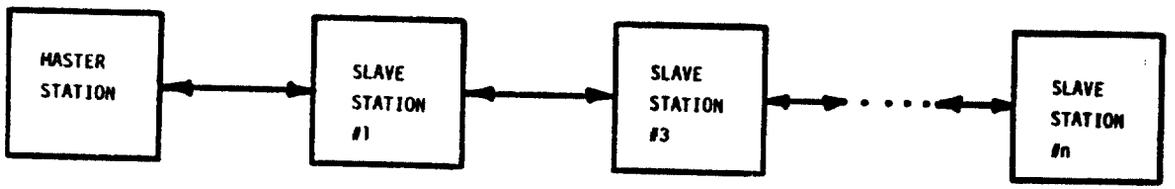

Figure III.2. A Chain of Stations Connected in MSRTS.

obtained from the phase of its immediate master by properly interpreting the quantities in eq.III.4. For example the phase of the signal input to the $(n+1)^{\underline{st}}$ slave in the link is given by

$$\text{Input Phase to the } n+1\underline{st} \text{ Station} = \theta_M + \frac{\Delta\tau_{12}}{2} + \frac{\Delta\tau_{23}}{2} + \ldots + \frac{\Delta\tau_{n-1,n}}{2} + \frac{\Delta\tau_{n,n+1}}{2}$$

$$= \theta_M + \frac{1}{2}\sum_{i=1}^{n}\Delta\tau_{i,i+1} \qquad \text{(III.6)}$$

where θ_M is the phase of the master oscillator to be transmitted to the slave stations. Ideally, with nondispersive cables, we will have $\Delta\tau_{i,i+1} = \tau_{i,i+1} - \tau_{i+1,i} = 0 \quad \forall i = 1, \ldots, n-1$, hence (III.6) gives us the phase input to the $(n+1)^{\underline{st}}$ station is the same as the master station.

III.4 Imperfect Compensation

The condition $\Delta\tau_{i,i+1} = 0$ for the ideal case assumes not only the cable be nondispersive but also that all the components in the system, especially the directional couplers are perfect. In actual practice, this is rarely the case hence it becomes reasonable to assume that each $\Delta\tau_{i,i+1}$ is a random variable with zero mean (unless the system implementation dictates otherwise) and a variance, say $\sigma^2_{i,i+1}$. It is also reasonable to assume that there is no correlation between any pair of random variables, in fact, we will assume that they are statistically pairwise independent random variables. Thus

$$E[\Delta\tau_{i,i+1}] = 0$$

$$E[\Delta\tau_{i,i+1}]^2 = \sigma^2_{i,i+1}$$

with

$$E\{[\Delta\tau_{i,i+1}][\Delta\tau_{j,j+1}]\} = 0 \qquad i \neq j \qquad \text{(III.7)}$$

Let

$$y_n \triangleq \frac{1}{2}\sum_{i=1}^{n} \Delta\tau_{i,i+1} \qquad \text{(III.8)}$$

$$E[y_n] = \frac{1}{2}\sum_{i=1}^{n} E[\Delta\tau_{i,i+1}] = 0$$

and using (III.7) we get

$$E[y_n^2] = \text{Var}[y] = \frac{1}{4}\sum_{i=1}^{n} E[\Delta\tau_{i,i+1}]^2 = \frac{1}{4}\sum_{i=1}^{n} \sigma^2_{i,i+1}$$

$$\triangleq \sigma^2_{y_n} \qquad \text{(III.9)}$$

Thus the disturbance to the phase input to the $(n+1)^{\underline{st}}$ station has a zero mean and a variance of $\sigma^2_{y_n}$. A simple application of the central limit theorem gives that for a large enough "n" we have

$$p_{y_n}(y) = \frac{1}{\sqrt{2n\sigma^2_{y_n}}}\, e^{-y^2/2\sigma^2_{y_n}} \qquad \text{(III.10)}$$

and

$$\text{Phase Input to the } (n+1)\underline{\text{st}} \text{ Station} \triangleq \phi_{n+1} = \theta_M + y_n \qquad \text{(III.11)}$$

then

$$E[\phi_{n+1}] = E[\theta_M + y_n] = \theta_M + E[y_n] = \theta_M \qquad \text{(III.12)}$$

and

$$\text{Var}[\phi_{n+1}] = \sigma^2_{y_n} \qquad \text{(III.13)}$$

III.5 Effect of Nonzero Mean of $\Delta\tau_{i,i+1}$ on the System

So far we have tacitly assumed that $E[\Delta\tau_{i,i+1}] = 0$ $\forall i = 1,\ldots,n$. If there is some reason to assume that $E[\Delta\tau_{i,i+1}] = c_{i,i+1} \neq 0$ then the mean of y increases in the following way:

$$y_n = \frac{1}{2}\sum_{i=1}^{n} \Delta\tau_{i,i+1}$$

$$E[y_n] = \frac{1}{2}\sum_{i=1}^{n} E[\Delta\tau_{i,i+1}] = \frac{1}{2}\sum_{i=1}^{n} c_{i,i+1} \neq 0$$

$$= \frac{nc}{2} \text{ if } c_{i,i+1} = c \ \forall i.$$

and

$$\text{Var}[y_n] = \frac{1}{4}\sum_{i=1}^{n} \sigma^2_{i,i+1} \qquad \text{(III.14)}$$

In such a case another mechanization of the system described in Fig.III.3 may prove more useful.

The key points to note in this mechanization is that the directional couplers in Fig.III.3 are replaced by diplexers and frequency dividers are included. Also the direction of flow of "ω" signals and "2ω" signals is alternated. Going through a similar analysis as before we can arrive at an equation similar to (III.11) giving us the phase of the input signal to $(n+1)^{\underline{st}}$ station in the steady state to be

$$\Phi_{n+1} = \theta_M + y_n \qquad \text{(III.15)}$$

where

$$y_n = \frac{1}{2}\sum_{i=1}^{n} (-1)^{i+1} \Delta\tau_{i,i+1}$$

Thus

$$E[y_n] = \frac{1}{2}\sum_{i=1}^{n} (-1)^{i+1} E[\Delta\tau_{i,i+1}]$$

$$= \frac{1}{2}\sum_{i=1}^{n} (-1)^{i+1} c_{i,i+1} \qquad \text{(III.16)}$$

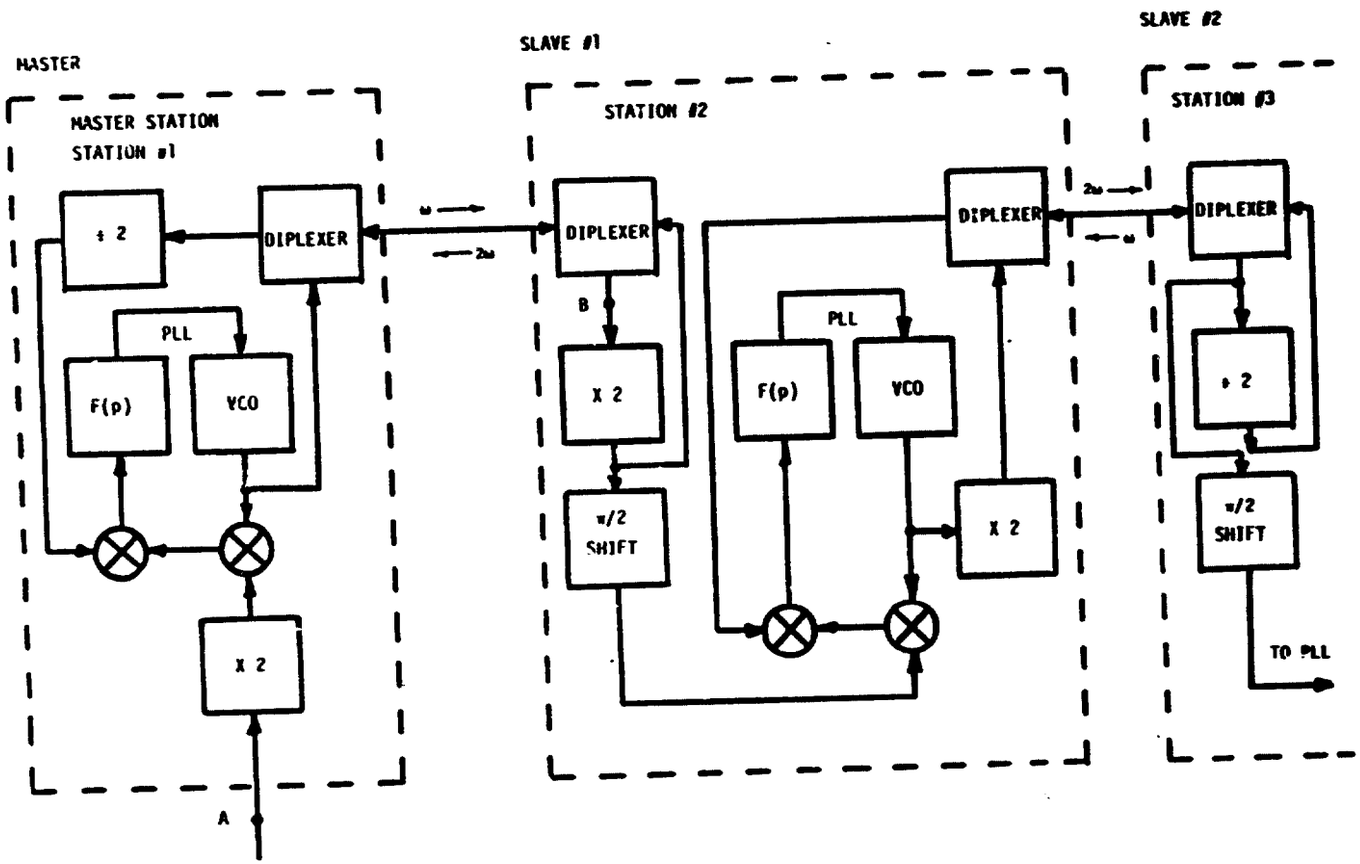

Figure III.3. System Minimizing the Constant Bias Added by Each Station.

If $c_{i,i+1} = c \quad \forall i = 1,\ldots,n$ then

$$E[y_n] = \frac{c}{2}\sum_{i=1}^{n}(-1)^{i+1} = \begin{cases} 0 & \text{if } n \text{ is even} \\ \frac{c}{2} & \text{if } n \text{ is odd} \end{cases}$$

and

$$\text{Var}[y_n] = \frac{1}{4}\sum_{i=1}^{n}\sigma^2_{i,i+1} = \sigma^2_{y_n} \qquad \text{(III.17)}$$

Comparing (III.14) with (III.17), we see that the mean of the phase disturbance has decreased by at least a factor of n while the variance remains the same.

III.6 Probability Distribution of the Phase

$$\text{input phase to } (n+1)\underline{\text{st}} \text{ Station} = \phi_{n+1} = \theta_M + y_n$$

where

$$y_n = \frac{1}{2}\sum_{i=1}^{n}\Delta\tau_{i,i+1}$$

with

$$E[y_n] = \frac{1}{2}\sum_{i=1}^{n}E[\Delta\tau_{i,i+1}] = \frac{1}{2}\sum_{i=1}^{n}c_{i,i+1} \triangleq c_n$$

and

$$\text{Var}[y_n] = \frac{1}{4}\sum_{i=1}^{n}\sigma^2_{i,i+1} \triangleq \sigma^2_{y_n}$$

$$E[\phi_{n+1}] = \theta_M + E[y_n] = \theta_M + c_n$$

$$\text{Var}[\phi_{n+1}] = \sigma^2_{y_n}$$

Assuming a large enough "n" using the central limit theorem, we have

$$p_{\phi_{n+1}}(\phi_{n+1}) = \frac{1}{\sqrt{2\pi\sigma_{y_n}^2}} \; e^{-(\phi_{n+1}-\theta_M-c_n)^2/2\sigma_{y_n}^2} \qquad \text{(III.18)}$$

Thus it becomes possible to find the probability that the phase input to the $(n+1)^{\underline{st}}$ station lies between $\pm\Delta$ of the master signal phase, θ_M. This is given by

$$P[\theta_M-\Delta \le \phi_{n+1} \le \theta_M+\Delta] = \int_{\theta_M-\Delta}^{\theta_M+\Delta} p_{\phi_{n+1}}(\phi_{n+1})\,d\phi_{n+1}$$

$$= \int_{\theta_M-\Delta}^{\theta_M+\Delta} \frac{1}{\sqrt{2\pi\sigma_{y_n}^2}} \; e^{-(\phi_{n+1}-\theta_M-c_n)^2/2\sigma_{y_n}^2} \; d\phi_{n+1}$$

$$= \text{erf}\left(\frac{\theta_M+\Delta-\theta_M-c_n}{\sigma_{y_n}}\right) - \text{erf}\left(\frac{\theta_M-\Delta-\theta_M-c_n}{\sigma_{y_n}}\right)$$

$$= \text{erf}(\Delta-c_n/\sigma_{y_n}) + \text{erf}(\Delta+c_n/\sigma_{y_n}) \qquad \text{(III.19)}$$

where

$$\text{erf}(x) \triangleq \frac{1}{\sqrt{2\pi}}\int_0^x e^{-y^2/2}\,dy$$

Thus we see from (III.19) how the mean value c_n enters into the equation to affect the probability of ϕ_{n+1} being in $(-\Delta,\Delta)$ interval. If $c_n=0$ then (III.19) reduces to $2\,\text{erf}(\Delta/\sigma_{y_n})$. In such a case with $P[\theta_M-\Delta \le \phi_{n+1} \le \theta_M+\Delta] = a$ and $\sigma_{y_n}^2 = \frac{1}{4}\sum_{i=1}^{n}\sigma_{i,i+1}^2 = n\sigma^2/4$ (i.e., $\sigma_{i,i+1}=\sigma\ \forall i$) we can get from (III.19) that

$$a = 2\,\text{erf}\left(\frac{\Delta}{\sqrt{\frac{n}{2}}\,\sigma}\right)$$

$$n = 4 \times (\Delta/\sigma)^2 \times \left(\frac{1}{\text{erf}^{-1}(\frac{a}{2})}\right)^2 \qquad \text{(III.20)}$$

The above equation tells us how many stations ("n") can be allowed in a chain of stations for fixed values of "a" and "σ" and a selected

value (variable) of Δ. The ratio $(\Delta/\sigma)^2$ can be intrepreted as

$$\left(\frac{\Delta}{\sigma}\right)^2 = \frac{\text{Max Allowable Spread}}{\text{System Spread}} \triangleq \text{Spread Ratio.} \qquad \text{(III.21)}$$

If we let $\Delta=\pi$ and change a to (1-a) (20) becomes

$$n = 4\left(\frac{\pi}{\sigma}\right)^2 \times \left[\frac{1}{\text{erf}^{-1}\left(\frac{1-a}{2}\right)}\right]^2 \qquad \text{(III.22)}$$

"n" gives us how many stations can be allowed in a chain for a pre-determined value of "a" and the system parameter value σ before slip of one cycle is expected to occur at the input to (n+1) station. Thus a large number of stations can be allowed if σ is sufficiently small before the cycle slipping occurs, alternatively the probability of slipping a cycle tends to zero.

III.7 Phase Noise Propagation in a Chain of Stations

The above analysis does not consider any form of noise either generated by the system components like the PLL or the channel noise. The analysis presented below considers the propagation of noise generated by the PLL through a chain of stations. Fig.III.4 describes the connection and signals at the $k^{\underline{th}}$ st tion. We will adopt a new notation $(\tilde{\cdot})$ means phase of the signal $(\cdot)$. At the $k^{\underline{th}}$ station

$$\tilde{s}_{k_0}(t) = \omega(t-\tau_{k,k-1}) + \theta_{k-1}(t-\tau_{k,k-1})$$

$$\tilde{r}_k = \omega t + \theta_k(t)$$

where $\theta_k(t) \triangleq \theta_k(t) + \psi_k(t)$ in which $\psi_k(t)$ is the phase noise generated by the $k^{\underline{th}}$ oscillator and $\theta_k(t)$ is the phase estimate of the $k^{\underline{th}}$ oscillator.

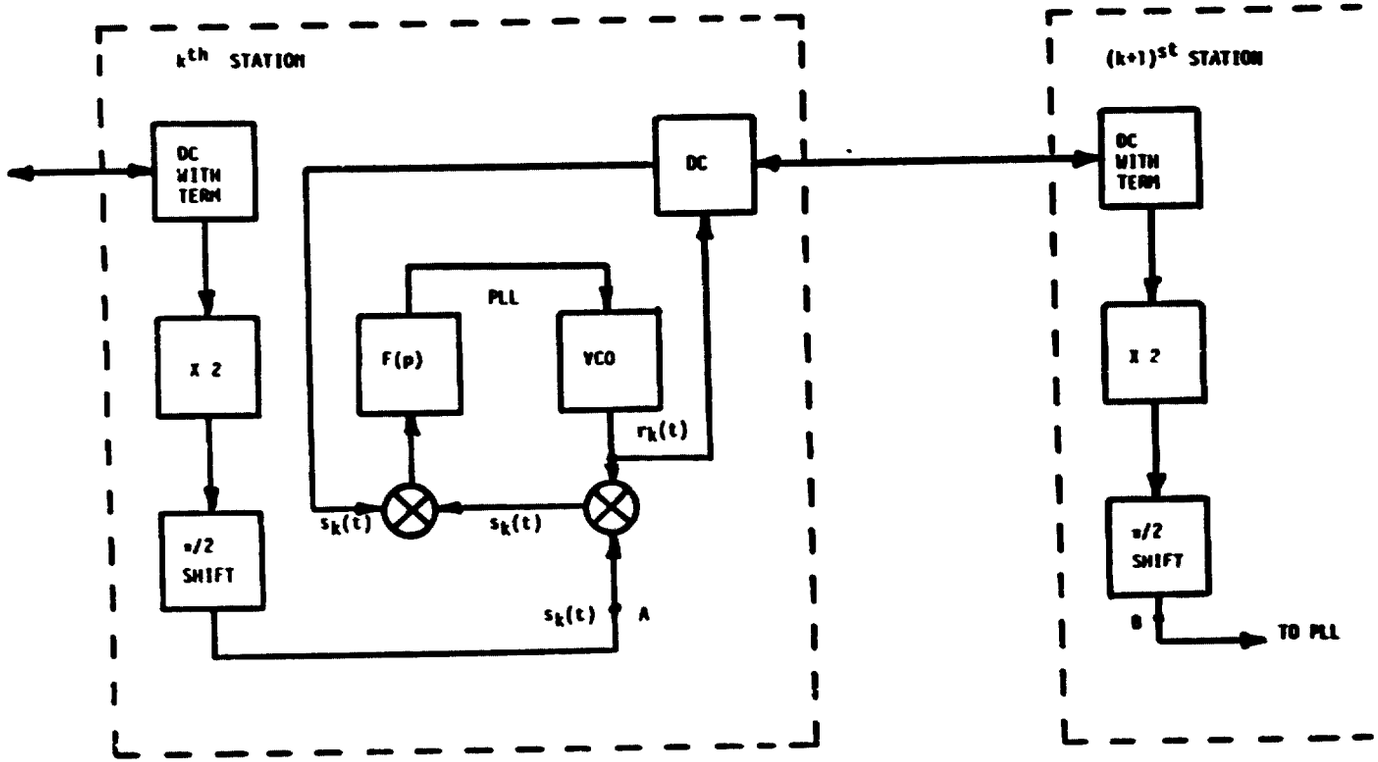

Figure III.4. Connections at the $k^{\underline{th}}$ Station in a Chain of Stations.

$$\tilde{s}_k(t) = 2\omega(t-\tau_{k,k-1}) + 2\theta_{k-1}(t-\tau_{k,k-1})$$

$$\tilde{s}_{k_1}(t) = \omega t - 2\omega\tau_{k,k-1} + 2\theta_{k-1}(t-\tau_{k,k-1}) - \theta_k(t)$$

$$\tilde{s}_{k_2}(t) = \omega(t-\tau_{k+1,k} - \tau_{k,k+1}) + \theta_k(t-\tau_{k+1,k}-\tau_{k,k+1})$$

$$\tilde{c}_k(t) = \omega(\tau_{k+1,k}+\tau_{k,k+1}-2\tau_{k,k-1}) + 2\theta_{k-1}(t-\tau_{k,k-1}) - \theta_k(t-\tau_{k+1,k}-\tau_{k,k-1}) - \theta_k(t)$$

Taking Fourier transform on both sides,

$$c_k(\omega) = 4\pi\omega(\tau_{k+1,k}+\tau_{k,k+1}-2\tau_{k,k-1}) + 2\theta_{k-1}(\omega)e^{-j\omega\tau_{k,k-1}} - \theta_k(\omega) \cdot e^{-j\omega(\tau_{k+1,k}+\tau_{k,k-1})} - \theta_k(\omega)$$

$$c_k(\omega) = 4\pi\omega(\tau_{k+1,k}+\tau_{k,k+1}-2\tau_{k,k-1}) + 2\theta_{k-1}(\omega)e^{-j\omega\tau_{k,k-1}} - \theta_k(\omega)[1 + e^{-j\omega(\tau_{k+1,k}+\tau_{k,k+1})}]$$

Now

$$\theta_k(\omega) = \frac{kF_k(\omega)}{j\omega}[c_k(\omega)] + \psi_k(\omega)$$

$$\theta_k(\omega) = \frac{kF_k(\omega)}{j\omega}[4\pi\omega(\tau_{k+1,k}+\tau_{k,k+1}-2\tau_{k,k-1}) + 2\theta_{k-1}(\omega)e^{-j\omega\tau_{k,k-1}} - \theta_k(\omega)\{1 + e^{-j\omega(\tau_{k+1}-\tau_{k,k-1})}\}] + \psi_k(\omega) \quad \text{(III.23)}$$

Assuming that proper filtering removes the δ's and solving for $\theta_k(\omega)$ from (III.23) yields

$$\theta_k(\omega) = \frac{kF_k(\omega)e^{-j\omega\tau_{k,k-1}}}{j\omega + kF_k(\omega)[1+e^{-j\omega(\tau_{k,k+1}+\tau_{k+1,k})}]}\theta_{k-1}(\omega) + \frac{j\omega k}{j\omega + kF_k(\omega)[1+e^{-j\omega(\tau_{k,k+1}+\tau_{k+1,k})}]}\psi_k(\omega) \quad \text{(III.24)}$$

let

$$R_k(\omega) = \frac{2kF_k(\omega)e^{-j\omega\tau_{k,k-1}}}{j\omega + kF_k(\omega)[1+e^{-j\omega(\tau_{k+1,k}+\tau_{k,k+1})}]}$$

and

$$H_k(\omega) = \frac{j\omega K}{j\omega + kF_k(\omega)[1+e^{-j\omega(\tau_{k+1,k}+\tau_{k,k+1})}]} \quad \text{(III.25)}$$

Then (III.24) becomes

$$\theta_k(\omega) = R_k(\omega)\theta_{k-1}(\omega) + H_k(\omega)\psi_k(\omega) \quad \text{(III.26)}$$

This is a recursive relation for $\theta_k(\omega)$ and can be solved for the $n^{\underline{th}}$ station phase output. This turns out to be

$$\theta_n(\omega) = \left\{\prod_{i=1}^{n} R_i(\omega)\right\}\theta_0(\omega) + \sum_{i=1}^{n}\left\{H_i(\omega)\prod_{j=i+1}^{n} R_j(\omega)\right\}\psi_i(\omega) \quad \text{(III.27)}$$

where

$$\theta_0(\omega) = \theta_M(\omega) + \psi_M(\omega)$$

Thus the system can be represented as in Fig. III.5 in a series form. Or this can be modelled as a parallel fed system shown in Fig. III.6 From (III.27) we have

$$\theta_n(\omega) - \left\{\prod_{i=1}^{n} R_i(\omega)\right\}\theta_0(\omega) \triangleq \phi_n(\omega) = \sum_{i=1}^{n}\left\{H_i(\omega)\prod_{j=i+1}^{n} R_j(\omega)\right\}\psi_i(\omega) \quad \text{(III.28)}$$

Now assuming that $E[\theta_i(\omega)] = 0 \ \forall i$ and $E[\psi_i(\omega)\psi_j(\omega)] = 0$ if $i \neq j$ we have

$$E[\phi_n(\omega)] = 0 \Rightarrow \theta_n(\omega) = \prod_{i=1}^{n} R_i(\omega)\ \theta_0(\omega) \quad \text{(III.29)}$$

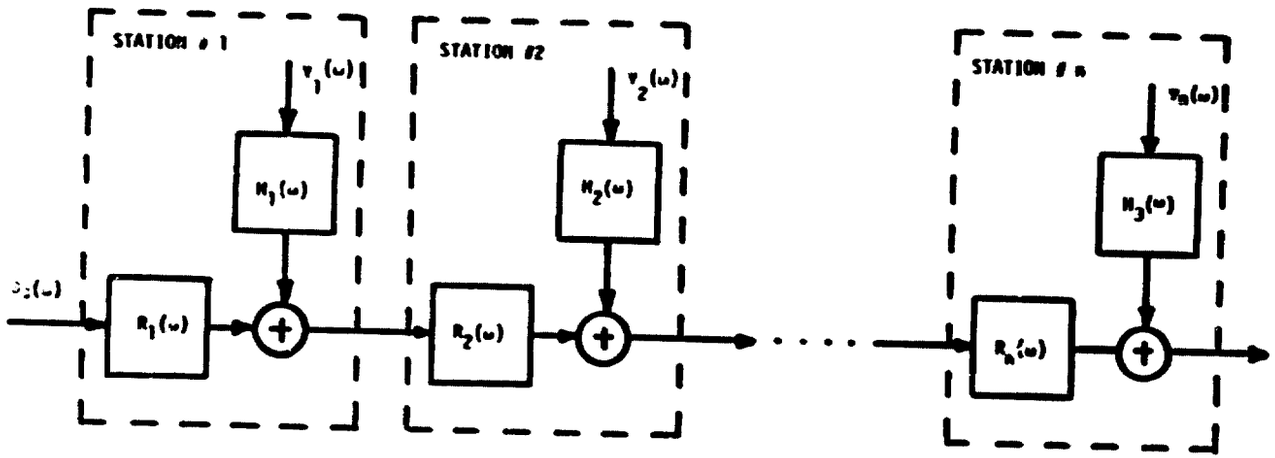

Figure III.5. Series Equivalent of a Chain of Stations Connected in MSRTS.

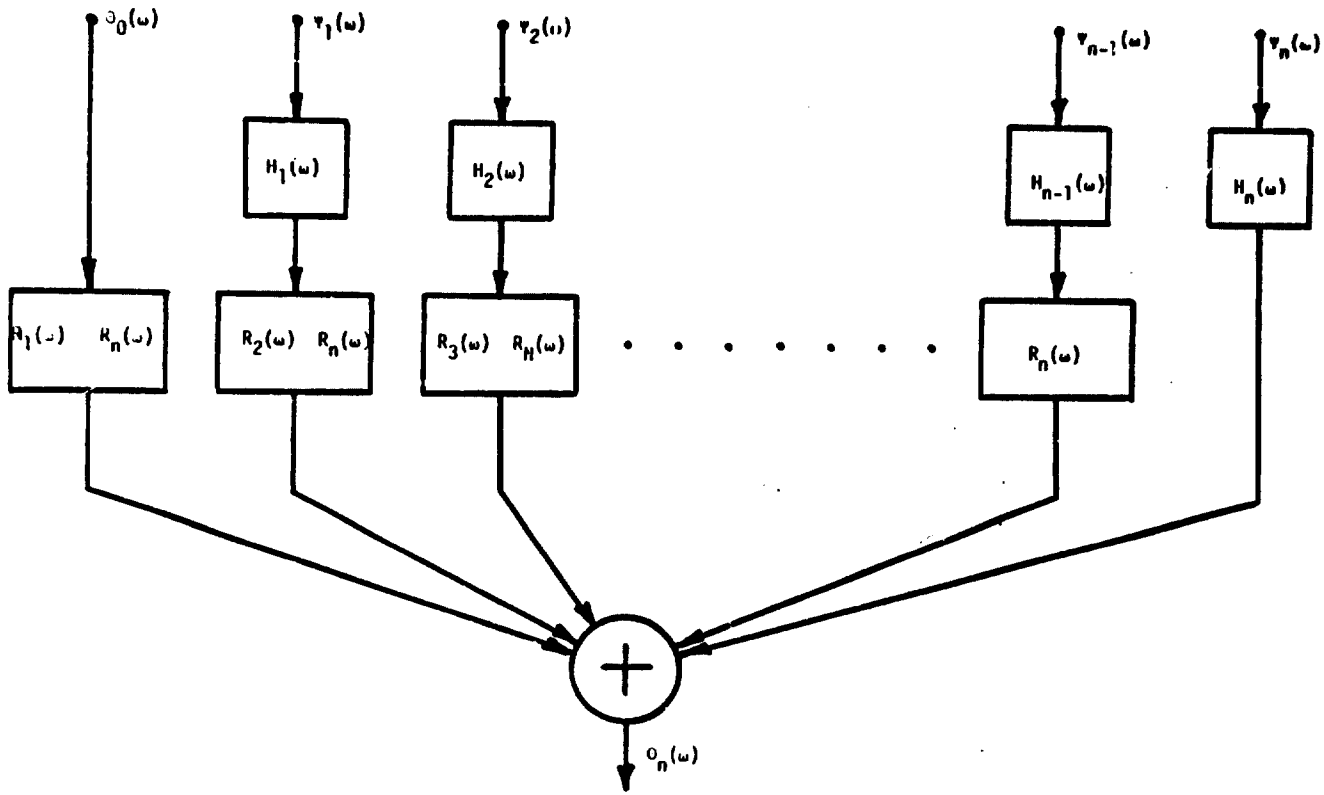

Figure III.6. Parallel Equivalent of the Chain of Stations Connected in MSRTS.

i.e. on the average, the output phase of the $n^{\underline{th}}$ station oscillator equals the master phase. We would be interested to find $\sigma^2_{\phi_n}$.

$$S_{\phi_n}(\omega) = \sum_{i=1}^{n} |H_i(\omega)|^2 \left\{ \prod_{j=i+1}^{n} |R_j(\omega)|^2 \right\} S_{\psi_i}(\omega) \qquad \text{(III.30)}$$

where $S_{\psi_i}(\omega)$ is the single sided spectral density of the ψ_i.

$$\sigma^2_{\phi_n} = \frac{1}{2\pi} \int_0^\infty \sum_{i=1}^{n} |H_i(\omega)|^2 \left\{ \prod_{j=i+1}^{n} |R_j(\omega)|^2 \right\} S_{\psi_i}(\omega) d\omega \qquad \text{(III.31)}$$

$$\sigma^2_{\phi_1} = \frac{1}{2\pi} \int_0^\infty |H_1(\omega)|^2 S_{\psi_1}(\omega) d\omega$$

$$\frac{\sigma^2_{\phi_n}}{\sigma^2_{\phi_1}} = \frac{\int_0^\infty \sum_{i=1}^{n} |H_i(\omega)|^2 \left\{ \prod_{j=i+1}^{n} |R_j(\omega)|^2 \right\} S_{\psi_i}(\omega) d\omega}{\int_0^\infty |H_1(\omega)|^2 S_{\psi_1}(\omega) d\omega} \qquad \text{(III.32)}$$

where $R_k(\omega)$ and $H_k(\omega)$ are defined in (III.25). Now if we assume that $\tau_{ij} = \tau \ \forall i,j$ we have $H_i(\omega) = H(\omega) \ \forall i$ and $R_i(\omega) = R(\omega) \ \forall i$. In such a case

$$\frac{\sigma^2_{\phi_n}}{\sigma^2_{\phi_1}} = \frac{\int_0^\infty |H(\omega)|^2 [|R|^{2(n-1)} S_{\psi_1} + |R|^{2(n-2)} S_{\psi_2} + \ldots + |R|^2 S_{\psi_{n-1}} + S_{\psi_n}] d\omega}{\int_0^\infty |H(\omega)|^2 S_{\psi}(\omega) d\omega}$$

Now we let $S_{\psi_i}(\omega) = S_{\psi}(\omega) \ \forall i$ hence

$$\frac{\sigma^2_{\phi_n}}{\sigma^2_{\phi_1}} = \frac{\int_0^\infty |H(\omega)|^2 \left\{ \frac{1 - |R|^{2n}}{1 - |R|^2} \right\} S_{\psi}(\omega) d\omega}{\int_0^\infty |H(\omega)|^2 S_{\psi}(\omega) d\omega} \qquad \text{(III.33)}$$

Now assuming $\tau_{ij}=0 \ \forall i,j$ and $F_k(\omega) = F(\omega) \ \forall R$ and $S_\psi(\omega) = 1/\omega$ we get

$$R(\omega) = \frac{2F(\omega)K}{j\omega + 2KF(\omega)}$$

$$H(\omega) = \frac{j\omega K}{j\omega + 2F(\omega)} = 1 - R(\omega)$$

Assuming

$$F(\omega) = \frac{1 + j\omega\tau_2}{1 + j\omega\tau_1}$$

$$R(\omega) = \frac{1 + j2\zeta x}{(1-x^2) + j2\zeta x} \quad \text{where } x = \omega/\omega_n$$

with $\omega_n = \sqrt{K/\tau_1}$ and $\zeta = (\tau_2/\tau_1)\omega_n$ which gives

$$H(\omega) = 1 - R(\omega) = \frac{-x^2}{(1-x^2) + j2\zeta x}$$

Substituting $H(\omega)$ and $R(\omega)$ in (III.33) one can compute the normalized mean squared random jitter after n stations (normalized by the mean squared random jitter produced by one station) is computed by the use of an IBM Computer. The results are presented in Fig. III.7. As can be seen, as ζ, the damping factor of the circuit increases, the noise variance at the end of n station chain decraases but this may create problems in acquisition mode of the stations.

III.8 MSRTS Tree Network

When there are a number of stations to be connected (phase locked) together to transmit phase information from one station to all the remaining stations, one possible way of connection is to connect all of them in a chain and let the master feed the chain. There are obvious disadvantages of a series connection with the above scheme,

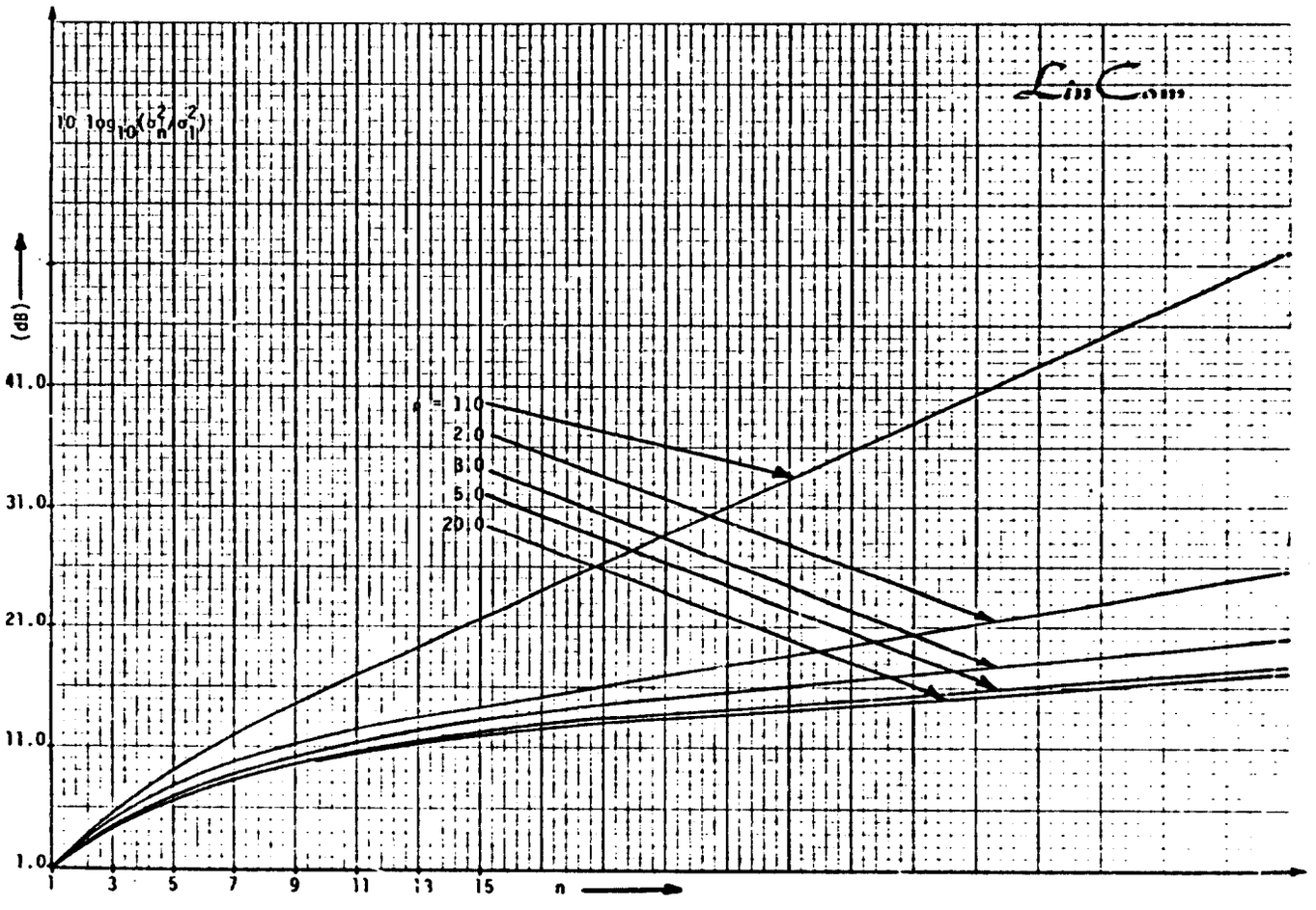

Figure III.7. Plot of the Relative Variance of a Chain of Stations Connected in MSRTS.

hence the well known master-slave hierarchial tree structure will be tried next. Fig.III.8 shows such a tree structure using MSRTS concept for the time transfer.

The master (station 1) in the figure feeds the phase to four physically close equidistant (from the feeding point) phase locked loops via a four way power splitter. These are level 1 slaves. Each of the level 1 slaves is connected to a four way power splitter as level 2 via the MSRTS. Again a group of 2nd level four PLLs are placed equidistant from the power splitter and each of these is connected to the third level power splitter via MSRTS. This is continued until all the oscillators (stations) are connected.

For each oscillator in the network there exists only one chain connecting the master to the oscillator and our analysis in the previous section holds.

III.9 Conclusion

MSRTS provides a new way of delay compensation which can use already existing Master Slave systems. Proper design of filters at each station can reduce the varianceof noise at the end of the chain of stations. MSRTS can also be useful in antenna theory, especially those reflector antennas where distribution of the master phase accurately is vital to the performance of the antenna. Also this method can be of use for sensing phase at a remote location for phase measurement purposes.

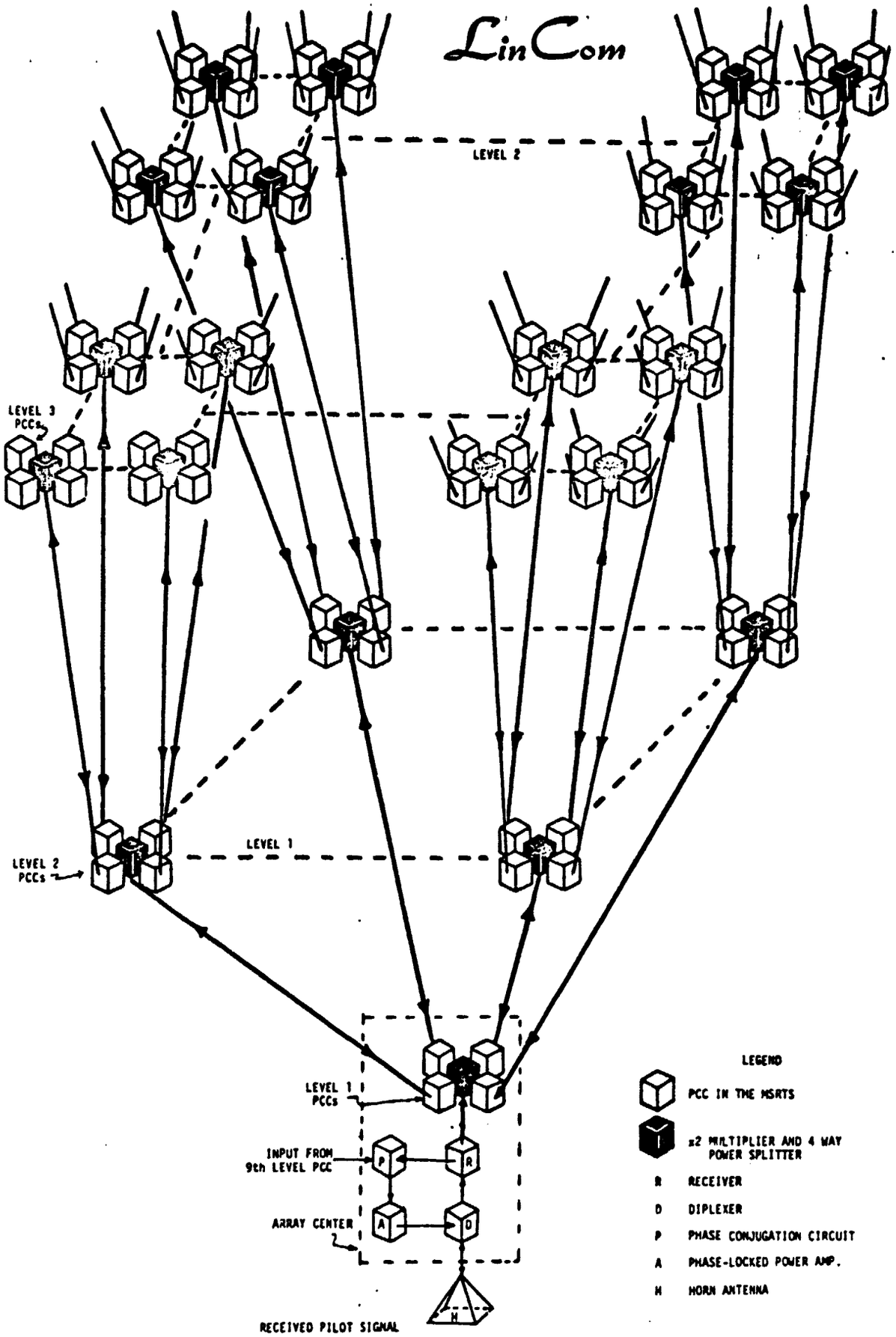

FIGURE III.8 THREE LEVELS OF THE PHASE CONTROL SYSTEM ILLUSTRATED IN ALL QUADRANTS

REFERENCES

1. H. Inose, H. Fujsaki and T. Saito, "Theory of Mutually Synchronized Systems," Electronic Communications in Japan, Vol. 49, April 1966

2. A. Gersho and B. Karafin, "Mutual Synchronization of Geographically Separated Oscillators," Bell System Technical Journal, Vol. 45, December, 1966, pp. 1689-1704.

3. W. C.Lindsey, A. Dobrogowski and A. V. Kantak, "Mutual Synchronization Properties of a System of Two Oscillators with Sinusoidal Phase Detectors," IEEE Transactions on Communications, December, 1976, pp. 1321 - 1326.

4. T. Yamato, M. Ono and S. Usuda, "Synchronization of a PCM Integrated Telephone Network," IEEE Transactions on Communication Technology, Vol. COM-16, pp. 1-11, Feb. 1968.

5. W. C. Lindsey, A. V. Kantak and A. Dobrogowski, "Network Synchronization by Means of Returnable Timing System," IEEE Transactions on Communications, Vol. COM-21, pp. 892-896, June 1978.

APPENDIX IV

SOLARSIM SOFTWARE DEVELOPMENT

This section describes the SOLARSIM programs and SOLARSIM capabilities to quantify the spacetenna performance parameter values. The overall setup of SOLARSIM computer simulation is shown in Figure IV.1 where the user inputs direct the central processor unit to pick the correct SOLARSIM subroutine from the subroutine package stored in the memory of the computer and after computation, produce the desired output either in the form of plots or printout or both. Figure IV.2 shows the capabiliteis fo the SOLARSIM subroutine package. As shown in the figure, SOLARSIM can compute the following quantities:

1. Antenna element covariance matrix.
2. Individual realization of random power pattern.
3. Mean far field power pattern.
4. Main beam gain losses.
5. RMS pointing error.
6. Tilt/mechanical error effects on gain with effect of conjugation at other than radiating element level.
7. Main beam power transfer efficiency.

There are two different types of inputs necessary for the operation of SOLARSIM subroutines, users inputs and the computer generated inputs. Both these inputs are shown in Figure IV.2. The computer generated inputs are automatic in the sense that once the user's input specifies the SOLARSIM subroutine, the subroutine calls for the necessary computer generated input for its execution.

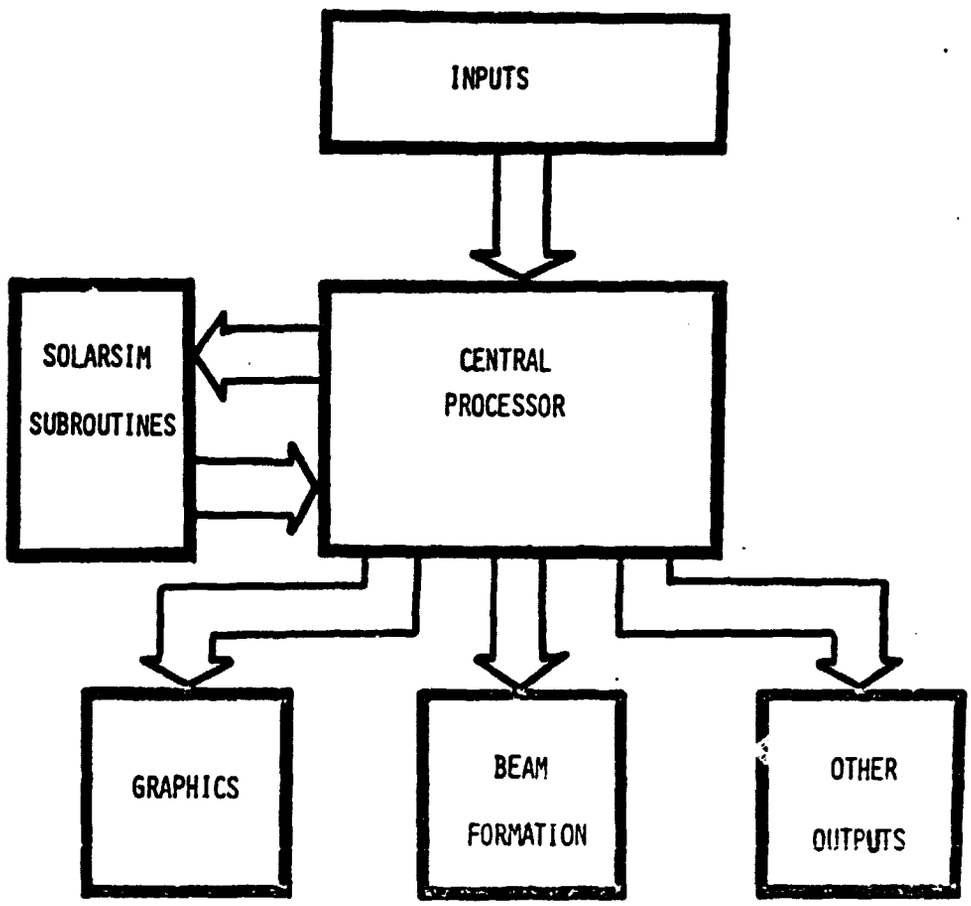

Figure IV.1. SOLARSIM Computer Simulation Package.

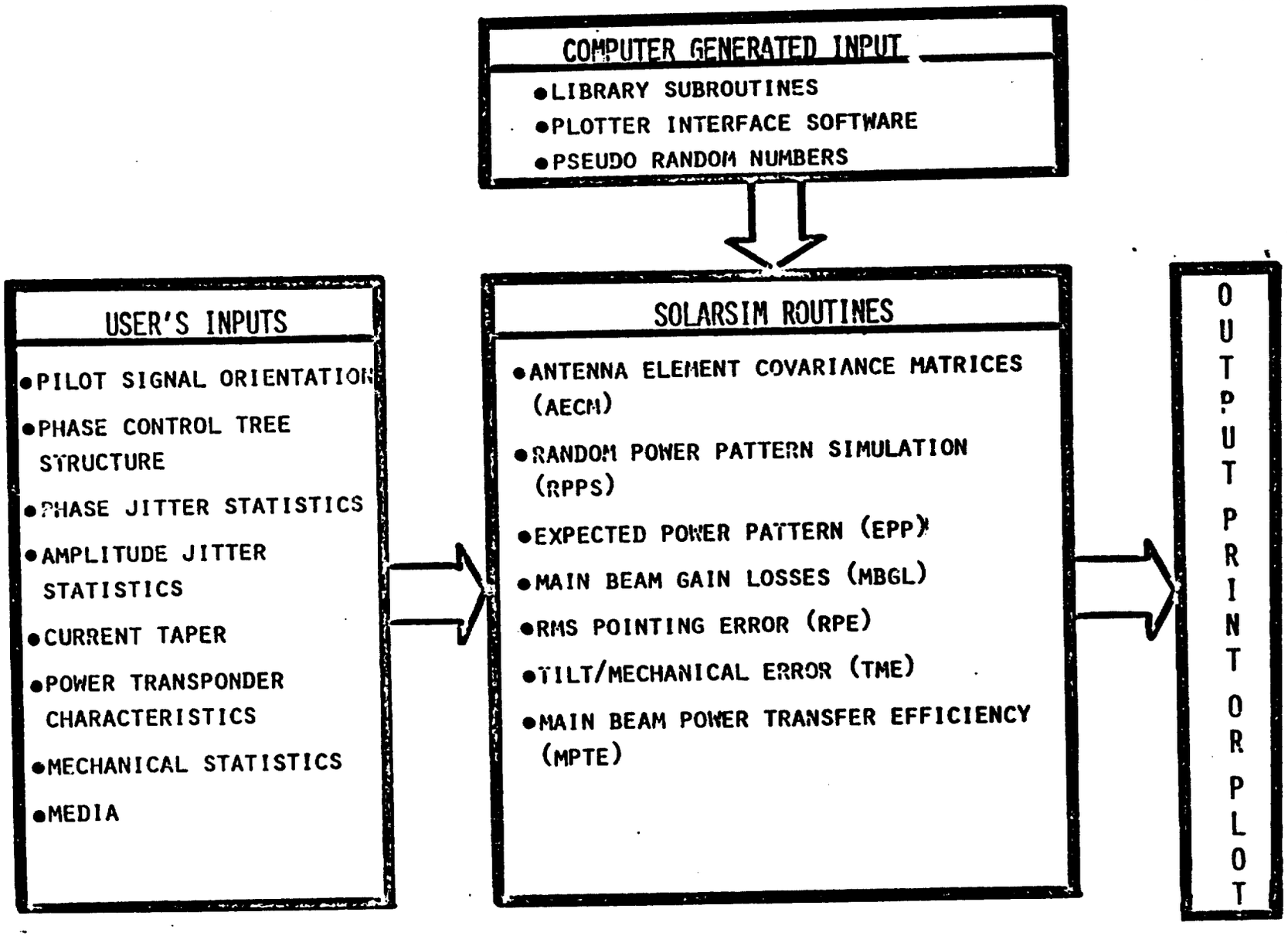

Figure IV.2. SOLARSIM Capabilities.

The SOLARSIM programs are configured such that all the user has to know are the inputs to the programs. In certain programs this step is made easier by having a question and answer session in the beginning of the programs.

The documentation below contains information necessary for the user to use the programs. The topics covered can be grouped into three headings. The first part gives an overall input output diagram for the program along with a short description of what the program does. The second part shows the flow chart of the program and the third part shows a typical output of the program.

SOLARSIM Subroutine PVRPAT

Purpose: PVRPAT simulates the SPSS antenna system and computes the actual (not the averaged) power patterns for the antenna, when the phase distribution system noises are present and not present. This program gives a probable pattern for the SPSS antenna.

Inputs:

L - Number of levels of the phase distribution tree structure.

LL - Number of current levels.

DB - Current taper in dB.

DX - Incremental distance in x direction.

DY - Incremental distance in y direction.

STEP - Increment in θ direction for the computation of power pattern.

NN - Number of θ values to be used to compute the power pattern.

THETAS - Starting value of θ direction

THETA0 - Pilot signal θ direction.

PHI0 - Pilot signal ϕ direction

PHI - Constant value of ϕ direction to be used in the power pattern.

SGMA - Array for the standard deviations in each branch of the phasing tree (in degrees).

SEED - Array of initial values for generating the Gaussian random variable representing the phasing system noise.

Outputs:

T - Array of θ values (minutes).

XC- Array of $u = \sin\theta\cos\phi$ values

YC- Array of computed power pattern.

A simple output of the PVRPAT is shown in Figure IV.4 where L = 6, LL = 4 and dB = 10. There are two columns under "ratio". The first one is the antenna power pattern with no phase distribution system error and the second one is with the phase distribution system errors specified in the input. Shifting of the maximum of the main lobe is evident in the second column of "ratio". This shifting of the main lobe is plotted in Figure IV.5 for the case of L = 5, 10 dB current taper and the phase error standard deviation of 10° at each level of the phase distribution tree in this particular case the main lobe has shifted from its mean position by 0.3'.

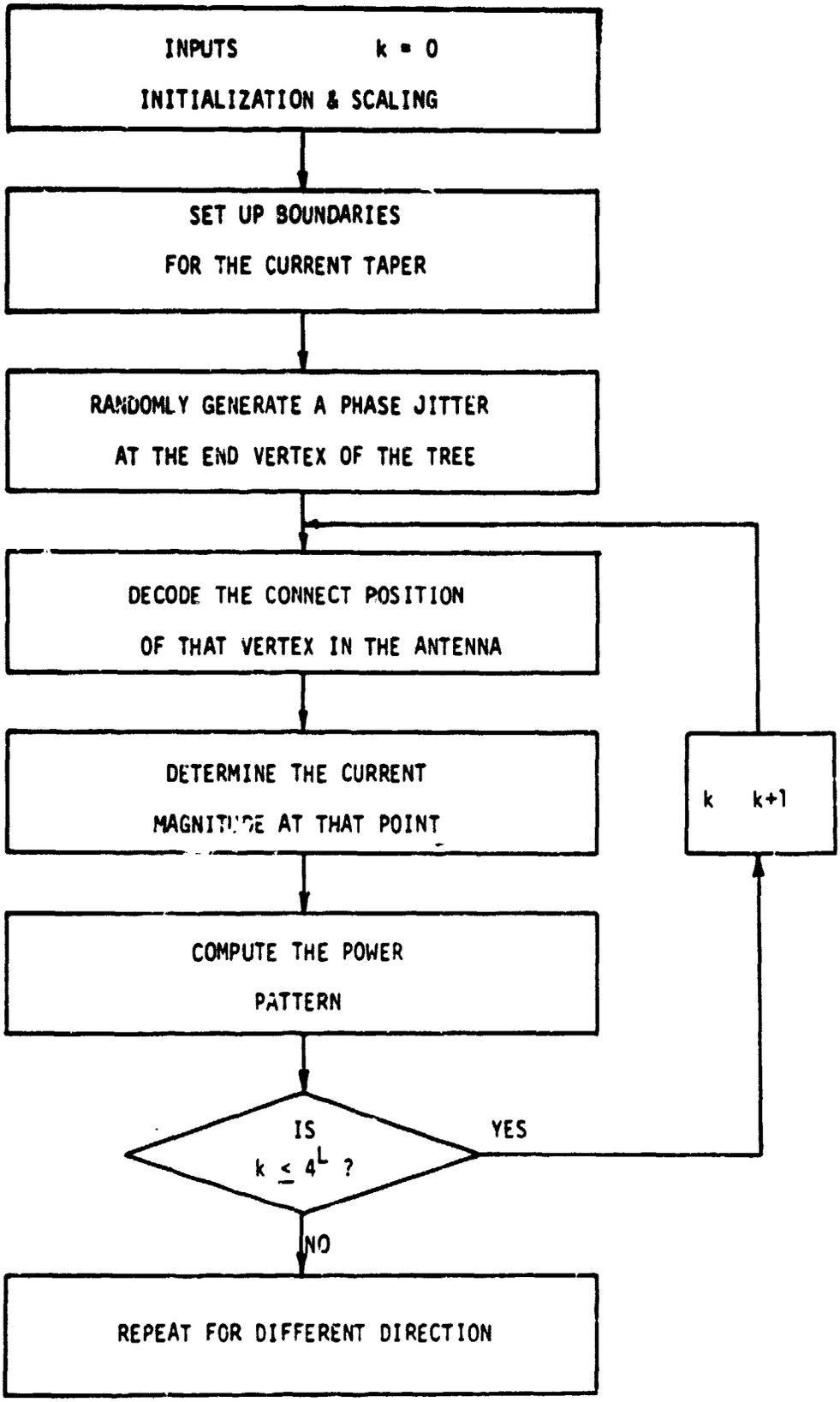

Figure IV.3. Flow Chart for "PVRPAT" Program.

LinCom

```
ɪʟʟʟ.ʌ ( ʊ·...ᴇ.
.ᵻ>ʲ ȷ

ʷ.,ɪ.,4,5,0.,ᴄ,ɪᴜ.,ᵃ.,ᵈ.,1.,1.,32ᴎ.
ɪ.,1.,1.,1.,!.,ɪ.
ɪ,ɪɪ,ɪɪɪ,ɪɪɪɪ,ɪɪɪɪɪ,ɪɪɪɪɪɪ
3:>ᴇXɪᴛ
LINES:3 FIELDATA
>

 @XQT
MAP23R2 RL71-3 07/17/78 11:36:52
START=013033, PROG SIZE(I/D)=5690/11009
SYS$*FLIB$. LEVEL 72-0
END MAP

>@ADD DATUM
```

THETAP	PHIE	RO	SGMA(1)	DD	DX	DY	LL	L
.000	.000	320.000	1.000	10.000	1.000	1.000	4	6

THETA	U	RATIO	
.00000000	.00000000	.0000000	-.5747175-001
1.00000001	.01492625	-.1037891+000	.0000000
2.00000003	.02985251	-.4157336+000	-.1494701+000
3.00000004	.04477876	-.9373706+000	-.5096344+000
4.00000005	.05970500	-.1670514+001	-.1086073+001

921421.10018014   301609.95946866

Figure IV.4. A Sample Outpuf of PVRPAT.

LinCom

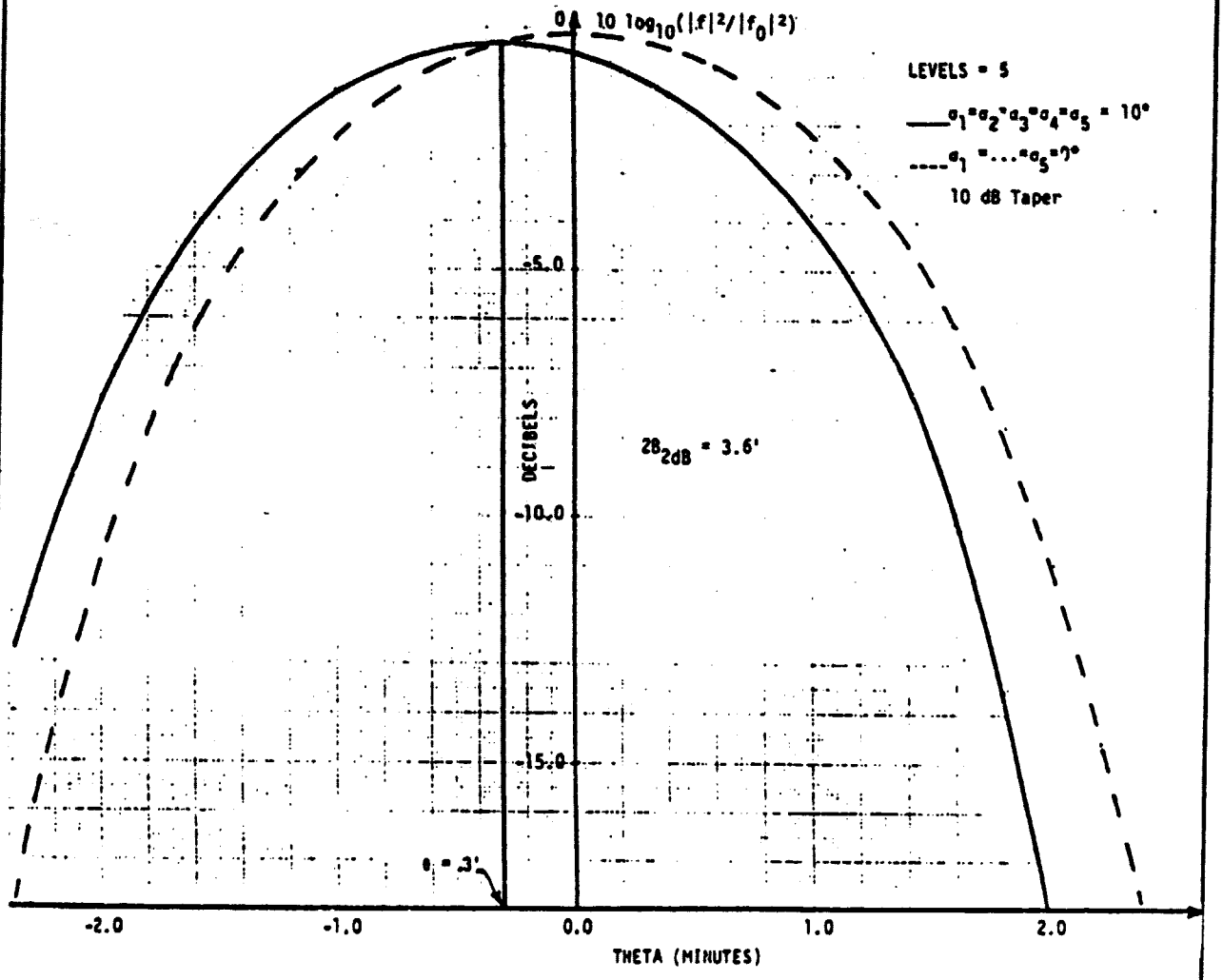

Figure IV.5. Figure Illustrating Shifting of the Main Beam.

SOLARSIM Subroutine EAPP

Purpose: EAPP computes the exact expected (averaged) power pattern for the SPS antenna for different configurations of the phase distribution system. It also allows the current taper to be a variable of the program.

Inputs: Figure IV.6 describes the inputs to the EAPP which are basically the same as the list of inputs to the PVRPAT except for the last entry which is changed to SGMD. Fig. IV.7 gives the flowchart of EAPP.

Outputs: The list of outputs is similar to that of the PVRPAT output list.

A sample program is run for the case L = 5, LL = 4, dB = 10 dB. The output θ is in minutes, $u = \sin\theta \cos\phi$ and the last column gives the normalized gain of the antenna. Figure IV.8 gives the particulars of the sample run.

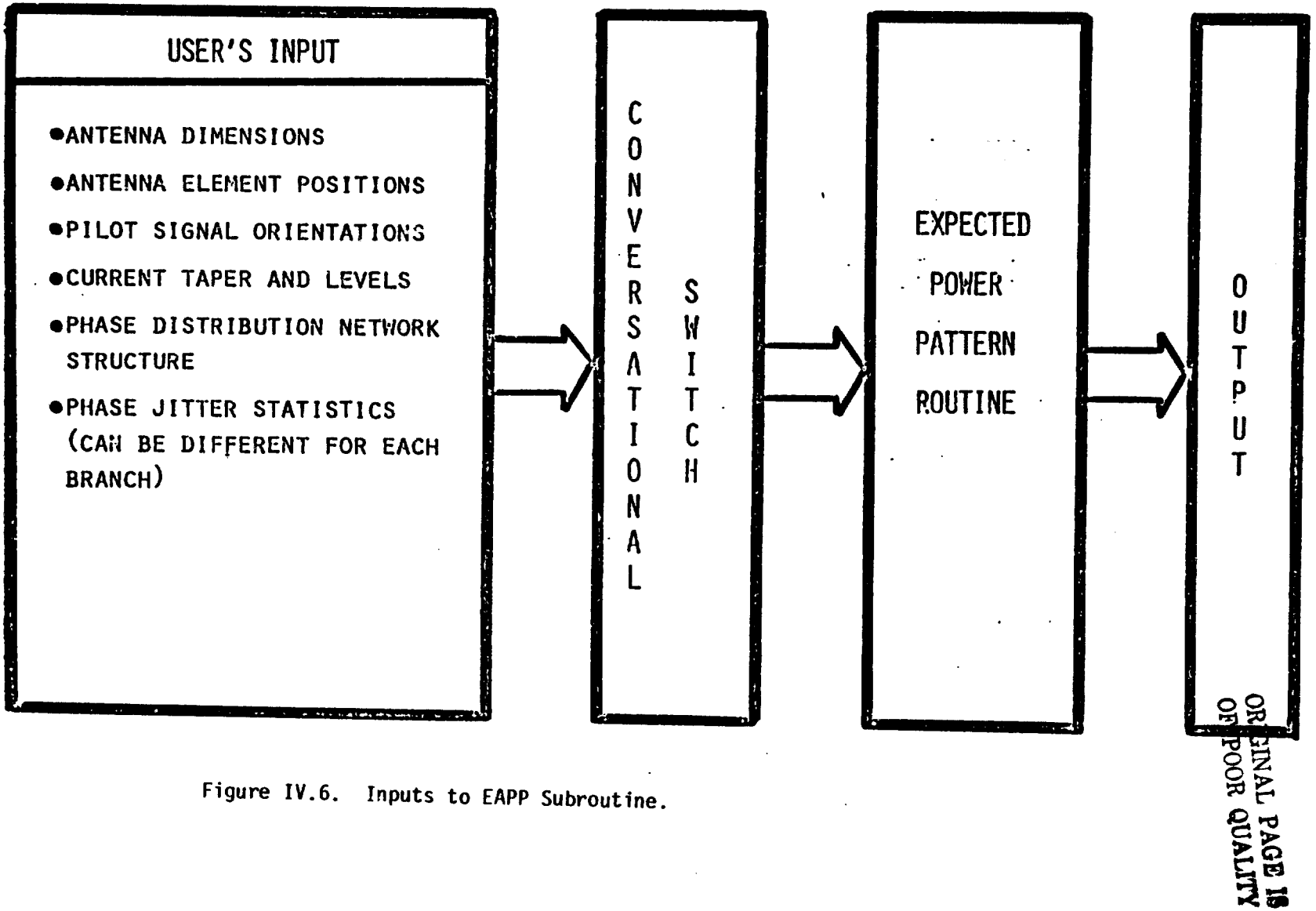

Figure IV.6. Inputs to EAPP Subroutine.

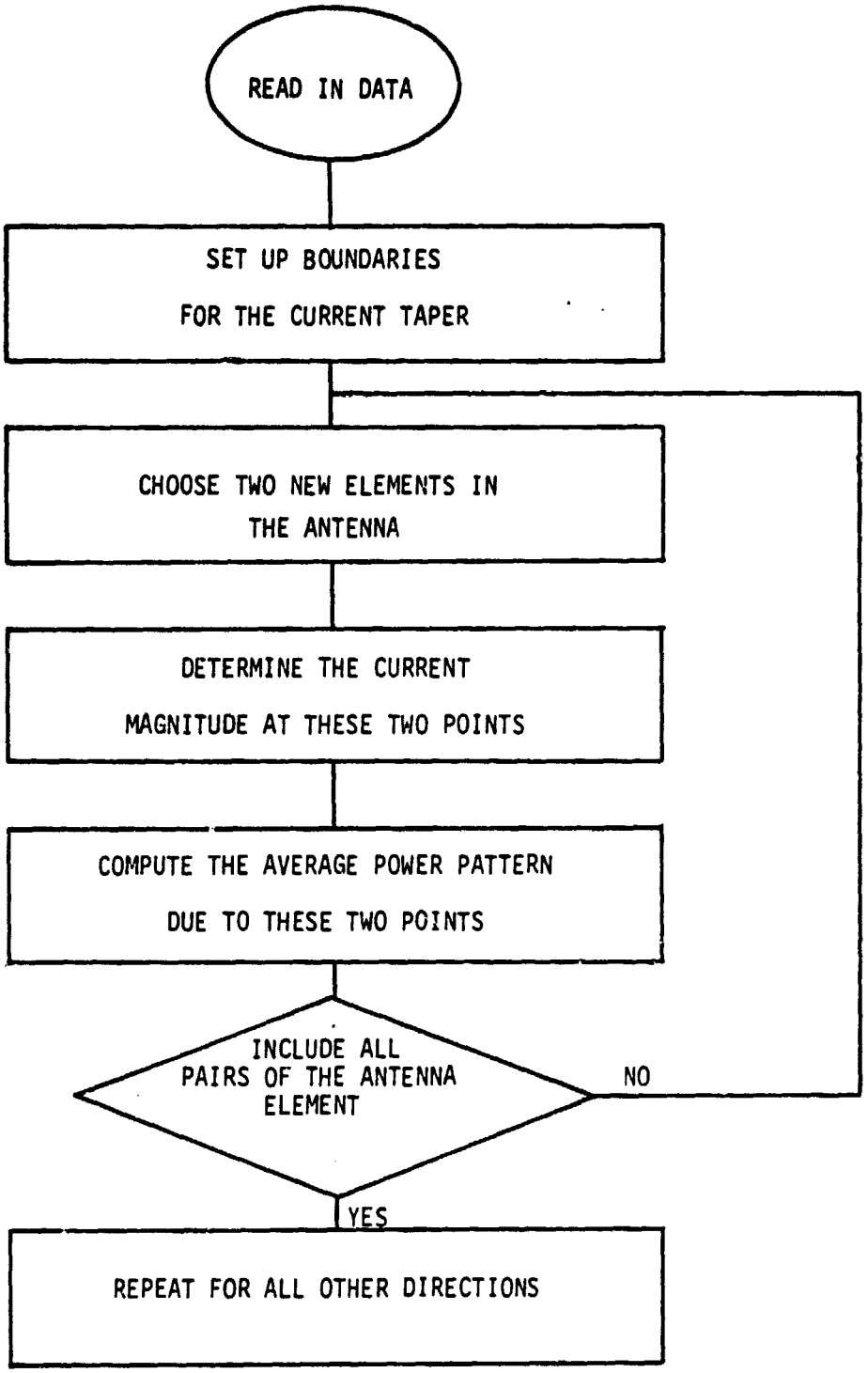

Figure IV.7. The Flow Chart of EAPP.

```
 0.,10.,4,10,0.,5,10.,0.,0.,1.,1.,320.
>5.,5.,5.,5.,5.

SIGMA( 1 ) =       5.00000000
SIGMA( 2 ) =       5.00000000
SIGMA( 3 ) =       5.00000000
SIGMA( 4 ) =       5.00000000
SIGMA( 5 ) =       5.00000000

 THETA0    PHI0      RO       DB       DX      DY       LL    L
   .000     .000 320.000  10.000    1.000   1.000     4     5

        THETA              U          (PERTURB)  RATIO

     .00000000          .00000000      .0000000
   10.00000000          .14926083     -.4152529+01
   20.00000000          .29852040     -.2011022+02
   29.99999976          .44777745     -.1548799+02
   39.99999952          .59703071     -.2231589+02
   49.99999905          .74627890     -.2111276+02
   59.99999905          .89552070     -.2155554+02
   69.99999809         1.04475510     -.2391221+02
   79.99999809         1.19398056     -.2326496+02
   89.99999809         1.34319593     -.2579810+02

364244.17187500
```

Figure IV.8. A Sample Output of EAPP.

SOLARSIM Subroutine APPRXPAT

Purpose: The previous subroutine computes the actual averaged power pattern but it is slow and uses a lot of CPU time. APPRXPAT computes the averaged power pattern by introducing an approximation to the phase error covariance matrix which makes the computations considerably faster and the results are very close to EAPP results. APPRXPAT, like the EAPP, handles various configurations of the phase distribution system and also different current tapers can be specified.

Inputs:

XRM - Alphanumeric array for generating the format of the output printer plot.

L - Number of levels of the phase distribution tree structure.

LL - Number of current levels.

NTER - Number of θ values to be used to compute the power pattern.

NB - Array containing number of branches per level of the phase distribution tree structure.

SGM - Array of standard deviations in each branch of the phasing tree (degrees).

START - Starting value of the θ direction.

PHIO - Pilot signal ϕ direction.

THEATAO- Pilot signal θ direction.

PHI - Constant value of ϕ direction to be used in computations.

DB - Current Taper in dB.

Figure IV.9 gives the flowchart of the subrouting APPRXPAT.

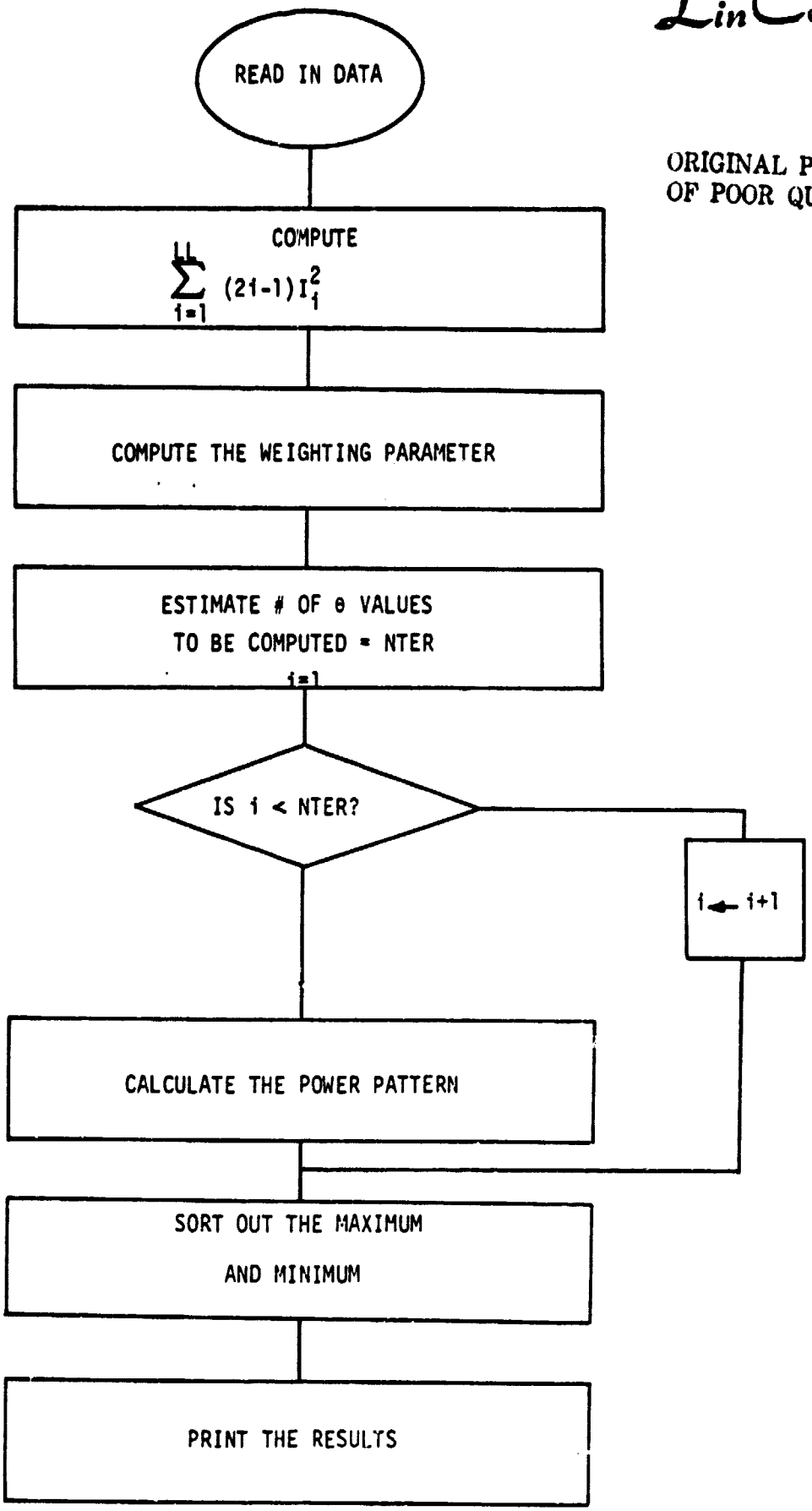

Figure IV.9. The Flowchart for the APPRXPAT.

Outputs:

T - Array of the theta values (minutes).

EFF - Array of the approximate power pattern.

Library Subroutines: PLOT1

Figure IV.9 shows the sample output run for the case of a four level phase distribution tree with 10 dB current taper induced by 10 current levels and no phase errors (i.e., L=4, LL = 10, dB = 10 and sigmas = 0). The branching of the phase distribution tree is 16 x 16 x 16 x 25. The last two columns represent θ and the associated approximate normalized power pattern.

Figure IV.10 depicts the plotted output of the APPRXPAT for the four level phase distribution tree structure described above with the standard deviations of phase error at each level equal to 7.5°. The current taper is 0 dB for the solid line curve and 10 dB for the dashed line curve. As can be seen from the figure, there is a widening of the half main beam width from 0.58 minute to 0.67 minute and a drop in the first sidelobe level from -13.4 dB to -17.5 dB.

Figure IV.11 shows the power patterns for a nine level phase distribution structure with four branches per node and 0 dB current taper. The standard deviation of the phase error added at each of the nine levels is a variable. The values are given in the figure. As is expected from the theory, we see from that the main lobe becomes wider, loss of gain is experienced and the nulls begin to fill up as the phase error variance is increased. Number 5 curve with 90° standard deviation of phase error at each level shows that the antenna is no longer distinguishable from an omni antenna.

```
0.00000      0.00000      0.00000      0.00000      1.000004+001

4.30817+004

9.70492-001

1.31546+000

0.00000      3.40243+009
8.76976-001  9.38603+008
1.31546+000  6.93758+007
2.19244+000  5.89675+007
2.63093+000  6.36931+006
3.50790+000  1.35490+007
3.94639+000  5.43427+005
4.82337+000  7.20323+006
5.26186+000  1.09719+005
6.13883+000  4.09431+006

0.00000      -4.27849+001

0.00000      0.00000
4.38488-001  -1.82974+000
1.31546+000  -1.71539+001
1.75395+000  -2.67903+001
2.19244+000  -1.78472+001
2.63093+000  -2.75250+001
3.06942+000  -2.67026+001
3.50790+000  -2.42469+001
3.94639+000  -3.82145+001
4.38488+000  -2.09957+001
5.26186+000  -4.27849+001
5.70035+000  -3.07191+001

.00000  I
.43849  I
.87698  I
1.31546  I
1.75395  I
2.19244  I
3.06942  0
3.50790  I
4.38488  0
4.82337  0
5.70035  0
```

ORIGINAL PAGE IS
OF POOR QUALITY

Figure IV.9. A Sample Output for APPRXPAT.

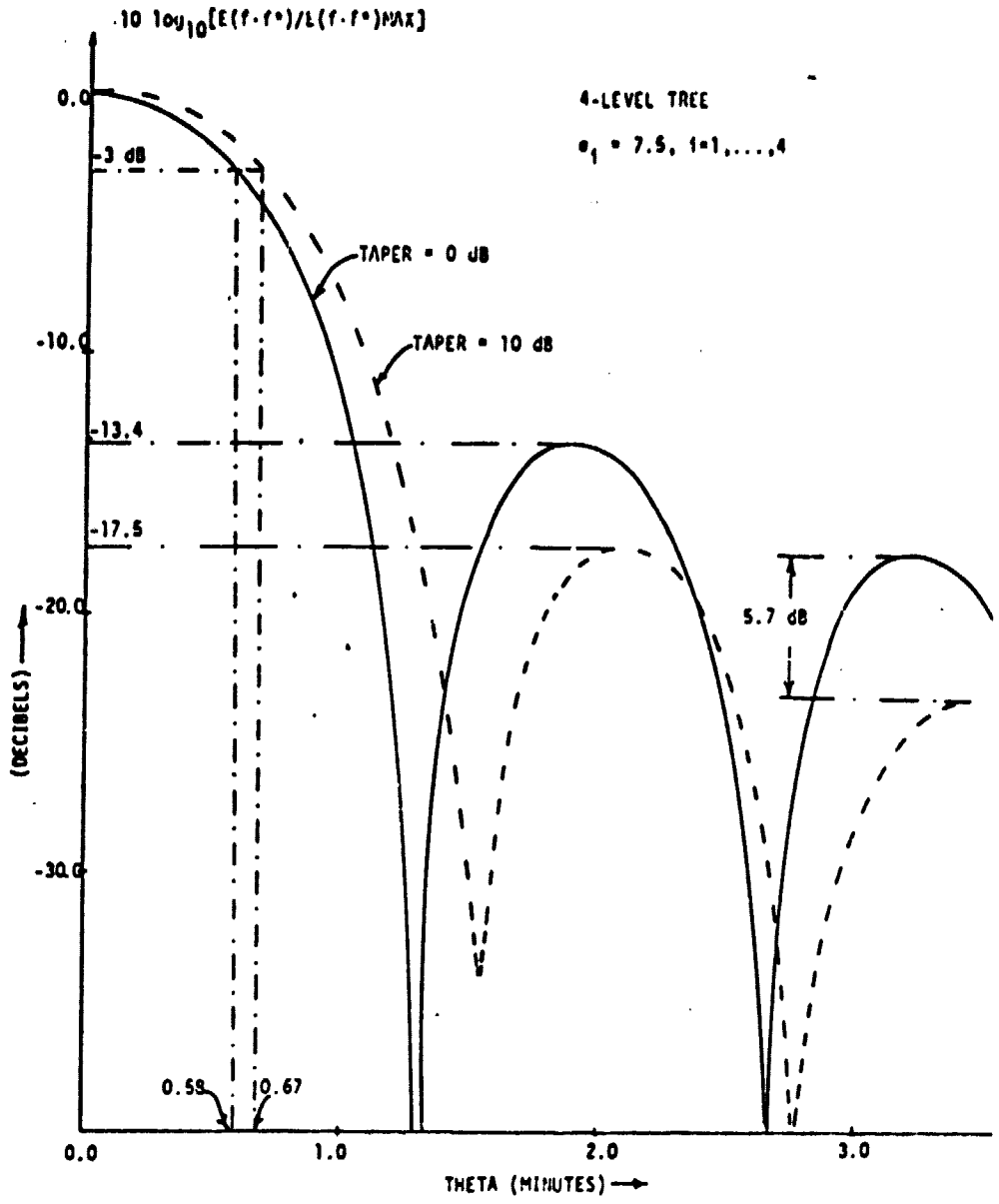

Figure IV.10. Power Pattern by APPRXPAT.

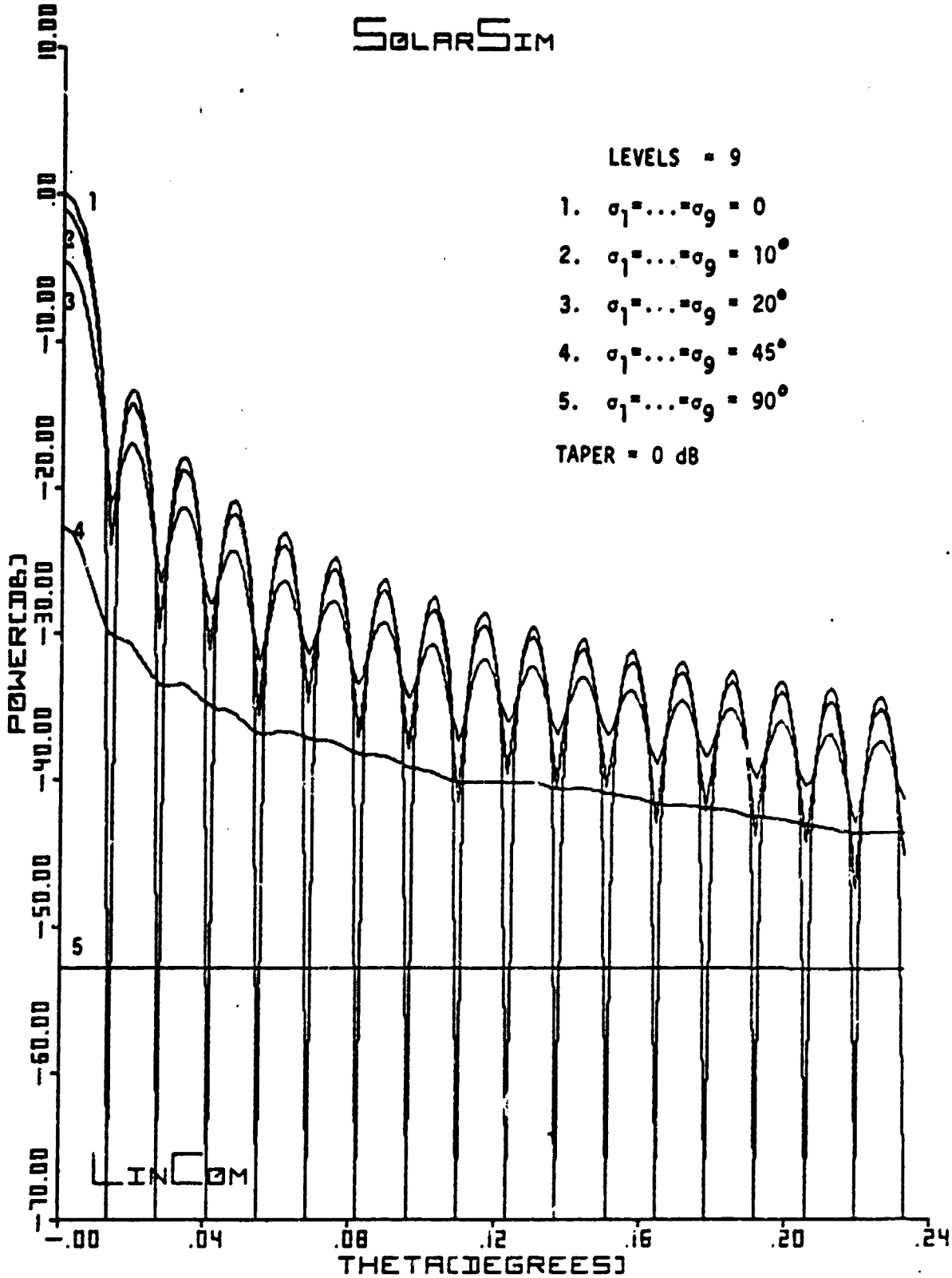

Figure IV.11. Power Patterns for Various Sigmas

SOLARSIM Subroutine TRUEGGO

Purpose: TRUEGGO computes the actual main beam gain of the SPSS antenna with and without the noise introduced by the phase distribution system.

Inputs:

L - Number of levels of the phase distribution tree structure.

LL - Number of current levels.

DX - Interelemental spacing in x direction.

DY - Interelemental spacing in y direction.

SGMA1 - Array for standard devistions in each level of the phase dsitribution tree structure.

Outputs: The output consists of two gains, one when the phasing system imperfections are present and the other when there are no imperfections. Ratio of these two generates the normalized gain sample run shows the output for L = 4, LL = 8 and σ for all levels = 5°

Figure IV.12 is the flowchart of the TRUEGGO program. Figure IV.13 is a plot of normalized gain in dB and the total phase error at the tip of the tree (equal amount of phase error added per level) as a result of the sample run of the APPRXPAT. The curves are drawn for the nine as well as four level phase distribution structure with current taper of 0 and 10 dB. As can be seen from the figure to achieve a gain efficiency of not less than 96% the total phase error at the tip of the tree cannot be allowed to become more than 12°.

APPRXPAT subroutine was used to determine the effect of the phase error variance added by the last level of the phase distribution tree

structure. A sample run of APPRXPAT for the four and nine level phase distribution tree structure was made with the last level sigma varying (the sum total of remaining level sigmas was held constant to 15°) for current taper equal to 0 and 10 dB. The resultant plot is shown in Figure IV.14.

Effect of phase error added by different levels in the phase distribution tree is shown in Figure IV.15. Two different structures are considered. One with eight levels of phase distribution system and the other with nine levels. The normalized gain is plotted when the standard deviation of the phase error added by the system at the $i^{\underline{th}}$ level is 5° while the remaining levels add no phase error $i = 1,\ldots,9$. It can be deduced from this figure that as far as the gain reduction is concerned, the last level is the most important level, i.e., the phase variance of the PAs will have a worse effect than the oscillator noises added at the first few levels. Fig. IV.16 is an extension of the above idea applied to a nine level phase distribution tree. Curve 1 is a plot of normalized gain with respect to the first level sigma varying (all other levels add no phase variance). Curve 2 is a plot of normalized gain against the RMS phase error build up with each level sigma varying. Curve 3 is the plot of normalized gain against phase error added at the ninth level (all other levels add no variance).

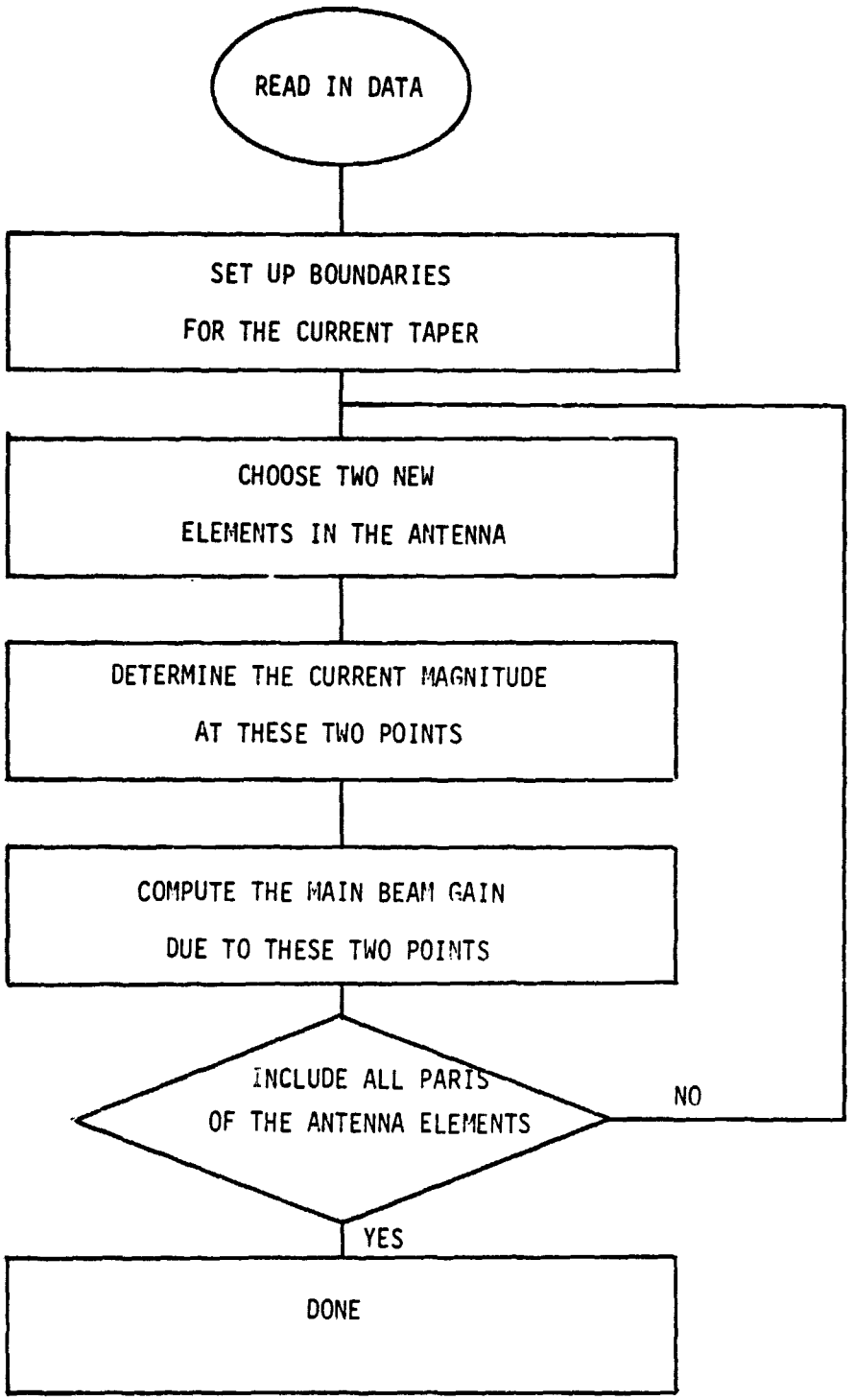

Figure IV.12. Flowchart of TRUEGGO.

ORIGINAL PAGE IS
OF POOR QUALITY

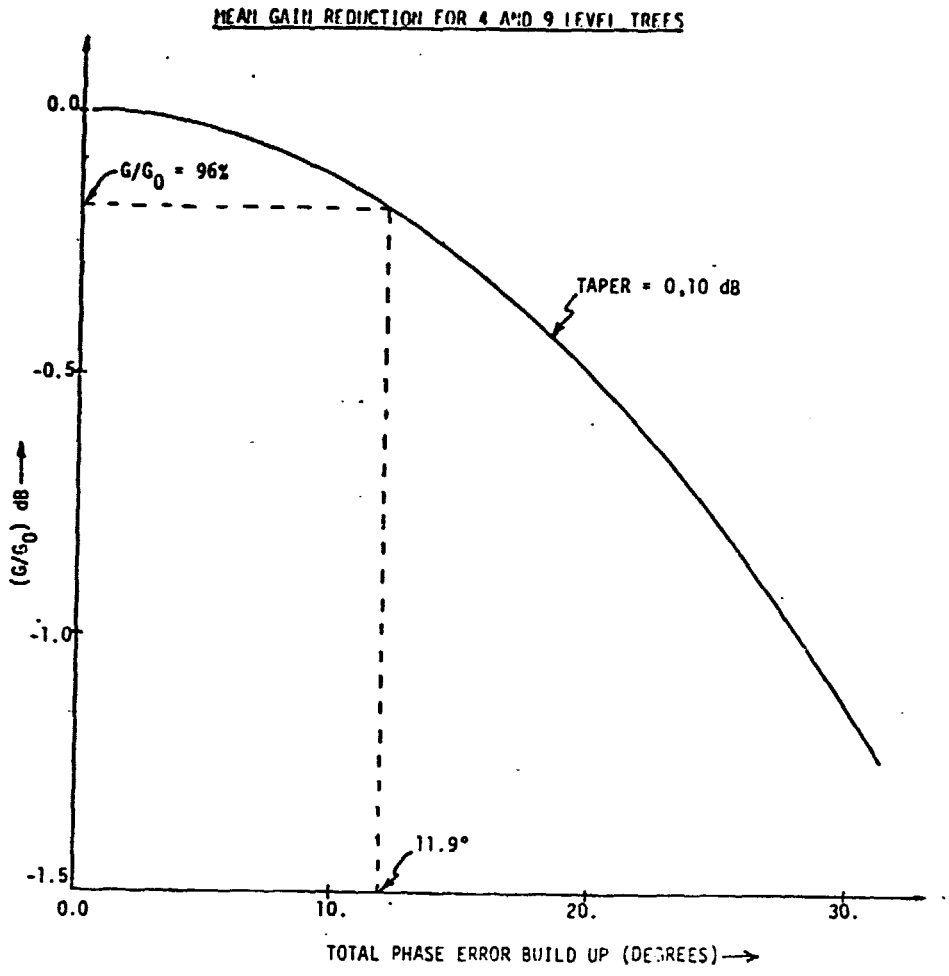

Figure IV.13. Effect of Phase Error Build Up on the Gain.

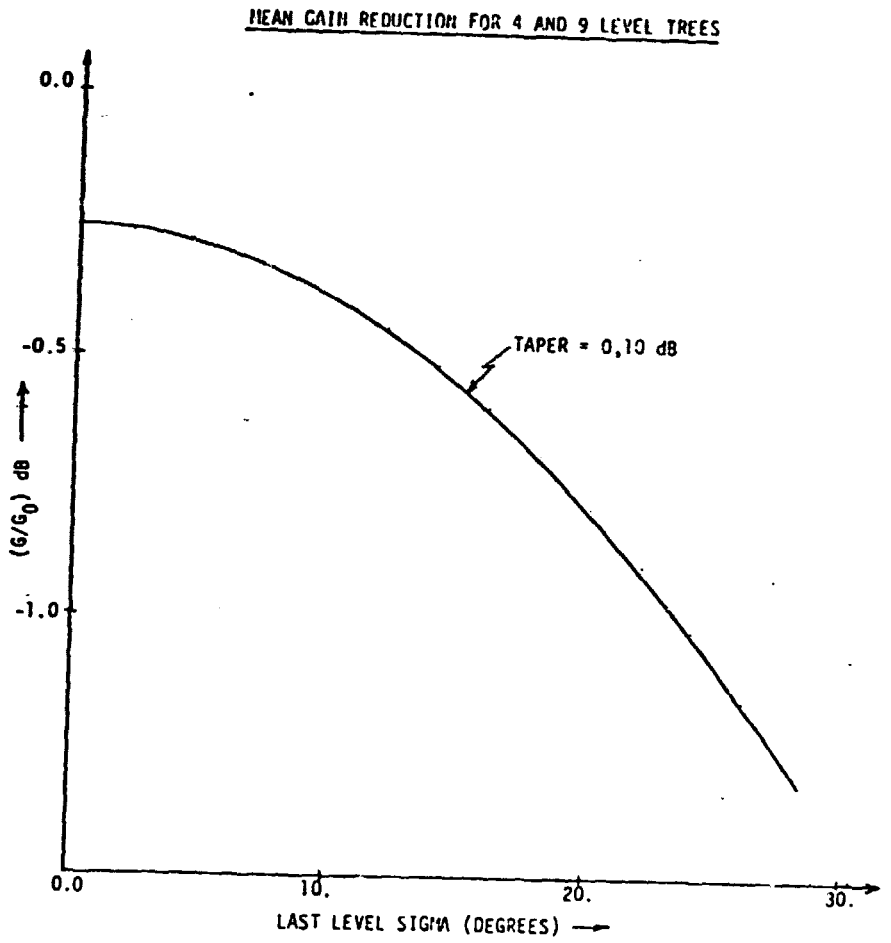

Figure IV.14. Effect of Last Level Phase Error Build Up on the Gain of the Spacetenna.

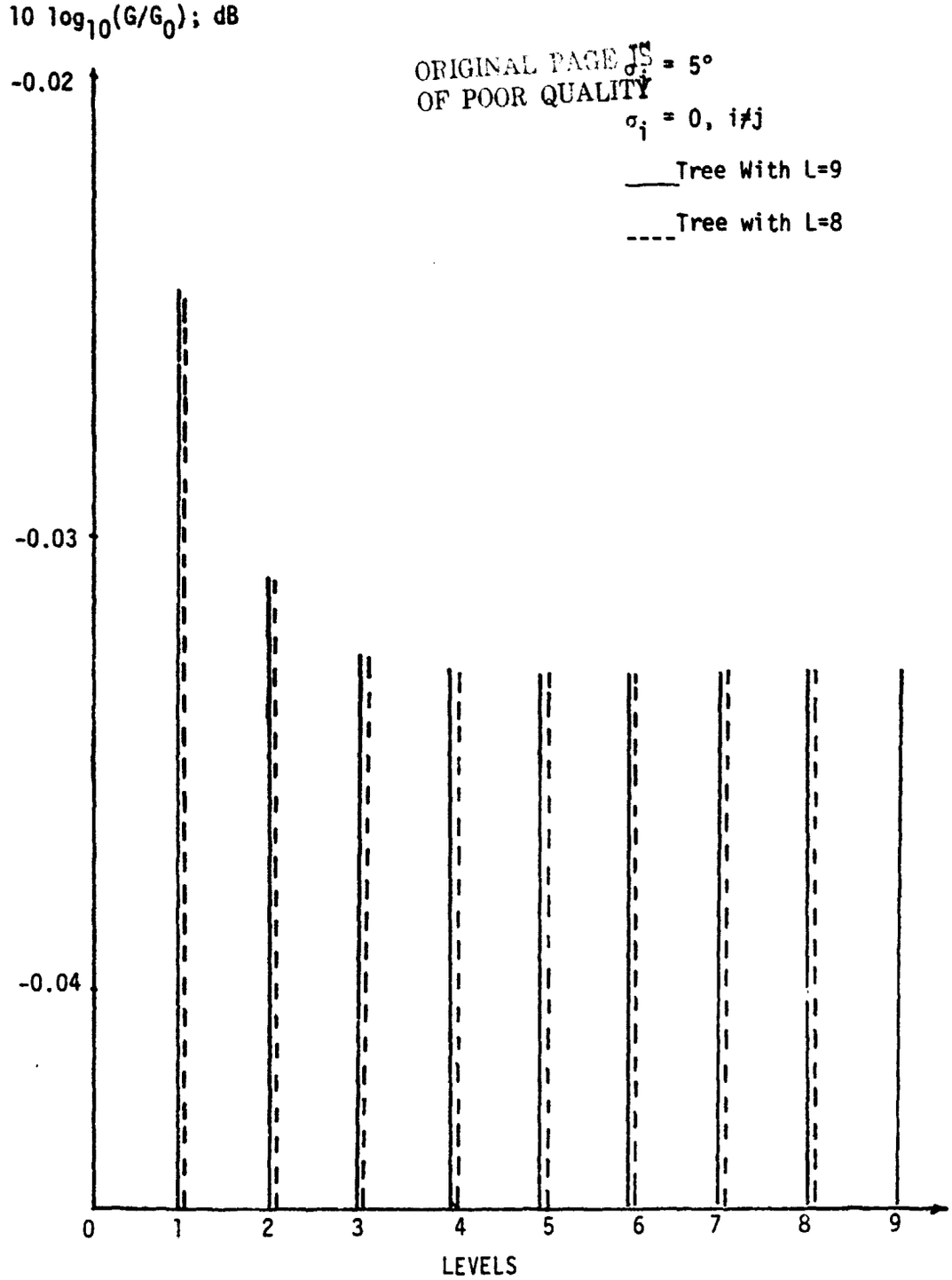

Figure IV.14. Effect of Each Level Phase Error on the Gain of the Spaceuenna.

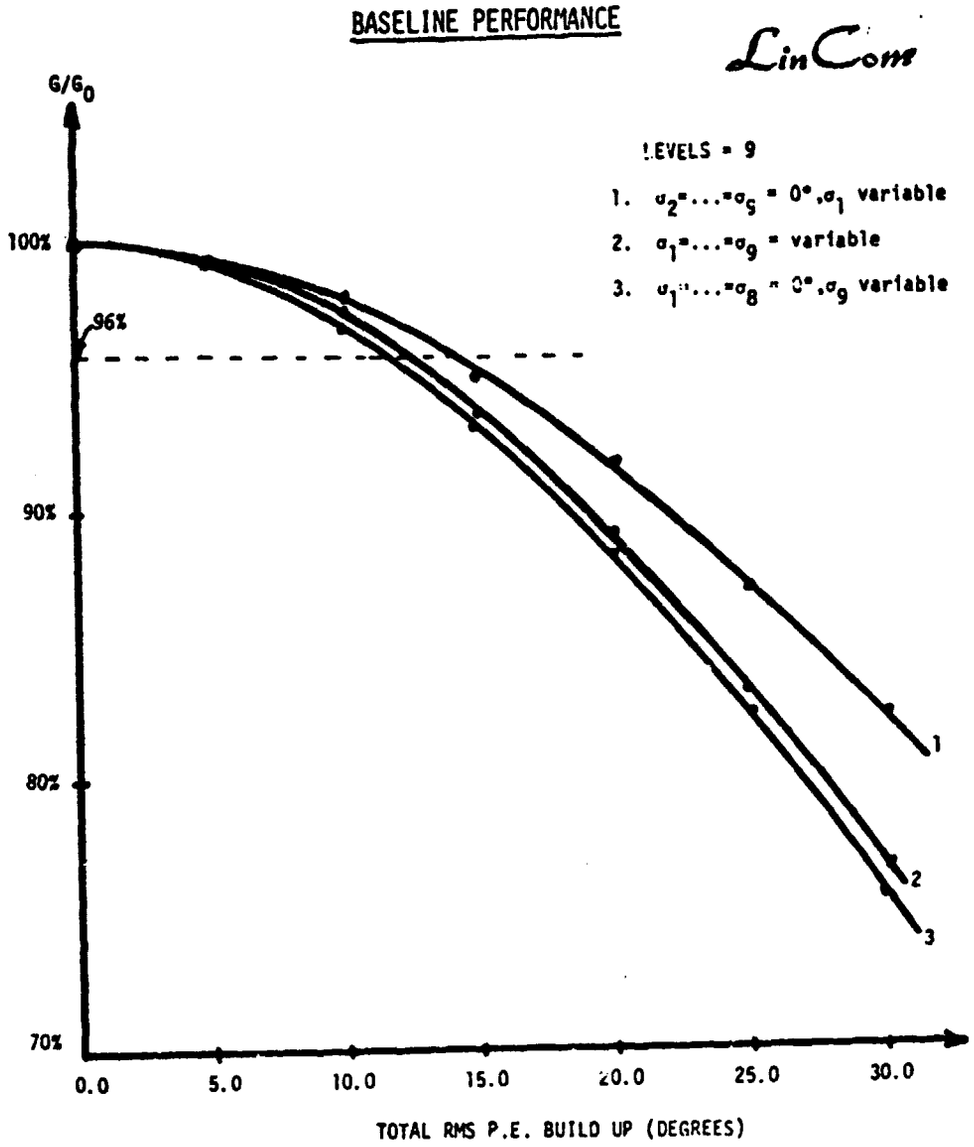

Figure IV.16. Effect of Phase Error Build Up on the Gain.

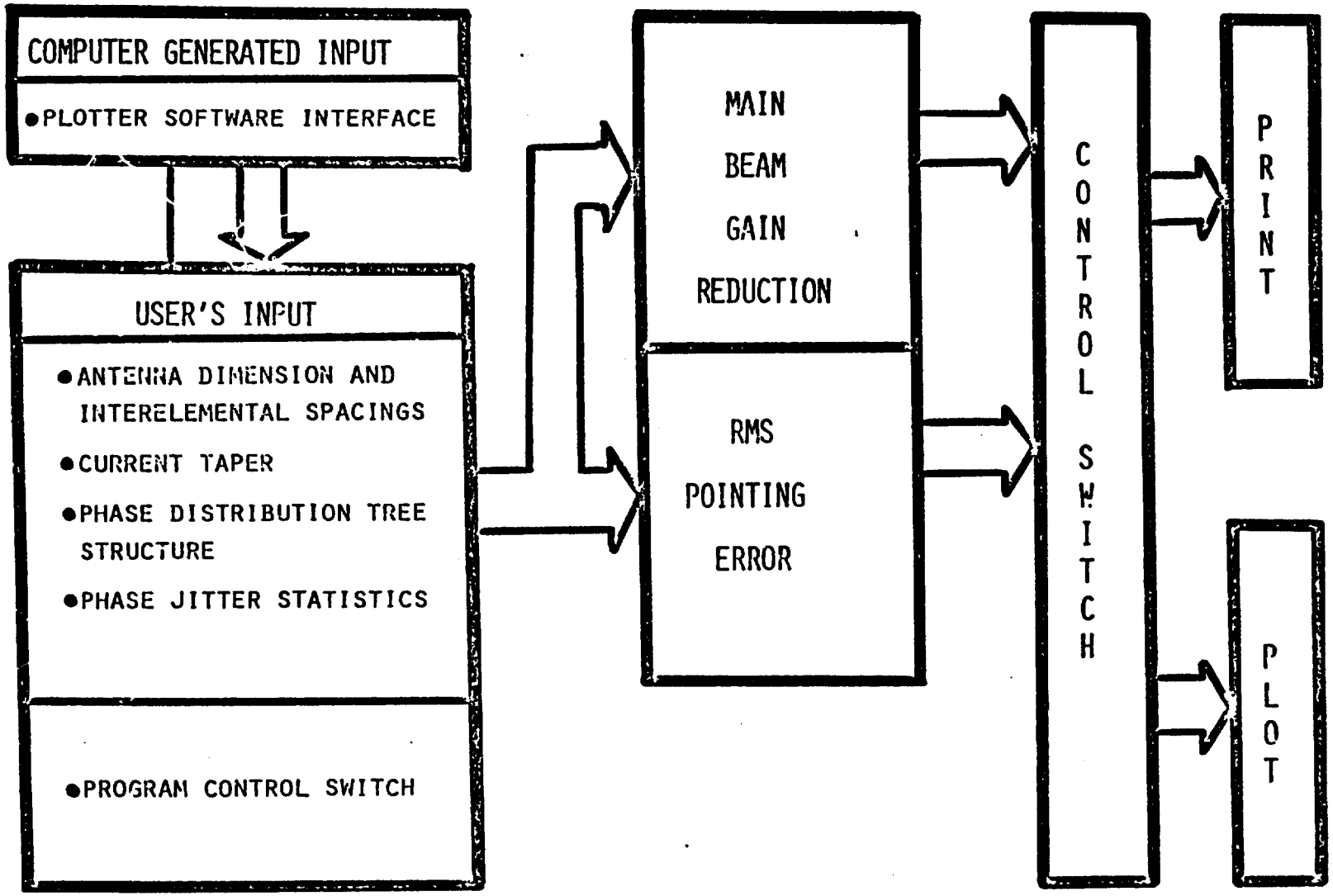

Figure IV.17. Inputs and Outputs of the Subroutine APPDEL.

SOLARSIM Subroutine APPDEL

Purpose: Given the phase distribution system, the imperfections (noises) associated with it, APPDEL computes the value of standard deviation of the pointing error. This program also takes into account the specified current taper. Figure IV.17 shows the inputs necessary and the outputs generated by APPDEL.

Inputs:

L - Number of levele of the phase distribution tree structure.

LL - Number of current taper.

DB - Current taper in dB.

LB - Array for number of branches per level of the phase distribution tree.

ICNTL - Control parameter.

1. For printout with supplied sigmas for the distribution tree.
2. For plot of $\sigma_{\Delta u}$ (S.D. of pointing error) vs RMS .
3. Stops the execution.

SGMS - Array for the standard deviation in each branch of the phasing tree.

NTER - Number of points desired on the plot.

ICNT - Control parameter.

1. For plot of $\sigma_{\Delta u}$ vs first level .
2. For plot of $\sigma_{\Delta u}$ vs RMS σ with all levels varying.

Outputs:

SIGLOW - Array for the lower bound on the $\sigma_{\Delta u}$.

SIGDLU - Array for approximate $\sigma_{\Delta u}$.

ISGDUP - Array for the upper bound on $\sigma_{\Delta u}$.

Library Subroutines: Plot 1.

The program has question and answer session, the output is self explainatory. Fig. IV.18 is the flowchart of subroutine APPDEL. A sample output is shown in Figure IV.19. Figure IV.20 is a plot of the RMS pointing error against the total phase error obtained from a typical run of APPDEL for four and nine level distribution trees for 0 and 10 dB current tapers. The taper broadens the beam but it becomes more susceptable to pointing error also this can be ascertained from the two curves in Figure IV.20. As the figure shows for 10 dB current taper for either four or nine level phase distribution structure for an allowable probability of 0.95 for the absolute pointing not to exceed 4% of the 3 dB beamwidth the maximum phase error build up can equal 10°.

Figure IV.20 shows the plot from another sample run of APPDEL. The phase distribution tree structure has eight and nine levels only one level had a phase error input of 5° all the remaining levels added no phase errors. The importance of the phase errors in the first few levels is evident from the figure.

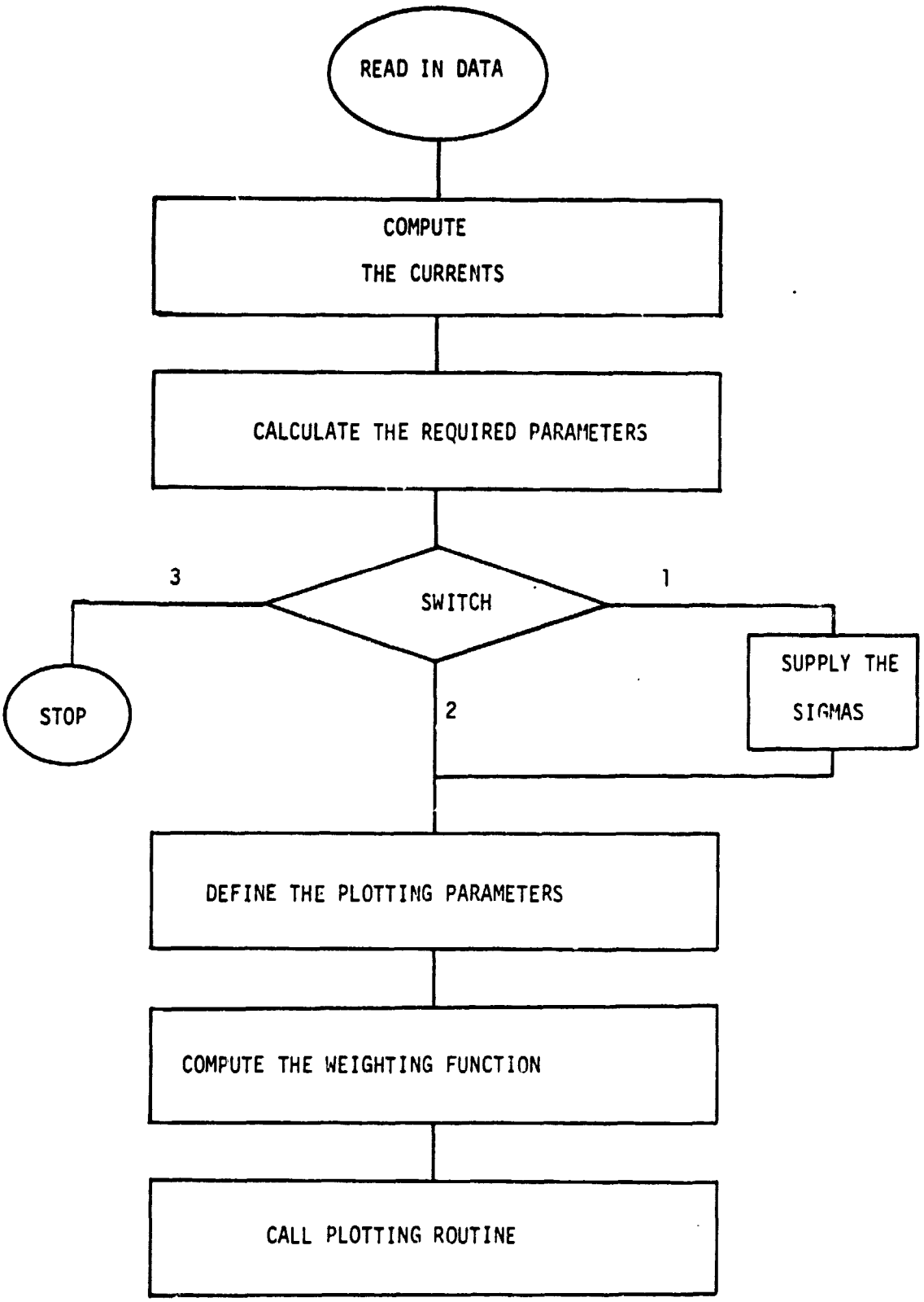

Figure IV.18. Flowchart of Subroutine APPDEL.

10.,5,10
>4,4,14,16,25

4 4 14 16 25

102400 5 10 10.00000000

.99427655 .97177283 .92828186 .86666746 .79082899 .70529383 .61477319 .52374151 .43609009 .35488892

.10799472+07 .10606078+09 .55740904+08

TYPE 1 FOR PRINTOUT WITH SUPPLIED SIGMAS, TYPE 2 FOR PLOT OF DELU VS THE RMS SIGMA, TYPE 3 TO STOP
>1

TYPE IN THE SIGMAS
>0.,5.,5.,5.,5.

.00108019
.02925606
.09809848

TYPE 1 FOR PRINTOUT WITH SUPPLIED SIGMAS, TYPE 2 FOR PLOT OF DELU VS THE RMS SIGMA, TYPE 3 TO STOP
>2

TYPE IN THE NUMBER OF POINTS DESIRED ON THE PLOT
>15

TYPE IN THE INCREMENT FOR X AXIS
>1.

TYPE 1 FOR PLOT OF DELU VS THE FIRST LEVEL SIGMA OR 2 FOR DELU VS RMS SIGMA WITH ALL LEVELS VARYING
>2

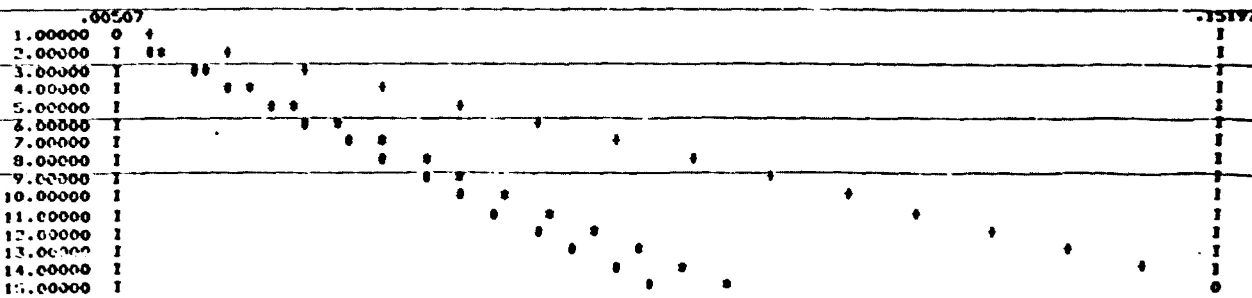

TYPE 1 FOR PRINTOUT WITH SUPPLIED SIGMAS, TYPE 2 FOR PLOT OF DELU VS THE RMS SIGMA, TYPE 3 TO STOP
>3

Figure IV.19. A Sample Output of APPDEL.

ORIGINAL PAGE IS OF POOR QUALITY

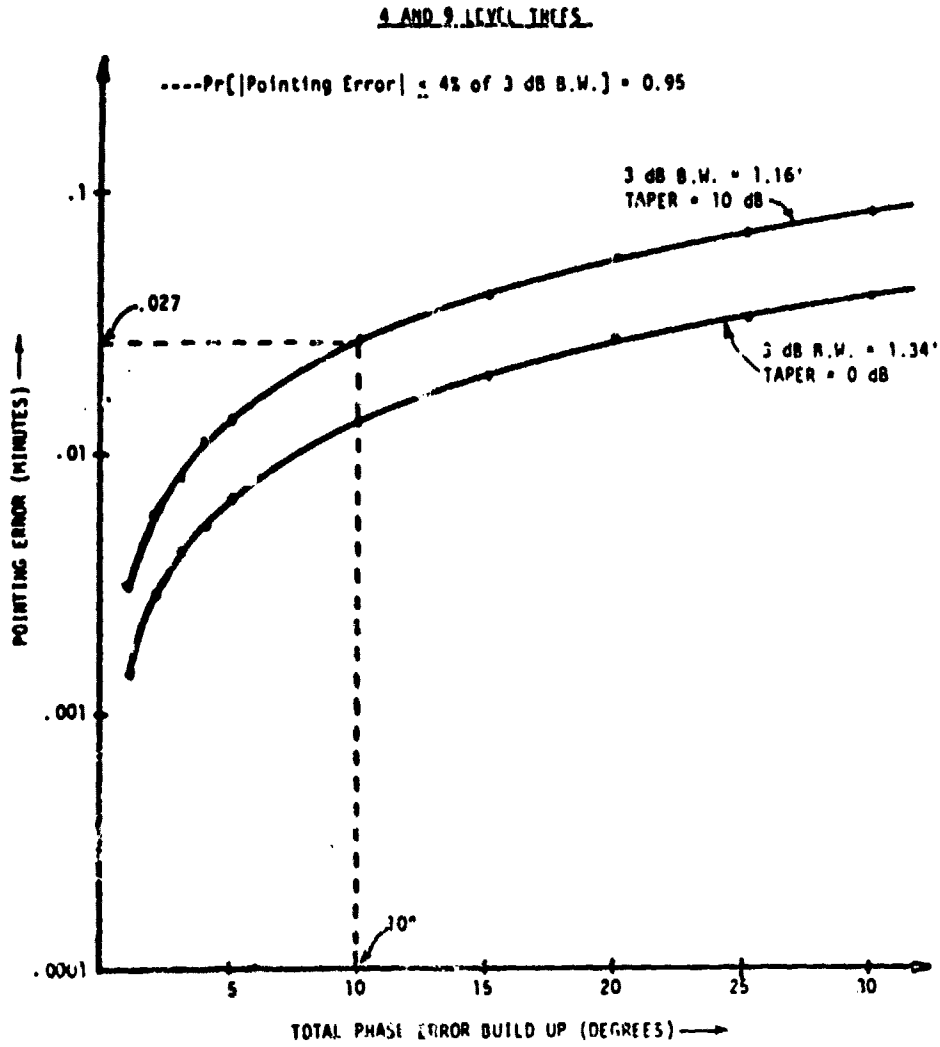

Figure IV.20. Effect of Phase Error Build Up on RMS Pointing Error.

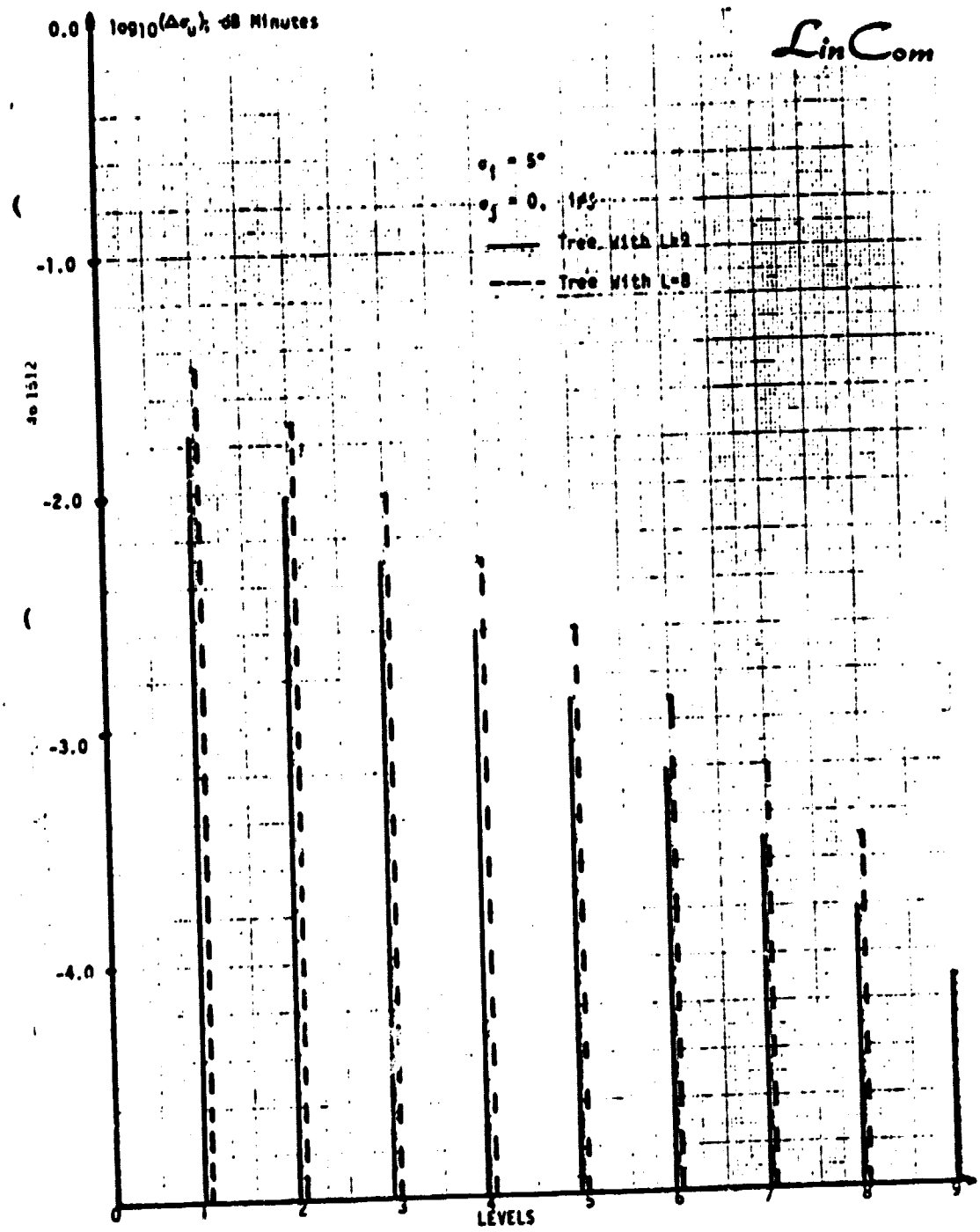

Figure IV.21. Effect of Each Level Phase Error on the Beam Pointing Error.

SOLARSIM Subroutine MPTS

Purpose: This subroutine computes the power transfer efficiency of the spacetenna by calculating the actual power received by the rectenna when the beam suffers deflection due to the phase errors in the phasing system and dividing this power by the power received by the rectenna when the main beam is ideally pointed.

Inputs:

M(I) - Number of amplifiers in the i^{th} level subarray, I = 1,...,10.

N(I) - Number of radiaging slots in the i^{th} level, I = 1,...,10.

NA(I) - Number of amplifiers in the i^{th} level, I = 1,...,10.

R(I) - Radius of i^{th} power density ring, I = 1,...,10.

SIGMAB(I)-The total standard deviation in the i^{th} power density level radiating elements, I = 1,...,10.

SIGPHI(I),SIGPSI(I) - The standard deviation of location errors of radiating and the receiving elements for the subarrays in the i^{th} power density level, I = 1,...,10.

SIGMAI(D) - The standard deviation of the current amplitude feeding the radiating elements in the i^{th} power level, I = 1,...,10.

CURNT(I) - The current output of the power amplifier in the i^{th} level, I = 1,...,10.

XMEAN(I),YMEAN(I) - The x and y components of mean subarray tilt in the i^{th} power level, I = 1,...,10.

SGMA(I) - The standard deviation of the x and y components of the subarray tilt in the i^{th} power density level, i = 1,...,10.

THETAR,PHIR - The (θ,ψ) direction of the incoming pilot signal.

NX,NY,XA,XB,YA,YB,IA,IB - The parameter values of the double integral subroutine.

Outputs: The output is shown in terms of a figure in Section 10 (Fig. 10.19).